Navigation intelligente dans des environnements virtuels

Yuyang Wang

HESAM UNIVERSITÉ

Arts et Métiers Sciences et Technologies

ÉCOLE DOCTORALE SCIENCES ET MÉTIERS DE L'INGÉNIEUR
[LISPEN, Institut Image - Campus de Cluny]

THÈSE

présentée par : **Yuyang WANG**
soutenue le : **14 Octobre 2021**

pour obtenir le grade de : **Docteur d'HESAM Université**

préparée à : **École Nationale Supérieure d'Arts et Métiers**
Spécialité : **Informatique-traitement du signal**

Intelligent navigation in virtual reality

THÈSE dirigée par :
M. MERIENNE Frédéric

et co-encadrée par :
M. CHARDONNET Jean-Rémy

Jury

M. Daniel MESTRE	Directeur de recherche ISM, Aix-Marseille Université	Président/ Rapporteur
M. Antonio CAPOBIANCO	Maître de conférences HDR ICube, Université de Strasbourg	Rapporteur
M. Ronan QUERREC	Professeur CERV, ENIB	Examinateur
M. Jean-Rémy CHARDONNET	Maître de conférences HDR LISPEN, Arts et Métiers	Examinateur
M. Frédéric MERIENNE	Professeur LISPEN, Arts et Métiers	Examinateur
Mme Jivka OVTCHAROVA	Professeure IMI, KIT (Allemagne)	Invitée

THÈSE

Acknowledgments

First and foremost, I want to give sincere gratitude to Prof. Frédéric Merienne and Dr. habil. Jean-Rémy Chardonnet for their constructive comments, valuable suggestions and discussions, enthusiastic encouragement, and infinite patience. They usually give me different advice and constant support in every aspect, which allows me to take advantage of both. It was a privilege to pursue a Ph.D. under their supervision. I wish that I could collaborate with them again in the future.

I also want to thank the members of Institut Image. Especially, thanks Thomas LAMY for technical support with multiple research facilities; thanks Julien Ryard and Jérémy Plouzeau for their support in code development; thanks Rémy Malin for his support for graphics resources; thanks Géraldine Roux for her help in many administrative procedures; thanks Dr. Ruding Lou for his kind help when I had difficulties in personal life; thanks my Ph.D. colleagues (Bo Li, Théo Combe, Cédric Di Loreto, Mahdiyeh Moosav, *etc.*) with whom we can share research experience and progress. Similar gratitude belongs to Prof. Dr. Jivka Ovtcharova for hosting my stay in the Institute for Information Management in Engineering (IMI), Karlsruhe Institute of Technology, for one year during my Ph.D. study. I want to thank the members of IMI, Thomas Maier, Karin Jenewein, Sonja Ohler, Mikhail Langovoy, Matthes Elstermann, Jieyang Peng, Andreas Kimming, Anjela Mayer, Felix Longge Michels, Victor Häfner and Polina Häfner, for their help in administrative issues, technical assistances in experimental work.

Thanks also to the thesis committee: Ronan Querrec, Daniel Mestre, Antonio Capobianco, for their constructive advice and comments on the thesis. I also want to thank the anonymous reviewers of the conference and journal papers for their critical comments on my work. Many anonymous individuals have participated in the user experiments and contributed meaningful data; I gratefully acknowledge their selfless support. Many of them showed significant interest in virtual reality after attending my tedious experiments and encouraged their friends to participate in the research. Thanks

to their presence, I have been productive and creative in my work.

I am indebted to the China Scholarship Council (CSC) for financially supporting my Ph.D. work in the past four years. I also thank the French-German Institute for Industry of the Future and the Erasmus Mobility programme that funded my stay at Karlsruhe Institute of Technology in Germany.

Finally, I would like to express my sincere gratitude to my family members.

Résumé

La réalité virtuelle (VR) connaît un développement rapide grâce aux technologies de jeux vidéo 3D et de casques immersifs abordables, permettant d'interagir plus facilement avec des environnements virtuels. Au cours du processus d'interaction, l'utilisateur est au centre de l'application et, par conséquent, il est primordial de comprendre les facteurs humains affectant l'expérience et la satisfaction de l'utilisateur. Ces facteurs sont cruciaux pour concevoir une navigation virtuelle aussi naturelle que ce que les utilisateurs font généralement inconsciemment dans le monde réel.

Cependant, les techniques de navigation dans les environnements virtuels peuvent être exigeantes sur le plan cognitif et induire un cybermalaise, conduisant au rejet des technologies de réalité virtuelle. Divers factors humains peuvent influencer l'expérience utilisateur, en particulier le niveau de cybermalaise pendant l'immersion en réalité virtuelle. Comme ces effets sont individuellement différents, son évaluation correcte est un préalable à la conception de différentes techniques de navigation. Pour utiliser ces différences individuelles et adapter la dynamique de navigation, nous avons introduit un modèle de logique floue pour analyser les caractéristiques humaines liées à l'apparition du cybermalaise et déterminer un indice personnalisé de cybermalaise. En plus des approches d'évaluation actuelles, nous avons démontré comment mesurer le cybermalaise et la charge cognitive en utilisant le *deep learning* (autoencodeur LSTM) et TOPSIS. La méthode d'évaluation proposée peut être considérée comme une amélioration des approches d'évaluation actuelles. Les résultats suggèrent que le *deep learning* représente une alternative innovante intéressante pour mesurer le cybermalaise en se basant sur des mesures comportementales comme la balance posturale, et que TOPSIS peut améliorer la précision de mesure de la charge cognitive.

Les progrès réalisés pour accroître le potentiel de la réalité virtuelle reposent également sur notre capacité à développer des techniques de navigation qui peuvent atténuer le cybermalaise de manière efficace. Nous avons introduit la navigation adaptative dans le sens de la personnalisation et conçu quatre

techniques différentes et originales de navigation tenant compte de différents facteurs humains. Dans un premier temps, nous avons proposé une navigation semi-automatique pour lisser les trajectoires de navigation lors des déplacements de l'utilisateur. Deuxièmement, connaissant l'importance des profils de vitesse de navigation sur l'expérience utilisateur, nous avons conçu un limiteur de vitesse capable de minimiser le *jerk* total lorsque l'utilisateur navigue dans des environnements virtuels. Troisièmement, le modèle de logique floue introduit pour déterminer un indice personnalisé de cybermalaise a été utilisé pour proposer une dynamique de navigation personnalisée. Enfin, sur la base de la théorie du contrôle PID et des réseaux de neurones, nous avons conçu une stratégie adaptative en ligne pour adapter la vitesse de navigation sur la base de l'état physiologique. Pour chaque technique de navigation, des expérimentations ont été réalisées pour valider leurs performances dans l'amélioration de l'expérience utilisateur, et les résultats montrent une réduction significative du niveau de cybermalaise.

Mots-clés : Réalité virtuelle, Navigation, Cybermalaise, Charge cognitive, Expérience utilisateur, Navigation personnalisée

Abstract

Virtual reality (VR) has experienced fast development thanks to technologies from 3D computer games and affordable head-mounted devices (HMDs), making it possible to interact with virtual environments more easily. During the interaction process, the user is at the center of the application, and therefore, it is paramount to understand the human-related factors affecting user experience and satisfaction. These factors are crucial for designing virtual navigation as natural as users usually conduct subconsciously in the physical world.

However, navigation techniques in virtual environments might be cognitively demanding and induce cybersickness, leading to the rejection of VR technologies. Various human-related factors can influence user experience, especially the level of cybersickness during immersion in VR applications. As these effects are individually different, its correct evaluation is a premise for designing different navigation techniques. To use these individual differences for adapting the navigation dynamics, we successfully introduced a fuzzy logic model to analyze human characteristics related to cybersickness and output a personalized cybersickness indicator. On top of the current evaluation approaches, we demonstrated how to measure cybersickness and cognitive workload based on deep learning (LSTM autoencoder) and TOPSIS. The proposed evaluation method can be regarded as an improvement for the current evaluation approaches. The results suggest that deep learning represents an interesting innovative alternative to measure cybersickness based on behavioral assets such as posture sway, and TOPSIS can improve the measuring accuracy for the cognitive workload.

The progress in unlocking the potential of VR also relies on our ability to develop navigation techniques that can mitigate cybersickness efficiently. We introduced adaptive navigation in the sense of personalization and designed four different original navigation techniques considering human-related factors. First, we proposed semiautomatic navigation to smoothen navigation trajectories during user displacement. Second, knowing the importance of navigation speed profiles on user experience, we

designed a speed protector that can minimize the total jerk when the user navigates in virtual environments. Third, the fuzzy logic model introduced to compute a personalized cybersickness indicator was used to propose personalized navigation dynamics. Last, based on the PID control theory and neural networks, we designed an online adaptive strategy to adapt the navigation speed based on physiological assets. For each navigation technique, user experiments were performed to validate its performance in improving user experience, and the results manifest a significant reduction of cybersickness severity.

Keywords: Virtual reality, Navigation, Cybersickness, Cognitive workload, User experience, Customized navigation

Contents

[1]Nous renvoyons à la section 4.1 pour une description détaillée.
[2]Nous renvoyons à la section 4.2 pour une description détaillée.
[3]Nous nous référons à la section 4.3 pour une description détaillée.
[4]Nous renvoyons à la section 5.1 pour une description détaillée.
[5]Nous renvoyons à la section 5.2 pour une description détaillée.
[6]Nous renvoyons à la section 5.3 pour une description détaillée.

[7]Nous renvoyons à la section 5.4 pour une description détaillée.

List of Tables

List of Figures

Chapter 1

Introduction

Contents

Virtual reality (VR) has become popular thanks to the fast development of affordable head-mounted devices (HMDs) with various available applications. Current VR HMDs mainly include high spatial and temporal resolution with dual displays (for example 1440×1600 pixels per eye and 90Hz to 120Hz refresh frame rate frequencies), achieving high-fidelity stereoscopic vision and image rendering, and low latency body tracking experience. Some international companies such as Google, Facebook, Microsoft, HTC, Samsung, and Apple are participating in the development of new VR hardware with their advantages (S. Chang and W. Chen 2017), bringing a total market size estimated to more than $100 billion in the next decades (Bellini *et al.* 2016; Framingham 2016; Merel 2017).

VR requires a user to be immersed in a computer-synthesized environment to perform tasks (Merienne 2016). Therefore, VR is user-centric, and all the created applications should focus on providing more user-centered to improve VR acceptance. According to a minimal set of assessments, the ability to predict human susceptibility to cybersickness is a promising work to develop personalized settings for VR users, thereby reducing or avoiding the side effects during and after the immersed experience. Currently, the community is searching for solutions to reduce cybersickness and provide VR users with a better experience. Users get cybersickness when exposed to locomotion-dominated navigation tasks. Although many techniques have been proposed to mitigate cybersickness in such navigation applications, few works have involved individual factors and physiological feedback. Many articles propose new techniques to reduce cybersickness but lack substantial explanation for their efficiency. The insufficiency of theoretical support is a problem. We believe that any approach to treat VR side effects should start from the reason for their occurrence. In addition, the cybersickness severity and susceptibility generally vary among users, leading to difficulties in the measurements.

Therefore, before we propose our solutions, we propose in this thesis to go deep into details regarding the effect of human-related factors on user experience, namely here cybersickness and cognitive workload, to develop *ad hoc* novel evaluation methods of cybersickness severity and cognitive workload. These methods will allow us to derive personalized navigation methods mitigating cybersickness while ensuring low cognitive workload.

1.1 Contributions

This thesis aims at developing navigation techniques that can mitigate cybersickness and cognitive workload, through which we expect to improve user's immersive experience in virtual environments. We describe several fields, including different reasons for the occurrence of cybersickness, different measurements for cybersickness and cognitive workload. We will find the limitations of current evaluation methods for cybersickness and cognitive workload, and we will propose our solutions. Aiming to develop adaptive navigation, we will present a series of work, including technical developments, user tests, and validation. The thesis achieves several contributions in terms of scientific and technical developments, including:

- A literature study on navigation in virtual environments and the associated effects on cybersickness and cognitive workload.
- The development of evaluation methods for cybersickness and cognitive workload considering the defects of current measurements.
- The development of adaptive navigation methods including semi-automatic trajectory, speed protector, adaptive navigation techniques considering cybersickness susceptibility and physiological response.

1.2 Content of the thesis

Figure 1.1 depicts the structure of the thesis and the relationship between each chapter. The research content sticks to navigation in virtual reality by improving navigation experience . We designed different navigation techniques by mainly focusing on cybersickness as well as cognition. Below, we summarize the content of the other chapters (excluding the current chapter):

In chapter 2, we perform a literature review on navigation and user experience. We will study the individual differences in the tolerance to cybersickness and the reason for its happening. The effects of individual factors including gender, age, postural stability, ethnic origin and genetic influences, gaming experience, personality, visual acuity will be analyzed. This chapter also summarizes the explanations for cybersickness based on several theories and highlights the correlations and differences from our

point of view. Based on these theories, we put forward recommendations for future work investigating 3D interaction interfaces, cybersickness reduction or avoidance, and other user experience related issues. In addition, we investigate approaches to measure cognitive workload in this chapter.

In chapter 3, we define the objectives of the thesis more in detail. Also, we expose the associated research questions.

In chapter 4, we propose our solutions to measure cybersickness and cognitive workload. To measure cybersickness, we train an LSTM model for each participant using a normal-state postural signal captured before exposure. If the postural sway signal from post-exposure is sufficiently different from the pre-exposure signal, it suggests that there is a severe cybersickness. To predict the susceptibility to cybersickness according to the individual difference, we further introduce a fuzzy logic model that can analyze human characteristics related to cybersickness. Last, to improve the measuring quality of the cognitive workload, we demonstrate a novel method of analysis of the NASA-TLX table based on TOPSIS.

In chapter 5, we present four different navigation techniques to improve the navigation experience. The idea is to adapt navigation settings such as human factors, the motion dynamics (trajectory, speed, or acceleration). First, we propose semiautomatic navigation to smoothen the navigation trajectory during navigation. Second, knowing the importance of navigation speed profile, we design a speed protector to minimize the total jerk when the user navigates in virtual environments while ensuring low cognitive workload. Moreover, we develop adaptive navigation based on user susceptibility to cybersickness computed from the fuzzy logic model presented in chapter 4, and also design an adaptive online strategy to adapt the navigation speed based on the PID control theory.

In chapter 6, we briefly summarize the thesis and derive several open perspectives related to our work for further research.

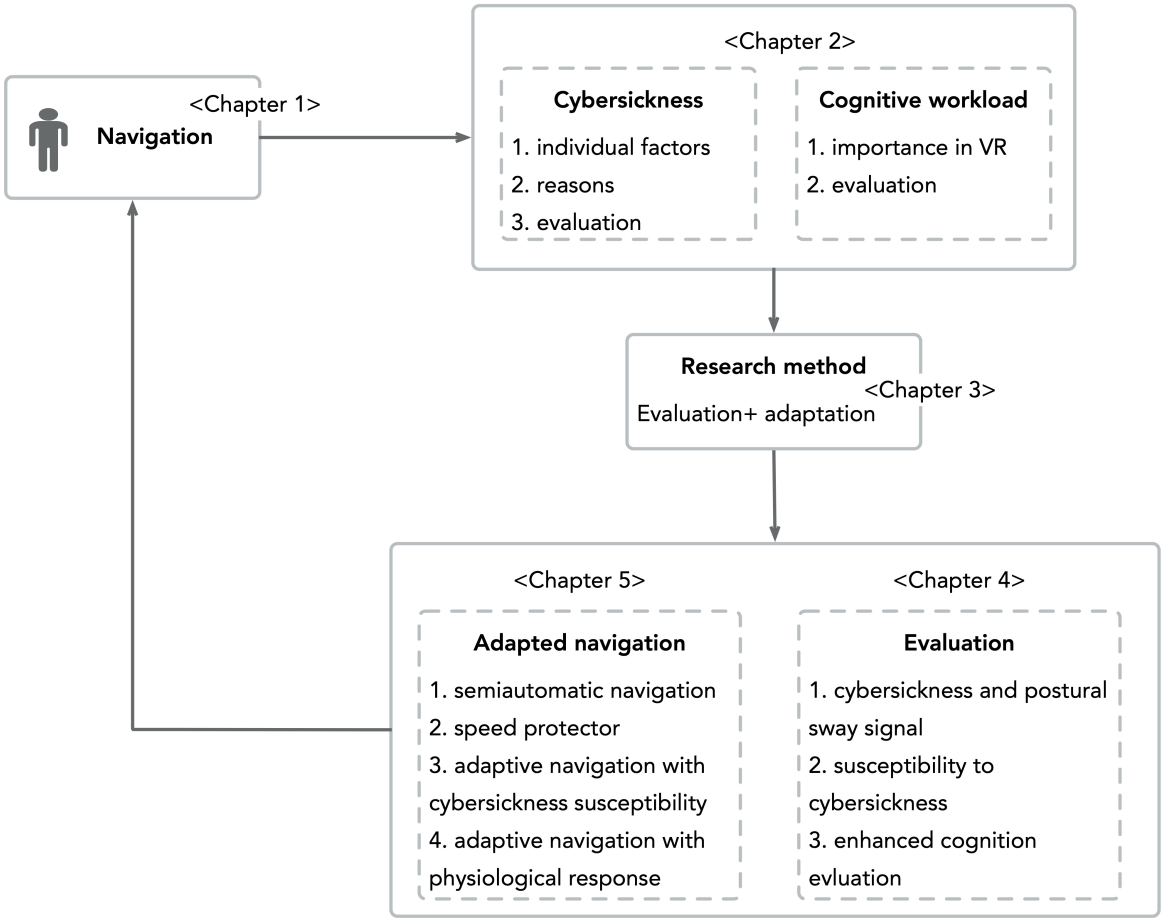

Figure 1.1: Overview of the thesis structure.

Chapter 2

Literature review

Contents

As immersive virtual reality (VR) systems have become available to public consumers, such technology reshapes the way how users interact with virtual environments (VEs). The easy access to these devices enables researchers and engineers to develop various VR applications for medical training (Javaid and Haleem 2019), education (Radianti *et al.* 2020) or patient rehabilitation (Negrillo-Cárdenas *et al.* 2020). VR also represents an excellent opportunity for companies to reorganize themselves and adapt their processes to new conditions imposed especially by the COVID-19 pandemic (Gibbons 2020). For example, G.-Z. Yang *et al.* (2020) reported that during the global pandemic, high-fidelity and low-latency VR technologies helped many conferences successfully going online, featuring participants' virtual avatars fully mobile and immersed in virtual conference environments, which contributed to preventing the virus from spreading.

The characteristic of VR is to enable a user to be immersed in a virtual environment (VE) and to interact with it (Sherman and Craig 2003), which means back and forth actions between the user and the VE. Currently, VR research focuses on many subfields related to human-computer interaction (HCI), e.g., displaying devices with more immersion, interaction with multisensory feedback, human factors. Merienne (2016) claimed that the perceiver is at the center of a VR application, and awareness of the technologies and human factors are essential to promote the efficiency of the application. Engineers try to produce environments that are immersive as much as possible based on new technologies (Lavalle *et al.* 2014; Bolton *et al.* 2014), while academic researchers tend to design and verify new types of user interfaces and interaction techniques in an immersive virtual environment (Aslandere *et al.* 2015; Jankowski and Hachet 2015). With the fast development of technologies coming from video games, new types of devices are frequently released, continually upgrading user interfaces and interaction techniques. We believe that VR should provide a more user-oriented and customized experience by involving human factors, rather than technological aspects.

In this chapter, we will focus on navigation, as a key task in virtual environments.

2.1 Navigation

2.1.1 Human walking

In physical environments, navigation tends to be a "no-brainer" task: once individuals formulate the target, body muscles work collaboratively to perform the movements (LaViola Jr *et al.* 2017).

It has been shown in neuroscience that humans carry out navigation tasks in a stereotyped manner at both geometric and kinematic levels (Hicheur *et al.* 2007). Given the background, the stereotype indicates that, among infinite possible trajectories to connect position A to position B (both are oriented points), all pedestrians would follow similar paths while walking from A to B. It is necessary to introduce virtual navigation conditions that can preserve such steering from physical walking, which will generate natural trajectories that conform to real ones as much as possible.

Many previous studies indicate that the trajectories of hands and whole-body movements share prevalent strategies. For example, Papaxanthis *et al.* (2003) found that kinematic analogies are shared between vertical whole-body and arm navigations in the sagittal plane, which implies that the central nervous system (CNS) uses common control mechanisms to perform arm and whole-body movements. Also, C. M. Harris and Wolpert (1998) presented a unifying theory showing that humans follow highly stereotyped trajectories where the motion profiles of both eyes as well as hands are smooth and symmetric during saccadic eye movements and goal-directed hand movements; the trajectory is generated from the CNS in a way to minimize a cost which is integrated along the movements, e.g., jerk (Hogan 1984; Flash and Hogan 1985) or torque (Uno *et al.* 1989), and also to minimize the variance of the final position of the eyes and hands.

2.1.2 Virtual navigation

Navigation is a fundamental task for a large number of domains using virtual reality (VR) applications. Before carrying out this primary task, users have to adapt their viewpoint in order to explore unknown virtual environments (VEs) (Kulik 2009). Humans can perform navigation in physical environments through multisensory feedbacks from visual, proprioceptive and vestibular systems, while in VR the only way to keep identical and consistent sensory feedbacks during virtual walking is to enable users to walk for real and map it to virtual environments. However, due to the limits of VR devices, VR displays and small available workspace of large immersive displays, users have to be constrained into a limited physical space, which means that it is impossible to directly map real walking to virtual walking, leading to unnatural sensory feedback. This issue has drawn much attention with many metaphors and apparatuses developed, e.g., the CyberWalk omnidirectional treadmill system that enables users to walk endlessly in any direction without leaving the confines of the limited physical space (Souman *et al.* 2008), or redirected walking techniques allowing real walking within

constrained physical spaces by subtly manipulating users' viewpoint (Razzaque 2005).

Natural navigation interfaces are favored as they intend to minimize the mismatch between proprioceptive information related to actions and sensory feedback arising from the VR system (Marsh *et al.* 2012). A natural navigation technique should consider providing with the best experience to its users. In product design, user experience is defined as "a person's perceptions and responses that result from the use of anticipated use of a product, system or service" (*Ergonomics of human system interaction-Part 210: Human-centred design for interactive systems* 2019). It does not concentrate merely on the user's responses during interaction (e.g., subjective measurements and action preferences) with a product but rather on the reactions (e.g., physiological reactions) that appear during interaction. Since these responses and reactions are influenced by diverse factors such as user's expectations, beliefs, preferences, perceptions, feelings and emotions, and attainments, designers are prompted to decide the importance of difference factors based on the type of product and planned application (Rebelo *et al.* 2012). As for virtual reality, many past works (Stanney *et al.* 1998; Takatalo *et al.* 2011; Sheik-Nainar *et al.* 2015; Shaw *et al.* 2018) have investigated cybersickness and cognitive workload during dual-task or multi-task virtual navigation in 3D VEs. Therefore, despite the different explanations of user experience provided in different domains (Rebelo *et al.* 2012; *Ergonomics of human system interaction-Part 210: Human-centred design for interactive systems* 2019), from now on, we will refer user experience to both VR sickness and cognitive workload because they are explicitly associated with navigation.

Various approaches for navigation have been proposed in past research, different from developing navigation interfaces or metaphors. Igarashi *et al.* (1998) implemented a path drawing technique for navigation in immersive 3D environments. This approach requires users to draw the trajectory as a predefined path with a free stroke, and in the meantime the path is projected onto the walkable surface to generate the final moving path. Then the viewpoint is moved automatically along the tangential direction of the path with an appropriate speed. A user study showed that path drawing is a preferred and more intuitive navigation method compared to other navigation approaches such as flying and driving. In this case, as users do not have to focus on maneuvers and path finding, they are more likely to perform other tasks easily during navigation (Renner *et al.* 2010), for example, perceive and recognize densely-occluded models (Elmqvist and Tsigas 2007).

Instead of drawing a path, automatic path planners from the humanoid robotics field focusing on

the evolution of humanoids in real environments also proved to be an efficient method (Mohanan and Salgoankar 2018). Yao *et al.* (2010) introduced the application of path planing to travel in VEs and they managed to control a virtual human motion with an improved A* algorithm, thereby allowing the system to plan automatically an optimal path from the starting point to the target point with the intention of committing a specific task such as *search* or *maneuvering*. Thanks to boosted computational performance with GPUs, the algorithm can also be extended to real-time applications used for multi-agent travel in VEs (Sud *et al.* 2008). A practical application is navigation in very constrained environments such as radioactive environments in order to protect users from being harmed under high radiation. Y. Liu *et al.* (2015) applied path-planning algorithms into a virtual-real mixed simulation program to provide a minimum dose navigational approach. In addition, further research on the application of *Dijsktra's algorithm* and *RRT* algorithm* (two other path-planning algorithms) were implemented, and the results were compared so as to verify the effectiveness and feasibility of path-planning algorithms in VEs (Chao *et al.* 2017). This work was developed with path-planning algorithms to make task optimization and evaluation intuitive, effective and secure, but they were not designed as a travel interface for first-person applications to address cybersickness.

Argelaguet and Andujar (2010) started considering speed adaptation on a predefined path and claimed that the path gives a sequence of viewpoints from part of the scene that will be shown to the user, while the speed is another paramount parameter which further determines when and how long the user can experience immersive environments; accordingly, the authors suggested to combine both components: the camera path and the corresponding speed profile. In addition, Argelaguet (2014) proposed an approach to adapt speed based on updating the current acceleration of the viewpoint to make sure that the optimal perceived speed is reached without abrupt speed changes, and with this rule, speed can be adjusted in accordance with the spatial relationship between the user, the environment as well as the optical flow. One significant contribution of these works is a decrease of jerkiness of the navigation profile which establishes smoother camera motions, making motion profiles closer to real navigation trajectories (Cirio *et al.* 2013).

Some works on goal-directed navigation models exist based on the minimization of a cost function in order to generate optimized motion profiles along a trajectory. In the context of hand trajectory generation (Richardson and Flash 2002), Pham *et al.* (2007) simulated and compared numerically the results for human walking trajectories with four different physical parameters, including velocity,

acceleration, jerk and snap, by setting initial and final conditions for velocity and acceleration, as well as the global trajectory duration; qualitative and quantitative analyses suggest that the minimum jerk and the minimum snap models can provide predictions significantly to match actual trajectories at the geometric and kinematic levels. Mombaur *et al.* (2008) found that trajectories are not always nonholonomic, and it is possible to join holonomic and nonholonomic constraints to formulate an optimal control problem with a cost function to minimize. The main defect of these methods is that they have to generate the motion profile before navigation and require the whole profile duration in advance, while such requirement is computationally demanding which excludes their application in dynamic environments where solvers have to find the optimal motion profile in real time.

2.2 Cybersickness

Navigation in virtual environments generally leads to cybersickness which poses a severe threat to the usability of VR applications. There exists a significant correlation between VR sickness discomfort levels and user comfort (Somrak *et al.* 2019). Currently, many navigation interfaces have been developed with the intention of enhancing user comfort but cybersickness is still an inherent problem to be overcome. In this section, we will summarize the individual susceptibility to cybersickness and different hypotheses to explain cybersickness, with which we can propose our solutions to mitigate it in the next chapters.

2.2.1 Effect of individual factors on cybersickness

Around 80 % to 95 % of VR users experience sickness symptoms when exposed to virtual environments (VEs), with from 5 % to 30 % of which have to quit the immersed exposure (Arns and Cerney 2005). For new users of the VR technology, around 60 % suffer these adverse symptoms and the substance of symptoms usually varies from one to another among individuals (Lawson *et al.* 2002). Therefore, this section aims to examine individual characteristics that could affect cybersickness during navigation in immersive 3D environments. Although lots of work have been carried out to reduce cybersickness based on technology-related factors (e.g., field of view, platform, resolution, frame rate, scene content, and time lag), very little attention is paid to the human-related factors systematically. These human-related characteristics should be clear to determine and explain the major reason for cybersickness among individuals. Consequently, we will discuss the effect of individual differences (e.g.,

gender, age, posture, gaming experience, ethnic influence, etc.) on cybersickness occurrence and severity. These factors are studied because they are human-related and individually independent, explaining why some participants experience severe sickness but nothing for other groups.

2.2.1.1 Age

Age can influence the proneness to cybersickness, despite debates on the evolution of the proneness over age. Figure 2.1 represents the evolution of the severity of sickness against increasing age, based on past studies conducted by L. Harm (1990a) and Kolasinski (1995). According to their results, the peak of severity is observed around 12 years old, with a quick decrease until 21, then a gradual drop thereafter, meaning that elderly people suffer less from sickness (Davis *et al.* 2014), or even very little around 50 (Kolasinski 1995). Similarly, children under 2 years old seem not to suffer from sickness, as they are often jostled during this period (Biocca 1992). To compare age-related differences in driving performance on a driving simulator, L. Liu, Miyazaki, *et al.* (1999) grouped the participants into eight categories (less than 16, 16-25, 26-35, 36-45, 46-55, 56-65, 66-75, and 76 and older) and demonstrated that the elderly participants (despite being unfamiliar with computers) are less susceptible to nausea compared to other groups.

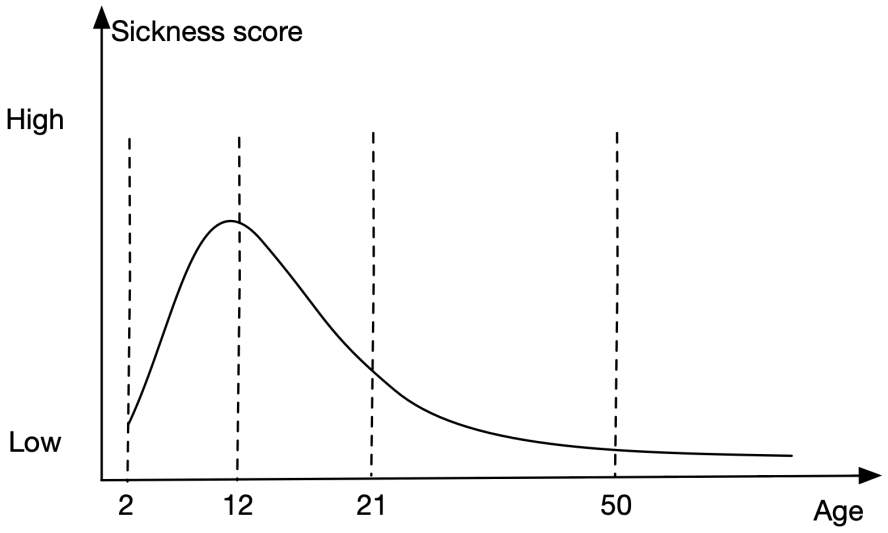

Figure 2.1: Trend of susceptibility to sickness against increasing age (inferred from (L. Harm 1990a) and (Kolasinski 1995)).

S.-N. Yang *et al.* (2012) exposed 203 teens and adults (44% female) to a movie in 2D and stereoscopic 3D. They found that the older group experienced higher dizziness and nausea in the presence

of 2D stimuli, whereas younger participants reported greater blurred and double vision, dizziness, and nausea symptoms in 3D viewing, which indicated that older adults are less sensitive to greater vergence demand, which was the latent source of blurred and double vision. To explain this observation, S.-N. Yang *et al.* (2012) argued that viewers older than 45 are mostly presbyopic, i.e., lacking the ability to accommodate differences in focusing retinal images and converging without causing any accommodative (focus) changes, so they frequently experience a mismatch or decoupled relationship between vergence and accommodation in daily life. Similarly, due to the lack of accommodation ability, the older group experienced greater cybersickness symptoms in 2D viewing because they had to preserve the same level of vergence or squinting responses. Meanwhile, younger viewers normally have strong accommodation ability to vergence processes, which is more likely to induce side effects during 3D viewing.

The effect of age can be explained in different ways. First, Reason and Brand (1975) stated that the senses of children are not fully formulated and they are still highly flexible and adaptable. Second, the ageing of the vestibular system for the older people could result in low cybersickness among older individuals (Paillard *et al.* 2013), which is especially the case for those more than 60 years old with a loss of vestibular nerve fibers (Bergström 1973) and the ageing of vestibular ganglion cells (Richter 1980). Several theories, such as the poisoning theory (Treisman 1977) and negative reinforcement (Bowins 2010) presented in subsection 2.2.2, provide explanation for the effect of age from their perspective.

However, there are also opposite findings. Using similar but slightly different age group method, Arns and Cerney (2005) splitted the participants into eight categories: 9-11, 12-14, 15-17, 18-20, 21-23, 24-26, 27-29, 30-39, 40-49, and 50-60, enabling to examine more closely the cybersickness score for those aged from 9 to 29, and find the sickness trend for adults aged 30 years and older: the majority of the elderly subjects are prone to simulator sickness than younger groups, and in terms of comparison with the total severity score, sickness symptoms are not negligible for older subjects, demonstrated in Figure 2.2.

2.2.1.2 Gaming experience

As more and more people play video games, past studies have observed a potential effect of gaming experience on the proneness to cybersickness. Indeed, since gamers regularly achieve fast and accu-

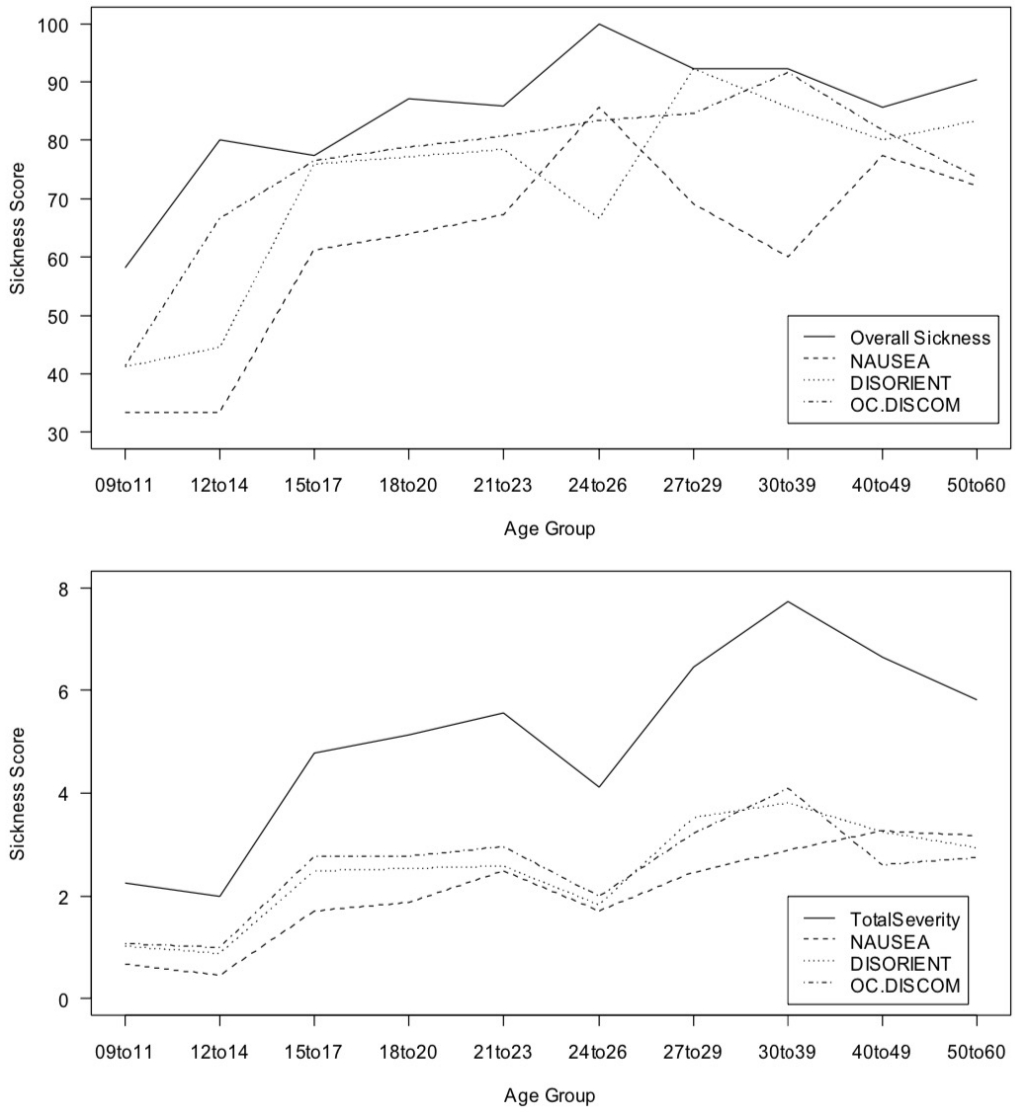

Figure 2.2: Sickness reports as a function of age group: (Top) Percentage of subjects reported sickness in each group, (Bottom): Mean sickness of each group; figure taken from Arns and Cerney (2005).

rate movements in virtual environments, they are able to develop strong abilities in terms of spatial awareness and navigation skills, which gives them an advantage over non-gamers in terms of severity of cybersickness (S. P. Smith and Du'Mont 2009). People with less computer proficiency or gaming experience can then be significantly more prone to cybersickness when exposed to stereoscopic stimuli, compared to people with prior gaming experience (Häkkinen *et al.* 2006). One reason given is that people with little computer or game experience are likely to have a neutral or even negative attitude towards immersive technologies, leading them to get more stressed and pay excessive attention to their

feelings rather than to the immersive environment itself.

We mentioned above that proneness to cybersickness can be maximal in young people. However, since more and more of them gain strong gaming experience, this proneness tends to fade away (Knight and Arns 2006), showing that habituation to immersive environments plays a role in reducing the occurrence of cybersickness, as found from correlation tests with the frequency of playing games (Iskenderova *et al.* 2017) or from physiological measurements (Dennison *et al.* 2016).

However, there are some literature presenting little relationship between gaming experience and cybersickness. Gamito, Oliveira, Morais, *et al.* (2010) designed a first person shooter game and asked 16 participants (without any gaming experience) to play the game; through training on different procedures, participants gained different gaming experience; however, no significant differences were found on the effect of gaming experience. Gamito, Oliveira, Santos, *et al.* (2008) examined cybersickness in a virtual test examination scenario in which the participants have to mark the right answer to each question; and no significant differences were observed regarding gaming experience.

2.2.1.3 Ethnic origin and genetic influences

Ethnicity is a characteristic that has been very little studied regarding its effect on the proneness to cybersickness. One work studied differences in sickness between Caucasian and Asian people by exposing them to nausea-inducing body rotation on a rotational chair along the yaw axis (Klosterhalfen *et al.* 2005). A motion sickness susceptibility questionnaire (MSSQ) was filled by the participants and the total rotation tolerance time (RT) was captured to measure the severity of sickness. The experiment showed that Caucasian participants seemed less affected than Asian participants, as their average RT was higher and the MSSQ score was lower than for Asian subjects, which is consistent with a former study in which Asian, European-American and African-American groups were exposed to a rotating optokinetic drum (R. Stern *et al.* 1993). Such observations may originate from a difference in the threshold for and/or sensitivity of the response against one or more of the physiological stimuli including stress hormones, osmolality, or blood pressure, that control the release of vasopressin and, consequently, affects gastric activity (R. M. Stern *et al.* 1996).

The susceptibility to sickness also shows hereditary features, according to some questionnaire surveys. Yanus and Malmstrom (1994) carried out two surveys. The first survey administered to 77 male graduate student indicates strong correlation between sons and their biological fathers regarding

the severity of sickness symptoms. The second survey from 95 male and female members of Air Force Reserve unit ageing 18 to 56 further reveals that the proportion of self-reported symptoms, including headache and fatigue, strongly correlates with that of both father and mother. Knox (2014) also found genetic effects from public technology reports: (1) if both parents are susceptible to cybersickness, their children are five times more likely to suffer from similar symptoms than other children; (2) another research on the 41% of British parents with driving experience also have a children susceptible to sickness. On the other hand, for monozygotic compared to dizygotic twins, evidence found through questionnaires reports a high concordance rate to motion sickness susceptibility (Abe *et al.* 1984; Reavley *et al.* 2006; Sharma *et al.* 2008), at around 2.5 times more (Bakwin 1971).

Genetic influences are proposed to explain the effect of ethnicity as a gene may co-control personal responsiveness to visual stimuli (R. M. Stern *et al.* 1996). For example, the serotonin-transporter gene (SERT) determining serotonin reuptake and other polymorphisms of the serotonergic system is linked to the severity of nausea and vomiting (Klosterhalfen *et al.* 2005). Additionally, Finley Jr *et al.* (2004) indicated that the susceptibility to cybersickness is associated with the genome of the alpha-2 adrenergic receptor, which can be 6.7Kb or 6.3Kb in size on Chromosome 10 for each subject. Those with a 6.7Kb gene size have a greatly higher tolerance to visually induced motion sickness. Based on the work from R. M. Stern *et al.* (1996) and Finley Jr *et al.* (2004), L. Liu, Yuan, *et al.* (2002) found: the frequency of alpha-2 adrenergic receptor "gg" phenotype ("gg" equals the 6.3Kb gene) in Chinese and Japanese is 5.8 and 7.8 respectively times than that in Englishmen, and the "gg" phenotype in those susceptible to cybersickness is 1.6 times higher than that of individuals with higher tolerance to cybersickness.

Knox (2014) argued that the sickness symptoms have a genetic basis arising from a long-term evolutionary adaptation process to avoid harmful risks or dangerous situations. However, it is worth mentioning that the effect of ethnicity on visually induced motion sickness so far remains inconclusive. Nevertheless, Klosterhalfen *et al.* (2005) advocated that attributing sickness symptoms to other forms of sensory hypersensitivity (e.g., chemical, olfactory, and gustatory stimuli) as descripted for hyperemesis gravidarum, or to genetic traits in functional bowel disorders would help accelerate the analysis for the genetic effect.

2.2.1.4 Gender

It has been widely found that females are more susceptible than males in terms of all kinds of motion sickness (Reason and Brand 1975; Jaeger and Mourant 2001; Holmes and Griffin 2001; Hakkinen *et al.* 2002; S.-N. Yang *et al.* 2012; Flanagan *et al.* 2005; Häkkinen *et al.* 2006; G. D. Park *et al.* 2006). However, finding that women do not differ in their sensory response to motion stumuli (Reason and Brand 1975), Biocca (1992) criticized such statement by arguing that the conclusion is derived from the self-reports of symptoms and males are likely to underreport their susceptibility. Dobie *et al.* (2001) also found greater cybersickness among females than among males in terms of equivalent exposure history, and the sex difference is stable across school age from 9 to 18 years, but the author did not find evidence that men are more restrained to report sickness. Still, the effect of gender has been occasionally linked to inconsistent symptom awarenesses and the willingness to recognize such symptoms under socially controlled psychology (Ladwig *et al.* 2000). Recalling a positive correlation between trait-anxiety and cybersickness (Collins and Lentz 1977), Paillard *et al.* (2013) performed an experiment to validate whether the gender effect is due to the trait-anxiety since women tend to report both higher trait-anxiety (Robin *et al.* 1987) and sickness susceptibility than men do (Reason and Brand 1975; Jaeger and Mourant 2001; Flanagan *et al.* 2005); despite the consistent result with the literature that women report greater trait-anxiety, the authors admit that cybersickness still exists after accounting for the anxiety effect.

Weech *et al.* (2019) found that users experiencing high presence tend to experience low level of cybersickness. Due to the individual sensitivity to sensory conflicts (Reason and Brand 1975; Rebenitsch and C. Owen 2016a), higher sensitivity will lead to high level of cybersickness and low presence, whereas low sensitivity to cue conflicts will result in low level of cybersickness and increased sense of presence. Melo *et al.* (2018) compared the score of both cybersickness and presence inside the real-world scene and computer-generated scene, and in the real-world scene, no differences were found for self-reported cybersickness and presence. However, in synthesized contents, female participants reported higher scores for presence, implying that they are more susceptible to the virtual environment. Recall that cybersickness is negatively associated with presence; it suggests that females are more prone to cybersickness because they experience more presence (Witmer and Singer 1998). Therefore, Viaud-Delmon *et al.* (1998) explained that men might have the superior ability to adapt themselves to sensory conflicts than women do.

In addition, the relationship between hormonal levels and susceptibility to cybersickness is also proposed for explaining the gender difference. For example, Schwab (1954) found that women tend to get severe cybersickness during menstruation, and Reason and Brand (1975) further added anecdotal evidence of increased cybersickness during pregnancy. Golding *et al.* (2005) found that cybersickness level could fluctuate during the menstrual cycle, and demonstrated that, except for those of 50-60 years old, the hormonal status cannot completely disclose the easily induced sickness of women; the authors suggest that the overall gender differences among all ages may be due to a "hard-wired" greater emetic and nausea susceptibility in females. Matchock *et al.* (2008) further investigated the effect if the susceptibility to cybersickness is attributed to the phase of the menstrual cycle: with 90 young females (42 users of oral contraceptives) exposed to a rotating optokinetic drum, the authors found that females without using oral contraceptives report more severe nausea and sickness symptoms during the peri-menses compared to that during the peri-ovulatory phase. In contrast, females using oral contraceptives report the same level of nausea and sickness symptoms. These findings suggest that fluctuating estrogen levels during the menstrual phases might influence the susceptibility to cybersickness.

The gender effect is also possible due to the fact that women have a wider field of view than men, which in turn increases the level of cybersickness (Kennedy and L. H. Frank 1985; LaViola Jr 2000). Dodgson (2004) examined the human inter-pupillary distance and reported that the average inter-pupillary distance for females is around 0.96 that of males. Read and Bohr (2014) believed the difference in inter-pupillary distance would affect the experience during 3D visual stimuli because disparities (i.e., differences in object position on the two retinal images) are restrained by the camera parameters which on average would be marginally larger for women in terms of the natural disparities, thereby leading to high proneness to cybersickness for female viewers.

Past studies also report null correlation across genders. On an investigation performed by Knight and Arns (2006), there is no difference across genders during an increasing self-reported susceptibility. Gamito, Oliveira, Santos, *et al.* (2008) designed a virtual exam to ask the students to answer each questions in the VE, and the statistical analysis shows no difference between men and women in terms of cybersickness on the measurement of simulator sickness questionnaire (SSQ, Kennedy, Lane, *et al.* (1993)). With user tests in three different virtual environments (i.e., non-stereoscopic neutral world, non-stereoscopic public speaking, stereoscopic public speaking world), Ling *et al.* (2013) did not find

any difference between genders in terms of SSQ.

2.2.1.5 Postural stability

Postural stability is generally measured and compared between pre-exposure and post-exposure to the virtual environment. According to the analysis between the pre/post-simulator postural stability and post-simulator sickness questionnaire (SSQ) performed on Navy helicopter pilots (Kolasinski 1995), pre-simulator postural stability is strongly associated with the *Nausea* and *Disorientation* subscale scores of the SSQ. In contrast, post-simulator postural stability does not correlate with the subscale score of *Oculomotor* (Kolasinski 1995). Riccio and Stoffregen (1991) believed that prolonged postural instability is the reason for sickness symptoms (i.e., postural instability appears prior to cybersickness). The authors further observed that animals get motion sick after they fail to maintain postural stability. Therefore, those with poor postural control may be more prone to cybersickness (N. Owen *et al.* 1998). With the subjects exposed to the optical flow in either sinusoidal (0.2Hz) or complex sum-of-sines stimulus, Stoffregen and Smart (1998) found that "Sick" and "Well" participants differed regarding their postural sway, which appears before the onset of cybersickness symptoms; such difference in postural sway implies that there is a corresponding susceptibility to cybersickness among individuals.

N. Owen *et al.* (1998) argued that the relationship between sickness and postural instability exists because of anxiety. The anxiety and fear of falling can deteriorate postural stability (B. E. Maki *et al.* 1991; B. Maki and Mcllroy 1996), and they are associated with bodily symptoms such as dizziness, excessive sweating or breathing difficulties. Therefore, anxious individuals could be under unbalanced body conditions and more likely to experience and report severe sickness symptoms, leading to a biased correlation between postural control and sickness susceptibility.

2.2.1.6 Visual acuity

It is reported that around 12% of the population suffers from different types of binocular vision, leading to partial or complete trouble in stereoscopic vision and binocular depth perception (Hale and Stanney 2006). Due to the retinal disparity projected to the two eyes, individuals may have struggled with extra stress and/or stronger oculomotor disturbances (Rinalducci 1996), compared with those in normal sighted viewers. Cybersickness and visual acuity likely have some correlation because both can

act on the oculomotor systems, which is why we include visual acuity as an individual factor to influence cybersickness. Much to our surprise, very limited evidence can support this hypothesis; we only find from the work of Webb and Griffin (2002) that subjects with poorer visual acuity generally report higher cybersickness, and the authors propose to perform further investigation on the mechanism.

In contrast, with 23 participants immersed in a VE maze for up to one hour to perform several stationary and movement-based tasks, Hale and Stanney (2006) stated that there are no significant differences observed between normal vision and low stereo acuity individuals evaluated in the experiment for cybersickness, and both groups report similar increase of SSQ scores and oculomotor disturbances after exposed to visual stimuli. Read and Bohr (2014) and Allen *et al.* (2016) reported that the proneness to cybersickness has no association with low stereo acuity and with pre-existing eye conditions when viewers are exposed to 3D virtual environments. An earlier study shows the effect of visual acuity in an extreme condition by including blind participants. Graybiel (1970) compared blind with normally sighted individuals, and it is reported that vision is not an essential but rather a less important etiologic factor during the occurrence of cybersickness.

2.2.1.7 Illness

Illness is also associated with user's susceptibility to cybersickness; therefore, users with physical problems such as illness, fatigue, sleep loss, hangover, upset stomach, periods of emotional stress, head colds, flue, ear infection, or upper respiratory illness are recommended to avoid using VR applications (LaViola Jr 2000).

Table 2.1 presents a summary of the relationship between individual characteristics and cybersickness.

2.2.2 Cybersickness: why?

The community has long been seeking theories to explain "why" and "how" cybersickness can occur. However, no unified theory can explain everything, so these theories are developed by refinement of each other for application in different situations. For instance, the sensory conflict, postural instability and eye movement theories are regarded as "how" theories, while the evolutionary theory is considered as "why" theory (Brooks *et al.* 2010). We summarize seven different theories in this section. When it

Table 2.1: Summary of how individual factors influence cybersickness

Individual factors	**Relation with cybersickness**	**References**
Age	1. Cybersickness severity increases until 12, and decreases afterwards Opposite finding: 2. The elderly are more prone to cybersickness than the young	L. Harm (1990a), Kolasinski (1995), Davis *et al.* (2014), Opposite finding: Arns and Cerney (2005)
Gaming experience	More gaming experience, less cybersickness	S. P. Smith and Du'Mont (2009), Häkkinen *et al.* (2006), Knight and Arns (2006), Iskenderova *et al.* (2017), Gamito, Oliveira, Morais, *et al.* (2010)
Ethnic origin and genetic influences	1. Caucasian group has longer rotation tolerance time than that of Asian subjects 2. Cybersickness shows hereditary features, depending on if parents are susceptible to cybersickness 3. Cybersickness is associated with the frequency of alpha-2 adrenergic receptor "gg" phenotype.	Klosterhalfen *et al.* (2005), R. Stern *et al.* (1993), Yanus and Malmstrom (1994), Knox (2014), Abe *et al.* (1984), Reavley *et al.* (2006), Sharma *et al.* (2008), Bakwin (1971), L. Liu, Yuan, *et al.* (2002)
Gender	Females are more susceptible than male in terms of all kinds of cybersickness	Reason and Brand (1975), Jaeger and Mourant (2001), Holmes and Griffin (2001), Hakkinen *et al.* (2002), S.-N. Yang *et al.* (2012), Flanagan *et al.* (2005), Häkkinen *et al.* (2006), G. D. Park *et al.* (2006)
Postural stability	1. Pre-simulator postural stability is strongly associated with nausea and disorientation. 2. Poor postural control is linked to cybersickness	Kolasinski (1995), Riccio and Stoffregen (1991), N. Owen *et al.* (1998), Stoffregen and Smart (1998), N. Owen *et al.* (1998)
Visual acuity	1. Subjects with poor visual acuity generally report higher cybersickness Opposite findings: 2. No significant relation between visual acuity and cybersickness	Rinalducci (1996), Hale and Stanney (2006) Opposite findings: Hale and Stanney (2006), Read and Bohr (2014), Allen *et al.* (2016)
Illness	Illness can increase the risk of severe cybersickness	LaViola Jr (2000)

comes to a specific theory, we firstly explain what it is and follow some strongly associated evidence and examples to demonstrate the effectiveness.

2.2.2.1 Sensory conflict theory

The sensory conflict theory proposed by Reason and Brand (1975) is seemingly the most commonly discussed when it comes to the explanation for cybersickness. Reason and Brand (1975) suggested that the conflict information arising from different sensory organs results in cybersickness. The conflict between visual motion from optic nerve and the actual motion in physical world, and conflict between the vestibular structures for the detecting the moving orientation and acceleration are considered to be two main contributors to cybersickness (Reason and Brand 1975; Brooks *et al.* 2010). Next, Reason (1978) formulated a neural mismatch model, revealing that the actual sensory information has to be in conflict with one's own past experience, and sickness symptoms appear when the sensory information remains contradictory constantly to one's expectation.

Oman (1982) provided a mathematical basis to the sensory conflict theory. In brief, the model claims that the muscle activity (m) arising from the desired position $\mathbf{x_d}$ results in a position $\mathbf{x}$ with the body dynamics (B). This signal, along with the external nose n_e, is noticed by the the senses (S), leading to the sensory information $\mathbf{a}$. Oman (1982) speculated that an internal model including the same architecture computes the expected sensory information $\hat{\mathbf{a}}$, and in addition, the difference $\hat{\mathbf{c}}$ between $\mathbf{a}$ and $\hat{\mathbf{a}}$ is computed and fed back into the system with a weight coefficient K_c, thereby achieving an estimate of the actual position. The difference vector $\mathbf{c}$ is associated with the severity of sickness.

In many cases, the instance of sensory conflict among systems are logically straightforward and recognizable. There are several kinds of conflict that can cause cybersickness, between/among sensory modalities (i.e., visual-vestibular), within a sensory system (i.e., otolith-canal, or ambient-focal) or between expected and experienced patterns of visual stimuli (Stoffregen and Riccio 1991). As one simple example, immersed in a moving 3D virtual environment, the subject receives visual cues as self-motion while the vestibular system will report no self-motion as the person is still in a stationary position. It is worth noting that the source of sensory conflict can also be sub-parts of the same body system (e.g., the visual system), not just a conflict between/among systems (Allen *et al.* 2016). One example is the mismatch that appears between naturally correlated motor and retinal cues to motion-

in-depth in 3D virtual environments. In the physical word, accommodation cues and disparity cues generally offer congruent information. When an object moves to a person in the real world, the retinal image becomes defocused and the disparity of the signal received by the two eyes adapts accordingly. However, in 3D immersive viewing, these two depth cues are mostly in conflict. In head-mounted devices, the disparity cues in 3D stereoscopic environment imply that an object is coming, but due to the fact that the focus of the retinal image relies on the distance between the eye and the VR display, which remains constant, these cues fail to show variation in depth. Allen *et al.* (2016) also reported that many other visual cues (i.e., those linked to vergence angle or velocity-based cues to depth where cues are found that an object moving in depth moves in diverse directions between eyes) can be in conflict with one another and with other retinal and motor cues. For instance, Hoffman *et al.* (2008) found that motor conflicts arising from inconsistent accommodation and vergence changes can lead to cybersickness symptoms such as fatigue, especially during rapid velocities (Lambooij *et al.* 2009), despite the fact the sickness severity relies on the distance and sign of the disparity (Shibata *et al.* 2011).

The sensory conflict theory implies that individual differences in sensory system sensitivity is linked to the severity of cybersickness; in other words, those individuals with greater sensitivity are likely to detect the conflict cues much more easily. Allen *et al.* (2016) validated this hypothesis by inviting 73 participants to complete a series of tasks within 3D virtual environments, and the authors measured individually the sensitivity to visual depth cues and a number of other basic visual functions. As predicted by the sensory conflict theory, participants who have better sensitivity to dynamic visual cues to depth can take the most benefit of 3D technology, but unfortunately, are also those who have the least tolerance due to strong proneness to cybersickness. Read and Bohr (2014) also argued that side effects of 3D immersion are arising from the cue conflicts between the depth information from binocular disparity and other cues from accommodation, motion parallax and vestibular input; hence, individuals' differences in sensitivity to stereo 3D stimuli imply their tolerance for cue conflict. Those with binocular eye disorders like strabismus tend to experience incorrect disparities during everyday life, but their visual systems have established mechanism to compensate for this. In this case, more tolerance to conflict information is provided due to a less reliable visual input, which demonstrates that individuals with visual problems are less likely to experience cybersickness.

Warwick-Evans, Symons, *et al.* (1998) exposed the participants to a film with two levels of con-

flict manipulated by changing the speed of visual stimulus, but there was no difference between the faster speed and normal speed of file presentation, indicating that the severity of cybersickness is not proportional to the magnitude of the sensory conflict. A lower visual stimulus speed might be useless to reduce cybersickness, and oppositely, Warwick-Evans and Beaumont (1995) found that a visual stimulus at a normal speed induces remarkably more cybersickness than a 20% higher speed.

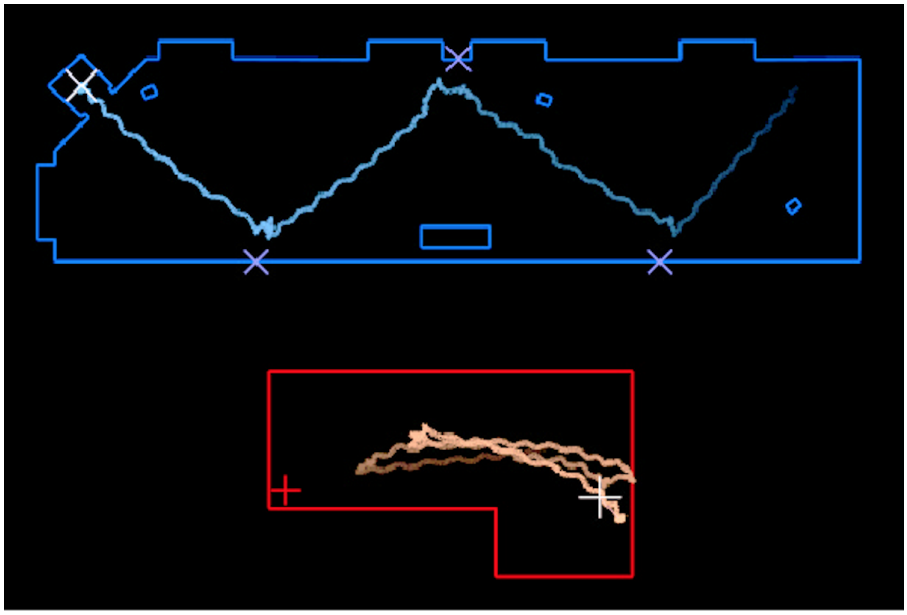

Figure 2.3: Overview of the trajectory taken by the user in the virtual environment (above in blue) and in the physical tracker area (below in red), figure from Razzaque (2005).

Encouraged by the fact that a person put blindfold and instructed to walk along a straight line unwillingly walks in an arc or circled trajectory instead, Razzaque (2005) designed the *Redirected Walking* (RW) technique which allows users to really walk inside very large virtual environments despite the physical limitation of the tracker area. Depending on the user's real orientation and position in the tracker area, the RW technique rotates interactively the virtual scenario so that the user is redirected regularly to the endless boundary of the tracker area, shown in Figure 2.3. The rotation is an unaware or imperceptible experience as the implementation is under the human perceptual level for sensing the position and speed. Although the main goal of the RW technique is to enable users to navigate in large virtual environments within limited physical spaces, it can reduce cybersickness as a byproduct, providing a validation for the sensory conflict theory. Similar strategies to avoid the conflict information by reproducing more consistent sense can be found: for example, walking-in-

place (Templeman *et al.* 1999) and treadmill walking (Darken *et al.* 1997) can not only extend the limit of physical space, but allow users to experience physical motion simultaneously during visual stimuli (Cao *et al.* 2018; Ng *et al.* 2019).

2.2.2.2 Subjective vertical conflict theory

The subjective vertical conflict (SV-conflict) theory suggests that cybersickness depends on the internal representation of the external verticality where only one mismatch of interest appears between the subjective vertical and sensed vertical. The SV-conflict theory can be regarded as a refinement of the sensory conflict theory, based on the observation that individuals only suffer sickness while there is an abrupt change of gravity in respect of their head, Bles *et al.* (1998) presented the definition of the SV-conflict theory: "All situations which provoke motion sickness are characterized by a condition in which the sensed vertical as determined on the basis of integrated information from the eyes, the vestibular system and the non-vestibular proprioceptor is at variance with the subjective vertical as predicted on the basis of previous experience." Bles *et al.* (1998) support their work by arguing that the SV-conflict theory proposes only one provocative conflict in common instead of considering different kinds of conflicts which is the case for the sensory conflict theory, and they found that the SV-theory fits and explains the experimental data better than the sensory conflict theory does. The importance of subjective vertical is given in two aspects (Bles *et al.* 1998): first, the vertical is responsible for the organism to keep the upright body posture, and for example, researchers propose that the control of body orientation is associated with cybersickness; second, the cardiovascular system requires information to maintain enough cardiac output for each segment of body.

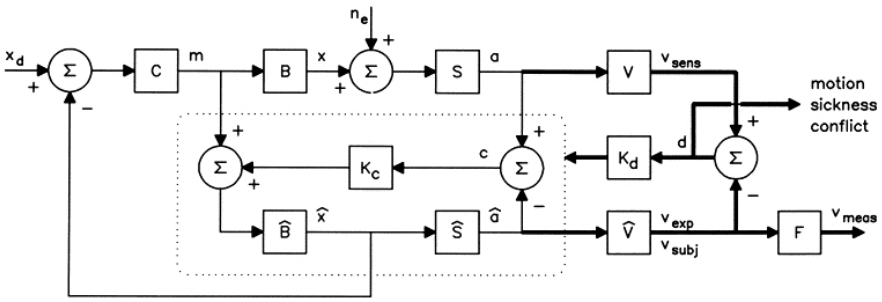

Figure 2.4: The subjective vertical conflict model, represented by thick lines, is an extension of the model of Oman (1982) for the computation of subjective vertical; the vector **d** is linked to cybersickness, figure from Bles *et al.* (1998).

The SV-conflict theory can be formulated mathematically as an extension of Oman (1982)'s model with extra modules to calculate the difference between the sensed and subjective vertical, shown in Figure 2.4. The SV-conflict model constructs the sensed vertical $\mathbf{v_{sense}}$ based on the sensory information with the network V, and also the expected vertical $\hat{\mathbf{v}}$ based on previous experience with another network $\hat{V}$. The difference vector $\mathbf{d}$ between $\mathbf{v_{sense}}$ and $\hat{\mathbf{v}}$ is applied to revise $\hat{\mathbf{v}}$, and the revised $\hat{\mathbf{v}}$ is hereinafter named the subjective vertical $\mathbf{v_{subj}}$. In opposition to the theory of Oman (1982), the SV-conflict model states that the vector $\mathbf{d}$ is responsible for cybersickness, instead of the vector $\mathbf{c}$.

However, the lack of specific data to prove the signal flow in the model presented in Figure 2.4 remains controversial (Bos, Bles, *et al.* 2008). An enhancement of the SV-conflict theory is the subjective vertical-horizontal (SVH) conflict model which takes the horizontal linear accelerations into account for predicting seasickness, which proves to be 20% better than the SV-conflict model (Khalid *et al.* 2011).

2.2.2.3 Postural instability theory

Stoffregen and Riccio (1991) argued that the sensory conflict theory cannot explain the existence of cybersickness from a theoretical point of view because regarding the discrepancies as conflict information instead of something else is just a hypothesis rather than a fact, and there are many cases that can lead to sensory conflict without inducing cybersickness. Besides, the lack of predictive validity of the sensory conflict theory limits the application of this theory to the design of virtual environments (Smart Jr *et al.* 2002). Riccio and Stoffregen (1991) believed that cybersickness results from prolonged instabilities, meaning that postural instability precedes the symptoms of cybersickness. Therefore, postural instability is a necessary condition to induce cybersickness. The authors found from data that a longer unstable posture is generally associated with higher likelihood and intensity of sickness symptoms, and the magnitude of postural instability is linked to the severity of cybersickness. However, with the postural instability theory, the authors admit that they do not know why the symptoms of cybersickness are what they are, and they are unable to account for the nature of symptoms.

The individual susceptibility to sickness depends on the personal ability to keep or reconfigure postural stability in a certain condition. For example, those who are more prone to cybersickness

would have difficulty in maintaining posture in provocative visual stimulus, which makes it possible to predict the susceptibility of individual before being been exposed to visual stimulus. Smart Jr *et al.* (2002) investigated whether postural motion collected with a tracking system can predict cybersickness; the authors observed that the postural instabilites appear prior to the onset of cybersickness and with a discriminant analysis, parameters of postural motion can predict cybersickness accurately. Chardonnet *et al.* (2017) successfully measured cybersickness via the analysis of postural sway signal in both time and frequency domains; they associated many features of postural signal with the self-reported SSQ score, indicating using postural information as an efficient indicator of cybersickness.

There are some evidence to validate the postural instability theory. With the objective of measuring cybersickness in console video games in an HMD, Merhi *et al.* (2007) asked participants to play one of two games on a standard Xbox platform for 50 minutes with either standing (7 participants) or sitting (17 participants) postural conditions for comparison, and the authors found that 90% of standing participants but only 59% of seated participants reported cybersickness, and further statistical analysis indicate that posture is a remarkable factor ($\chi^2(1) = 6.75, p < .05$) affecting self-reported level of cybersickness among users of console video games. This research works further on the effect of posture on cybersickness, so under a similar experiment condition, Stoffregen, Faugloire, *et al.* (2008) observed a significant difference in head and torso motion between sick and well participants before the onset of self-reported cybersickness, which conforms to the postural instability theory.

The difference between sitting and standing posture provides an opportunity to reduce cybersickness. Keshavarz, Novak, *et al.* (2017) invited 16 older to engage in a simulated driving task using a console video game while seated. Participants had to complete the experiments in two conditions: with or without passive restraint of the head and torso to the backrest and headrest of the seat. Measurement with the Fast Motion Sickness Scale and SSQ indicates that aged users prone to cybersickness in the unrestrained condition reported remarkably less severity of symptoms when they were passively restrained. However, Warwick-Evans, Symons, *et al.* (1998) observed a difference between lying and free-standing conditions regarding the onset time of cybersickness, but they found no significant difference in posture through an equal-time and equal-distance exposure to visual stimulus, and also no relationship between the severity of cybersickness and the magnitude of postural instability. Koslucher *et al.* (2016) observed that sex differences in postural sway is related to sex differences in the incidence of visually induced motion sickness, suggesting that the control of postural balance

could also explain the gender effect that females are more prone to cybersickness than males. Munafo *et al.* (2017) claimed no difference between men and women when the experiment is performed in seated condition, while cybersickness severity among women (77.8%) is remarkably larger than among men (33.33%). The authors further found correlation between the patterns of postural sway and sex differences: sex-related differences in pose control exist before the onset of cybersickness; females have smaller feet than males of comparable height, and with a purely physical sense, there is an increased likelihood that disturbing visual stimulus will result in posture instability due to the difference in body shape.

2.2.2.4 Rest frame theory

In addition to the sensory conflict theory and the postural instability theory above-mentioned, Prothero (1998) proposed the rest frame theory. The rest frame theory claims that humans tend to select certain things and treat them as stationary references. The idea of this theory is from physics where the coordinate system is required to define spatial positions, angular orientations and motion speeds, providing the observer with a stationary reference called "rest frame". In real environments, our brain regards the Earth's surface as a stationary reference and uses it for spatial comparisons. Once humans recognize what is stationary or non-stationary, the brain will judge and measure the relative motions of other objects on or near the reference (e.g., bicycles, cars and aircrafts), and the information received by the visual and inertial system are used to organize its next perceptions and actions.

The classical sensory conflict theory claims that cybersickness is arising from inconsistent visual and inertial motion cues, while Prothero and D. E. Parker (2003) regarded the rest frame theory as a slight refinement of the sensory conflict theory. The rest frame theory states that rest frames are vital to spatial perception, and the incapability of choosing an appropriate rest frame results in cybersickness. In other words, cybersickness is not due to the congruent information between orientation and motion cues, but instead, resulting from conflicting rest frames implied by many motion cues that are decoded to affect one's judgement on moving or stationary objects. Despite a little refinement of sensory conflict theory, the rest frame theory implies that focusing on particular visual stimuli that can influence the selection of rest frame could be a rewarding strategy to reduce cybersickness. In order to find the rest frame, the rest frame theory decomposes the virtual environment into two parts, one as "content of interest" (CI) in the foreground and another as "independent visual background" (IVB) which matches

inertial orientation and motion cues. The selected rest frame is strongly affected by the IVB implying that the spatial comparisons and perceptions is performed in connection with the IVB. The importance of the IVB suggests that if we can make the IVB aligned with the inertial cues even if the CI is not, then it is possible to reduce cybersickness (Prothero, Draper, *et al.* 1999).

There are some experiments that can be explained by the rest frame theory to reduce cybersickness. Whitinghill *et al.* (2015) demonstrated that a virtual nose can reduce cybersickness when added into some games, depicted in Figure 2.5. The authors organized 41 participants to their VR applications on a VR headset with varying visual stimulus (i.e., city navigation walking game, and white-knuckle roller coaster game), and some of the participants played games with a virtual nose while others play without virtual nose. With the virtual nose, participants reported lower sickness scores, and the cybersickness onset time was 94.2 seconds longer in the city navigation game and 2.2 seconds longer in the roller coaster game compared to that of without the virtual nose. Apart from the evaluation through the sickness onset time, researchers also observed the significance of a virtual nose through the electro dermal activity (EDA) measurement.

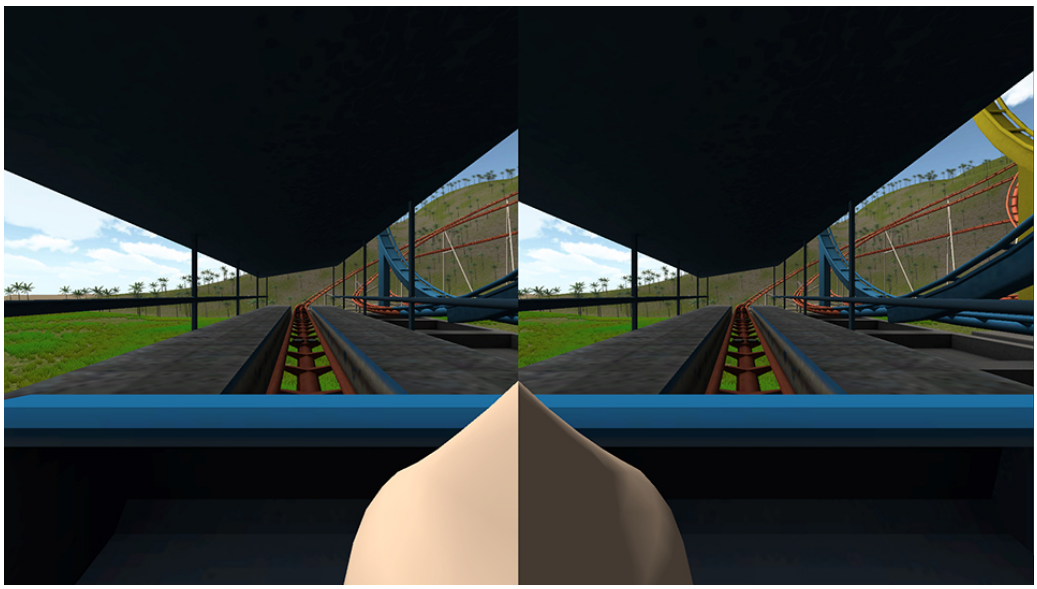

Figure 2.5: The inserted virtual nose for reducing cybersickness in virtual environments, figure from Whitinghill *et al.* (2015).

Although the virtual nose experiment validates the rest frame theory, Cao *et al.* (2018) criticized that the virtual nose is in a head reference frame instead of a real-world reference frame, but the typical rest frame is in the latter one, and further, the possibility of a see-through typical rest frame

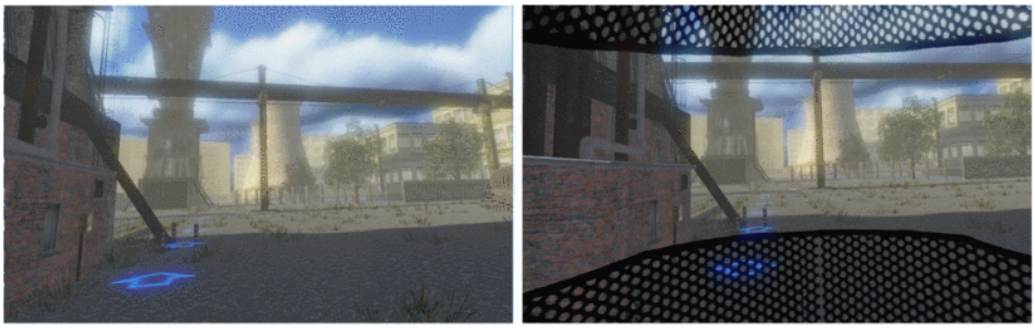

Figure 2.6: Virtual scenario without rest frame (left) and with a black metal net working as a rest frame (right); a function is defined to control the transparency of the rest frame in the right subfigure, figure extracted from Cao *et al.* (2018).

is not enabled by the virtual nose. Including a visual cue and an independent visual background as a stationary reference, J. J. W. Lin *et al.* (2004) developed a *Virtual Guiding Avatar* represented as an abstract airplane to enable the user to follow a horizontal motion trajectory. With the motion cues and independent visual background, the *Virtual Guiding Avatar* (VGA) enables the user to estimate the upcoming visual flow and to adapt gaze as compensation at the corresponding direction. The experiments were performed in projection-based system and the results from a revised SSQ manifested that the earth-fixed VGA with rotational prediction cues or non-earth-fixed VGA with rotational and translational prediction cues can reduce the severity of sickness significantly. Considering that the HMD system tends to induce more severe cybersickness than with projection-based simulators, Cao *et al.* (2018) employed two different strategies including static and dynamic rest frames in an HMD-based system to extend the user's travel distance in virtual environments, shown in Figure 2.6. The dynamic rest frame means that the opacity varies according to visually perceived motion during navigation; otherwise, it is the static rest frame. The reported SSQ score and discomfort score showed no difference between two different rest frames because of the small sample size; however, both rest frames proved to be efficient for reducing cybersickness.

2.2.2.5 Eye movement theory

Riccio and Stoffregen (1991) mentioned that gaze instability is associated with cybersickness because uncontrolled eye movements prevent the optic nerve from collecting relevant spatial information, thereby inducing postural instabilities. However, the mention of gaze instability in their study is not to formulate the eye movement theory but to support the postural instability theory, and the authors

suppose that the association between eye movements and cybersickness would be excluded if the body is under passive restraint.

It was found that most oculomotor systems are formulated with a negative feedback mechanism, but the systems become insensitive or fail to respond to external stimulus if it exceeds a certain range (Ebenholtz 1992). Ebenholtz (1992) related cybersickness to eye movement, arguing that any condition producing error in eye movement control, proceeding with feedback and error-correcting signal, is a potential reason for cybersickness. If visual stimuli are applied, it is likely to induce oculomotor instability and errors in eye movement control due to unsuccessful response to the same stimulus. Thus when the error is small, the subject is able to correct it with muscular effort; however, the continuous effort for correction could make troubles, because the constant strain imposed subconsciously on the subject may give rise to muscular and nervous fatigue and eye tension. Further, the afferent signal can stimulate the vagus nerve which is adjacent to the vestibular nuclei, resulting in symptoms of cybersickness (Ebenholtz *et al.* 1994; Webb and Griffin 2002).

Webb and Griffin (2003) believed that since a functioning vestibular system holds the key to cybersickness, eye movements may be attributed to the vestibular input leading to cybersickness through an unknow mechanism. Ebenholtz (2001) found that two kinds of eye movement, including optokinetic nystagmus and vestibular ocular response, are strongly linked to cybersickness. In the optokinetic nystagmus, the subjects tracks or pursuits a moving target with their eyes, and when the object moves out the field of vision, their eyes snaps back to the original position where the subjects first see the object, like saccadic movements. On the other hand, the vestibular ocular response is associated with maintaining a moving object on the fovea (the center of the retina with the sharpest vision) during head turning process. Therefore, for vestibular ocular response, if the subject rotates her/his head to the right while fixating the object straight ahead, the eye has to be rotated to the left accordingly. Ebenholtz (2001) mentioned that errors during these eye movements can cause symptoms of sickness such as headache, eye strain and difficulty concentrating. Similar sickness symptoms are also reported for car or boat passengers who suffer an irregular series of impulses; these impulses may need modification or interruption of the eye movement if the passenger is struggling to fixate or track an object visually (Treisman 1977).

Some studies are in line with the eye movement theory. Holmes and Griffin (2001) employed the optokinetic nystagmus as a strategy to induce cybersickness, with the aim to study the variation

of heart rate along with severity of sickness. Ji *et al.* (2009) investigated the effect of optokinetic nystagmus on participants by suppressing vection with an additional peripheral visual field rotating in the reversed direction to the rotating environments. The head is fixed by a chin rest in order to avoid interaction effects between postural instability and head sway when a visual stimulus is projected on the retina; the result measured through SSQ score offers powerful evidence for the positive correlation between optokinetic nystagmus and cybersickness in the absence of vection. Webb and Griffin (2003) designed an experiment with single or five horizontal rows of moving dots presented on a VR head-mounted display, in which the subjects were requested to track visually these moving dots and then return instantly to the starting point. The nystagmic eye movements were induced with an approximated amplitude of 18° at $27° \cdot s^{-1}$. Two conditions (i.e., single or five moving dots) presented two level of vection, but there was no difference regarding the severity of cybersickness. The results indicate that vection is not the primary cause of cybersickness, and cybersickness is induced by eye movements or the movement of images on the fovea. Therefore, an appropriate control of eye movements or gaze fixation is feasible to help reduce cybersickness (Webb and Griffin 2002; Webb and Griffin 2003).

2.2.2.6 Poison theory

Not limited to humans, susceptibility to visual stimuli appears across species including cats and dogs and other vertebrate species such as birds and fish, but rodents and rabbits, horses and other ruminants are unlikely to vomit because of their exceptionally adapted stomach anatomy (Oman 2012). All species are under evolutionary press to establish protection mechanisms against ingesting or ingested toxins. Cybersickness is provoked by a minor degree of disruption or difficulty during the programming of eye or head movement when information from visual, vestibular or proprioceptive inputs are irregularly and unpredictably perturbed by certain types of stimuli. The body constitutes an ideal warning system for detecting early central effects of neurotoxins when these have not activated more basic levels of defense. The produced toxins which influence the nervous system tend to adjust sensory inputs or coordination, or both. The emetic response to persistent disrupted signals would be a benefiting adaptation for nonprofessional feeders who eat both plants and carrion. Treisman (1977) postulated that nausea and vomiting in responding to visual stimuli could be an accidental byproduct of this protection system. From the evolutionary point of view, there should be some

survival superiority through which the life entities can gain benefits from the susceptibility; otherwise, the nature selection should have acted positively to abandon it (Oman 2012). This is an adaptationist explanation for cybersickness because it presumes that all phenotypic traits for survival benefit are correlated and shaped the during long-term evolution process.

Treisman (1977) underlined that the humans have not evolved to adapt themselves to relatively fashions of transportation as we are using nowadays, and therefore, the body reacts to sensory conflicts as they were ingested toxin, following symptoms like vomiting, which could be a unbiased side effect of a favorable gene or genes. This work has been widely accepted as an evolutionary explanation for cybersickness. In support of the poison hypothesis, Treisman (1977) pointed out the relatively strong immunity of infants or small age of individuals to cybersickness, and he explained that young mammals rely mainly on milk or shortlisted food which is rarely toxic, and they are regularly suffering random and unstable movements when carried; however, species with particular or controlled diets or tolerant of toxins are excluded. However, it hardly proves the lack of sickness symptoms of other younger animals and fact that the lack of susceptibility in infants can be associated with the immaturity of spatial orientation mechanisms (Reason and Brand 1975; Oman 2012). Another evidence is based on the fact that vestibulectomy renders humans and animals immune to cybersickness. Money and Cheung (1983) carried out this experiment in seven dogs by removing surgically their vestibular apparatus of the inner ear and observing the damaged emetic response to certain poisons. It was found that the vestibulectomy rendered the dogs immune to swing tests of motion susceptibility, indicating that the inner ear is part of the normal mechanism for vomiting in reply to poisons, and that one of the physiological roles of the inner ear is to promote the emetic response to poisons; therefore, the linkage between vestibular apparatus and the corresponding emetic response to poisons is regarded as the foundation of cybersickness.

Although the "poison" theory from Treisman (1977) is continually cited as an accepted explanation for cybersickness, the evolutionary point of view has been vigorously challenged by a number of domain experts mentioned in Oman (2012).

2.2.2.7 Negative reinforcement model

Bowins (2010) claimed that cybersickness has evolved as a negative reinforcement system to visual stimuli involving sensory conflict and postural instability, and abnormal stimuli of this form would

have significantly increased the risk of injury or signaled illness or vulnerability to predators, thereby lowering evolutionary fitness. With the symptoms of cybersickness, users would naturally reduce or cease the related activities to escape the horrible experience. At the beginning of a neural mismatch between experienced and expected motion and/or postural instability, sickness symptoms appear to provide a negative reinforcement for action requested to terminate the offending visual stimulus. If the stimulus continues, the symptoms intensifies to the point of resulting in an alert to vomit. These actions activated by the sensation of cybersickness includes early avoidance, reduction or cessation of visual stimulus, and shifting away from the offending situation. Positive reinforcement does so through positive feedback, while the negative reinforcement does so by punishment or diminishing a behavior.

Watt *et al.* (1992) observed that the prolonged active motions, i.e., rapid rhythmic voluntary rotation of the whole body, head and gaze together, can induce sickness symptoms for many individuals within 30 minutes, and these side effects including disordered posture and gaze control strategies pose a threat to survival; then other symptoms such as nausea and vomiting evolve to urge against such stimuli. The negative reinforcement mechanism of cybersickness symptoms is much similar to how pain facilitates evolutionary fitness. The perception of pain is a negative reinforcement paradigm actively prompting the organism to stop the pain-inducing state through avoidance, reduction, cessation or removal of the damaging situation (Bowins 2010). Analogously, cybersickness affords an effective negative reinforcement for coping with disgusting visual stimuli. However, due to the lack of physical capacity to avoid, reduce, or abort the offending stimulus, infants and toddlers are mostly or completely immune to cybersickness until they acquires the ability to operate the negative reinforcement system. As a hypothetical support for this theory, Bowins (2010) anticipated that those humans or animals prone to cybersickness would elect to stop or abort provocative visual stimuli earlier than the non-susceptible group. However, Oman (2012) considered this prediction to be plausible because it is still unclear from the point of the evolutionary aspect or the putative relationship between postural instability and predation.

One benefit of the negative reinforcement model is that it can be tested with both animal and human subject models under specifically designed conditions, compared to other cybersickness theories (Bowins 2010). This model helps easily to understand other cybersickness symptoms including escalation, seemingly dysfunctional induced state, termination of disgusting visual stimulus; on the other hand, the negative reinforcement model accounts for the presence of anxiety symptoms in cybersick-

ness, because that circumstances can arouse the sensation of threat throughout the evolution (Bowins 2010).

Table 2.2 presents different above-mentioned theories to explain cybersickness.

Table 2.2: Summary of theories to explain cybersickness

Cybersickness theory	Standpoint	References
Sensory conflict theory	The conflict information arising from different organs results in cybersickness	Reason and Brand (1975), Oman (1982), Brooks *et al.* (2010)
Subjective vertical conflict theory	Cybersickness appears when the sensed vertical conflicts with the subjective vertical	Bles *et al.* (1998)
Postural instability theory	Cybersickness results from prolonged instabilities, which precedes the symptoms of cybersickness	Stoffregen and Riccio (1991), Riccio and Stoffregen (1991), Smart Jr *et al.* (2002), Chardonnet *et al.* (2017)
Rest frame theory	The rest frames are vital to the spatial perception, and the incapability of choosing an appropriate rest frame leads to cybersickness	Prothero (1998), Prothero, Draper, *et al.* (1999), Prothero and D. E. Parker (2003)
Eye movement theory	Any condition producing error in eye movement control, preceding with feedback and error-correcting signal, is a potential reason for cybersickness	Riccio and Stoffregen (1991), Ebenholtz (1992), Ebenholtz *et al.* (1994), Ebenholtz (2001)
Poison theory	1. The body reacts to sensory conflicts as they were ingesting toxins 2. Nausea and vomiting in responding to visual stimuli could be an accidental byproduct of this protection system	Treisman (1977)
Negative reinforcement model	With the symptoms of cybersickness, users would naturally reduce or cease the related activities to escape the horrible experience	Bowins (2010)

2.2.3 Cybersickness evaluation

Crampton categorised the measures for motion sickness into two ways: qualitative and quantitative (L. Harm 1990b). Qualitative test scores are based primarily on psychological description or reports of signs and symptoms from experimenters and test subjects. For example, motion sickness questionnaires are commonly used to estimate sickness. However, multiple sources of error are inherent and inevitable as questionnaires heavily rely on subjective evaluations of the indicators being measured; thus the errors tend to undermine the reliability of the measurement procedure or experiment.

In parallel, quantitative assessments through physiological body signals arising from simulator sickness provides experimenters with opportunities to have precise direct comparisons between and within subjects. Another benefit of quantitative measurements from physiological manifestations is the possibility to continuously collect data throughout an experimental session, thereby achieving better accuracy and detail to characterize the progression and effectiveness of sickness symptoms. This also enables to design a real-time estimation system as an efficient sickness indicator.

2.2.3.1 Subjective evaluation

Subjective evaluation of cybersickness relies on different questionnaires which are designed to measure the sickness levels in different contexts.

In the early 1980s, the motion sickness questionnaire (MSQ) was designed to measure motion sickness arising from different kinds of transportation such as cars, buses, ships and airplanes (L. Frank *et al.* 1983). To focus on the sickness resulted from the simulator, Kennedy, Lane, *et al.* (1993) proposed a short version of the MSQ, the well-used Simulator Sickness Questionnaire (SSQ), considering only 16 items of the MSQ and removing MSQ symptoms that rarely or infrequently occur in simulator exposures. Factor analysis methods including principal-factor analysis and normalized varimax rotation were used to identify the coincidence or clusters of symptom items. The SSQ can be divided into three categories: nausea, oculomotor and disorientation.

Practical performance and easiness of use have become the most fundamental features of the SSQ when used to evaluate sickness after simulator tests on relevant platforms. Up to now, the SSQ is used in most VR applications. For example, many past studies have been conducted with the SSQ to assess simulator test conditions on educational devices for training (Dziuda *et al.* 2014) and compare the user experience of navigation paradigms (W. Chen *et al.* 2013), or to research on the effect of the field of view and image delay of head-up displays on simulator sickness and try to find optimal settings, which is receiving increasing attention (Alshaer *et al.* 2017; Meehan *et al.* 2003). Second, it becomes an effective measurement to quantify the level of simulator sickness and the SSQ generally provides a reference score to be compared with during the development of new indicators as we will see in the following sections. For example, Padmanaban *et al.* (2018) used ratings on a varied dataset of steroscopic 3D videos based on characterized video features such as the stereoscopic depth, vection and motion velocity to correlate these variables as a function of cybersickness. Meanwhile, the SSQ

was introduced to evaluate the level of the corresponding sickness after each experiment.

Kim *et al.* (2018) argued that VR sickness is a subset of simulator sickness, and therefore, some items in the SSQ might not suitable for measuring VR sickness. Further, they proposed a simplified version of the SSQ: the virtual reality sickness questionnaire (VRSQ). Compared with the SSQ, VRSQ results can be divided into two components including oculomotor and disorientation, and it has nine items. This questionnaire was shown to be more appropriate in VR studies than the SSQ.

To develop VR applications that can mitigate cybersickness, researchers are often fascinated with the overall level of cybersickness. In this case, it might be meaningful to repeatedly ask participants a single question about their wellbeing, instead of asking multiple questions in SSQ and VRSQ, which should significantly alleviate the workload during the user studies (Bimberg *et al.* 2020). The Misery Scale (MISC) (Bos, MacKinnon, *et al.* 2005; Bos, Vries, *et al.* 2010), and Fast Motion Sickness Scale (FMS) (Keshavarz and Hecht 2011) can be used in such purpose to quickly capture the severity of cybersickness. The MISC, which rating ranges between 0 (no problems) and 10 (vomiting), exploits the knowledge that the nausea antecedes other individually different symptoms such as dizziness, headache, sweat, and stomach awareness. Once the nausea is experienced, a minimum MISC of 6 is rated. When participants are familiar with this scale, the rating process can be repeatedly quickly. Similarly, the FMS is a verbal rating scale ranging between 0 (no sickness at all) and 20 (frank sickness), participants during visual exposure can rate the severity of cybersickness every minute, which is fast and efficient and can be carried out online in virtual reality applications.

Aforementioned questionnaires can measure the cybersickness after the user being exposed to visual stimuli, while the more fascinating way is to predict how susceptible to cybersickness the user is before the exposure. The motion sickness susceptibility questionnaire short-form (MSSQ-Short, also called motion history questionnaire,Golding (1998)) can estimate one's susceptibility to cybersickness by analyzing different sorts of motion that can induce sickness, for example, cars, buses or coaches, trains and so on. In addition, the MSSQ-Short can be used to weight the scores among different users for each experiment considering individual differences and to integrate ratings into a single and comprehensive rating (Golding 2006).

2.2.3.2 Physiological evaluation

Although well-established questionnaires in terms of motion sickness are widely used, there is one evident drawback of such methods if compared to physiological evaluations; for instance, lengthy questionnaires are generally administered after a user has performed an experiment; therefore he/she has to shift attention away from the experiment to personal feelings (Dennison *et al.* 2016). On the contrary, physiological indicators are developed based on physiological signals such as heart rate variability, blood pressure, electrogastrography and galvanic skin reaction (Brundage *et al.* 2016; Higuera-Trujillo *et al.* 2017), and can be used during exposure without requiring any verbal or written feedback from the users. Dennison *et al.* (2016) proposed other indicators that were not much studied in the scope of cybersickness, such as stomach activity, blinking and breathing. From these quantitave measurements, past work proposed strategies to prevent cybersickness from increasing while navigating, typically, the users' electrodermal activity was shown to be an efficient indicator to estimate the level of sickness and was used as a parameter in the navigation control law to adapt navigation in virtual environments, thus significantly reducing cybersickness (Plouzeau *et al.* 2018).

Behavioral indicators have received large attention for several years, for example postural sway, as it has been shown to be important indicators of motion sickness (Riccio and Stoffregen 1991). Chardonnet *et al.* (2017) focused on the features of postural sway during immersion and navigation in VR. They collected the postural sway signals in the Left/Right (L/R) and Forward/Backward (F/B) directions and analyzed them in both the time and frequency domains. They correlated the results with sickness scores obtained from questionnaires. As for the time-domain analysis, the resulting signals of L/R and F/B movements for the marginally stable and the stable states were projected onto an XY plane in order to monitor dynamic changes of the area and shape of the projected signals. The frequency domain analysis revealed two main components: low frequency and high frequency components; the former is usually linked to stable body states in which users do not feel any sickness (voluntary movements) while the latter is more related to marginally stable body states in which sickness arises (involuntary movements).

Unnatural viewing mechanism in virtual environments is also responsible for visual fatigue and cybersickness (Matsuura and Takada 2016). The observation of depth gaze associated with veridical depth information during exposure in VEs becomes paramount. Wibirama and Hamamoto (2014)

carried out a comprehensive study on cybersickness with respect to the SSQ, electrocardiography (ECG) as well as 3D gaze tracking. The occurrence of cybersickness was investigated with the SSQ, then the result was utilized for the analysis of user behaviors according to ECG and 3D gaze tracking; they found that participants immersed in 3D visual contents can have less dominant sympathetic nerves activated due to voluntary gaze fixation at one point, which suggests that depth gaze oscillates more frequently when cybersickness appears.

2.2.3.3 Learning-based evaluation

Machine learning is attracting great attention recently as it is supposed to be a powerful tool for data analysis and has already shown many advantages in video games, computer vision, speech recognition (Deng and D. Yu 2014; Goodfellow *et al.* 2016) or to develop health management systems (Khan and Yairi 2018; Faust *et al.* 2018). Consequently, learning-based algorithms can be extended to detect and predict cybersickness if robust neural networks can be trained based on physiological or visual signals.

From the ratings collected through questionnaires, Padmanaban *et al.* (2018) constructed a dataset of stereoscopic 3D videos across a wide spectrum of sickness so that comparative analyses of sickness can be performed in a significant way. A machine learning approach was employed to build a model of the nonlinear relationship between video contents and their corresponding nauseogenicity. However, this method requires artifacts to select features from the videos, which may lead to unavoidable biased results.

Another promising online motion sickness level prediction system was developed for a dynamic vehicle environment based on a learning system (C.-T. Lin *et al.* 2013); electroencephalography (EEG) signals are used to characterize the physiological changes that occur during the transition of passengers' cognitive states. This information is trained and compared through a self-organizing neural fuzzy inference network (SONFIN) to forecast a sickness level, achieving an overall accuracy of about 82% through experiments. Although this system is built mainly for estimating sickness for passengers in a vehicle, it can also be used to measure cybersickness in virtual reality as the symptoms between motion sickness and cybersickness are quite similar, which has already been demonstrated (Kennedy, Drexler, *et al.* 2010).

Table 2.3 presents different approaches to measuring cybersickness.

2.3 Cognitive workload

Referring to the development of navigation interfaces in a VR application, cognitive workload is another important factor to involve as the choice of navigation technique can influence cognition in a virtual environment (Zanbaka *et al.* 2005). Reimer and Mehler (2011) reported a positive trend between an increasing speed and a rising cognitive workload. Strategies to control speed during virtual navigation are of great significance regarding cognitive workload. Marsh *et al.* (2012) claimed that an unnatural navigation is likely to worsen user's task performance and results in high cognitive workload because it requires additional working memory to establish and support a mental model; the authors further proposed to develop a body-based navigation technique that requires less cognitive resources since such navigation is based on natural skills that have already been proceduralized, e.g., real walking in the physical environment.

Despite this growth and the capabilities of the latest devices, if a VR-based task is not designed with an appropriate level of cognitive workload to match a user's expertise, the task completion performance may be restrained (L. Zhang *et al.* 2017). Cognitive workload in this case is a term that refers to the cost of completing a task (Hart 2006a). It can be defined as the amount of cognitive resources used per unit time to reach the performance required by the task (Wickens *et al.* 2015). For pragmatic purposes, Blackwood (1900) proposed a simple definition that the workload is the ratio of time required to time available (time required/ time available). When the time required to complete a task is longer than the time available, it is cognitive overload, and vice versa. For example, when a user navigates in a virtual environment as a primary task, he/she may have to interact with internal objects as a secondary task, and because of this, a non-skilled user would keep overloading for longer time. More introduction to cognitive workload can also be found in (Paas *et al.* 2003).

Although workload is defined at a qualitative level, researchers are still trying to find measurable criteria on a multi-dimensional basis to quantify this phenomenon. The approaches used in the literature to measure cognitive workload include subjective measurements via questionnaires, physiological measurements via biosensors and performance measures (Paas *et al.* 2003; L. Zhang *et al.* 2017). The subjective and physiological evaluation methods are similar to those performed in measuring cyber-

Table 2.3: Summary of approaches for measuring the severity of cybersickness

	Variants	Features	References	Error analysis
Subjective evaluation	Simulator sickness questionnaire (SSQ)	1. users report the level of sixteen symptoms on a four point scale; 2. the cybersickness level is divided into three types: nausea, disorientation, oculomotor	Kennedy, Lane, *et al.* (1993)	1. individually different ability, sensitivity or awareness to detect early low-level symptoms; 2. inter-rater differences in assessing sickness symptoms, inter-laboratory differences of understanding of and explanation for the questionnaires
	Motion sickness susceptibility questionnaire (MSSQ)	Asks for previous sickness occurrences in cars, busses, trains, aircraft, boats, ships, swings, and so on	Golding (1998), Golding (2006)	
	Virtual reality sickness questionnaire (VRSQ)	1. revised version of SSQ for usage in VR environments; 2. the nausea component in SSQ is removed, only nine symptoms to report	Kim *et al.* (2018)	
	Misery scale (MISC), Fast motion sickness scale (FMS)	1. asks for a single value as the level of cybersickness; 2. easily be applied repeatedly	Wertheim *et al.* (2001), Bos, MacKinnon, *et al.* (2005), Bos, Vries, *et al.* (2010), Keshavarz and Hecht (2011)	
Physiological evaluation	Heart rate variability (HRV), blood pressure, electrogastrography (EGG), galvanic skin reaction (GSR)	1. Physiological signals are collected through various sensors; 2. Extra work is required to interpret the signal into a sickness level	Chardonnet *et al.* (2017), Brundage *et al.* (2016), Higuera-Trujillo *et al.* (2017), Dennison *et al.* (2016), Riccio and Stoffregen (1991)	1. differences in the general physiological state of the subject on different days; 2. individual differences in cognitive and psychological factors; 3. individual differences in reactivity of various physiological systems to motion provocation; 4. differences in blood levels of caffeine, nicotine, alcohol;
Learning-based evaluation	Deep/machine learning, signal analysis	1. using deep/machine learning to extract information from physiological signals; 2. using subjective-reported sickness levels as ground truth to train the neural network	Padmanaban *et al.* (2018), C.-T. Lin *et al.* (2013)	Performance relies on physiological signals and ground truth data

sickness, and therefore, they are sharing almost identical error sources. The performance measures are to report cognitive workload based on some performance variables related to task completion such as reaction time, accuracy, and error rate.

Physiological means for measuring cognitive workload have progressed due to the development of new types of biosensors, while subjective measurement methods are mainly based on long-living existing questionnaires such as the Subjective Workload Assessment Technique (SWAT) (Reid and Nygren 1988), the Modified Cooper Harper scale (MCH) (Kilmer *et al.* 1988), or the NASA-TLX table (Hart and Staveland 1988; Hart 2006a). The pre-defined questions enable experimenters to carry out experiments and analyse the data more easily than with biofeedback. However, the subjective evaluation process can bias the results because of unperceived internal changes and unknown factors among users. In addition, this evaluation method generally fails to reduce dispersion effects, noise and uncertainty during subjective investigation (Katicic *et al.* 2015a), posing a threat to what we refer to the measuring precision.

2.3.1 Subjective evaluation

Subjective measurements require users to provide feedback of their experience through questionnaires. Among well-known questionnaires, the MCH method was developed by Harper and Cooper (1986), which is still being used nowadays as a reliable measurement of aircraft performance. The user evaluates the performance of a specific task in terms of controllability, workload, and attainable performance goals, on a 1-10 scale; then, the assessment is analysed through a statistical study. On the other hand, the SWAT method consists of three criteria to measure workload: time load, effort load and psychological stress load (Reid and Nygren 1988). The user is asked to sort these factors, then to rate each of them in a 3-scale table, and the final evaluation is derived through a conversion table that provides the relationship between the 1-3 scale table and the final score. NASA-TLX (Hart and Staveland 1988; Hart 2006a) is another widely accepted subjective workload evaluation method applied in the computer-human interface (CHI) field (Ma and Kaber 2006; Cannavò *et al.* 2020). Based on a multi-dimensional rating procedure, NASA-TLX obtains an overall workload score according to a weighted average of ratings on six criteria: *Mental Demand* (MD), *Physical demand* (PD), *Temporal Demand* (TD), *Performance* (Pe), *Effort* (Ef) and *Frustration* (Fr). Despite the simplicity of implementing these different methods, subjective evaluation cannot generally be performed in real time

(while performing the tasks), which can lead to biased results because of unaware internal changes, e.g., the psychosocial environment (Casner and Gore 2010), thus resulting in high uncertainty. Since subjective evaluation can be easily conducted and interpreted on one-dimensional or multi-dimensional scales, it is the most preferred approach (Eraslan *et al.* 2016).

2.3.2 Physiological evaluation

Many researchers have investigated the possibility of measuring cognitive workload through the physiological response of users, which does not require a direct response from the user. Contrary to subjective measures, results from physiological evaluation are representative of the actual task workload (Miller 2001). Some of the frequently applied physiological methods include cardiac activity, eye gaze and electroencephalography (EEG) (L. Zhang *et al.* 2017; Gerry *et al.* 2018). Cardiac activity is the most common approach for measuring workload in driving and flight simulators and is measured through blood pressure, heart rate and heart rate variability (HRV) (Hoover *et al.* 2012). Heartbeats can be analysed in the time and frequency domains to determine the HRV. Some early studies found that heart rate and HRV correlate with workload: the higher the mental workload, the higher the heart rate and the lower the HRV (Mulder 1986; Metalis 1991). Pupil dilation has recently been used as an indicator for mental workload in the HCI community since eye gaze signals indicate a user's cognitive state (Kosch *et al.* 2018). EEG signals are hypersensitive and credible for regular memory load evaluation, especially the alpha and theta wavebands of EEG that are reflective of the task difficulty (Gevins, M. E. Smith, *et al.* 1998). Physiological measurements alleviate the complexity of the experiment in that users do not have to conduct a second test or to be asked for feedback. However, these measures are subject to several sources of error: the accuracy of physiological data heavily relies on the performance and precision of the sensors; such signals are sensitive to disturbances.

2.3.3 Performance-based evaluation

Performance-based techniques are the third type of workload measurements. Paas *et al.* (2003) reported that performance variables (e.g., reaction time, accuracy, and error rate) from a secondary task could reflect the cognitive workload imposed by a primary task. These criteria have been found to be correlated with cognitive workload (Son and S. Park 2011). However, the insensitivity of some of the measurements while using performance-based methods is one drawback (Shakouri *et al.* 2018).

For instance, a task with a low demanding workload can enable an excellent performance during the beginning stage of the task but then performance will degrade as the user becomes fatigued or distracted (Casner and Gore 2010), leading to mixed and noisy results. Accordingly, using this method along with other workload evaluation methods may improve the quality of the measure.

Table 2.4: Summary of approaches for measuring cognitive workload

	Variants	Comments	References
Subjective evaluation	Subjective workload assessment technique (SWAT)	Containning three criteria: time load, effort load, physiological stress	Reid and Nygren (1988)
	Modified cooper harper scale (MCH)	Widely used in aircraft performance	Harper and Cooper (1986)
	NASA-TLX	1. widely used in the CHI field; 2. including six criteria	Hart and Staveland (1988)
Physiological evaluation	Electroencephalography (EEG), heart rate variability (HRV), eye gaze	1. no need of response from the user; 2. results much close to the actual workload	Miller (2001), L. Zhang *et al.* (2017), Gerry *et al.* (2018), Hoover *et al.* (2012), Kosch *et al.* (2018)
Performance-based evaluation	Reaction time, accuracy, error rate	1. insensitivity; 2. better to be used with other evaluation	Paas *et al.* (2003), Son and S. Park (2011), Shakouri *et al.* (2018)

Table 2.4 presents a summary of different evaluation methods for measuring cognitive workload.

2.4 Summary

In this chapter, we summarized the evaluation methods for cybersickness and cognitive workload. Both of them can be evaluated through subjective and physiological methods. However, they have different error sources. Error sources for subjective evaluation are manifold, but a partial list of error sources are easy to find. For instance, individuals have different ability, sensitivity or awareness to detect early low-level symptoms, tend to use diverse approaches for reporting symptom characteristics. Besides, it is also possible to lead to errors due to inter-rater differences in assessing overt signs, inter-laboratory differences of understanding of and explanation for the criteria to characterize these symptoms.

Like subjective measures, physiological measures are also subject to various sources of error. It generally takes as input physiological signals, but the accuracy of physiological data relies closely on the performance and precision of the signal collector; normally such signals are sensitive to disturbance.

A partial list of other error sources includes: 1) differences in the general physiological state of the subject on different days; 2) individual differences in cognitive and psychological factors; 3) individual differences in reactivity of various physiological systems to motion provocation; 4) differences in blood levels of caffeine, nicotine, alcohol, or over-the-counter medications on different testing occasions; and 5) variations in vestibular receptor sensitivity across testing occasions.

Despite multiple measures for cybersickness and cognitive workload, these evaluations still fail to overcome different error sources. As the evaluation is a premise for designing different navigation techniques, we will propose a new evaluation approach. Through the literature study, we found that cybersickness is an individually different side effect depending on factors such as age, gaminge expereince and ethnic origin, and consequently, the solution to mitigate cybersickness should be individually different. Therefore considering different human factors, we will also design different navigation techniques to reduce cybersickness and cognitive workload.

Chapter 3

Research method

Contents

In response to the quickly increasing virtual reality market for practical application, navigation interfaces in virtual environments (VEs) have been recognized as the most fundamental feature to provide user satisfaction, sense of presence, reduced cybersickness and entertainment when designing a product, a building, or when showing reconstructed places to general public (Janeh *et al.* 2017). Navigation is paramount in VEs for two primary reasons: first, navigation is the most common and universal way enabling users to interact with objects and explore VEs as if in a physical world; second, navigation is often performed to support another task, for example, pick up treasures, fight enemies, and obtain spatial information (LaViola Jr *et al.* 2017).

To achieve successful navigation in VEs, appropriate navigation devices and techniques should be intuitive and should allow users a realistic perception of VEs. For instance, devices such as joysticks or head orientation tracking based devices using *Gyro* in virtual reality headsets are widely used to navigate in VEs. This kind of navigation devices is easy to use and effective for novice users to control movements in VEs (F. Zhang *et al.* 2017). However, joysticks are unable to provide smooth movements towards a target location but allow to move suddenly and irregularly. Such navigation technique fails to provide natural movements and is more likely to induce cybersickness (Vinson *et al.* 2012), resulting from serious discrepancies between visual information and the vestibular system.

3.1 Research questions

VR headset manufacturers try to provide higher immersion with their products. The counterpart is that users tend to suffer from more cybersickness, getting even worse as the immersed time passes (Padmanaban *et al.* 2018). The susceptibility to cybersickness varies among VR users. So far, the lack of efficient methods to evaluate and mitigate VR sickness in virtual environments attracts much attention from both academic and industrial communities. Therefore, the research issues related to cybersickness are:

Q1 How to evaluate cybersickness considering individual characteristics, as well as according to physiological signals such as EDA or posture sway?

Q2 How to design navigation techniques adapted to the user so that VR sickness can be mitigated?

Because the complexity of a task in a virtual environment can affect information processing, per-

formance and user attention (Ma and Kaber 2006), a virtual environment can act on the user at both the cognitive and perceptual levels (Milleville-Pennel and Charron 2015). Although there are multiple subjective methods to evalute cognitive workload, the lack of accuracy leads to difficulty in comparing different workload levels. Thus, the research issue for cognitive workload is:

Q3 How to improve the evaluation of cognitive workload?

3.2 Proposed approach

3.2.1 LSTM model for measuring cybersickness (Q1)

The susceptibility to cybersickness is affected by many factors including individual characteristics and displayed devices. It is important to investigate how to measure and quantify the amount of VR sickness after a user plays with VR systems. The LSTM model is one of the algorithms in the deep learning family, and it has special advantage to analyzing sequential data. This thesis proposes to tackle this issue by introducing the LSTM model to evaluate VR sickness based on physiological signals.

3.2.2 Adaptive navigation in VR (Q2)

We wish to design an online feedback evaluation system to optimize VR navigation interfaces according to the user's level of VR sickness. A real-time adaptive navigation system was developed following the evaluation of cybersickness. Four techniques have been developed, such as a speed protector that can optimize the navigation speed, and an adaptive model that can adjust the navigation acceleration based on a PID controller and user's physiological signals (e.g., EDA).

3.2.3 TOPSIS for measuring cognitive workload (Q3)

Considering that most current methods often fail to take into account inherent uncertainties during subjective judgment and comparison processes (Zhou and Chan 2017), we propose to use the *Technique for Order Performance by Similarity to Ideal Solution* (TOPSIS) (K. P. Yoon and Hwang 1995) model to enhance the precision of the subjective evaluation of workload. TOPSIS was developed for decision-makers to measure and compare the relative performance among different alternatives; it has been widely used in many evaluation processes such as supply chain management, manufacturing system

design, business and marketing management and health management (Behzadian *et al.* 2012). In this thesis, the TOPSIS method is used to analyze the NASA-TLX table for measuring the overall cognitive workload instead of using the classical weighted sum method.

Chapter 4

Measuring user experience

Contents

Through the literature study in chapter 2, we found that there are many methods of evaluating cybersickness and cognitive workload. However, these methods are blamed for multiple error sources, deteriorating the reliability of the evaluated results. In this chapter, we will focus on proposing a new evaluation technique to improve the evaluation performance of cybersickness and cognitive workload during or after navigation in virtual environments.

4.1 Evaluation of cybersickness with postural signal

4.1.1 Introduction

This section concentrates on cybersickness during navigation in an immersive virtual environment. A set of symptoms may appear on users owing to their susceptibility to cybersickness during or after being exposed to dynamic visual displays for a long time. Body postural instability is one of the behavioral phenomena that has already shown effectiveness to capture cybersickness (Chardonnet *et al.* 2017). In order to measure the user's cybersickness, we proposed a new method based on the deep long short term memory (LSTM) network and build a network to characterize the user's level of VR sickness. Compared to other neural networks like multilayer perceptrons (MLP) and convolutional neural networks (CNN) which have no internal memory and only process each input data independently, the LSTM model can perform better in processing long-term dependencies among sequential data with gates including the forget gate, the input gate and the output gate, and overcome gradient explosion and vanishing issues at the same time (Bengio, Simard, *et al.* 1994). It motivates our choice for the LSTM model to detect cybersickness. Here the LSTM model will be used to analyze the postural sway signal.

Chardonnet *et al.* (2017) extracted multiple features from the postural sway signal to measure the cybersickness, and validated the performance with SSQ. As an extension of such work, this section expects to extract a different feature correlated with the SSQ. While current approaches for measuring VR sickness can only be used in pre-exposure and post-exposure in the VE, we showed our method's advantage, as it can measure cybersickness and had the potential to be implemented for real-time applications, which enabled the experimenter to get rid of intermittent evaluation methods. The long-term objective was to extend these results to more cases and find objective and online measures to quantify simulator sickness with physiological signals. The most important contribution was the

proposition of a new method to evaluate VR sickness based on an LSTM network.

4.1.2 Principles of VR sickness evaluation

4.1.2.1 LSTM in deep learning

A deep long short term memory (LSTM) network is designed with the aim of detecting and measuring the degree of cybersickness. LSTM is one of the methods in the large deep learning family. Deep learning is a method trying to learn representations from source data with successive layers; the term *deep* in *deep learning* is not linked to any kind of deeper understanding of the solution achieved by the approach; instead, it is related to the idea of successive representation layers.

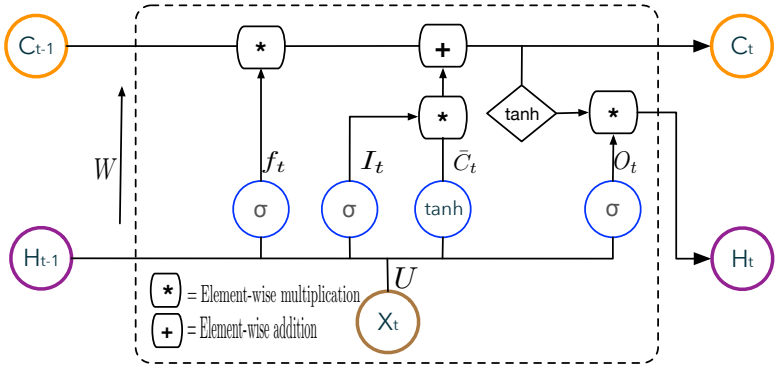

Figure 4.1: Diagram for an LSTM cell at time step t; W and U are weight vectors for the forget gate (f), the candidate ($\bar{C}$), the input gate (I) and the output gate (O); X_t: input vector, H_{t-1}: previous cell output, C_{t-1}: previous cell memory, H_t: current cell output, C_t: current cell memory; σ: sigmoid activation function.

Figure 4.1 explains the components of one LSTM cell and how it works. The LSTM cell takes inputs from the current step state (X_t), the previous hidden state (H_{t-1}) and the previous memory state (C_{t-1}), and returns outputs including the current hidden state (H_t) and the current memory state (C_t). The internal computational flow is controlled by four different gates which can also be understood as filters: a forget gate (f), a candidate ($\bar{C}$), an input gate (I) and an output gate (O), described in Equation 4.1 where X_t and H_{t-1} are processed by the corresponding weight vectors W and U. To further include history information, current outputs have to join a previous cell memory C_{t-1}, described in Equation 4.2.

$$\begin{cases} f_t = \sigma(X_t * U_t + H_{t-1} * W_f) \\ \bar{C}_t = \tanh(X_t * U_c + H_{t-1} * W_c) \\ I_t = \sigma(X_t * U_i + H_{t-1} * W_i) \\ O_t = \sigma(X_t * U_o + H_{t-1} * W_o) \end{cases} \tag{4.1}$$

$$\begin{cases} C_t = f_t * C_{t-1} + I_t * \bar{C}_t \\ H_t = O_t * \tanh(C_t) \end{cases} \tag{4.2}$$

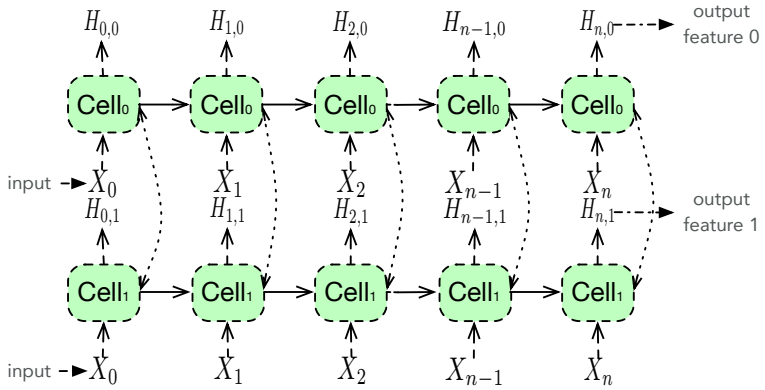

Figure 4.2: One LSTM layer is composed of two cells that can work in parallel and communicate between each other during the learning process; the input layer is the sequence consisting of a vector with length n; each cell is fed with the same input sequence.

A single LSTM cell can be extended along the sequence direction in order to process sequential data, which is the original LSTM model with one layer, as shown in Figure 4.2. The deep LSTM model, which is an extension of the original model, contains multiple hidden LSTM layers to learn the description of the original sequential data accurately. Based on different problem types, the model can output sequence data or only a single scalar. Especially when the model learns the features of the input sequence itself and tries to reconstruct such input in the output, the network is called an autoencoder. The so-called features of the sequence are the intermediate and equivalent representations of the original input within a latent space.

Figure 4.3 presents an overview of the proposed method for objectively measuring the cybersickness score based on the LSTM model. This figure shows that the model consists of an encoder that tries to represent the raw postural sway signal in a latent space, followed by a decoder that tries to reconstruct the original signal from the encoded features. Two stages compose the method: a training stage and an evaluation stage.

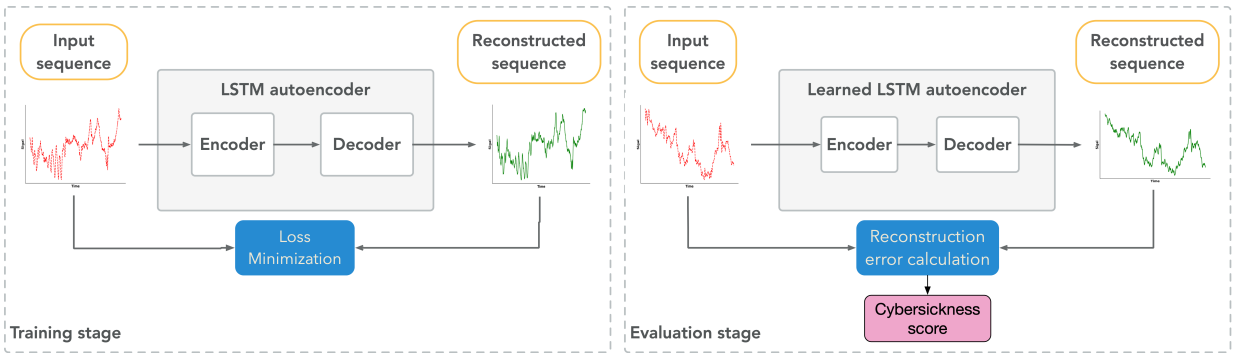

Figure 4.3: Overview of the proposed method for estimating the cybersickness score using an LSTM model.

4.1.2.2 Deep LSTM model for normal sway signals

In the training stage (Figure 4.3 left), the LSTM neural networks learns to extract features of the input consecutive signal information by minimizing the loss (mean-absolute error, MAE) between the original inputs and the reconstructed outputs, thanks to Equation 4.3:

$$\arg\min_{w} \mathcal{L} = \frac{1}{N}\sum_{i=1}^{N} ||\mathbf{X}_i - \hat{f}_w(\mathbf{X}_i)|| \tag{4.3}$$

where w is used to describe the parameterized model; $\mathbf{X}_i$ is the i^{th} sampling point of the postural sway signal $\mathbf{X}$; N is the length of the signal (number of sampling points); $\hat{f}_w$ is the non-linear function of the neural network that reconstructs the original input with the network. The input signal is a normal sway signal, representing the user's body postural sway when the user is in his/her usual state of fitness (no sickness).

Figure 4.4 shows the LSTM model aiming at retrieving the input postural sway signal. The model is built by stacking ten LSTM layers and one fully connected layer (also called dense layer in some literature). The number of layers was determined with the grid-search method, where we tried to find the best performance by tuning the model. Deep LSTM layers are used to learn the sequence features. The model includes two main parts: the encoder and the decoder; it can reconstruct the original input with high accuracy (i.e., small MAE). It is worth noting that high accuracy is valid only when the model reconstructs the signal from a similar body state, not to reconstruct every signal from diverse body states with high precision. A dropout function follows each layer to avoid overfitting (Srivastava

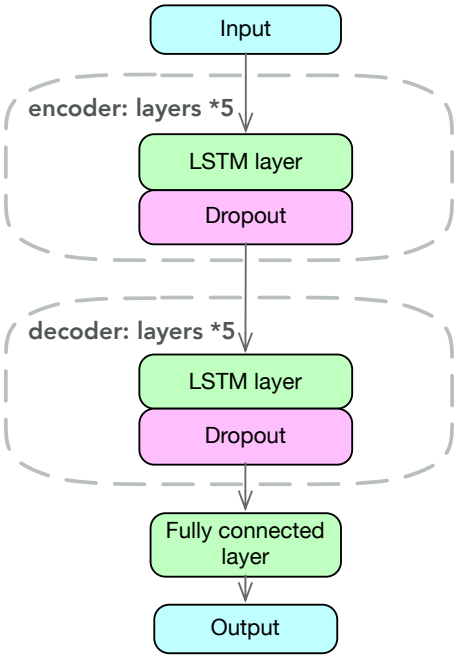

Figure 4.4: Overview of the proposed method to reconstruct the input signal using LSTM neural networks including five layers for the encoder and five layers for the decoder; dropout is introduced to avoid overfitting.

et al. 2014). Since we wanted to reconstruct the original input, a dense layer was used to reshape the output feature from the last LSTM layer. This process can be assimilated as a *reshape* function in many programming languages.

4.1.2.3 Detection of abnormal sway signals

After training our LSTM neural networks, the cybersickness score can be calculated according to the reconstruction errors, as done in (Hasan *et al.* 2016) (Figure 4.3 right). Based on the learned model, the reconstruction error E of a test signal $\mathbf{Y}$ can be written as

$$E = \frac{1}{N}\sum_{i=1}^{N} ||\mathbf{Y}_i - \hat{f}_w(\mathbf{Y}_i)|| \tag{4.4}$$

where $\hat{f}_w$ is the learned LSTM model.

Because the deep network is trained with the postural sway signal obtained before the user is immersed in VEs, the trained model is supposed to capture the features of a person without any feeling of cybersickness. Therefore, it can reconstruct the original sway signal. However, when such

a trained model is used in the evaluation stage where the postural sway signal is obtained after the user is exposed to VEs, the reconstruction error shall be larger. Consequently, by evaluating the cybersickness score based on the reconstruction loss with a trained model, the level of VR sickness is expected to be estimated and predicted in real-time without providing additional information.

A lower reconstruction error means that our model can retrieve the signal with more accuracy. In other words, when we train the model with a postural sway signal obtained from a normal state of the person (without any feeling of VR sickness), the encoder extracts the features of such state, and the decoder reconstructs the signal accordingly with high accuracy. However, during the evaluation stage, when we feed the network with a postural sway signal obtained from a different body state, the decoder will not be able to reconstruct the input signal with accuracy as the network does not recognize the learned features: the reconstruction error is thus supposed to be large.

4.1.3 User study

We conducted a user study in order to build the datasets to train our deep LSTM model and validate the general method. We carried out an experiment to estimate the level of VR sickness during navigation in a virtual environment through both the postural sway signals and the SSQ. The final results from both measurements were then fitted and correlated to our proposed evaluation method to validate its efficiency.

4.1.3.1 Participants

We asked 11 participants including 4 females ($M_{age} = 25.83$, $SD = 4.58$) to take part in the experiment. All participants were recruited through word of mouth. No compensation was given after the experiment. Before the experiment, a brief training was provided to let the subjects understand their main task in the virtual environment. All participants were requested to fill a pre-exposure questionnaire (Q1) to get general information about their health condition and their background knowledge on computers and virtual reality. According to the results from Q1, all subjects were in normal or corrected-to-normal health conditions, reported no disorders or unusual circumstances concerning their hearing or balancing, and did not report any severe susceptibility to motion sickness.

Figure 4.5: Virtual scene where the participants complete the task.

4.1.3.2 Experimental equipment

An HTC Vive head-mounted device (HMD) was used together with the two wireless handheld controllers provided with the HMD to control navigation. In our experiment, the trigger button and the trackpad of the handheld controller were mainly used to control the speed and the direction of navigation. To move forward, users pressed the trigger button and the movement started with a speed depending on how much the trigger was pressed, while turning was done through a gaze-directed technique in which the moving direction was the gaze direction (here, we assimilated the gaze direction to the head orientation). Users could stop navigation if they released the trigger button or when they arrived at the target position. The HMD was connected to Unity3D via SteamVR and VRTK SDK which provides many built-in APIs for developing VR user interfaces. With this SDK, users and the VE interaction could be achieved in real-time with negligible delay.

The postural sway signal of the participants was collected through a Stabilotest balance board from TechnoConcept[1]. It has internal sensors that can capture left/right and forward/backward sway signals in real-time for 51.2 s with a frequency of 40 Hz, providing 2048 sampling points.

4.1.3.3 Experimental procedure

The procedure was designed as follows:

1. All participants were requested to fill questionnaire Q1 before the experiment. Considering that the participants were unfamiliar with the HTC Vive, we gave them a brief training on the tasks, including what they were going to do and how to control navigation with the controllers.

2. In order to measure the difference of user's level of cybersickness before and after the main task, each participant had to fill an SSQ_{pre} (Q2) to get a pre-exposure cybersickness score then had to stand on the balance board while looking at a fixed point displayed on the wall to record the corresponding sway signal. Note that though past work has recommended not to administer an SSQ before exposure (Young *et al.* 2007), rather than considering participants to have no sickness at all, we chose to administer the SSQ to get a baseline of participants' actual state.

3. The participants navigated through the VE and completed the given task. In order to provoke cybersickness at different levels, each participant had to search and collect the coins scattered in the VE (Figure 4.5). We set the maximal navigation speed to 2m/s which is slightly higher than the normal walking speed. The participants were urged to explore and pick up a total of 30 coins as fast as possible. All along with the experiments, they were in a standing position, which is supposed to favor cybersickness more compared to a sitting position (Riccio and Stoffregen 1991). Note that the movement speed might be less than the maximal speed during task completion, depending on the input from the controller.

4. After the participants finished the navigation task in the VE, they took off the HMD then stood again on the balance board to collect another sway signal. Besides, another SSQ_{post} (Q2) was filled to calculate the ground truth cybersickness score after navigation in the VE.

5. The participants were invited to do the navigation task again within the same experimental conditions on another day in order to have more data samples, repeating the procedure between 2 and 4.

The whole procedure of the experiment is given in Figure 4.6. The participants were exposed to the VE each time between 3 and 5 minutes. After finishing the whole experiment, we obtained twice

[1] http://www.technoconcept.fr/shop/index.php

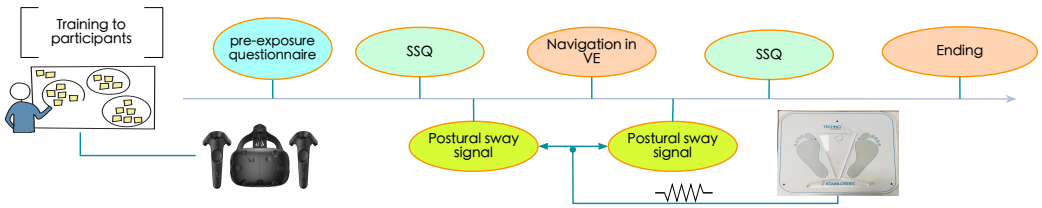

Figure 4.6: Experimental procedure conducted to obtain the datasets.

four different data for each participant: a pre-exposure postural sway signal and the corresponding SSQ_{pre} score, a post-exposure postural sway signal, and the corresponding SSQ_{post} score. Although the participant may become familiar with the environment and its procedure in the second experiment, this would not affect the final result from the participants as the idea was to find the variance of the SSQ score and the corresponding postural sway signal. The LSTM model was then created and implemented using a deep learning framework called Tensorflow[2]. Before the training and evaluation stages, the signal data was pre-processed by centering and scaling between -1.0 and 1.0. The pre-exposure signals were used to train the model to extract the features for the normal state and save them into the LSTM cells. The training stage stopped when the reconstruction error converged to a stable value. Then the post-exposure signals were fed into the model, which led to a jump of loss (strong variation of reconstruction loss) in the same way as described in subsubsection 4.1.2.3. This jump of loss was then considered to originate from the presence of VR sickness.

4.1.4 Performance and validation of the proposed method

To be sure that the sudden variation of reconstruction error between the training stage and the evaluation stage was due to the onset of VR sickness, we correlated it with the level of sickness provided by the sickness scores from the simulator sickness questionnaires. We computed for each experiment the difference between the pre-exposure and the post-exposure scores, and we will call it from now on the SSQ score:

$$SSQ = SSQ_{post} - SSQ_{pre} \tag{4.5}$$

and similarly, the variation of reconstruction error, that we will call from now the loss L, was computed by finding the difference between the average of the last five minimized pre-exposure reconstruction losses and the average of the initial five post-exposure reconstruction losses (we chose to take five values

[2]https://www.tensorflow.org

in each reconstruction loss to get a representative loss considering the instabilities and oscillations during the deep learning process):

$$L = \frac{1}{5}\left|\sum_{j=1}^{5} E - \sum_{k=N_L-5}^{N_L} \arg\min_{w} \mathcal{L}\right| \tag{4.6}$$

where E and $\arg\min_w \mathcal{L}$ were defined in Equation 4.4 and Equation 4.3 respectively; N_L is the length of the trained reconstruction error.

Figure 4.7 shows the reconstruction losses for one participant provided by the normal state sway signal (pre-exposure, blue curve) and the post-exposure sway signal (green curve). We splitted the normal state signal into small pieces (one signal with length of 2048 to 32 signals with length of 64) as a pre-processing step to train the model. We can observe the changes of the reconstruction loss during the training stage (80% of the signal pieces) and the evaluation stage; a validation loss (20% of the signal pieces) was also plotted to make sure that there was no overfitting with the dropout method. The procedure started from epoch 0 (an epoch corresponds to the period of an entire processed dataset) with an initial reconstruction loss of around 0.576 that was due to the random initialization of the deep neural network. The loss then decreased significantly as the epoch evolves, then it converged to a stable value. The training stage stoped at epoch 1000 as the reconstruction error was stable enough, at around 0.184. The model can be deployed subsequently for the evaluation stage where the model was fed with the signal obtained after the user was exposed to the VE. The green curve starting after the 1000 epoch was to demonstrate how the loss would evolve if the model continued to learn the feature of the post-exposure signal, although only the first five points of the curve interested us. As the model had never been trained to recognize a signal obtained from post-exposure in the VE, it was impossible to extract the features. Accordingly, we observed a significant reconstruction error at around 0.564, indicating that the model failed to reconstruct the signal. The jump of error and the first five values of the post-exposure reconstruction error were the only parts that interest us, as it showed that an abnormal signal was detected, i.e., an equivalent description of cybersickness occurs. In this example, the jump of loss L is 0.385 and corresponding measured SSQ score was equal to 7.48.

Since all the participants performed the experiment twice, we collected 22 groups of data to be correlated. Table 4.1 shows the correlation matrix that was obtained by computing the Pearson correlation coefficients between all the measured variables, and after decomposing the SSQ score into the three categories (nausea, oculomotor, disorientation). We saw that the Pearson correlation

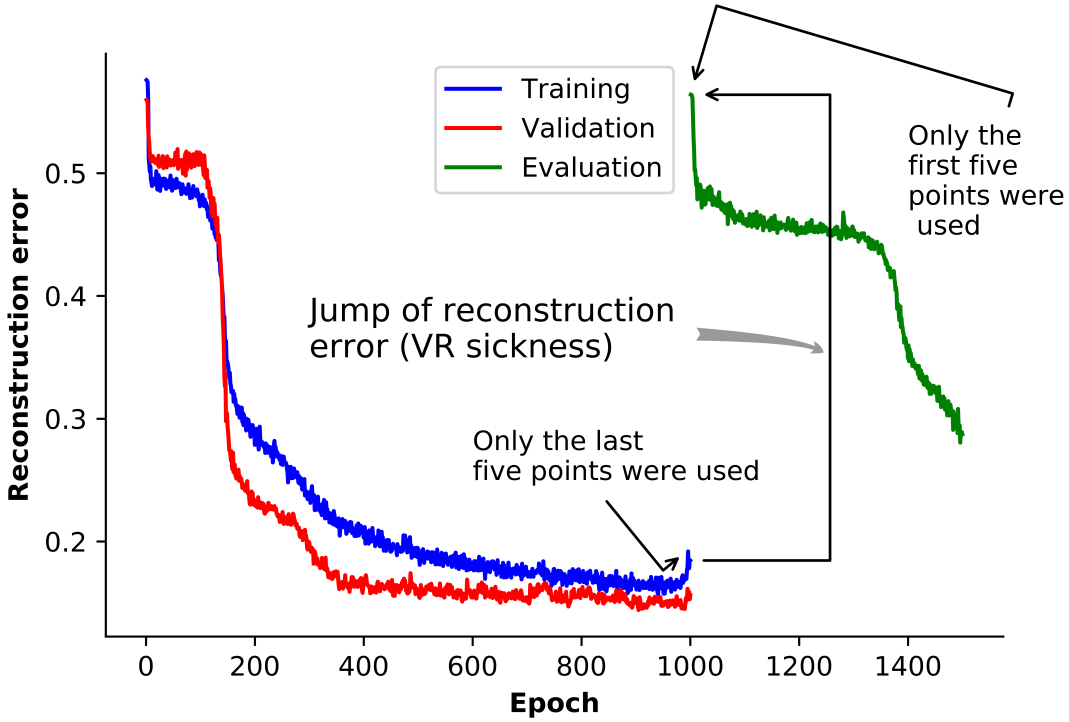

Figure 4.7: Demonstration of the proposed method to detect VR sickness from the signals of one participant.

coefficient is $r = .89$ between the SSQ score and the loss. The correlation between the loss and nausea is .75, the correlation between the loss and oculomotor was .77, and the correlation between the loss and disorientation was .84. All these correlation values ranged from .6 to .9, $p < .05$ which implied that our new method had enough accuracy to be effective. Figure 4.8 shows the correlation obtained between the SSQ scores and the losses. The loss is scattered along a regression line, implying the correlation matrix of Table 4.1. It suggested that the loss can be an effective method to capture the user's VR sickness level. However, we also found that this method became deficient when the SSQ score was too large, more than 120.

4.1.5 Prediction of cybersickness with a closed-loop system

We separated the experiment into "pre-exposure" and "post-exposure" with two distinct measurements in the previous section. We wanted to carry out a correlation test with the SSQ to validate the model's reliability. However, from the results, since we found a strong correlation between the loss

Table 4.1: Correlation matrix

	Loss	SSQ	Nausea	Oculomotor	Disorientation
Loss	1.00	⋱	⋯	⋯	⋯
SSQ	.89	1.00	⋱	⋱	⋮
Nausea	.75	.90	1.00	⋱	⋮
Oculomotor	.77	.87	.70	1.00	⋱
Disorientation	.84	.86	.68	.61	1.00

and the SSQ score, it is also possible to develop an online system with the proposed method without interrupting the experiment. Figure 4.9 shows the architecture of a real-time implementation of the system. The system consists of two steps, but only the second step is implemented as a closed-loop:

1. The user has to take the HMD on and get immersed in the VE. In order to collect normal

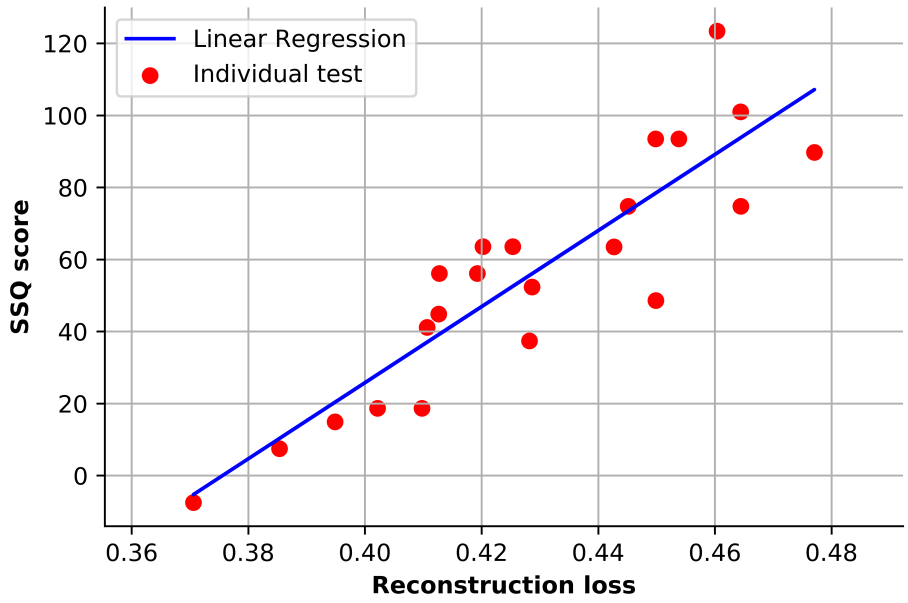

Figure 4.8: Correlation between the SSQ score and the loss computed from the model, regression line: $y = 1062.94x - 399.24$; the point $(0.385, 7.48)$ corresponds to the participant mentioned in Figure 4.7.

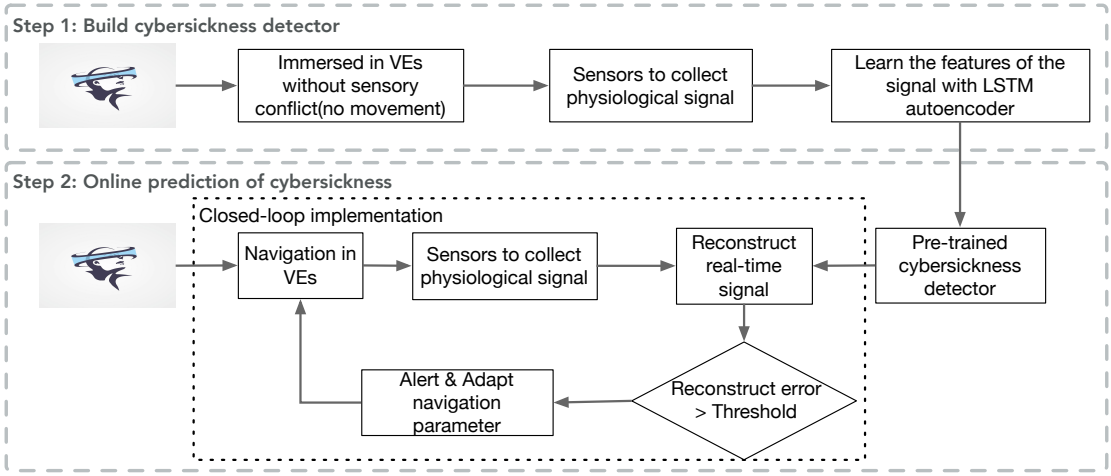

Figure 4.9: Schematic process of the proposed closed-loop system for navigation in VEs including a cybersickness detector: the first step is to collect signals to train the model network and the second step allows to deploy the pre-trained detector in a real application.

physiological signals (no VR sickness felt as at this stage there will no visual vection), she/he just has to stay in place without navigating, avoiding any occurrence of cybersickness. In addition, the signal can also be collected without getting immersed in the VE, which also makes sure that the user produces absolutely normal physiological signals. In either case, the user should not feel VR sickness during this stage so that the model can characterize the normal state. After the data acquisition, the LSTM model (also named cybersickness detector) can be trained to learn the features of the input signals.

2. The pre-trained model is deployed in the navigation system. Sensors keep tracking the user's physiological signals and send the information to the cybersickness detector, which will calculate online the reconstruction loss. If the reconstruction loss is larger than a pre-defined threshold, then the system detects VR sickness successfully; the system can then alert the user or adapt navigation parameters according to the detector. This step is a closed-loop implementation that shall improve efficiency and user experience significantly.

4.1.6 Conclusion

We proposed a new metric where we took into account dynamic information of the postural sway signal and extracted its features using a long short term memory (LSTM) encoder; then, the level

of VR sickness was measured according to the reconstruction error from the LSTM network. This method included two steps in terms of implementation: firstly, to train the network with signals from the VR user's normal state and then deploy the pre-trained model on a VR application. Since the model is designed to learn the features when the user does not feel any VR sickness, it can detect and alert abnormal signals obtained when the user is in another physiological state and feels VR sickness. As we trained the model for each user independently, the model was customized individually. The reliability of the network prediction was validated with the SSQ score. It achieved high enough Pearson correlation coefficients, meaning that the proposed method can be used in personalized VR navigation to detect cybersickness with real-time performance.

4.2 Prediction of cybersickness with human factors

4.2.1 Introduction

This section aims to develop fuzzy models including the fuzzy inference system (FIS) and Adaptive neuro-fuzzy inference system (ANFIS) to predict the susceptibility to cybersickness arising from immersive virtual navigation based on individual differences (e.g., age, gaming experience and ethnicity), enabling VR application designers to set navigation parameters that can provide a user-customized experience. The novelties of this work are summarized as follows:

- Using a model-based FIS approach by integrating existing knowledge from the literature, we can have an overall understanding of the proneness to simulator sickness depending on explicit individual differences.
- Using a data-driven ANFIS approach, we can get rid of the literature knowledge but still extract knowledge from input-output datasets to predict an overall tendency to simulator sickness, which proved to have better performance than with the FIS approach.
- Our work opens the possibility to design adaptive VR applications based on individual characteristics.

In this section, we first presented the approach to fuse knowledge from the current literature, based on the FIS and neural network algorithms, which can infer the quantized cybersickness indicator; next,

we validated its reliability. In the long term, we intended to develop a customized navigation interface by deploying such an indicator so that a VR system could better adapt to users. Our choice for fuzzy logic was because numberless regression techniques are data-driven models that can predict individual susceptibility to cybersickness. However, they are not suitable for the current situation. Fuzzy logic models are formulated from existing rules or learned from data to formulate the rules, enabling researchers to apply expert knowledge to an application. At the same time, regression techniques are only nonlinear fitting of data correlation. Also, regression techniques rely heavily on the dataset's quality, which is a challenge and cannot make the most of prior information based on expert knowledge. We argued that prior expert knowledge, accumulated over decades of intense research, should not be dismissed and ignored.

4.2.2 Fuzzy Inference Systems

A fuzzy inference system (FIS) is a nonlinear mapping which deduces outputs according to fuzzy reasoning and a class of fuzzy if-then rules. FIS is primarily applied to situations where either the expression about the investigated problems is vague and uncertain or the systems are difficult to be exactly modeled (Z. Yang *et al.* 2011). FIS relies heavily on the knowledge and experience from professional and domain experts, and therefore it is hard to attain satisfactory outcomes if enough prior information is lacking (Y.-S. Chen *et al.* 2016; Benmouiza and Cheknane 2019). The structure of a FIS is depicted in Figure 4.10. The database defines membership functions (MFs) used to partition linguistic variables (small, middle, large, and so on), and then, the inference engine carries out a reasoning procedure based on the fuzzy rules and given inputs to determine a reasonable output or consequence. In this work, as the correlation between influence factors and cybersickness can be acquainted with domain experts or past literature, FIS can include this knowledge naturally and predict cybersickness conveniently.

The literature reports three types of FIS: Mamdani-type, Sugeno-type and Tsukamoto-type (J.-S. R. Jang and Sun 1996). Our work here will use the Mamdani-type and the Sugeno-type models. The Mamdani-type system needs to find the centroid of a composed MF by integrating across a continuously varying function. The Sugeno-type system uses a singleton (constant value or linear mathematical functions) as the MF of the rule consequent (J.-S. R. Jang and Sun 1996). The Mamdani method is advantageous to utilize expert knowledge in a more intuitive and human-like manner despite sub-

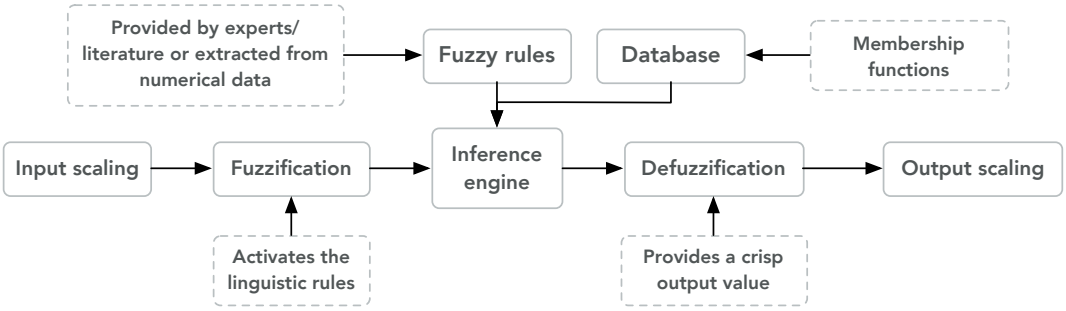

Figure 4.10: Block diagram for a fuzzy inference system.

stantial computational burden, while the Sugeno method is computationally beneficial and works well with optimization and adaptive techniques.

On the other hand, the ANFIS is a hybrid method that incorporates the benefits of both FIS and artificial neural networks (ANN) to derive the fuzzy if-then rules with suitable MFs acquired from numerical data (J.-S. Jang 1993). The main advantage of ANFIS is to automatically determine the optimal parameters of FIS from data instead of using prior knowledge and information from experts or past literature. This is achieved thanks to the strong learning ability of ANN, so that optimizing the unknown parameters with the input-output data sets is workable, and the optimization of these parameters during the training process is carried out to minimize the error between the predicted output and the actual output (Goyal *et al.* 2014). The parameters optimized by ANFIS consist of the premise parameters that represent the shape of the MFs, and the consequent parameters that illustrate the comprehensive output of ANFIS (Srisaeng *et al.* 2015). With these optimal parameters, ANFIS can be deployed to predict or estimate the output with new inputs. Back to Figure 4.10, when the fuzzy rules are constructed with experts or literature knowledge, FIS is commonly referred as Mamdani-type system, and when the fuzzy rules are derived from numerical data, FIS is noted as ANFIS.

FIS has been employed in various computer-human interface (CHI) areas to develop subject-dependent systems. Wu *et al.* (2010) suggested including linguistic rules instead of precise functions to model uncertainties, and also to create fuzzy rule-based controllers to describe the user's affective or cognitive state. Ota *et al.* (1995) proposed applying rule-based fuzzy logic to measure the competence and surgical skills of the trainee of a VR educational simulator, and this evaluation can be conducted together with the teaching session.

There exist also many studies based on fuzzy logic to support adaptive systems. Cueva-Fernandez *et al.* (2016). presented an adaptive speed interface for users to create software applications in the automotive context only with their voice. The interface can suit the user's level of experience based on fuzzy rules. With seven fuzzy rules considering ten characteristics, they computed a single output: the level of expertise and concentration of the user, i.e., beginner, intermediate, or advanced; then the system presents a higher or lower level of options and information depending on the user's level. Nyongesa *et al.* (2003) developed a fuzzy logic-based approach for webpage adaptation to improve users' shopping experience. As fuzzy logic can help analyze ambiguous presentations of shopping activities, much information such as purchase frequency, last purchase time and product presentation is obtained from users to facilitate interface personalization and adaptation. Hamam *et al.* (2008) proposed a taxonomy for measuring a haptic VR application's experience quality based on the Mamdani-type FIS. Their model contained five inputs (media synchronization, quality of perception, haptic rendering, degree of immersion, user satisfaction) described in a linguistic scale and presented by different MFs, and the fuzzy logic infers the quality of experience using the output: intolerable, unacceptable, average, excellent, and perfect.

4.2.3 Model Architecture

Many individual factors can affect the susceptibility to cybersickness, but, as an exploratory study, we focused on *Age*, *Gaming experience* and *Ethnicity* at this stage, because we can obtain this information easily through questionnaires and fuzzify them straightforward through MFs. It should be noted that the correlation between these factors and cybersickness was summarized from the literature, and in this work, we accepted their findings as they were, which was a premise of our fuzzy logic model.

In this section, we briefly presented the Sugeno-type ANFIS and Mamdani-type FIS methods. Their implementation is detailed clearly in the MATLAB fuzzy logic toolbox (*Fuzzy Logic Toolbox: User's Guide (R2020a)* 2020).

4.2.3.1 Sugeno-type ANFIS architecture

The architecture of ANFIS used in this study is illustrated in Figure 4.11. The system starts with three inputs, x, y and z, representing *Age*, *Gaming experience* and *Ethnicity*, respectively. The MF $O_{1,i}$ implies the degree to which the given t belongs to a quantifier, for example, little, middle and

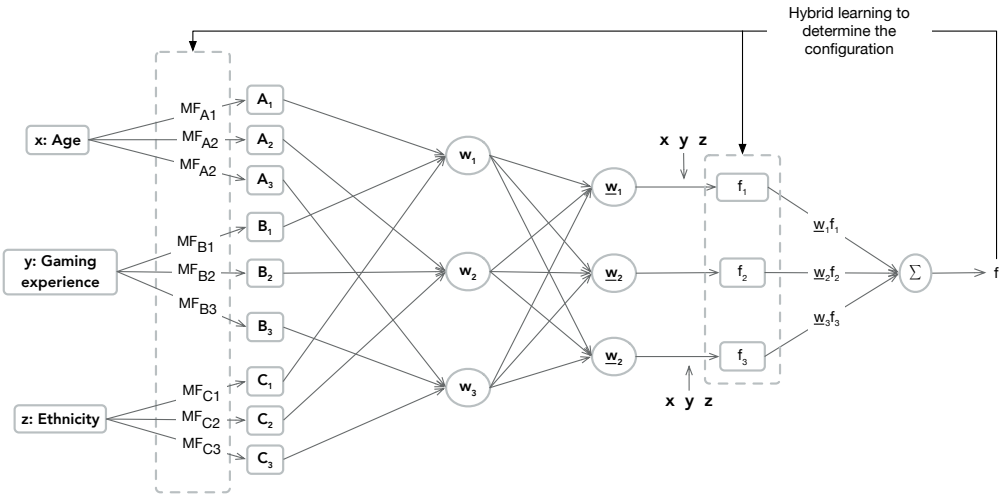

Figure 4.11: Adaptive neuro-fuzzy inference system architecture; note that the MFs and consequent functions are determined by expert knowledge in FIS, which is the main difference between ANFIS and FIS.

high. The MFs are minimum equal to 0 and maximum equal to 1. Some MFs, such as triangular, trapezoidal and Gaussian, are qualified to use, but the most common is the Gaussian bell-shaped function, given as,

$$MF(t) = \frac{1}{1 + (\frac{t-c_i}{a_i})^{2b_i}} \tag{4.7}$$

where a_i, b_i and c_i are the premise parameters to be optimized through the learning algorithm. When changing their values, the bell-shaped functions vary consequently, displaying various configurations of MFs.

Then the rule base embraces three fuzzy if-then rules of the Sugeno-type (Takagi and Sugeno 1983),

Rule 1: If x is A_1, y is B_1 and z is C_1, then $f_1 = p_1x + q_1y + r_1z + s_1$

Rule 2: If x is A_2, y is B_2 and z is C_2, then $f_2 = p_2x + q_2y + r_2z + s_2$

Rule 3: If x is A_3, y is B_3 and z is C_3, then $f_3 = p_3x + q_3y + r_3z + s_3$

MF_{Ai}, MF_{Bi}, MF_{Ci}, f_i are parameterized functions, $i = 1, 2, 3$. The purpose of the neural network is to adapt the premise parameters for MF_{Ai}, MF_{Bi}, MF_{Ci} and the consequent parameters (p_i, q_i, r_i and s_i for f_i. The optimal settings of these parameters are searched through a hybrid learning algorithm to minimize the error between the observed and predicted outputs. The bell-shaped functions vary as

the values change, displaying various configurations of MFs. A detailed explanation about the ANFIS architecture and related examples can be found in (J.-S. Jang 1993; Y.-S. Chen *et al.* 2016; Şahin and Erol 2017).

4.2.3.2 Knowledge-based Mamdani-type FIS architecture

In the ANFIS model (Figure 4.11), the if-else rules should be constructed through the learning algorithm by adapting the parameters of the Gaussian bell-shaped function, while in the FIS model, instead of obtaining the configuration of the MFs and consequent functions through optimization, we can define them by summarizing from the existing literature directly. The consequent function in FIS is also represented by an MF. According to the effects of age, gaming experience and ethnicity reported in Section 2.2.1 and considering that in our database, participants were higher than 12 years old and included primarily Asian and European populations, we could design the following fuzzy if-else rules,

- – If the age is low, the level of cybersickness is high
  - – If the age is middle, the level of cybersickness is middle
  - – If the age is high, the level of cybersickness is low
- – If the gaming experience is little, the level of cybersickness is high
  - – If the gaming experience is middle, the level of cybersickness is middle
  - – If the gaming experience is high, the level of cybersickness is low
- – If the ethnicity is Asian, the level of cybersickness is high
  - – If the ethnicity is a miscegenation between European and Asian, the level of cybersickness is middle
  - – If the ethnicity is European, the level of cybersickness is low

FIS relies on these predefined fuzzy rules as premises to construct the inference system. The Mamdani-type FIS is regarded as a knowledge-based system, since predefined if-else rules based on human knowledge from the experts or references are of great importance for this architecture. A detailed computing process is given in (J.-S. R. Jang and Sun 1996).

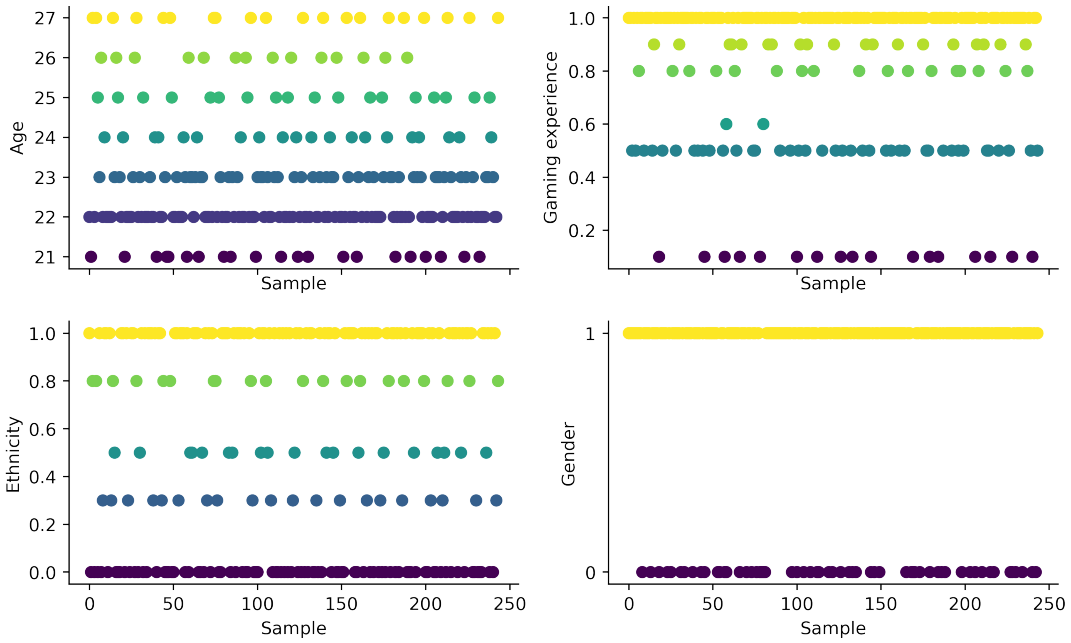

Figure 4.12: Individual characteristics of each sample, including *Age*, *Gaming experience*, *Ethnicity* and *Gender*.

4.2.3.3 Sampled data

From our past studies (performed in the same condition) related to cybersickness, we accumulated 270 samples among which 26 samples were not included since the associated participants did not finish the test. Each sample consists of age, gaming experience, ethnicity, and cybersickness levels. Figure 4.12 presents the individual characteristics of each sample from which we can observe the distribution. For the convenience of notation, the *Ethnicity* value of the Asians was assigned to 0 while that of the Caucasians was 1. To our knowledge, we did not found any ethnic effects for participants from another ethnicity. Therefore, an *Ethnicity* value between 0 and 1 was selected considering their ancestors. Each sample's characteristics are scattered uniformly in the given range, which can help avoid data bias in the validation.

The experimental steps to collect data are illustrated in Figure 4.13. First, the participants signed a consent form, and they were given instructions about what they were asked to do in the virtual environment and how to control their navigation with an HTC Vive hand controller or a Flystick controller in a CAVE system. Before the task started, participants had to fill a questionnaire about their health condition and information about age, gaming experience and ethnicity; they also had

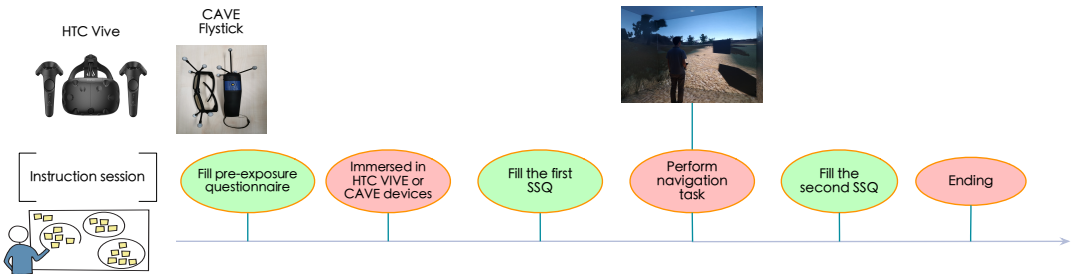

Figure 4.13: Experimental procedure conducted to collect data.

to fill the Simulator Sickness Questionnaire (SSQ) to record a pre-exposure level of cybersickness. They were allowed to drop out if they felt severe sickness. During the experiment, the participants navigated through the virtual scenario presented in Figure 4.15, inside either an HTC Vive or a 5-sided 4K CAVE system, and using a controller-based navigation technique. All participants had to walk on the same path and navigate for an equal distance as fast as possible, during which they had to frequently accelerate, decelerate or make a turn to avoid obstacles on the path. The aim of these frequent changes in speed was to induce VR sickness easily. Each test lasted around 5.5 minutes on average. Because of the visual stimuli displayed to the participants, they could experience sickness symptoms. Hence, a second SSQ was requested to be filled after finishing the task in the immersive environment. The SSQ score was measured as the difference between the post- and pre-exposure questionnaires. The distribution of the SSQ scores resulting from the experiment for each sample is depicted in Figure 4.14.

A preprocessing of the data was performed to convert the linguistic answers in the questionnaires to a crisp value that will constitute the input of the proposed fuzzy models. For example, “Caucasian” was assigned a value of 1 while “Asian” was assigned a value of 0.

4.2.4 Validation of the proposed methods

According to a given *Age*, *Gaming experience* and *Ethnicity*, FIS and ANFIS are supposed to predict the proneness to cybersickness, and we noted the proneness as O_{fis} and O_{anfis}, respectively. During the validation, we expected to find an effective correlation between the predicted proneness and the ground truth simulator sickness questionnaire (SSQ) score. We made the following hypotheses,

- O_{fis} is correlated with the SSQ score

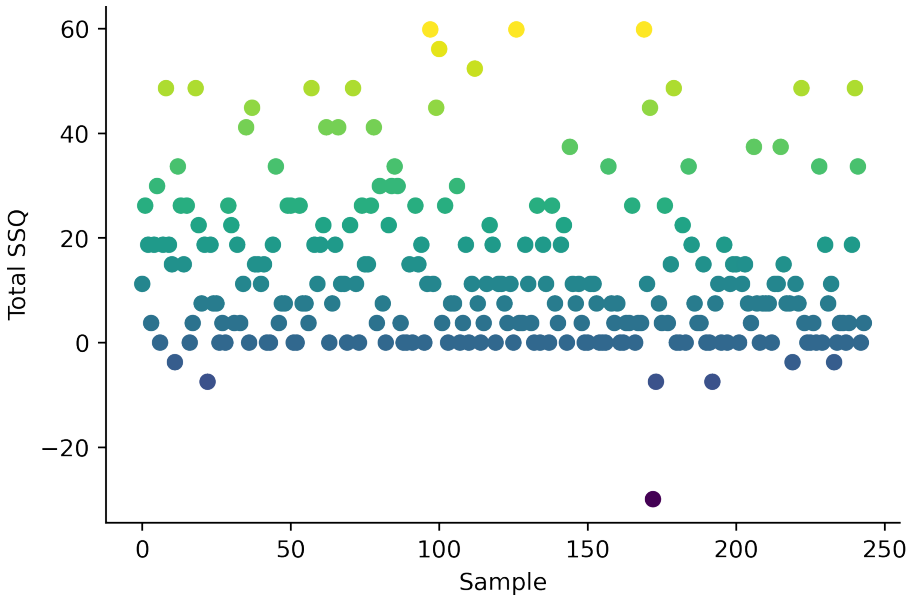

Figure 4.14: SSQ score with respect to each sample in Figure 4.12.

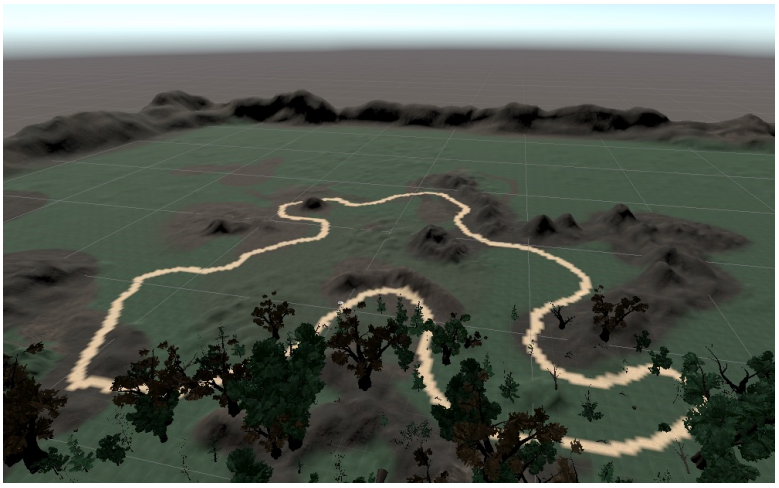

Figure 4.15: View of the virtual scenario in which the user had to navigate through the path.

- O_{anfis} is correlated with the SSQ score

Note that we were interested in the SSQ score rather than its sub-scales (Nausea, Oculomotor, Disorientation) because we did not found enough expert knowledge from previous studies to link these sub-scale scores to individual characteristics.

Figure 4.16: Example of a 4-fold cross validation: the data is split into four folds and in each division, the model is built with three folds and validated with one fold; the overall performance is obtained by computing the arithmetic mean.

4.2.4.1 Principle of validation

Our validation relied mainly on theoretical aspects at the current stage. Performance validations were carried out based on the correlation coefficient and a k-fold cross-validation. We will highlight the related concepts and explain why our architectures are reliable.

The correlation coefficient r between two variables is represented by a value ranging from -1 to 1, where a value of zero indicates the strongest disagreement and ± 1 reveals a perfect fit and agreement (Taylor 1990). With the correlation coefficient, we expected to see how much the output from fuzzy models can be associated with the SSQ, and if the fuzzy models worked well to composite individual differences, we would get a proper value of r between the composite value and the SSQ.

The k-fold cross-validation (Picard and Cook 1984) is a statistical method to assess the performance of machine learning models on unseen data. This model is easy to handle and implement with lower bias than other methods (Bengio and Grandvalet 2004). The procedure contains a single parameter k indicating the number of sets that the assigned data is divided into around equal size. Every set is sequentially used to test the model constructed from $k-1$ training sets. Figure 4.16 shows the validation process for a $k = 4$-fold cross-validation. In ANFIS, we implemented a 4-fold cross-validation method to validate the outputs' reliability: 3-fold of data for training the ANFIS model and the remaining fold of data for computing the correlation coefficient. In Mamdani-type FIS, since there is no training process, we computed each fold of data's correlation coefficient and took their average as the mean correlation coefficient.

Table 4.2: Correlation coefficients and p-values between inputs and Mamdani-type FIS outputs

	O_{fis}		Ethnicity		Age		Gaming experience		SSQ	
	correlation	p-value	correlation	p-value	correlation	p-value	correlation	p-value	correlation	p-value
O_{fis}	1	⋱	⋱	⋱	⋱	⋱	⋱	⋱	⋱	⋱
Ethnicity	-0.736	0.005	1	⋱	⋱	⋱	⋱	⋱	⋱	⋱
Age	0.215	0.114	-0.1626	0.359	1	⋱	⋱	⋱	⋱	⋱
Gaming experience	-0.509	0.001	0.030	0.439	-0.371	0.009	1	⋱	⋱	⋱
SSQ	0.438	0.029	-0.238	0.297	-0.048	0.545	-0.367	0.022	1	⋱

Table 4.3: Correlation coefficients and p-values between inputs and ANFIS outputs

	O_{anfis}		Ethnicity		Age		Gaming experience		SSQ	
	correlation	p-value	correlation	p-value	correlation	p-value	correlation	p-value	correlation	p-value
O_{anfis}	1	⋱	⋱	⋱	⋱	⋱	⋱	⋱	⋱	⋱
Ethnicity	-0.365	0.005	1	⋱	⋱	⋱	⋱	⋱	⋱	⋱
Age	-0.078	0.596	-0.163	0.359	1	⋱	⋱	⋱	⋱	⋱
Gaming experience	-0.573	0.001	0.030	0.439	-0.371	0.009	1	⋱	⋱	⋱
SSQ	0.624	0.001	-0.238	0.297	-0.048	0.545	-0.367	0.022	1	⋱

4.2.4.2 Correlation between Mamdani-type FIS outputs and SSQ

Table 4.2 contains the correlation coefficients among individual factors, the level of cybersickness (i.e., the SSQ score) and the Mamdani-type FIS output (i.e., O_{fis}), and the p-value associated with each correlation coefficient aside to show the statistical power. If our assumption was true, the correlation between the SSQ score and individual differences should be congruent with the correlation between O_{fis} and individual differences. The significance level in this work was set to .05.

A significant negative correlation was observed between O_{fis} and *Ethnicity* ($r_{59} = -.736$, $p < .01$) and *Gaming experience* ($r_{59} = -.509$, $p < .01$), while the correlation between O_{fis} and *Age* was very weak, $r_{59} = .215$, $p = .114$. The negative symbol validated the if-else rules for the effect of *Ethnicity* and *Gaming experience*, but the if-else rule for the effect of *Age* needed further investigation.

The SSQ score illustrated a similar trend as O_{fis} in terms of correlation with other factors, but only the correlation between SSQ and *Gaming experience* was significant, $r_{59} = -.367$, $p = .022$. The correlations between SSQ and *Ethnicity* ($r_{59} = -.238$, $p = .297$), and between SSQ and *Age* ($r_{59} = -.048$, $p = .545$) did not demonstrate any significance. Last, O_{fis} and SSQ were found to be significantly correlated, $r_{59} = .438$, $p = .029$.

4.2.4.3 Correlation between ANFIS outputs and SSQ

Under the same statistical approach and data splitting, Table 4.3 reports the correlation coefficients among individual factors, the SSQ score and the ANFIS output (i.e., O_{anfis}), and the corresponding p-value for each correlation coefficient. Since the correlation between SSQ and other individual factors has been reported in Table 4.2, these values did not change in Table 4.3. Therefore we focused on reporting the correlations between O_{anfis} and the related individual factors.

A significant negative correlation was observed between O_{anfis} and *Ethnicity* ($r_{59} = -.363$, $p < .01$) and *Gaming experience* ($r_{59} = -.573$, $p < .01$), while the correlation between O_{anfis} and *Age* was not significant, $r_{59} = -.078$, $p = .596$. Similarly, O_{anfis} was inversely correlated with *Ethnicity* and *Gaming experience*, which was also consistent with the respective if-else rules developed in the previous section. O_{anfis} and SSQ were found to be better correlated compared with the Mamdani-type output, $r_{59} = .624$, $p < .01$.

4.2.5 Discussion

This study aimed to find a way to composite individual factors to predict the susceptibility to cybersickness, and we proposed our approach with fuzzy logic. With predefined if-else rules and data learned features, the outputs of FIS and ANFIS demonstrated significant correlations with the SSQ. The FIS and ANFIS architectures were formulated differently, but it validated both architectures and the feasibility of our proposal that VR developers could use fuzzy logic to involve individual factors during the design of navigation interfaces.

Many individual factors can affect the proneness to cybersickness (LaViola Jr 2000; Weech *et al.* 2019), but the models comprised only three factors (*Ethnicity*, *Age* and *Gaming experience*), which might be the reason why the correlation magnitude was moderate, .438 for the Mamdani-type FIS and .624 for ANFIS. Thanks to the scalability of FIS and ANFIS, we can introduce additional factors to characterize cybersickness more precisely. To introduce new factors into the Mamdani-type FIS, we need to provide clearly the if-else rules for this factor.

Simultaneously, ANFIS can automatically construct the if-else rules based on the fed data. Depending on the situation, if we knew the potential effect of such factor on the susceptibility to cybersickness, we could apply the Mamdani-type FIS model; otherwise, the data-driven ANFIS can be an

advantageous alternative. However, we cannot add an arbitrary factor to this model. Fuzzy logic is a computing method based on the "degree of truth" instead of the usual "true or false" (1 or 0) Boolean logic. The membership function expresses the degree of truth. For example, when participants are asked to report their gender, two choices are usually proposed in past studies, male or female, which is not fuzzy but Boolean logic.

As we involved three human factors and an SSQ score in our dataset, the dataset reliability validation should find some correlations among these factors. However, only a correlation between SSQ and the *Gaming experience* reported from our dataset ($r_{59} = -0.367, p = .022$) was close to the one reported in (Iskenderova *et al.* 2017) ($r_{31} = -0.38$, $p = .04$). The absence of significant correlations between SSQ and *Ethnicity* and between SSQ and *Age* might be due to the lack of enough participants with different ethnicity and ages. According to past literature (L. Harm 1990a; Kolasinski 1995), *Age* is supposed to be an influential factor that affects the level of cybersickness. However, ANFIS also did not find any significant effect of *Age* despite its learning ability, and such insignificance was also observed from the Mamdani-type FIS output. This finding needed to be interpreted with similar caution: the *Age* of the participants considered here ranged from 18 to 35, which only covered a small range of age, and a further study with participants from the adolescent to the elderly might provide more substantial support. As a cybersickness predictor, O_{fis} or O_{anfis} were significantly correlated with *Ethnicity* and *Gaming experience* whereas SSQ was not. Reasons might be that the SSQ value from the questionnaires could contain unreliable, ambiguous and arbitrary emotional feedback (Katicic *et al.* 2015b). Instead, O_{fis} or O_{anfis} derived from either Mamdani-type FIS or ANFIS can avoid noisy information and strongly link to both sides (SSQ and individual factors).

We presented two strategies to integrate individual factors to propose a cybersickness indicator. With existing knowledge about the effect of personal characteristics, FIS could alleviate the amount of data required to produce a successful estimation of cybersickness, keeping the consumption of data to a minimum, as data are expensive to produce and obtain. On the other hand, with the available data, ANFIS proved to have better performance than FIS because ANFIS can learn and extract features from numerical data. Theoretically, artificial neural network (ANN) or other regression approaches can also learn the feature actively from the data to associate individual attributes with the level of cybersickness. It is also important to distinguish between a regression problem and a fuzzy logic problem: a regression problem aims to find the unknown correlation among variables, but the

fuzzy logic method will take advantage of existing correlation (i.e., expert knowledge) for prediction. Additionally, there are many studies comparing their performance, suggesting that both approaches could present competitive achievement if fine-tuned (Khoshnevisan *et al.* 2014; Şahin and Erol 2017). However, this section aims to engage individual differences into VR navigation systems. We preferred to use the fuzzy logic method because it can utilize prior expert knowledge naturally without using any data.

4.2.6 Conclusion

The aim of this section is to engage individual differences into VR navigation systems to predict cybersickness occurrences and severity, and we opted for fuzzy logic methods since they can be naturally connected with existing knowledge. We devised a strategy to composite existing knowledge about the effect of individual factors on cybersickness, and we demonstrated significant correlations between the composited value from fuzzy logic and the level of cybersickness as measured by SSQs.

We involved only three individual factors (age, ethnicity and gaming experience) in this study, which lowered the magnitude of the observed correlations, however the significance of these values assessed the reliability of the cybersickness indicator predicted by fuzzy logic. Other individual characteristics, such as physical illness, controllability of postural stability, visual acuity, personal traits and emotional states, can be easily integrated in FIS thanks to its scalable architecture, which may further strengthen the reliability of the proposed model. In chapter 5 , we will carry out user experiments on a VR platform in which the navigation interface can be adapted according to the output of fuzzy logic.

4.3 Enhanced cognitive workload evaluation

4.3.1 Introduction

We have proposed evaluation methods for cybersickness, either with postural sway signals, or with individual factors. As analyzed in chapter 2, cognitive workload is another important experience when performing tasks in virtual environments, but current evaluations of cognition through subjective methods are blamed for accuray due to various errors. In this section, we will present an enhanced cognitive workload evaluation method.

This section does not aim to develop a new approach to deduce mathematical operations and equations for measuring cognitive workload, but rather, to improve the precision and quality of current evaluation approaches with existing models. The improvement of precision would enable VR designers and experimenters to better discriminate differences among settings and to optimize their applications easily. The VR domain requires many evaluation methods to obtain user's feedback regarding the interaction design, but the application of appropriate methods ensuring the quality of the feedback in this field is rather scarce, which motivated us to involve TOPSIS and fuzzy AHP to improve the measuring quality of cognitive workload in VR. It is worth noting that the proposed method can be applied not only to VR, but also to any human-computer interaction application for which cognitive load is important to consider.

The proposed model was validated by a user study in subsection 4.3.4: two factors known to influence cognitive workload during a navigation task in a virtual environment are supposed to demonstrate the effectiveness of the TOPSIS method. These factors include the VR platform (HMD and CAVE) and the scenario density. For each of them, the overall workload score was computed by the classical weighted sum method (Hart 2006a) and our TOPSIS model. The overall workload measured from TOPSIS was firstly validated by ensuring consistency of the results with the literature. In addition, compared to the weighted sum method, the TOPSIS model significantly reduced the data dispersion, showing more accurate workload scores.

4.3.2 Methods for computing the cognitive workload scores

Throughout this paper, we will focus on the NASA-TLX table to demonstrate our methodology, since the criteria are well defined and widely accepted for the analysis of workload in virtual reality.

4.3.2.1 Weighted sum method

The calculation of the overall workload from the NASA-TLX table consists of two steps. First, participants have to perform a pairwise comparison of the criteria provided in the NASA-TLX table, based on the task they conducted and experienced; for example, if the user thinks that *Mental demand* is more important than *Physical demand*, then the weight of *Mental demand* is incremented by one while that of *Physical demand* remains unchanged. After a total of 15 comparisons, the weighting coefficients for the six criteria are obtained by normalisation. These comparisons are used to determine

the weighting coefficient for each criterion. In the rest of the paper, this weighting coefficient calculation method will be named *Hart*. Second, participants are given another questionnaire to quantify the score for each criterion. The overall workload score is computed as a sum of the scores for each criterion weighted by their respective weighting coefficient (Equation 4.8) (Hart and Staveland 1988; Hart 2006a). Subjective workload evaluation can be completed directly by the participants without any requirement of sophisticated devices, which is nearly straightforward and inexpensive to perform.

$$\begin{aligned} TLX_{Hart} = W_{MD} * MD + W_{PD} * PD + W_{TD} * TD \\ + W_{Pe} * Pe + W_{Ef} Ef + W_{Fr} * Fr \end{aligned} \tag{4.8}$$

TLX_{Hart} is the overall cognitive workload measured by the weighted sum method, W with a subscript is the corresponding weighting coefficient for each criterion.

Past research in many areas reports another approach to process the NASA-TLX table and obtain the cognitive workload score in a straightforward manner: a uniform weight is applied to each criterion (Tubbs-Cooley *et al.* 2018; Kamaraj *et al.* 2016), which means W_{MD}, W_{PD}, W_{TD}, W_{Pe}, W_{Ef} and W_{Fr} are equal to 16.67%. This approach is a particular case of the *Hart* weighting method. However, this approach is not adapted to different situations where the importance of each criterion needs to be differentiated.

4.3.2.2 Fuzzy Analytic Hierarchy Process

In the *Hart* weighting approach, participants have to compare the criteria in pairs to determine which one is more important than the other one. However in practice, the process of comparison and decision making is associated with the strong vagueness of human thinking: decision-makers generally give some or all pairwise comparison values with an uncertainty degree instead of precise ratings, and such uncertainty degree is represented from an appropriate semantic scale (C.-S. Yu 2002; Singh *et al.* 2013). As they usually are unable to explicit about their preference due to the fuzzy nature of the comparison process, decision-makers (VR users in the current context) usually tend to give interval judgments with a semantic scale than a fixed value (Gumus 2009).

To cope with it, mathematicians proposed the fuzzy method in real practice in which an uncertain pair-to-pair comparison exists. Mouzé-Amady *et al.* (2013) proposed a fuzzy integral approach based on the Sugeno integrals to determine the weighting coefficients. The weighting coefficients are

determined with at least one global measure (either a subjective rating or an objective cue, e.g., HRV, reaction time) to serve as an aggregation criterion. Then data-driven models (e.g., minimum specificity principle, simulated annealing technique) are used to find the optimal weighting coefficients and to fit the global criterion. In this approach, the weighting coefficients are no longer set based on the participant's subjective evaluation. To focus on evaluation with only subjective ratings, we will rather use the fuzzy AHP proposed by D.-Y. Chang (1996) to compute the weighting coefficients, as an alternative to the *Hart* weighting approach. Here we briefly described the basic concepts behind the fuzzy AHP. More theoretical details can be found in the literature (D.-Y. Chang 1996).

4.3.2.2.1 Definition of triangular fuzzy numbers Each fuzzy number can be represented by a membership function. A fuzzy number is called a triangular fuzzy number (TFN) when it can be described by the following function $\mu_M(x)$: $\mathbb{R} \to [0, 1]$,

$$\mu_M(x) = \begin{cases} \frac{x-l}{m-l} & x \in [l, m] \\ \frac{x-u}{m-u} & x \in [m, u] \\ 0 & otherwise \end{cases} \tag{4.9}$$

where $l \leq m \leq u$, l, m, u are the lower, modal and upper values of the TFN. This function is called the membership function.

The TFN has some pre-defined arithmetic operators. If $M_1 = (l_1, m_1, u_1)$ and $M_2 = (l_2, m_2, u_2)$ are two TFNs, the operation rules between the two TFNs are given as,

$$\begin{cases} M_1 \oplus M_2 = (l_1 + l_2, m_1 + m_2, u_1 + u_2) & \text{(4.10a)} \\ M_1 \otimes M_2 = (l_1 l_2, m_1 m_2, u_1 u_2) & \text{(4.10b)} \\ \lambda M_1 = (\lambda l_1, \lambda m_1, \lambda u_1) & \text{(4.10c)} \\ M_1^{-1} = (l_1, m_1, u_1)^{-1} \approx (\frac{1}{u_1}, \frac{1}{m_1}, \frac{1}{l_1}) & \text{(4.10d)} \end{cases}$$

where $\oplus$ denotes the extended summation of two TFNs and $\otimes$ denotes the extended multiplication.

4.3.2.2.2 Formulation of a fuzzy synthetic extent analysis Assuming a triangular fuzzy comparison matrix $\widetilde{A} = (a_{ij})_{n \times n}$, the extent analysis first sums up each row of this matrix, then normalizes the row sums with respect to the i^{th} row,

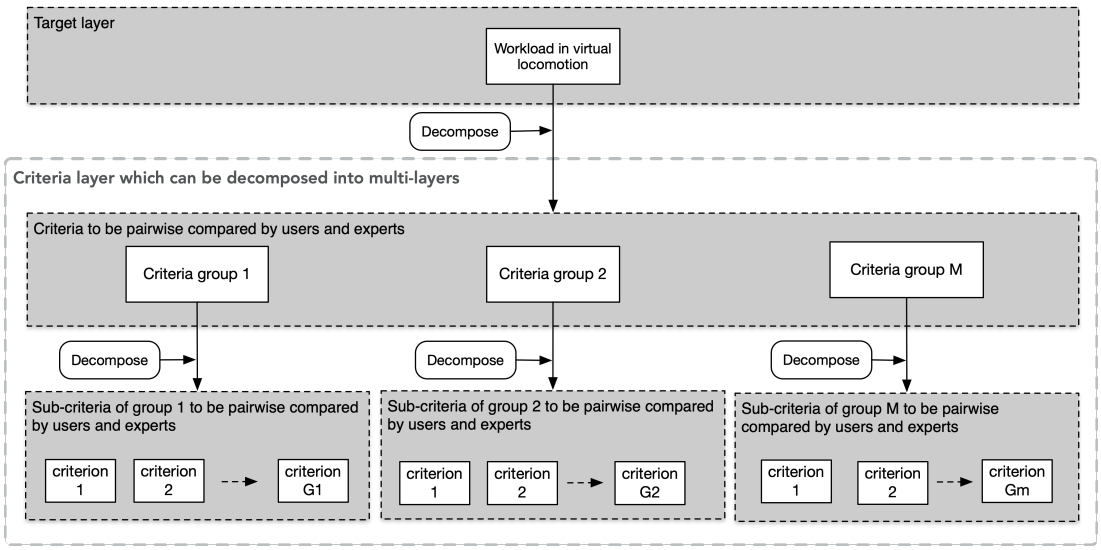

Figure 4.17: General hierarchical structure of workload evaluation; this structure can include related indices from different groups or sources.

$$S_i = \sum_{j=1}^{n} a_{ij} \otimes \left[\sum_{i=1}^{n} \sum_{j=1}^{n} a_{ij} \right]^{-1} \tag{4.11}$$

where $a_{ij} = (l_{ij}, m_{ij}, u_{ij})$ is a triangular fuzzy number. According to the operations rules, S_i is also a triangular fuzzy number.

Given two triangular fuzzy numbers, $S_1 = (l_1, m_1, u_1)$ and $S_2 = (l_2, m_2, u_2)$, the degree of possibility that $S_2 \geq S_1$ is defined as

$$V(S_2 \geq S_1) = \begin{cases} 1 & m_2 \geq m_1 \\ 0 & l_1 \geq u_2 \\ \frac{l_1 - u_2}{(m_2 - u_2) - (m_1 - l_1)} & otherwise \end{cases} \tag{4.12}$$

To compare S_1 and S_2, both values of $V(S_1 \geq S_2)$ and $V(S_2 \geq S_1)$ must be computed. Further, the degree of possibility for a convex fuzzy number S to be larger than k convex fuzzy numbers $S_i, i = 1, 2, ...k$ can be defined by

$$\begin{aligned} & V(S \geq S_1, S_2, ..., S_k) \\ & = V[(S \geq S_1) \text{ and } (S \geq S_2) \text{ and} \\ & ... \text{ and } (S \geq S_k)] = \min V(S \geq S_i) \end{aligned} \tag{4.13}$$

4.3.2.2.3 Procedures to perform a fuzzy AHP analysis

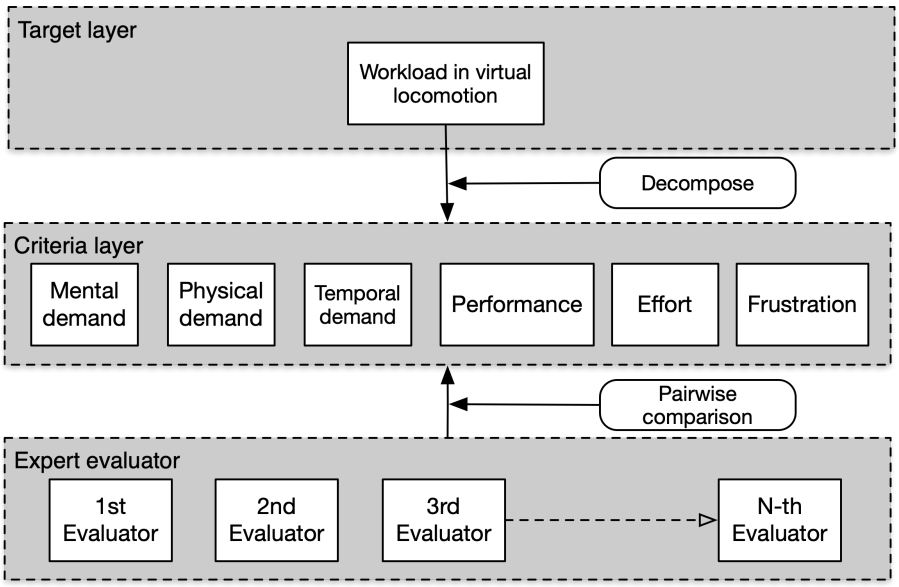

Figure 4.18: A specific case of hierarchical structure to measure workload with the NASA-TLX criteria.

Step 1: Problem analysis and hierarchical structure formulation Following the general procedures used in the AHP method, it is necessary to define factors that affect the goal. For example, a complex problem like workload can be decomposed into many criteria, and each criterion can be decomposed into many sub-criteria which can also be further decomposed (Figure 4.17), as in the NASA-TLX table. It is worth mentioning that the proposed approach can be applied to other workload measurement methods during a simulation experience, and not only to the NASA-TLX, as long as the measuring criteria from multi-groups can be validated. For example, D. Harris *et al.* (2019) propose a simulation task load index (SIM-TLX) where the criteria are introduced by integrating the NASA-TLX, the SURG-TLX and external indexes (Wilson *et al.* 2011). In this case, there are three groups of criteria, and each group has its own sub-criteria that should be placed according to the structure presented in Figure 4.17. And thanks to the hierarchical structure, the total number of comparisons would exponentially reduce despite increasing measuring criteria. In our case, we applied this structure to the NASA-TLX and for a navigation task in a virtual environment; the target or the goal was: which criterion is more important to reduce workload during virtual navigation? Pairwise comparisons are performed for each criterion based on the announced target. The corresponding hierarchical structure is shown in Figure 4.18.

Step 2: Determining the fuzzy linguistic scale When requested to compare or evaluate objects, individuals generally use linguistic expressions such as "very important", "little important", "good" and "bad". These linguistic expressions contain uncertain and fuzzy information that needs to be processed. To best fit subjective evaluations, we adapted pre-defined linguistic expressions from previous studies (Novák and Perfilieva 1999; Hong *et al.* 2018) that relied on the original work of Saaty (1987). Comparative judgment generally uses expressions from a linguistic set $\mathcal{F}$={Equally important, Weakly more important, Strongly more important, Very strongly more important, Absolutely important} that maps a corresponding fuzzy number, as presented in Table 4.4.

Table 4.4: Linguistic rating scales and corresponding fuzzy numbers

Linguistic scales	TFNs
Equally important (EI)	(1, 1, 1)
Weakly more important (WI)	(1, 1, 3/2)
Strongly more important (SI)	(3/2, 2, 5/2)
Very strongly more important (VI)	(5/2, 3, 7/2)
Absolute important (AI)	(7/2, 4, 9/2)

Step 3: Fuzzy comparison using the fuzzy linguistic scale Experienced evaluators are invited to fill a comparison table where they perform pairwise comparisons. Considering NASA-TLX, questions can be "what is the relative importance of criterion $C_i, i = 1, 2, .., p$ compared to $C_j, j = 1, 2, .., p, i \neq j$ to measure cognitive workload during a virtual navigation". The filled comparison table forms a fuzzy comparison matrix, denoted by $\widetilde{C}$,

$$\widetilde{C} = \begin{array}{c} \\ C_1 \\ C_2 \\ C_3 \\ C_4 \\ C_5 \\ C_6 \end{array} \begin{array}{c} \begin{array}{cccccc} C_1 & C_2 & C_3 & C_4 & C_5 & C_6 \end{array} \\ \begin{pmatrix} 1 & c_{12} & c_{13} & c_{14} & c_{15} & c_{16} \\ c_{21} & 1 & c_{23} & c_{24} & c_{25} & c_{26} \\ c_{31} & c_{32} & 1 & c_{34} & c_{35} & c_{36} \\ c_{41} & c_{42} & c_{43} & 1 & c_{45} & c_{46} \\ c_{51} & c_{52} & c_{53} & c_{54} & 1 & c_{56} \\ c_{61} & c_{62} & c_{63} & c_{64} & c_{65} & 1 \end{pmatrix} \end{array} \tag{4.14}$$

where $c_{ij} = \frac{1}{c_{ji}}$, and

$$\begin{cases} c_{ij} = (l_{ij}, m_{ij}, u_{ij}) \\ \frac{1}{c_{ji}} = \left(\frac{1}{u_{ij}}, \frac{1}{m_{ij}}, \frac{1}{l_{ij}}\right) \end{cases} \tag{4.15}$$

An example of matrix is provided in Annex A.1.

Each evaluator provides a fuzzy comparison matrix. The final evaluation matrix $\widetilde{C}^h$ aggregates the responses from all evaluators. Assuming we have H evaluators, we here take the average of all fuzzy comparison matrices,

$$c_{ij} = \left(\frac{1}{H}\sum_{h=1}^{H} l(c_{ij}^h), \frac{1}{H}\sum_{h=1}^{H} m(c_{ij}^h), \frac{1}{H}\sum_{h=1}^{H} u(c_{ij}^h)\right) \tag{4.16}$$

where $l(\cdot)$, $m(\cdot)$ and $u(\cdot)$ are functions to find the lower, modal and upper values of the TFN.

Step 4: Weighting vector determination using the extent analysis With the extent analysis method formulated in Equation 4.11, we are able to describe each criterion with a triangular fuzzy number. In order to determine the weighting vector of the criteria, the principle of comparison of fuzzy numbers must be used.

Assume that $d'(C_i) = \min V(S_i \geq S_j)$ for $j = 1, 2, ...p, i \neq j$, the weighting vector of p criteria is defined as,

$$W' = [d'(C_1), d'(C_2), ..., d'(C_p)]^T \tag{4.17}$$

where $C_i, i = 1, 2, ..., p$ are the criteria. Applying a normalisation operation, the final normalised weighting vector is

$$\begin{aligned} W = &\left[\frac{d'(C_1)}{\sum_{i=1}^{p} d'(C_i)}, \frac{d'(C_2)}{\sum_{i=1}^{p} d'(C_i)}, ..., \frac{d'(C_p)}{\sum_{i=1}^{p} d'(C_i)}\right]^T \\ =&[d(C_1), d(C_2), ..., d(C_p)]^T \end{aligned} \tag{4.18}$$

4.3.3 TOPSIS method

The TOPSIS method proposed by Hwang and K. Yoon (1981) is a comprehensive within-group evaluation method that can make full use of raw data and reflects the gap between the evaluated objects. The basic idea is developed based on normalised original data represented in the matrix form to find the optimal and the worst solutions within a finite set of alternatives. Then, the distance

between each evaluation object and the optimal and the worst solutions is calculated separately, which gives the relative closeness. This value is used as the basis for evaluating the merits and demerits. The method does not strictly rely on the data distribution and sample content, and the calculation process is simple and easy.

4.3.3.1 Data homogenization

The TOPSIS method uses the distance scale to measure the difference among samples. To use the scale, it is necessary to normalise the index attributes in the same manner (e.g., for attribute A, the bigger the number, the better the result, while for attribute B, the smaller the number, the better the outcome. Such inconsistency can lead to inconvenience and confusion for the calculation in the next steps). Usually, a cost-type indicator is converted to a benefit-type indicator (that is, the higher the value, the better the result; in fact, almost all evaluation methods need this step to homogenise the raw data).

4.3.3.2 Construction of the normalised matrix

Let n be the number of objects to be evaluated, each object has m attributes; then the original data matrix is constructed as,

$$X = \begin{pmatrix} x_{1,1} & x_{1,2} & \cdots & x_{1,m} \\ x_{2,1} & x_{2,2} & \cdots & x_{2,m} \\ \vdots & \vdots & \ddots & \vdots \\ x_{n,1} & x_{n,2} & \cdots & x_{n,m} \end{pmatrix} \tag{4.19}$$

To perform dimensionless calculations, we need to construct a weighted canonical matrix in which the attributes are normalised vectors, that is, each column element is divided by the norm of the current column vector (using the cosine distance measure),

$$z_{ij} = \frac{x_{ij}}{\sqrt{\sum_{i=1}^{n} x_{ij}^2}} \tag{4.20}$$

The normalised non-dimensional matrix becomes,

$$Z = \begin{pmatrix} z_{1,1} & z_{1,2} & \cdots & z_{1,m} \\ z_{2,1} & z_{2,2} & \cdots & z_{2,m} \\ \vdots & \vdots & \ddots & \vdots \\ z_{n,1} & z_{n,2} & \cdots & z_{n,m} \end{pmatrix} \tag{4.21}$$

4.3.3.3 Identification of the optimal and the worst solutions

There exist two idealised goals. One is the positive ideal goal or the optimal goal, and the other one is the negative ideal solution or the worst goal. The positive optimal solution Z^+ consists of the maximum value of each column element in Z:

$$Z^+ = \begin{pmatrix} \max(z_{1,1}, z_{2,1}, \cdots, z_{n,1}) \\ \max(z_{1,2}, z_{2,2}, \cdots, z_{n,2}) \\ \vdots \\ \max(z_{1,m}, z_{2,m}, \cdots, z_{n,m}) \end{pmatrix} \tag{4.22}$$

The negative worst solution Z^- consists of the minimum value of each column element in Z:

$$Z^- = \begin{pmatrix} \min(z_{1,1}, z_{2,1}, \cdots, z_{n,1}) \\ \min(z_{1,2}, z_{2,2}, \cdots, z_{n,2}) \\ \vdots \\ \min(z_{1,m}, z_{2,m}, \cdots, z_{n,m}) \end{pmatrix} \tag{4.23}$$

4.3.3.4 Calculation of the separation distance

The TOPSIS algorithm can be easily adapted to process subjective evaluations by considering that the best criterion to evaluate should be the closest to the optimal solution, and the farthest to the worst one. The separation distance is used to measure the distance between the current sample and the optimal/worst solution, and can be defined as the following,

$$\begin{cases} D_i^+ = \sqrt{\sum_{j=1}^{m} w_j (Z_j^+ - z_{i,j})^2} & \text{(4.24a)} \\ D_i^- = \sqrt{\sum_{j=1}^{m} w_j (Z_j^- - z_{i,j})^2} & \text{(4.24b)} \end{cases}$$

where w_j is the weight of the j^{th} attribute (importance) and can be derived from the fuzzy AHP method, *Hart* weighting method, or uniform weighting method.

4.3.3.5 Determination of the relative closeness coefficient

Since the separation distance has two independent values (D_i^+ and D_i^-), to get a unified measurement in one dimension, the relative closeness coefficient (RCC) of each entry is defined as,

$$RCC_i = \frac{D_i^-}{D_i^+ + D_i^-}, \quad RCC_i \in [0, 1] \tag{4.25}$$

When $RCC_i \to 1$, D_i^+ is small and D_i^- is large, it means that the measured object is close to having the best performance. However, depending on how the index attributes are formulated, it may be preferable to have a value of RCC_i close to 0, e.g., if the attributes are homogenised as a cost-type problem.

The performance of each object can be defined by the values of the RCC, ranking from large RCC to small RCC or in reverse order. Applying this principle to our case, a larger RCC value suggests a higher workload. In addition to observing the performance of each object individually, the RCC can be grouped according to the factors tested in the experiment and the difference of RCC can be compared among groups (e.g., HMD vs CAVE).

4.3.3.6 Composed multiple criteria evaluation system

Figure 4.19 presents the whole diagram of the proposed method to evaluate cognitive workload using TOPSIS from the fuzzy AHP and the *Hart* weighting approaches. The framework requires two steps. The first step is to compute the weighting coefficients from either the fuzzy AHP approach, the pairwise comparisons suggested by Hart and Staveland (1988) and Hart (2006a), or the uniform weighting approach. The second step is to use TOPSIS to compute the relative closeness coefficient using the weighting information obtained from the first step.

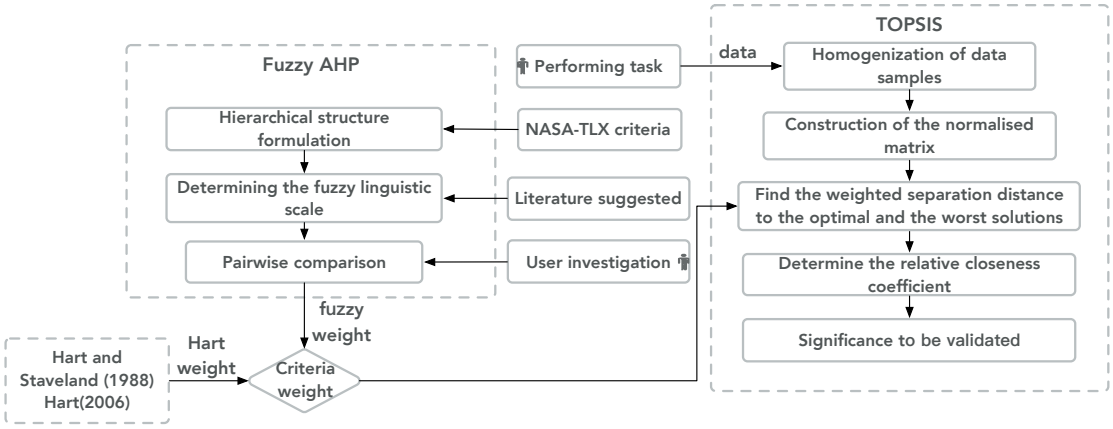

Figure 4.19: Schematic process of the proposed TOPSIS evaluation procedure; the TOPSIS method can use different weighting approaches.

4.3.4 User study

We designed an experiment to investigate the effectiveness of the proposed method to enhance the precision of the cognitive workload evaluation. We applied our tool in a navigation case in a VR application. In this experiment, we considered two factors that encounters in navigation experience in terms of cognitive load: the VR platform type (Sevinc and Berkman 2020) and the scenario density (Parsons *et al.* 2009). Based on this principle, we conducted the experiment to study the effect of these two factors on cognitive workload.

If the proposed methods can measure cognitive workload with the expected performance after a VR task, we shall obtain the following results:

R1 The *RCC* can measure the cognitive workload arising from different VR platforms and scenario densities, with consistent results with the literature

R2 The *RCC* provides more precise information on cognitive workload than the classical weighting sum method.

R1 helps identifying the effectiveness of the proposed method as it could lead to results similar to the other methods and measure cognitive workload successfully. R2 further shows the advantage of this method over the others in terms of data dispersion, represented by the coefficient of variation (CV).

4.3.4.1 Experiment equipment

The experiment was conducted in both a CAVE system and an HTC Vive head-mounted display to compare the effect of different displays on workload. The CAVE system consists of five walls with 4096×2160 px projectors that display stereoscopic images at a refresh frame rate of 120Hz. An in-house interface written in C++ was developed to connect all the devices of the system. On the other hand, the HTC Vive has a display resolution of 2160×1200 px with a refresh rate of 90Hz.

Navigation in virtual environments (forward/backward and left/right movements) was achieved using the joystick of an ART Flystick controller in the CAVE and the touchpad of the Vive controller with the HMD.

4.3.4.2 Participants

We invited fifteen subjects including engineers and students ($M_{age} = 23.1, SD_{age} = 1.82$) from the university to participate voluntarily without any compensation in the experiment. Each of them was given a brief introduction to the experiment and the potential risks that could be encountered. They were allowed to terminate the experiment if they felt strong discomfort. Also, a pre-exposure questionnaire was filled by these participants to gain information about their health condition and background that would be utilised for data analysis if necessary. To minimise random noise, we performed a within-subject test. A consent form was also signed by participants.

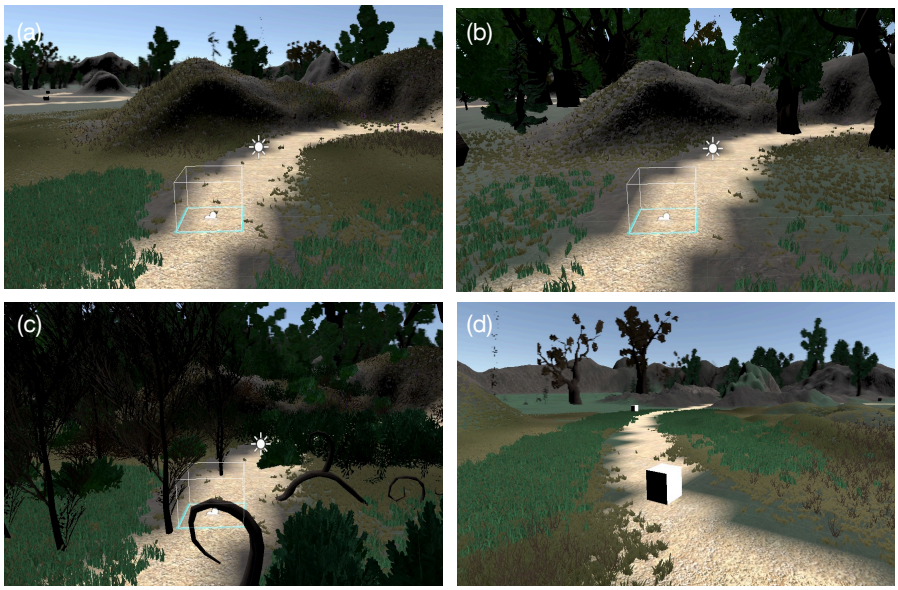

Figure 4.20: Scenarios with (a) low, (b) middle and (c) high densities; (d): scenario with checkpoints where the user has to stop and interact with.

4.3.4.3 Task design

Figure 4.21 shows how users conducted the task in the CAVE system and an overview of the 3D VE with the trajectory to follow highlighted in beige colour. The task performed in the HTC Vive followed the same settings as in the CAVE. The scenario consisted in walking in a forest area. By changing the density of objects present in the environment such as trees and flowers, we generated three different scenarios that we denoted by low (few objects), middle and high (many objects) densities (Figure 4.20). According to the definition of cognitive workload in subsection 4.3.1, such a setting

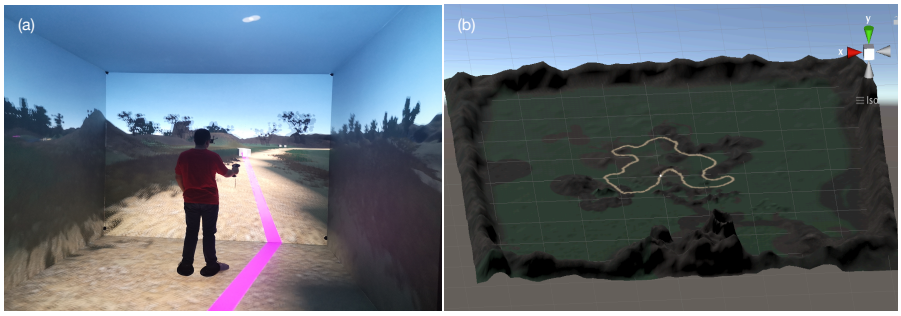

Figure 4.21: (a) One user is doing the experiment inside the CAVE system, the pink line instructs the initial navigation direction to prevent the user from getting lost once immersed; (b) overview of the 3D virtual environment with the trajectory to follow in beige colour.

should impose to participants different levels of cognitive workload: the high-density scenario should be more cognitively demanding than the low-density scenario because the user needs more cognitive resources to interact with the different objects and perform tasks. In the low density scenario, the user should be rarely affected and distracted when performing tasks, thus implying less workload. The general experimental procedure was organised as follows:

- Participants filled a pre-exposure questionnaire. Each participant was given a training about how to use the CAVE or the HTC Vive, and what they had to do in the 3D VE.
- With the help of the experimenter, participants put on the devices and were exposed to the virtual environment. Then, participants started to navigate in the VE following a predefined path. To increase the task difficulty level, users had to touch each checkpoint represented by the cube and avoid touching obstacles (trees, flowers) in the scenario with the handed device (shown in Figure 4.22, the HTC Vive controller in the HMD condition or the Flystick controller in the CAVE condition), then resume navigation (Figure 4.20d).
- When participants reached the destination inside the VE, they were removed from the CAVE or the HTC Vive and were requested to fill a NASA-TLX table based on their experience and impression.
- The experiment was repeated three times under the same conditions on three separate days.

The experimental conditions are listed in Table 4.5. They were uniformly distributed and balanced, to minimise random errors and hybrid effects. Six different conditions had to be tested in random

Table 4.5: Experimental conditions

Experiment number	1	2	3	4	5	6
Platform type	HTC Vive	HTC Vive	HTC Vive	CAVE	CAVE	CAVE
Scenario density	Low	Middle	High	Low	Middle	High

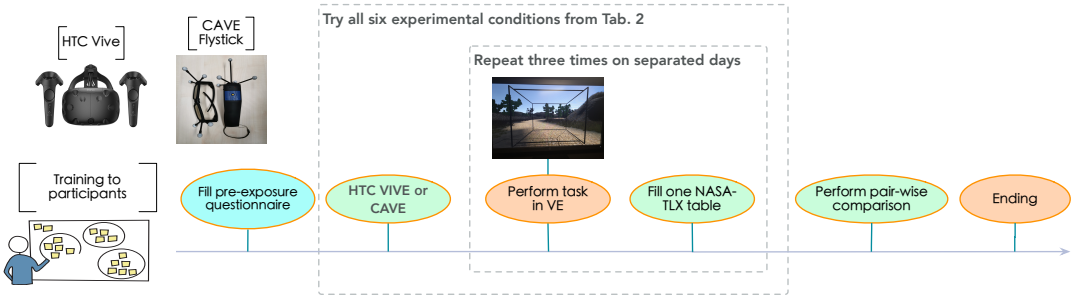

Figure 4.22: Flow chart of the experiment.

order, and each condition was repeated by one user three times on separate days. Totally, one user had to perform 18 (6×3) tests as we had six conditions. The flow chart of the experimental protocol is represented in Figure 4.22.

4.3.4.4 Determination of weighting coefficients

We computed two different sets of weighting coefficients. The *Hart* weighting coefficient approach explained in subsubsection 4.3.2.1 was operated strictly following the instructions from Hart and Staveland (1988) and Hart (2006a).

Participants who attended the experiments and also two professors were invited to form an individual pairwise comparison matrix using the linguistic expressions given in Table 4.4; those raters were chosen because of their expertise in cognitive workload evaluation in VR applications: participants knew what was important for them and therefore they can set appropriate pair-wise comparisons among different items, and the two external raters performed pair-wise comparisons based on their academic knowledge. A detailed procedure about the rating method can be found in Gumus (2009). The comparison among the criteria was conducted by considering which one was more important concerning the cognitive demand. To this end, participants were asked to fill the comparison questionnaire given in Appendix A.1, which led to a fuzzy comparison matrix. As explained in subsubsection 4.3.2.2, the normalised weightings of the aggregated responses were derived from the fuzzy synthetic extent

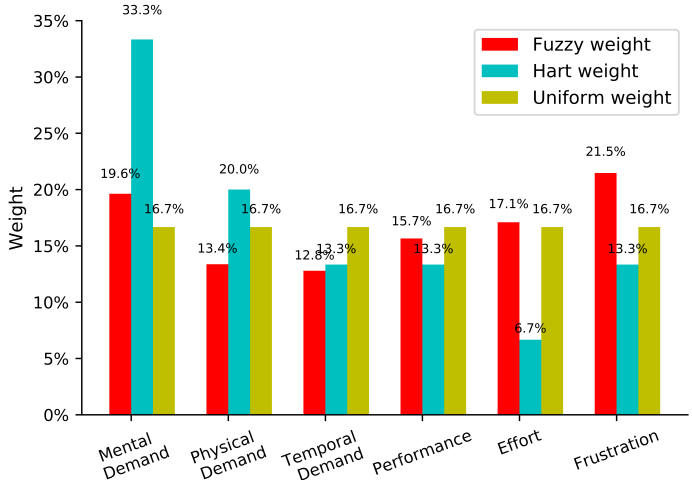

Figure 4.23: Aggregated normalised weights of the NASA-TLX criteria from three different approaches: the fuzzy AHP approach, the *Hart* weighting approach and the uniform weighting approach.

analysis.

4.3.5 Results

After the experiments, we collected all the questionnaires. We first computed the weighting coefficients using the *Hart* weighting and the fuzzy weighting approaches. Then, with these weighting coefficients available, we computed the RCC based on the TOPSIS method and the TLX_{Hart} score according to the weighted sum method. A statistical analysis was then performed to compare the RCC and TLX_{Hart}.

4.3.5.1 Weighting coefficients

Figure 4.23 illustrates the final weighting values each NASA-TLX criterion according to the weighting determination approach including the fuzzy AHP, the classical comparison process (*Hart*) and the uniform weighting. The uniform weights were obtained by setting the same weighting coefficient to all indices, and were used in this study as a control group, which helped to find the effect of different weighting coefficients determination approaches. From Figure 4.23, we can observe that the weights of the NASA-TLX indices strongly vary depending on the approaches. From the fuzzy AHP, *Frustration* and *Mental Demand* were the top two important factors, with a weighting coefficient of 21.5% and 19.6% respectively; *Effort* weight was relatively low (17.1%) followed by *Performance*

Table 4.6: Effect of factors on workload from different determination methods. Significance level: .05 (*), .01 (**)

	Fuzzy weight		Hart weight		Uniform weight	
TLX						
Factors	Platform	Scenario	Platform	Scenario	Platform	Scenario
Sum sq	7.46	22.93	4.88	27.47	6.94	16.42
NumDF	1	2	1	2	1	2
DenDF	236.09	236.17	235.96	236.04	236.02	236.11
F	2.10	3.23	1.46	4.12	2.15	2.55
p-value	.14	.04*	.23	.02*	.14	.08
η_p^2	.01	.03	.01	.03	.01	.02
RCC						
Factors	Platform	Scenario	Platform	Scenario	Platform	Scenario
Sum sq	0.0008	0.07	0.0003	0.08	0.0003	0.05
NumDF	1	2	1	2	1	2
DenDF	236.03	236.11	235.91	235.99	235.95	236.23
F	.12	4.72	.04	5.37	.05	4.12
p-value	.73	.009**	.84	.005**	.83	.02*
η_p^2	<.01	.04	<.01	.04	<.01	.03

weight (15.7%); *Temporal Demand* and *Physical Demand* had the lowest weights, 12.8% and 13.4% respectively. In parallel, the classical pairwise comparison indicated the highest weighting coefficient for *Mental Demand* (33.3%), followed by *Physical Demand* (20.0%); *Temporal Demand*, *Performance* and *Frustration* got equal weights (13.3%), while *Effort* got the lowest weight (6.7%).

The obtained weighting values from the three approaches were then provided to the TOPSIS model in order to get the RCC with Equation 4.25. The resulting overall workload scores were then compared with the classical weighted sum method (denoted TLX_{Hart} in Equation 4.8).

4.3.5.2 Workload assessment

Three participants performed only part of the eighteen conditions due to their availability. Therefore, this was not a perfect within-subject experiment because of the unbalanced samples, and we decided to analyze the variance with a mixed-effects model which is an extension of the repeated-measures ANOVA but with more flexibility (Galecki and Burzykowski 2013). Independently from the platform type and scenario density, individual differences (e.g., the way of thinking, judgment criteria) can be a potential factor that affects the overall workload score. In order to reduce these individual effects, we set the effect of individual difference as a random factor while we set the effect of the scenario density and the platform type as fixed effects. Statistics were conducted in *R* (R Core Team

Table 4.7: Post-hoc analysis for the scenario type considering different determination methods; Lower and Upper represent the boundaries of the 95% confidence interval (CI). Significance level: .05 (*), .01 (**)

	Fuzzy weight			Hart weight			Uniform weight		
TLX									
Scenario type	low	low	middle	low	low	middle	low	low	middle
Scenario type	middle	high	high	middle	high	high	middle	high	high
Mean difference	-0.44	-0.74	-0.30	-0.52	-0.81	-0.29	-0.38	-0.63	-0.25
Lower	-1.01	-1.33	-0.89	-1.07	-1.37	-0.86	-0.92	-1.18	-0.81
Upper	0.12	-0.16	0.29	0.03	-0.24	0.29	0.16	-0.07	0.31
p-value	.12	.01*	.31	.06	.005**	.32	.17	.02*	.39
η_p^2	.01	.03	<.01	.01	.03	<.01	.01	.02	<.01
RCC									
Scenario type	low	low	middle	low	low	middle	low	low	middle
Scenario type	middle	high	high	middle	high	high	middle	high	high
Mean difference	-0.03	-0.04	-0.01	-0.03	-0.04	-0.01	-0.02	-0.03	-0.01
Lower	-0.05	-0.07	-0.04	-0.05	-0.07	-0.04	-0.05	-0.06	-0.04
Upper	-0.001	-0.01	0.01	-0.003	-0.02	0.01	-0.001	-0.01	0.01
p-value	.04*	.003**	.31	.03*	.002**	.33	.05*	.006**	.39
η_p^2	.02	.04	<.01	.02	.04	<.01	.02	.03	<.01

2020) along with the related packages: *lme4*, *afex*, *lmerTest* and *effectsize*.

A mixed-effects model was conducted to determine the influence of two independent variables (platform, scenario) on cognitive workload considering both the TLX_{Hart} and RCC methods (Table 4.6). Normality of the data was checked. Three coefficient weighting approaches were applied for each cognitive workload determination method. Considering first the TLX_{hart} evaluation, the level of scenario density was found to have significant effects on the overall workload only when it was measured with the fuzzy AHP ($F_{2,236.17} = 3.23, p = .04, \eta_p^2 = .03$) and the *Hart* approaches ($F_{2,236.04} = 4.12,\ p = .02, \eta_p^2 = .03$). On the contrary, the VR platform did not have any significant effect whatever the weighting determination approach (fuzzy weighting: $F_{1,236.09} = 2.10,\ p = .14, \eta_p^2 = .01$, *Hart* weighting: $F_{1,235.96} = 1.46,\ p = .23, \eta_p^2 = .01$ and uniform weighting: $F_{1,236.02} = 2.15,\ p = .14, \eta_p^2 = .01$). With the RCC evaluation, the level of scenario density revealed a significant effect with all three weighting approaches (fuzzy weighting: $F_{2,236.11} = 4.72,\ p < .01, \eta_p^2 = .04$, *Hart* weighting: $F_{2,235.99} = 5.37,\ p < .01, \eta_p^2 = .04$, uniform weighting: $F_{2,236.23} = 4.12,\ p = .02, \eta_p^2 = .03$); the effect of the platform still showed no significant difference whatever the weighting approach (fuzzy weighting: $F_{1,236.03} = 0.12,\ p = .73, \eta_p^2 < .01$, *Hart* weighting: $F_{1,235.91} = 0.04,\ p = .84, , \eta_p^2 < .01$ and uniform weighting: $F_{1,235.95} = 0.05,\ p = .83, \eta_p^2 < .01$).

Post-hoc analyses were performed to understand the differences between the three levels of scenario density. Pairwise comparisons were done using Tukey HSD tests. Results are shown in Table 4.7. In addition to p-values, we considered the confidence interval (CI) to provide additional information that p-values do not convey, for example the actual mean difference between groups. The width of the CI for the difference reveals the precision of the estimate, and narrower intervals suggest a more precise estimate (Lee 2016). With the TLX_{hart} evaluation, statistical significance was observed only between the low and high densities and with two weighting approaches (the fuzzy weighting: $p = .01,\ 95\%\ CI : -1.33 \sim -0.16, \eta_p^2 = .03$, *Hart* weighting: $p < .01,\ 95\%\ CI : -1.37 \sim -0.24, \eta_p^2 = .03$, uniform weighting: $p = .02,\ 95\%\ CI : -1.18 \sim -0.07, \eta_p^2 = .02$). In contrast, the *RCC* evaluation reported more significant effects. Statistical significance was found between the low and middle densities (fuzzy weighting: $p = .04,\ 95\%\ CI : -0.05 \sim -0.001, \eta_p^2 = .02$, *Hart* weighting: $p = .03,\ 95\%\ CI : -0.05 \sim -0.003, \eta_p^2 = .02$ and uniform weighting: $p = .05,\ 95\%\ CI : -0.05 \sim -0.001, \eta_p^2 = .02$), as well as between the low and high densities also with all three weighting methods (fuzzy weighting: $p < .01,\ 95\%\ CI : -0.07 \sim -0.01, \eta_p^2 = .04$, *Hart* weighting: $p < .01,\ 95\%\ CI : -0.07 \sim -0.02, \eta_p^2 = .04$ and uniform weighting: $p < .01,\ 95\%\ CI : -0.06 \sim -0.01, \eta_p^2 = .03$). We can also remark that the CIs from the *RCC* are much narrower than with TLX_{Hart}.

4.3.5.3 Advantage of TOPSIS over the weighted sum method

When the overall workload was measured with the weighted sum method, the range of the CIs was wider than with the TOPSIS method, as shown in Table 4.7, revealing that TOPSIS provided more precise estimates than TLX_{Hart}. As a supplementary support, we considered the CV in addition to the mean (M) and the standard deviation (SD), obtained for each platform and scenario type with the three different weighting approaches and the two evaluation methods (Table 4.8). The CV is defined as the ratio of SD to M and represents a statistical measure of the dispersion of the data (Kesteven 1946; Lovie 2005). The higher the CV, the higher the dispersion and the less reliable the measure.

Another mixed-effects model was carried out to analyze the CV from Table 4.8, where the random effects were the platform type and the scenario density and the fixed effects were the evaluation methods (TLX_{Hart}, *RCC*) and the weighting approaches (fuzzy weighting, *Hart* weighting, uniform weighting). Table 4.9 presents the results of the statistical analysis. A significant difference was found between the evaluation methods in terms of CV, $F_{1,30} = 38.23, p < .01, \eta_p^2 = .56$. The weighting

Table 4.8: Descriptive statistics with the mean (M), the standard deviation (SD) and the CV with the different approaches

		Fuzzy weighting			Hart weighting			Uniform weighting		
TLX_{Hart}										
		M	SD	CV	M	SD	CV	M	SD	CV
Platform	HTC	7.53	2.90	0.39	7.4	2.93	0.40	7.48	2.83	0.38
	CAVE	7.26	3.16	0.44	7.21	3.22	0.45	7.22	3.10	0.43
Scenario type	low	7.04	2.74	0.39	6.92	2.80	0.40	7.05	2.74	0.39
	middle	7.45	2.91	0.39	7.37	2.89	0.39	7.4	2.84	0.38
	high	7.79	3.42	0.43	7.72	3.50	0.45	7.69	3.31	0.43
RCC										
Platform	HTC	0.40	0.13	0.33	0.38	0.14	0.37	0.40	0.13	0.33
	CAVE	0.40	0.14	0.35	0.38	0.15	0.39	0.40	0.14	0.35
Scenario type	low	0.38	0.13	0.34	0.36	0.13	0.36	0.39	0.13	0.33
	middle	0.40	0.13	0.33	0.39	0.13	0.33	0.41	0.12	0.29
	high	0.42	0.16	0.38	0.40	0.17	0.43	0.42	0.15	0.36

approach also influenced the CV significantly, $F_{2,30} = 3.54, p = .04, \eta_p^2 = .19$. Post-hoc analyses revealed that the *RCC* led to significantly smaller CVs than with TLX_{Hart}, $p < .01, \eta_p^2 = .56$. Furthermore, it was found that the CV from the *Hart* weighting was significantly higher than with the uniform weighting, $p = .01,\ 95\%\ CI : 0.007 \sim 0.05, \eta_p^2 = .19$. However, as an exploratory study, we did not find difference at the given significance level between the fuzzy weighting and *Hart* weighting, $p = .09,\ 95\%\ CI : -0.04 \sim 0.003, \eta_p^2 = .09$.

Therefore, the evaluation from TOPSIS illustrated a significantly lower dispersion of the data compared to TLX_{Hart}, which confirms our expectation that TOPSIS provides enhanced precision of subjective evaluation.

Table 4.9: Statistical analysis of CV for the different evaluation methods and weighting approaches. Significance level: .05 (*), .01 (**)

			Sum Sq	NumDF	DenDF	F	p-value	η_p^2
Mixed-effects model	TLX v.s. RCC		0.30	1	30	38.23	.00**	.56
	Weighting methods		0.005	2	30	3.54	.04*	.19
				Mean Difference	Lower	Upper	p-value	η_p^2
Multi-comparison	TLX	RCC		-0.06	-0.08	-0.04	.00**	.56
	Fuzzy weight	Hart weight		-0.02	-0.04	0.003	.09	.09
	Fuzzy weight	Uniform weight		0.01	-0.01	0.03	.39	.02
	Hart weight	Uniform weight		0.03	0.007	0.05	.01*	.19

4.3.6 Discussion

We proposed to use the *RCC* as an enhancement for the measurement of cognitive workload, with the expected outcomes that: the *RCC* is a more precise metric than classical methods to quantify cognitive workload resulting from different tasks or systems. In the considered use case, we could investigate the effectiveness of the *RCC* to discriminate cognitive workload in different VR platforms and scenario densities. Figure 4.24 shows the two steps operated to study the performance of our approach. First, evaluation results from TOPSIS were checked for consistency with results from the literature (R1). Then, the precision of the evaluation methods was checked by comparing the CVs between *RCC* and TLX_{Hart} (R2).

4.3.6.1 Validation of R1

No evidence was found that different VR platforms can lead to significantly different levels of workload, neither the *RCC* nor TLX_{Hart} showed such effect. In this sense, our results conformed to the findings of past research (Riley and Kaber 1999; Porssut and Chardonnet 2017; Freitas 2018; Sevinc and Berkman 2020) and confirmed that the *RCC* could represent well the level of cognitive workload, with respect to the VR platforms. Concerning the scenario density, past work proved that the type of scenario can affect cognitive workload (Parsons *et al.* 2009). From Table 4.6, both the *RCC* and TLX_{Hart} methods behaved consistently.

No significant difference was found between the middle and the high-density scenarios whatever the evaluation method. Past research showed that depending on the task difficulty, there exist three workload states that are cognitive under-load, adequate workload and cognitive saturation (Harrison *et al.* 2014; McKendrick *et al.* 2019). In our experiment, we set densities to produce these different states. From the *RCC* results, when participants performed the task in the low-density scenario, as it was less demanding, they were in an under-load state, resulting in significantly lower cognitive load than in the middle density case. As the scenario density increased, their cognitive ability to receive and process the spatial information was around overload or had already become overloaded, which explains why there was no significant difference between the middle and the high-density scenarios, whatever the evaluation method.

From these observations, our first expected outcome was achieved.

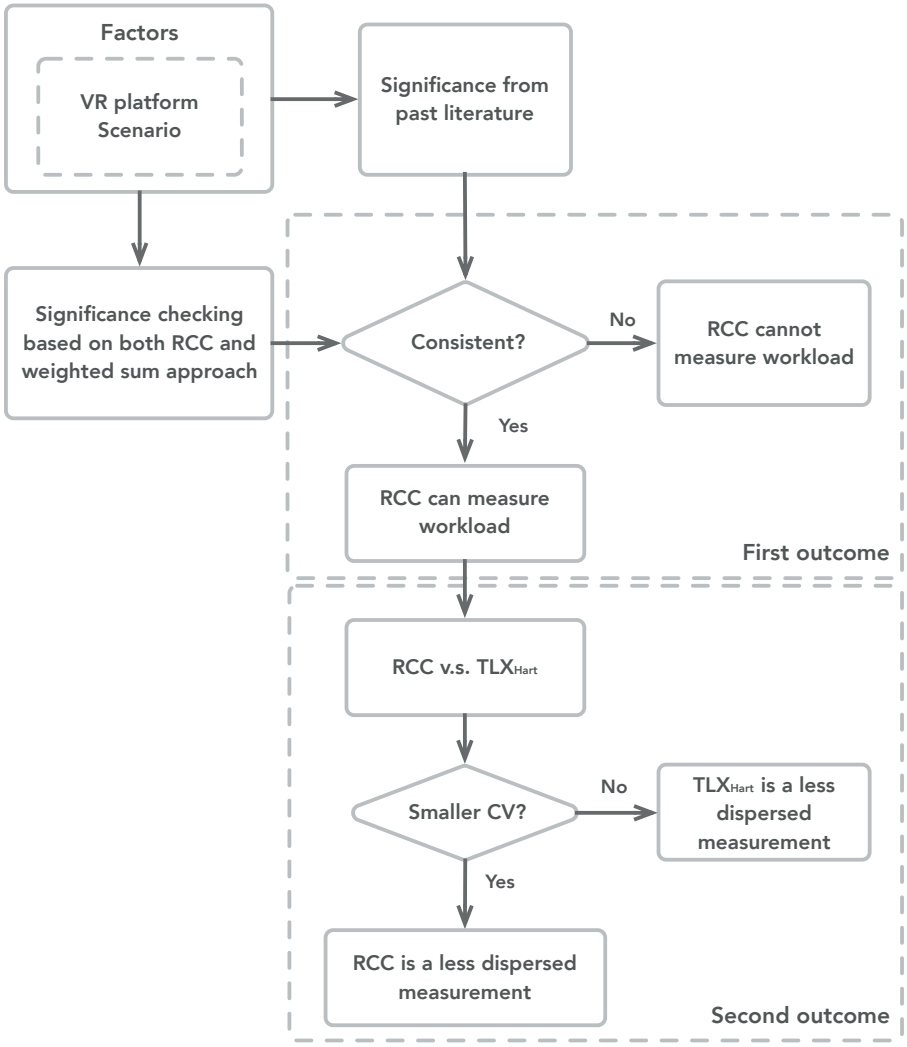

Figure 4.24: Flowchart of the validation process for the two factors considered here: first to check if there is a consistent result to show the proposed method working; second to compare the dispersion of measurements based on the CV.

4.3.6.2 Improved workload measurement by reducing dispersion

Much research has been done over the last decades to measure cognitive workload during a task, especially in fields related to human-computer interaction (Gevins and M. E. Smith 2003), driving (Patten *et al.* 2006) and flight (Sterman and Mann 1995; Kantowitz and Casper 2017), in which users have to process amounts of information simultaneously, resulting in high cognitive workload. Many past literature methods try to apply biosensors to measure cognitive workload, while evaluation through subjective questionnaires did not progress significantly. During the subjective evaluation process, par-

ticipants find it difficult to quantify their impressions towards the experience, but they are forced to give answers, leading to subjective results with high uncertainties (Katicic *et al.* 2015a). However, we believed that a proper analysis approach can address this drawback and enhance the reliability of individual feedback. Therefore, we introduced an alternative evaluation method to the straightforward weighted sum method to quantify workload based on subjective evaluation results more precisely. We compared the weighted sum method to the TOPSIS method considering three different weighting approaches.

From the experimental results, regarding the scenario type, with the classical weighted sum calculation method, statistical significance could be detected only between the low and high densities, implying a lack of precision of this method to discriminate the overall workload in smaller scales. In contrast, with the TOPSIS method, more significant effects were detected, as differences between low and middle densities were found. TOPSIS could therefore more precisely detect small changes in cognitive workload. The reason lies in the significantly smaller CV of the RCC, meaning a lower dispersion of the data and therefore an improved quality of discrimination among data.

Regarding the weighting approaches, we did not find a significant difference between the fuzzy AHP and the *Hart* weighting approaches as both of them gave similar significant results when applied to TLX_{hart} and RCC, but the *Hart* weighting resulted in a higher CV than with the uniform weighting approach. In other words, the fuzzy AHP and the *Hart* weighting approaches provided effective results, while particularly the fuzzy weighting could be used as an alternative to the *Hart* weighting and the uniform weighting approaches to determine the weighting coefficients for the overall cognitive workload score. This finding implies that applying weights to each criterion according to its importance is an essential step for computing the overall workload.

The comparison of CV validates our second outcome R2. It suggested that the cognitive workload measured from the TOPSIS is more reliable, which would be particular important for those wishing to compare and manage the workload difference in smaller scales.

4.3.7 Conclusion

We introduced a new method to improve the precision and reduce the CV of cognitive workload quantification thanks to the TOPSIS. The model was tested with three different weighting approaches: fuzzy weighting, *Hart* weighting and uniform weighting. Thanks to its hierarchy structure, the fuzzy

AHP method for computing the fuzzy weighting extended the possibility to measure the workload with other questionnaires instead of the NASA-TLX. The proposed method was applied in a VR user experiment to validate its performance by studying two factors in a navigation task: the type of VR platform and the scenario density. Results were compared with a classical weighted sum method. The *RCC* computed from TOPSIS was found to be a comprehensive metric for quantifying and comparing the level of workload among various VR applications, with a reduced CV on subjective evaluation compared to the classical weighted sum method. Validation results were consistent with the corresponding literature, which suggested that our new framework can be useful in assessing workload measurement by reducing subjective uncertainty and improving measuring quality.

Because of the increasing popularity of VR, it is important to consider cognitive workload in this domain. Therefore, the TOPSIS method for measuring cognitive workload was designed and validated in the field of VR, while it can also benefit to the measurement of cognitive workload arising from other domains by following our experimental steps. Nevertheless, one substantial limitation was that only two factors were considered to determine the effectiveness of our approach; future research shall consider more factors as well as more use cases to test the generality of this approach entirely.

4.4 Deployment of evaluation tools

The previous sections have presented and validated different methods for measuring cybersickness and cognitive workload. This section summarizes the proposed evaluation methods exposed in this chapter, and further, explicitly turn the methods into effective measuring tools for cybersickness and cognitive workload. The focus is not to propose a new research outcome, but to give a straightforward procedure concerning how to use our evaluation methods as standard tools.

As the previous sections (section 4.1, section 4.2 and section 4.3) have demonstrated how to use the evaluation methods in the context of navigation, we will not detail the associated computing process, but instead, focus on the general workflow.

4.4.1 Procedure for measuring cybersickness

4.4.1.1 Using postural signal

The procedure for measuring cybersickness according to the postural signal is,

1. A user stands on a balance board while looking at a fixed point in the front, through which the experimenter can collect the postural sway signal when the user is in a normal state.

2. The experimenter creates an autoencoder model with which the feature of the normal state can be extracted and saved in the model.

3. The user starts to navigate in the virtual environment.

4. The user stands on the balance board again while looking at a fixed point in the front, through which the experimenter will collect the postural sway signal after exposure. Note that the frequency and duration of the second collected signal should be the same as the previous one.

5. The experimenter substitutes the second signal into the abovementioned autoencoder, and the model will compute the reconstruction error, which indicates the level of cybersickness.

4.4.1.2 Using individual factors

Using the individual factors, we can obtain the user's susceptibility to cybersickness before the user is exposed to visual stimuli, implying a predictive ability. The procedure for predicting the susceptibility to cybersickness with individual factors is,

1. The experimenter prepares a questionnaire to investigate individual factors including age, gaming experience, and ethnic origin.

2. Based on the relationship between individual factors and cybersickness (discussed in chapter 2), the experimenter can formulate the fuzzy inference system.

3. With the fuzzy inference system, the experimenter can compute the user's susceptibility to cybersickness. The susceptibility to cybersickess indicates the individual proneness to sickness symptoms during navigation.

As the study investigates many user-related factors, the experimenter has to respect the rules related to privacy protection.

4.4.2 Procedure for measuring cognitive workload

The measurement of cognitive workload is developed from the NASA-TLX questionnaire. Therefore, the experiment process is the same as in past research using the NASA-TLX, but the difference is at the post-processing of the NASA-TLX data, for which the TOPSIS method will be used.

The procedure for measuring the cognitive workload with TOPSIS method is,

1. The user performs the navigation task in a virtual environment, after which he/she has to fill the NASA-TLX.

2. The user also needs to perform the pair-wise comparisons among different items in the NASA-TLX. The comparisons can reflect the importance of each NASA-TLX item concerning the current task. Regarding the pair-wise comparisons, we mentioned three different methods in section 4.3.

3. After the experimenter finishes all the user studies, TOPSIS will compute an overall cognitive workload for each user.

4.5 Summary

Finding the importance of evaluating user experience in a navigation task, we proposed different evaluation methods to measure user experience, i.e., cybersickness and cognitive workload in this context. The measure of cybersickness includes two aspects. One is to measure cybersickness after user navigation in a virtual environment. For example, by comparing the postural sway signal from pre-exposure and post-exposure to visual stimuli, we can compute the user's sickness level. However, this is a posterior measure, which can not predict users' susceptibility to cybersickness. Therefore, we used fuzzy logic to involve individual differences to predict cybersickness susceptibility, before the user is exposed to visual stimuli. In addition, it is essential to measure cognitive workload: when navigating in a virtual environment, the user also needs cognition to process information, interact with virtual objects, and perform tasks. However, current subjective evaluation methods generally fail to control dispersion effects, noise, and uncertainty. Hence, we proposed the TOPSIS model to enhance the precision of the subjective evaluation of cognitive workload.

Chapter 5

Improving navigation experience

Contents

Chapter 2 has summarized different mechanisms for cybersickness in virtual environments, which provides us with inspiration and viewpoint for designing new navigation techniques in this chapter. Chapter 4 presents multiple evaluation methods for cybersickness and cognitive workload. Evaluation is a partial premise for the reduction of cybersickness and cognitive workload. The objective of the thesis is not only to evaluate but also to design navigation techniques that can reduce efficiently cybersickness and cognitive workload. In this chapter, we proposed four novel original navigation techniques, for each of them validating its performance in improving user experience in terms of cybersickness and cognitive workload.

5.1 Semiautomatic navigation

5.1.1 Introduction

A path drawing technique was designed by Igarashi *et al.* (1998) to navigate in virtual 3D spaces. This method allows users to draw the desired path with a free stroke, then the system automatically projects the stroke onto the walking surface to generate the final moving path. With the intention of developing a navigation interface to provide better user experience and reduce cybersickness, in this section we presented a new semiautomatic technique to navigate in immersive virtual environments. The path planning algorithm is similar to the one used in humanoid robotics. The novelties and contributions of the proposed navigation techniques include the following aspects:

- Design a semiautomatic navigation method: we proposed to integrate real-time automatic navigation through the path planning algorithm to allow smooth and optimized navigation, but still enabled users to manually adjust the path with a gaze-directed navigation method, providing more freedom to modify the generated path in VEs, depending on the task to be performed. The design of our navigation method will be presented in subsection 5.1.2.

- Analyzing the effectiveness and user satisfaction of our proposed navigation technique. In most cases, semiautomatic navigation outperformed joystick-based navigation especially regarding cybersickness, as shown in subsection 5.1.4.

5.1.2 Design of semiautomatic navigation

Currently, many navigation interfaces have been developed with the intention of enhancing user comfort but cybersickness is still an inherent problem to be overcome in virtual reality (Davis *et al.* 2014). Considering the sensory conflict theory introduced in Chapter 2, the problem becomes: can we design a navigation interface that reduces the conflicted signal as much as possible? In order to answer this question, we designed the semiautomatic navigation system and we hypothesized that the user should suffer from less cybersickness.

5.1.2.1 Semiautomatic navigation

The original purpose of semiautomatic navigation is that a virtual reality system provides basic control rules and dynamics during navigation while still allowing users to control the system if necessary (Galyean 1995). In this work, a semiautomatic navigation interface was developed based on an automatic path planner together with a gaze-directed technique to allow to manually modify the generated path if needed. Among manual navigation techniques, we chose the gaze-directed technique as it is easy to use while being close to real situations: when we are walking in the physical world, we usually look in the target direction.

One general issue of gaze-directed navigation is that it couples gaze direction and navigation direction, which means that users cannot look in one direction but move to another direction simultaneously. However, considering real life experience that people may look in a direction other than their navigation direction during walking, cycling, or driving in the physical world, the introduced automatic path planner fills up such deficiency. In addition, if a complete 3D motion (e.g., "flying") is enabled in VEs, the gaze-directed technique has to tackle two problems: a) users may navigate up and down when they navigation in a horizontal plane since it is difficult to keep the head in the same level precisely. b) even if users manage to control the head direction, it is also awkward to correct the navigation trajectory vertically up or down by looking straight up or down.

In order to overcome these two deficiencies of the gaze-directed technique, we added a path planner that can control the trajectory and avoid the "up or down" effect. The implementation of the semiautomatic navigation technique is explained in Algorithm 1. A user firstly specifies a target to the VE platform, the system reads the current states of the avatar position and orientation and the

Algorithm 1 Semiautomatic navigation technique in immersive virtual environments

Input: The user sends a command to the VE platform to navigate
Output: The user reaches the destination in the VE
Initialize the system
Read the initial position and orientation of the avatar $\mathbf{P}_a$, $\mathbf{O}_a$ and the destination $\mathbf{P}_d$, $\mathbf{O}_d$
while Destination not reached **do**
    if path from the motion planner **then** ▷ default navigation is with the path planner
        function MotionPlanner($\mathbf{P}_a$, $\mathbf{O}_a$, $\mathbf{P}_d$, $\mathbf{O}_d$) ▷ Run the function
            Substitute $\mathbf{P}_a$, $\mathbf{O}_a$, $\mathbf{P}_d$, $\mathbf{O}_d$ into the path planning system
            Generate the trajectory with the A* path planning algorithm
            Smoothen the trajectory with Bézier curves
            Translate the user with speed V along the tangent line of the path
        end function
    else
        function GazeDirectedNavigation($\mathbf{P}_a$, $\mathbf{O}_a$, $\mathbf{P}_d$, $\mathbf{O}_d$) ▷ Run the function
            Get the gaze direction $\mathbf{T}_g$ of the user at state $\mathbf{P}_a$, $\mathbf{O}_a$
            Normalize $\mathbf{T}_g$
            Translate the user with speed V along the direction of $\mathbf{T}_g$ in the VE's coordinate system
        end function
    end if
    Update the current position and orientation of the avatar and target
end while

destination. The path-planning algorithm connects the avatar position to the target position with the shortest trajectory using an A* path planning algorithm (see the work of Tiwari *et al.* (2012) for a detailed explanation of A*) by taking into account environmental constraints simultaneously. However, the original trajectory generated by the A* algorithm has only C^0 continuity which is unnatural and very similar to the path generated from a joystick controller. In order to smoothen the trajectory, we can implement numerical methods like clothoid curves, polynomial curves and Bézier curves to define the final shape of the path, but we chose Bézier curves as in Equation 5.1, because it has the lowest computational cost (Gonzalez Bautista 2017),

$$\mathbf{B}(t) = \sum_{k=0}^{n} P_k \binom{n}{k} (1-t)^{n-k} t^k \tag{5.1}$$

where n is an integer related to the degree of the Bézier curve, P_k is the selected control point from the original A* trajectory, and t is a parameter, $t \in [0, 1]$. In a real case, the control point computed on the raw path generated from the A* algorithm is given in Equation 5.2,

$$\begin{cases} P_0 = T_i + l_1 \frac{T_{i-1} - T_i}{||T_{i-1} - T_i||} \\ P_1 = T_i + l_2 \frac{T_{i-1} - T_i}{||T_{i-1} - T_i||} \\ P_2 = T_i + l_3 \frac{R - T_i}{||R - T_i||} \\ P_3 = T_i + l_2 \frac{T_{i+1} - T_i}{||T_{i+1} - T_i||} \\ P_4 = T_i + l_1 \frac{T_{i+1} - T_i}{||T_{i+1} - T_i||} \end{cases} \tag{5.2}$$

where, as shown in Figure 5.1, T_{i-1}, T_i and T_{i+1} are the raw path points coming from the path planner; P_0, P_1, P_3 as well as P_4 are set to lie in the raw path; l_1 is the distance from T_i to P_0 and P_4; l_2 is the distance from T_i to P_1 and P_3; l_3 is the distance along the angular bisector (obtuse angle) of the intersection; R is a point on the angular bisector. Here the hyper-parameters are l_1, l_2 and l_3, but since l_1 and l_2 lie in the same direction, to simplify, we can define a new hyper-parameter r,

$$r = \frac{l_1}{l_2} \tag{5.3}$$

and if we fix l_2, the final hyper-parameters become r and l_3, which makes it easier to control the shape of the smoothed path.

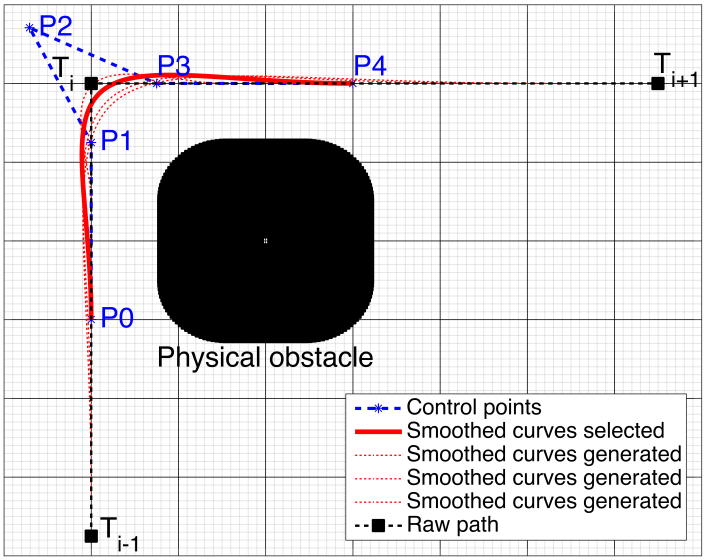

Figure 5.1: Application of a 4^{th} degree ($n = 4$) Bézier curve to smoothen an intersection. The thick red line is the selected trajectory.

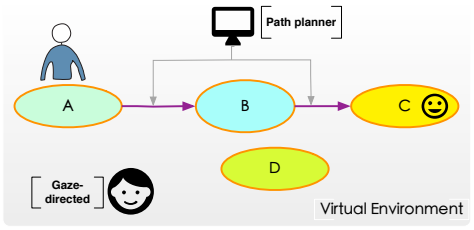

(a) The user simply navigates from A to C by following the path generated from the path planner during the whole process, passing position B. This may happen when the user does not have to conduct activities in position D.

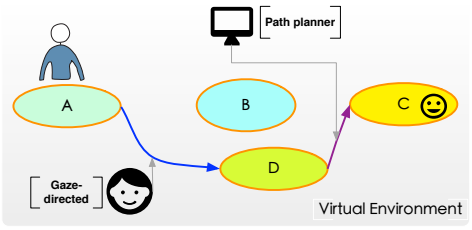

(b) The user firstly navigates to position D with gaze-directed technique to conduct a task since B is not the desired position, while she/he can activate the path planner again in the later stage to go to position C .

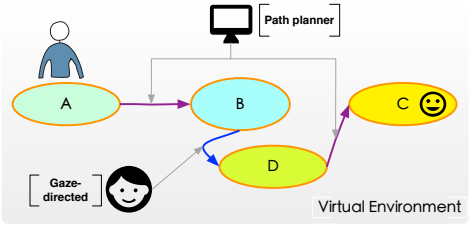

(c) The user firstly arrives at position B with the path planner but then she/he can go to position D with the gaze-directed method to perform a task; finally she/he uses the path planner to go to position C.

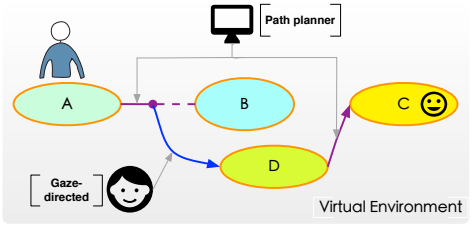

(d) The user initially decides to go with the default path planner but she/he changes her/his mind before arriving at position B, so the gaze-directed technique enables her/him to move to position D. After finishing the task in D, she/he moves to C with the path planner.

Figure 5.2: Semiautomatic navigation technique to navigate from position A to position C in a VE: the purple line is the trajectory generated from the path planner while the blue line is the trajectory generated from the gaze-directed technique. A, B, C and D are arbitrary positions of the walkable surface in the VE.

Figure 5.2 presents four different examples for the application of the semiautomatic navigation technique. The user has to navigate to position C from position A, and in the simplest case, if there is no specific reason motivating her/him to pass through position D, the path from the path planner would be the best choice. On the other hand, one user may not want to follow the trajectory from the path planner but to navigation with a personalized way where the gaze-directed technique provides a natural interaction between the VE and the user. For example in a game, users want to pick up treasures along the way "$A \rightarrow D \rightarrow C$" instead of "$A \rightarrow B \rightarrow C$" in the VE, so the gaze-directed technique enables them to change the motion path towards another position D, which works as a supplement to the automatic motion planner. Finally, the user will be translated successfully to

the destination with the trajectory from either the path planner or the gaze-directed method, both providing smooth trajectories.

In general, semiautomatic navigation follows the principle: users can accept the default and optimized (shortest) path to conduct the assigned task, but they can refine or modify the path with the gaze-directed technique if the shortest one is not preferred or for a specific task. However, at any time and position if users get lost in the VE during navigation, they can activate the path planner again.

5.1.3 User study

5.1.3.1 Navigation techniques setup

All the tests for this study were run using an HTC Vive head-mounted display. We compared our semiautomatic navigation with joystick-based navigation. Joystick-based navigation was set as a performance baseline as it tends to induce more cybersickness (Rebenitsch and C. Owen 2016b; Vinson *et al.* 2012), and we expected that semiautomatic navigation will lead to less cybersickness by avoiding unnecessary and noisy movement.

5.1.3.1.1 Joystick-based Joystick-based navigation was implemented to enable users to control movements in the VE, i.e., navigating in both translational and rotational directions. Note that the position and orientation of the joystick was independent of that of the user, meaning that the user's position and orientation in the physical world must be initialized to be consistent with that in the VE. The maximal speed was set to $2\,m.s^{-1}$ but the actual speed depended on the user's input from the controller.

5.1.3.1.2 Semiautomatic As explained in subsection 5.1.2, the semiautomatic navigation was designed by combining the advantage of a path planner and gaze-directed navigation. The designed path planner was implemented on top of NavMeshAgent which is a navigation mesh agent implemented with the A* algorithm in Unity3D, while the implementation of the gaze-directed technique was based on an open source library, VRTK[1]. As mentioned, the user has two options: navigation following a smooth path towards the desired position, or navigation using the gaze-directed technique to modify the default if necessary. When the user presses the trigger button of the HTC Vive handheld controller, she/he will be translated along the generated path, but if the user touches the touchpad of

[1] https://vrtoolkit.readme.io

the controller, she/he will be translated to the direction of gaze. The maximal speed was also set to be $2\,m.s^{-1}$, but the real speed depended on how much the button was pressed. The generated path is displayed to the users so that they can decide whether following the generated path or modifying it with the gaze-directed technique.

5.1.3.1.3 Hypotheses In order to assess the performance of the semiautomatic navigation method, we hypothesized that

H1 Compared to joystick-based navigation, our semiautomatic navigation technique is much more efficient and provides more immersion since it enables users to concentrate on the assigned task instead of learning how to use the navigation interface.

H2 The semiautomatic navigation technique can help users find an optimized and smoothed path, thereby significantly alleviating cybersickness, while joystick-based navigation normally translates users with irregular and jerky trajectories resulting in increased sensory conflict.

5.1.3.2 Participants

We invited 13 participants including 4 females (mean age 25.83, SD=4.58) to the experiment. Before the experiment, a pre-exposure questionnaire (Q1) was filled in to get a better insight of the participants' background and health condition. From this questionnaire, all subjects had normal or corrected-to-normal vision and reported no disorders or unusual circumstances with respect to their hearing or balancing. During the experiment, one participant dropped out due to strong cybersickness, and the corresponding results were not taken into account for statistical analyzis. None of them had experienced VR before the experiment.

5.1.3.3 Task design and experimental procedure

The experiments were carried out in a large space free of any obstacles to make sure there was no interference that could affect user experience. The virtual environment, implemented in Unity3D, was a 3D model of a building including many office rooms where the participants were asked to explore and pick up a total of 30 coins scattered in different places as fast as possible inside the VE. The coins had to be collected in a specific order: the coins were numbered from 1 to 30, and the participants had to

catch them in an ascending order. To avoid biased results from users' evaluation, the two navigation techniques were presented in a random order. The evaluation of user experience and cybersickness was conducted with the following two methods.

5.1.3.3.1 Subjective evaluation Participants were given a training on the two different navigation interfaces and they were allowed to stay a given period in the virtual environment before conducting the experiment. Each session of the experiment ended with the simulator sickness questionnaire (SSQ, Q2) to report cybersickness (Kennedy, Lane, *et al.* 1993), and a brief questionnaire (Q3, to evaluate each navigation method in terms of efficiency, likability, accuracy, learnability, immersion, naturality, consistence and concentration) as a feedback about general impressions on the navigation method just used. It is worth noting that here Q3 was designed mainly according to some quality factors from the work of Bowman *et al.* (1997) to measure the navigation interfaces; the factors include the speed (appropriate velocity or the total time spent to complete the task), accuracy (proximity to the desired target), spatial awareness (the participant's implicit knowledge of her/his position and orientation within the environment during and after navigation), ease of learning (the ability of a novice user to use the technique), ease of use (the complexity or cognitive load of the technique from the participant's point of view), and presence (the participant's sense of immersion or "being within" the environment). We extracted some questions from the Witmer-Singer presence questionnaire (Witmer and Singer 1998) in order to help participants evaluate the navigation interfaces from different perspectives.

5.1.3.3.2 Objective evaluation The questionnaires represent a subjective evaluation which may lead to biased results in some situations, therefore in addition we measured the evolution of the participants' center of gravity (COG) with the TechnoConcept balance board[2], as past literature showed postural sway to be a reliable feature to measure cybersickness (e.g., (Chardonnet *et al.* 2017)). The embedded sensor can gather the postural sway signal in Forward/Backward and Left/Right directions and allows to compare the body's variance of COG before and after navigation in the VE.

5.1.3.3.3 Procedure All the participants followed the same experimental procedure, starting with a clear and careful explanation, then a training session to the experiment with a basic description of VR knowledge. The whole procedure was designed as follows:

[2]http://www.technoconcept.fr/shop/index.php

1. Before being immersed in the VE, participants were requested to fill an SSQ (Q2) to check if they had already felt any cybersickness. The postural sway signal was also collected through the balance board with the intention of comparing the variance of the COG's area before and after the experiment.

2. The participants were assigned randomly one of the navigation method (joystick or semiautomatic) to navigation in the VE and were requested to pick up all the coins.

3. After the participants finished the task, the total time for completing the task was recorded immediately. Again, they were asked to stand on the balance board in order to measure the variance of the COG's area after immersion in the VE. Then, Q2 and Q3 were filled at this stage.

4. On another day, the participants were invited to test the remaining navigation method following the same procedure as before.

5.1.4 Results and discussion

5.1.4.1 Statistical Tests

Since we did not collect an extremely large sample for the statistical analysis, we first validated the normality and homogeneity of the collected data with the Shapiro-Wilk test and the Levene test, respectively. Then, we performed a one-way ANOVA on data that were normally distributed and had equal variance. Otherwise, the Kruskal-Wallis H-test was used. The statistical value and the p-value for each measured item are summarized in Table 5.1, with a detailed description in the next subsection. The significance level was set to .05.

5.1.4.2 Results

Figure 5.3 shows the difference between the two different navigation interfaces in the VE in terms of the total time and the geometrical size of the COG's area. The COG's area was derived by projecting Forward/Backward (F/B) and Left/Right (L/R) postural sway signals onto the XY plane, then was defined as the optimum ellipse surrounding 90% of the sampled points as used for example in the work of Chardonnet *et al.* (2017). For each navigation method, the variation of the COG's area was considered to be an objective behavioral indicator and was measured as the difference before and after navigation in the VE. The joystick controller ($M = 303.83\,s$, $SD = 44.91\,s$) significantly

Table 5.1: Statistical results for the different measured items.

Item	Test	Statistical value	p-value	Sig.
Total time	H-test	17.468	.00003	**
Variation of area	ANOVA	4.573	.043	*
Total SSQ	ANOVA	5.638	.028	*
Nausea	ANOVA	5.876	.024	*
Oculomotor	ANOVA	5.882	.023	*
Disorientation	ANOVA	1.666	.210	
Efficiency	H-test	3.990	.046	*
Likability	ANOVA	4.330	.049	*
Accuracy	ANOVA	6.760	.016	*
Learnability	H-test	8.270	.004	**
Immersion	H-test	10.958	.00093	**
Naturality	H-test	1.381	.240	
Consistency	H-test	8.416	.004	**
Concentration	H-test	7.879	.005	**

required much more time to navigate in the VE compared to that of the semiautomatic technique ($M = 227.59\,s$,$SD = 16.83\,s$), while we can also see that the COG's area significantly changed from ($M = 58.92\,mm^2$, $SD = 41.90\,mm^2$) to ($M = 27.63\,mm^2$, $SD = 42.55\,mm^2$).

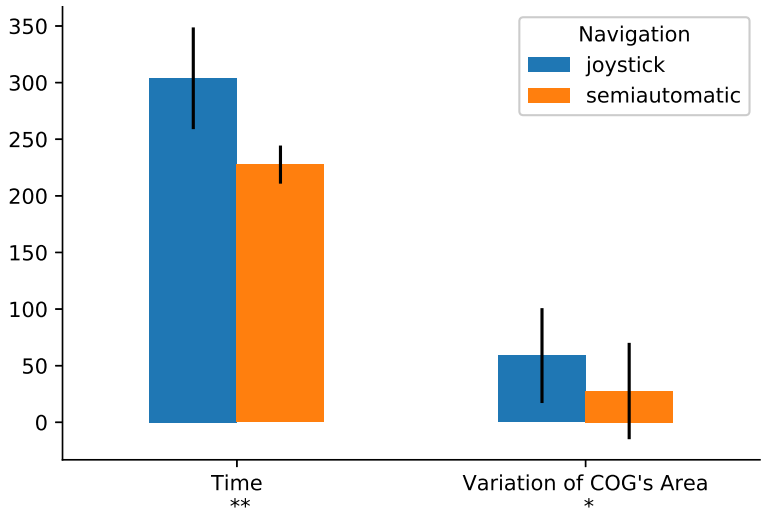

Figure 5.3: Comparison of objective indicators for both navigation techniques.

Figure 5.4 depicts the results of the SSQ scores obtained from the questionnaires. The participants were requested to rate the amount of sickness they felt before and after each experiment. Among the three categories of the SSQ (nausea, oculomotor, disorientation), we found a significant decrease for the total SSQ score, nausea and oculomotor categories (34.13%, 41.63% and 40.00% respectively). The disorientation score decreased slightly of about 19.05%, but no significance was found.

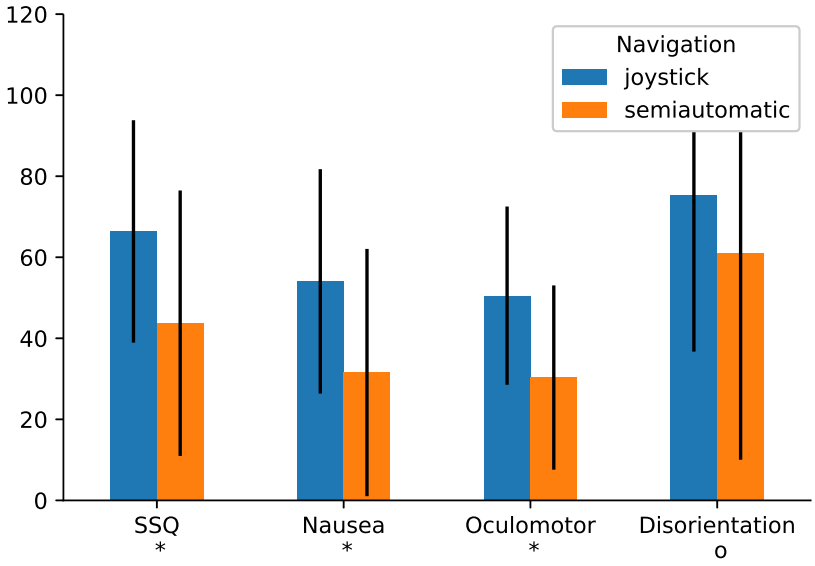

Figure 5.4: Comparison in terms of SSQ scores.

Figure 5.5 shows the results from the participants after rating each navigation method in terms of efficiency, likability, accuracy, learnability, immersion, naturality, consistence and concentration based on a 5-point Likert scale (1=not at all, 5=extremely). The semiautomatic navigation technique significantly outperformed the joystick-based technique for all items except naturality. The joystick was reported to be easier to know how to use since the participants already experienced this kind of controller. However, there was no significant difference concerning naturality because navigation in the VE was still considered as different compared to navigation in the physical world as the participants reported after the experiment.

We also got a general feedback from the participants after the experiments. They liked the joystick's learnability more than with the semiautomatic technique, because they had already played or seen video games and could therefore control movements unconsciously; however, every time they wanted

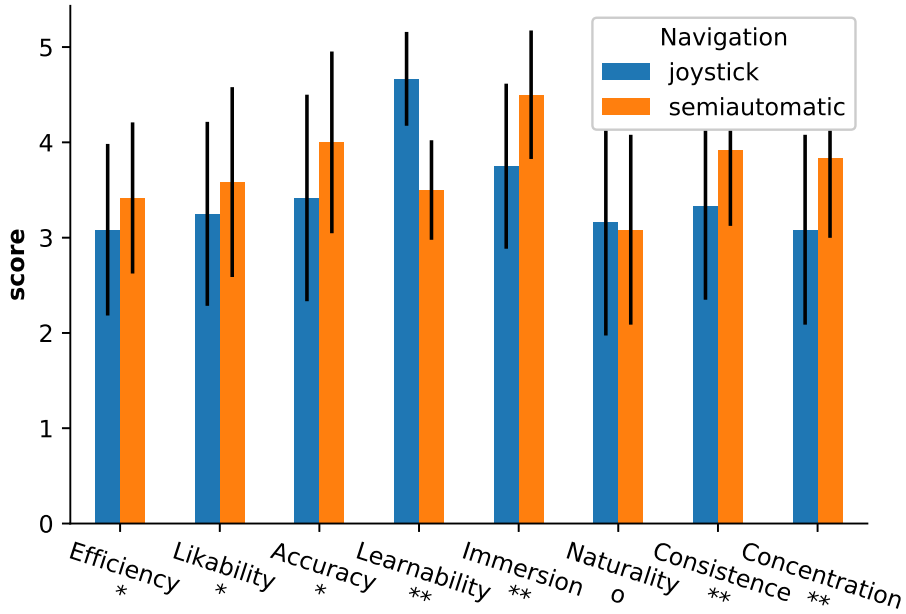

Figure 5.5: Comparison in terms of quality factors.

to move to one coin in the VE they had to constantly adjust their movements and therefore found it hard to locate themselves exactly. The experience with the joystick was also reported to be jerkier and less smooth during navigation. Concerning the semiautomatic navigation method, all the participants mentioned that they liked seeing the generated path as it could give them more motion cues about the moving direction, but some users also complained that they did not want to be constrained in the path and with pre-defined movements along the generated path.

5.1.4.3 Discussion

Recall that we proposed two assumptions in order to show that the semiautomatic navigation technique could provide better user experience, and especially reduced cybersickness.

5.1.4.3.1 Validation of hypothesis 1 Semiautomatic navigation was much more efficient in comparison with the joystick method since the semiautomatic method generates optimized paths towards the desired position, and in this case, users can focus on the task instead of considering how to control navigation in the VE, which can be evidenced from the total time of task completing and also subjec-

tive evaluation shown in previous subsubsection 5.1.4.2. With semiautomatic navigation, users only needed to set the target, then to follow the trajectory, and to use the gaze-directed method to make corrections if the path was not the preferred one. Participants seemed to appreciate the semiautomatic method considering all criteria except learnability because they were familiar with the joystick, which coincides to previous studies (Tregillus *et al.* 2017).

5.1.4.3.2 Validation of hypothesis 2 The significant decrease of the COG's area indicated that there was less sensory conflict in the semiautomatic navigation method, therefore the CNS could control the postural sway more easily as also reported in the work of Chardonnet *et al.* (2017). Other past studies also observed a similar conclusion that low sensory conflict normally induces less cybersickness (Llorach *et al.* 2014). However, the disorientation score did not witness any significant difference between the two different navigation methods, although the participants reported less disorientation when using the semiautomatic method. The reasons can be: a) the participants were requested to finish the task as fast as they could so they focused more on the task instead of looking around and exploring the VE, but concerning other items of the SSQ, semiautomatic navigation achieved better performance with the assistance of the motion planner which could get rid of unnecessary movements and involuntary visual stimuli. b) The sample size was not enough large since we had only 13 participants. Further studies with much more participants should be conducted.

5.1.5 Conclusion

Considering the sensory conflict theory, we designed a semiautomatic navigation method trying to reduce the generation of conflicted signals. We analyzed user experience in terms of cybersickness and other quality factors and we compared them with joystick-based navigation. Statistical analyses showed significant improvement in reducing cybersickness especially symptoms of nausea and oculomotor. This validates our hypotheses that when navigating using a joystick controller, users have to frequently change the speed and direction of movement and always look around for the target, consequently, leading to more sensory conflict. On the other hand, the motion planner in semiautomatic navigation may help users navigate in a VE with less unnecessary and jerky visual stimuli, therefore reduce cybersickness. In addition, semiautomatic navigation achieves better performance among several quality factors such as efficiency, likability, accuracy, immersion, consistency and concentration.

Future work shall focus more on user's intention and also the optimisation of navigation speed.

In this section, the focus of the work was to adapt the navigation trajectory to avoid unnecessary movements. However, considering that the visual motion stimuli is directly linked to the speed profile, we were wondering if adapting the navigation speed can improve the user experience. In the next section, we will propose a speed protector that can control the speed during navigation.

5.2 Navigation with speed protector

5.2.1 Introduction

The main purpose of this section is to investigate whether an optimized speed profile of the navigation with proper acceleration and jerk can improve user experience. The idea is to design what we call a *speed protector* that prevents users from negative experience due to irregular speeds. The long term objective is to further extend this protector in a feedback navigation interface that can adjust the motion conditions according to the user's physiological response. For instance, if the navigation system detects that a user gets VR sick or experiences high cognitive workload, it can restrict irregular navigation and optimize the speed accordingly, and not simply stop abruptly which is likely to induce posture imbalance due to inertia (Merienne 2016). Our objective is a wide one. However, this section focuses on designing the speed protector and validating its performance with a user study.

We believed that the control of physical walking according to the body mechanism will make the difference to virtual navigation especially in improving comfort in a VR experience. In addition, it enables us to answer some challenging questions, such as how to reduce cybersickness and cognitive workload efficiently and achieve a more comfortable experience, to study user behaviors during complex navigation in immersive environments, and further to motivate the application of VR into various fields.

The contributions of this section include the following aspects:

- Design of a speed protector based on a minimal-jerk model. We explained our choice for the minimal-jerk model rather than other models. We also presented the algorithm that can be directly implemented as a speed protector during virtual navigation. This will be presented in subsection 5.2.2.

- User test arranged in an orthogonal table which allows exhaustive parameter studies. As we

considered several factors during the experiment, the orthogonal experiment design is a powerful tool to reduce the total number of experiments, making our experiment results more reliable with less effort. The results indicated that the magnitude of acceleration and jerk influence user experience. This will be addressed in subsection 5.2.3.

5.2.2 Design of the Speed Protector

Previous studies had developed navigation techniques by adding extra trajectories (Igarashi *et al.* 1998) to follow or adapting speed (Argelaguet 2014) to keep smooth navigation. Here we proposed a new speed adaptation method considering that the rule of human walking and hand movement is usually a minimization problem. It represented a novel idea to treat navigation in 3D VEs with a similar principle as human movements in physical environments. This section explains how to design the speed protector and how to embed it into a navigation system. We developed two types of protectors: a nonlinear one and a linear one. The nonlinear speed protector suggests that the speed is a nonlinear function and the linear speed protector implies that the speed is a linear function.

5.2.2.1 Nonlinear speed protector

The nonlinear speed protector is derived from the minimum-jerk model where the speed profile is found as a high-order polynomial function. The problem is to find the speed v defined on $[0, T]$ which minimizes the cost functional

$$\min J(v) = \frac{1}{2}\int_0^T (v'')^2 \mathrm{d}t \tag{5.4}$$

Subject to

$$\begin{cases} v(0) = v_0, \quad v(T) = v_T, & \text{(5.5a)} \\ v'(0) = v'_0, \quad v'(T) = v'_T, & \text{(5.5b)} \\ \text{the speed constraint: } v \in \Omega = [v_{\min}, v_{\max}] & \text{(5.5c)} \\ \text{the acceleration constraint: } a \in \Omega = [a_{\min}, a_{\max}] & \text{(5.5d)} \\ \text{and the control constraint: } j \in \Omega = [j_{\min}, j_{\max}] & \text{(5.5e)} \end{cases}$$

The purpose is to find the solution of $v(t)$ such that it makes $J(v)$ minimal, which implies that the change $\mathrm{d}J(v)$ of $J(v)$ should be zero in any small variations of v. Translating this into mathematical

interpretation, we firstly define a family of functions of the following form,

$$h(\epsilon, t) = v(t) + \epsilon\delta(t) \tag{5.6}$$

where $h(\epsilon, t)$ is a family of functions including the potential solution, and $\delta(t)$ is an arbitrary function with $\mathcal{C}^1$ continuity to perturb $v(t)$ by small changes of magnitude ϵ. For $h(\epsilon, t)$ to meet the boundary conditions given in Equation 5.5a and Equation 5.5b, the following conditions are prescribed to $\delta(t)$,

$$\begin{cases} \delta(0) = 0 \quad \delta(T) = 0 & \text{(5.7a)} \\ \delta'(0) = 0 \quad \delta'(T) = 0 & \text{(5.7b)} \end{cases}$$

$J(v)$ to be minimal requires that

$$\frac{\mathrm{d}J(h)}{\mathrm{d}\epsilon}|_{\epsilon=0} = \frac{1}{2}\int_0^T (h'')^2 \mathrm{d}t = 0 \tag{5.8}$$

Note

$$\begin{aligned} \frac{\mathrm{d}J(\epsilon)}{\mathrm{d}\epsilon}|_{\epsilon=0} &= \int_0^T (v'' + \epsilon\delta'')\delta'' \mathrm{d}t \\ &= \int_0^T v''\delta'' \mathrm{d}t \end{aligned} \tag{5.9}$$

Recall that $\delta'(0) = 0$, $\delta'(T) = 0$, using integration by parts

$$\begin{aligned} \int_0^T v''\delta'' \mathrm{d}t =& v''\delta'|_0^T - \int_0^T v^{(3)}\delta' \mathrm{d}t \\ =& -\int_0^T v^{(3)}\delta' \mathrm{d}t \end{aligned} \tag{5.10}$$

Recall that $\delta(0) = 0$, $\delta(T) = 0$, using integration by parts again

$$\begin{aligned} \int_0^T v^{(3)}\delta' \mathrm{d}t =& v^{(3)}\delta|_0^T - \int_0^T v^{(4)}\delta \mathrm{d}t \\ =& -\int_0^T v^{(4)}\delta \mathrm{d}t \end{aligned} \tag{5.11}$$

Since $\frac{dJ(\epsilon)}{\mathrm{d}\epsilon}|_{\epsilon=0} = 0$, it requires that

$$\int_0^T v^{(4)}\delta \mathrm{d}t = 0 \tag{5.12}$$

which must be the case for an arbitrary function δ, meaning that, $\forall t \in [0, T], v^{(4)} = 0$.

It is obvious that in order to ensure both null 4^{th} derivative and satisfied constraints, the profile of v must be a third order polynomial function, which is also the reason why we defined the speed protector as nonlinear, i.e.,

$$v = \sum_{k=0}^{3} \xi_k t^k \tag{5.13}$$

It is then required to determine the four parameters ξ_0, ξ_1,...ξ_3. The first two parameters can be determined from the initial conditions. For $t = 0$

$$\begin{cases} \xi_0 = v_0 & \text{(5.14a)} \\ \xi_1 = v_0' & \text{(5.14b)} \end{cases}$$

The last two parameters can be determined from the terminal conditions

$$\begin{cases} v_T = \xi_0 + \xi_1 T + \xi_2 T^2 + \xi_3 T^3 & \text{(5.15a)} \\ v_T^{'} = \xi_1 + 2\xi_2 T + 3\xi_3 T^2 & \text{(5.15b)} \end{cases}$$

This can be solved for ξ_2 and ξ_3, expressed in matrix form

$$\begin{bmatrix} \xi_2 \\ \xi_3 \end{bmatrix} = \begin{bmatrix} T^2 & T^3 \\ 2T & 3T^2 \end{bmatrix}^{-1} \begin{bmatrix} v_T - \xi_0 - \xi_1 T \\ x_T' - \xi_1 \end{bmatrix} \tag{5.16}$$

Once the ξ_k parameters are known and substituted into Equation 5.13, the entire motion profile from the starting time 0 to the terminal time T can be determined.

5.2.2.2 Why minimizing jerk and not other temporal derivatives?

The third derivative of position with respect to time is called jerk. The fourth, fifth, and sixth derivative are called snap, crackle, and pop, respectively. The problem is to ensure that the minimum-jerk model can provide the best description of human motion profiles: why not for example other temporal derivatives?

To answer this question, Richardson and Flash (2002) considered how position x changes as a function of the derivative order n in the following expression:

$$J\left(x(t)\right) = \frac{1}{2} \int_0^T \left(\frac{\mathrm{d}^n x}{\mathrm{d}t^n}\right)^2 \mathrm{d}t \tag{5.17}$$

They found that as n increases, the solution to the functional $x(t)$ approaches to a step function.

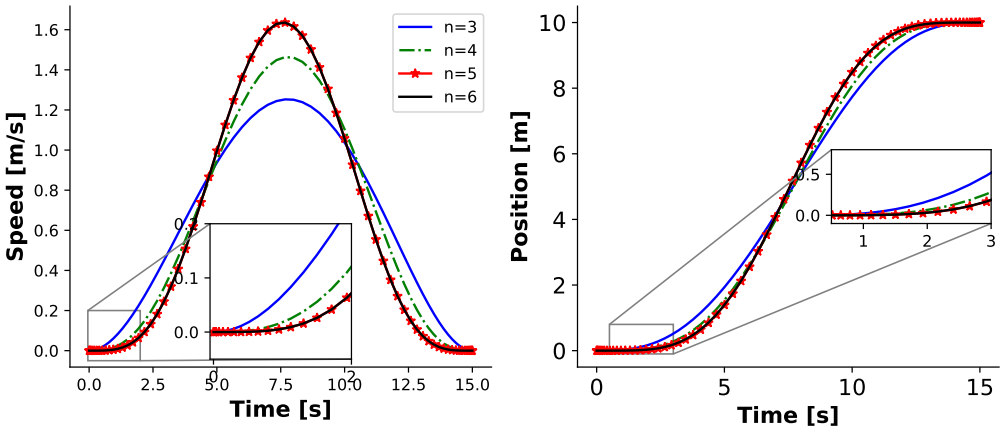

Figure 5.6: Motion speed for each trajectory; the ratio of peak speed to average speed increases as n increases: motion with minimum jerk ($n = 3$), minimum snap ($n = 4$), minimum crackle ($n = 5$) and minimum pop ($n = 6$).

Figure 5.6 shows minimum jerk, snap, and crackle trajectories. Note how the first derivative (speed) of each trajectory becomes narrower and taller when jerk, snap and crackle appear in the minimized functional. Therefore, if snap is minimized, we get a movement with a higher peak speed than a trajectory that minimizes jerk. This implies that as n increases in Equation 5.17, the solution yields a trajectory with a larger peak relative to average speed.

If we call r the ratio of peak speed to average speed, then a minimum-acceleration trajectory, i.e., $n = 2$ in Equation 5.17, has a ratio of $r = 1.5$. For a minimum-jerk trajectory, $n = 3$ and $r = 1.875$; for a minimum-snap trajectory, $n = 4$ and $r = 2.816$. Psychophysical experiments revealed that navigation movements have a ratio r that is about 1.75, and thus most resemble minimum-jerk trajectories (Flash and Hogan 1985).

5.2.2.3 Linear speed protector

The linear speed protector is based on the motion sickness dose value (MSDV). The MSDV has been widely used as a measurement for motion sickness (Eriksson and Svensson 2015) and VR sickness (Plouzeau *et al.* 2018; So 1999): the larger the value, the higher the level of VR sickness. The MSDV is defined by

$$\min M = \frac{1}{2}\int_0^T a^2 \mathrm{d}t = \frac{1}{2}\int_0^T (v')^2 \mathrm{d}t \tag{5.18}$$

where a is the acceleration, T is the total navigation time. By integrating the square of acceleration during the whole navigation time, the MSDV provides an absolute value to characterize the level of motion sickness or VR sickness.

Instead of using the MSDV as a measurement method, we can also obtain a speed profile that automatically meets the definition of the MSDV: we can get the analytical solution of Equation 5.18 if we employ the variational method as done in the minimum-jerk model, which leads to the following final solution

$$\forall t \in [0, T], v'' = 0 \tag{5.19}$$

This suggests that the speed profile should be a linear function of $t, \forall t \in [0, T]$ parameterized by ϑ_0 and ϑ_1, i.e.,

$$v = \vartheta_0 + \vartheta_1 t \tag{5.20}$$

In order to determine the unknown parameters ϑ_0 and ϑ_1, we only need two conditions from the following three options,

$$\begin{cases} v(0) = v_0 & \text{(5.21a)} \\ v(T) = v_T & \text{(5.21b)} \\ \vartheta_1 = a_{\max} & \text{(5.21c)} \end{cases}$$

where $a_{\max}$ is the maximal allowed acceleration. In either cases, the final navigation speed profile will be only piecewise linear and just $\mathcal{C}^0$ continuous.

5.2.2.4 navigation constraints

Putting constraints on motion parameters is mandatory. Indeed, a high magnitude of acceleration and jerk generally leads to a lose of balance and worse experience within a short period of time; further users have to abandon the allotted task to do postural adjustment (Crossland and Rich 1998). Therefore, it is necessary to set constraints on the levels of acceleration and jerk. Although such constraint values may vary among different studies and works, they normally fall within similar ranges. For example, for acceleration the threshold for discomfort lies around 1m/s^2, ranging up to 1.47m/s^2 (Kilinç and Baybura 2012); the jerk threshold for discomfort lies around 0.5m/s^3, ranging up to 0.9m/s^3 (Kilinç and Baybura 2012; Förstberg 2000). The *Mechanical Vibration and shock- Evaluation of human exposure to whole-body vibration- Part 1- General Requirements* (1997) defines

acceleration thresholds that are widely used regarding user comfort, as given in Table 5.2. Most of these studies on the magnitude are carried out for the railway and the automotive industries, but we considered that navigation in general should have the same impact on users whatever the environment. In this work the motion constraints for our speed protector will be chosen from the above-mentioned settings.

Table 5.2: Acceleration limits and corresponding comfort levels

Comfort levels	Acceleration limits ($\mathcal{A}_{\max}$)
Not uncomfortable	0.315m/s^2
A little uncomfortable	0.63m/s^2
Fairly uncomfortable	1.0m/s^2
Uncomfortable	1.6m/s^2
Very uncomfortable	2.5m/s^2

5.2.2.5 Algorithm implementation

Considering the whole problem given in Equation 5.4, we would firstly present the bisection method so that the constrained optimization problem can be solved in an iterative manner. In mathematics, the bisection method is the simplest method to find a root of any continuous functions (e.g., $r(t)$) on an interval $[T_m, T_n]$ with opposite signs on the boundary, hence $r(T_m)r(T_n) < 0$. The procedure goes as follows: find the midpoint of $[T_m, T_n]$, i.e., $T_k \leftarrow \frac{1}{2}(T_m + T_n)$. If r_m and r_k have opposite signs, the interval $[T_m, T_k]$ has the optimal solution and will be substituted for the next iteration. Likewise, if r_n and r_k have opposite signs, the interval $[T_k, T_n]$ will be retained for the next iteration. Such process is repeated until the length η of the most recent interval $[T_m, T_n]$ is less than the desired accuracy κ. Once the optimal time T_o is found, it computes the corresponding optimal state variables including speed v_o, acceleration a_o and jerk j_o. It is worth noting that the classical bisection method tends to compare the signs (e.g., +, -) of the solution on the boundary of a given interval. Here we rather used boolean values (e.g., **true**, **false**), which follows the same philosophy for optimization.

Figure 5.7 presents an overview of the algorithm developed for the proposed speed protector. Algorithm 2 integrates both the nonlinear and the linear speed protectors, and is the main part of our implementation which shows a frame-based motion protector to be embedded in current devices for controlling virtual walking. Algorithms 3, 4 and 5 are complementary functions required for the calcu-

Algorithm 2 Implementation of the speed protector in a real application considering user inputs

$\mathcal{I} \in \mathbb{R}$ ▷ Input speed from user's controller
$\mathcal{V} \in \mathbb{R}$ ▷ Real navigation speed in the VE
$\mathcal{V}_{-1} \in \mathbb{R}$ ▷ Real navigation speed in the VE of the last frame
$\mathcal{A} \in \mathbb{R}$ ▷ Real navigation acceleration in the VE
$\mathcal{A}_{-1} \in \mathbb{R}$ ▷ Real navigation acceleration in the VE of the last frame
$t \leftarrow 0$, $t \in \mathbb{R}^+$ ▷ Current time since program starts
$t_{-1} \leftarrow 0$, $t \in \mathbb{R}^+$ ▷ Time of the last frame
$\Delta \leftarrow 0$, $\Delta \in \mathbb{R}^+$ ▷ Time difference since the last frame
repeat Frame-by-frame animation
    Get $\mathcal{I}$ from user's controller
    $\Delta \leftarrow |t - t_{-1}|$
    if nonlinear speed protector **then**
        $T_o \leftarrow$ findOptimalTime
        $\mathcal{V}_o, \mathcal{A}_o \leftarrow$getStates($T_o$, Δ, **false**, $\mathcal{V}_{-1}$, $\mathcal{A}_{-1}$, $\mathcal{I}$)
        $\mathcal{A} = \mathcal{A}_o$ ▷ Use the optimal acceleration as the current acceleration
        if $\mathcal{I} > \mathcal{V}_{-1}$ **then**
            $\mathcal{V} \leftarrow \min(\mathcal{V}_o, \mathcal{I})$ ▷ Avoid sharp increase
        else
            $\mathcal{V} \leftarrow \max(\mathcal{V}_o, \mathcal{I})$ ▷ Avoid sharp decrease
        end if
        $\mathcal{A}_{-1} \leftarrow \mathcal{A}$
    else ▷ Linear speed protector case
        if $\mathcal{I} > \mathcal{V}_{-1}$ **then**
            $\mathcal{V}_o \leftarrow \mathcal{V}_{-1} + a_{\max}\Delta$ ▷ $a_{\max}$ is from the comfort limit
            $\mathcal{V} \leftarrow \min(\mathcal{V}_o, \mathcal{I})$ ▷ Avoid sharp increase
        else
            $\mathcal{V}_o \leftarrow \mathcal{V}_{-1} - a_{\max}\Delta$
            $\mathcal{V} \leftarrow \max(\mathcal{V}_o, \mathcal{I})$ ▷ Avoid sharp decrease
        end if
    end if
    $t_{-1} \leftarrow t$
    $\mathcal{V}_{-1} \leftarrow \mathcal{V}$
until Program close

lation and serve for the nonlinear speed protector. The physical meaning of parameters including $\mathcal{I}$, $\mathcal{V}$, $\mathcal{V}_{-1}$, $\mathcal{A}$, $\mathcal{A}_{-1}$, t, t_{-1}, Δ are explained inside the algorithm tables. Here parameters with the subscript -1 mean values from the last frame. With all these parameters available, the system will firstly read the user's inputs from the VR controller, and depending on the values, the optimization problem and the corresponding boundary conditions defined in Equation 5.4, Equation 5.5a and Equation 5.5b are formulated simultaneously by setting

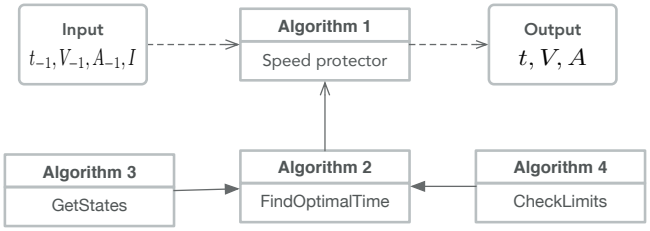

Figure 5.7: Schematic diagram showing the relationships between the implemented algorithms; the inputs $t_{-1}, \mathcal{V}_{-1}$ and $\mathcal{A}_{-1}$ are from the last frame, and the outputs $t, \mathcal{V}$ and $\mathcal{A}$ are to be used for the current frame.

$$\begin{cases} v(0) = \mathcal{V}_{-1} & \text{(5.22a)} \\ v'(0) = \mathcal{A}_{-1} & \text{(5.22b)} \\ v(T_o) = \mathcal{I} & \text{(5.22c)} \\ v'(T_o) = 0 & \text{(5.22d)} \end{cases}$$

According to Equation 5.22a and Equation 5.22b, speed and acceleration will be calculated based on information from the last frame, and the final speed is expected to reach the command speed from the user's input with a smooth concatenation, as expressed in Equation 5.22c and Equation 5.22d. Then, a smooth speed profile is computed accordingly. Subsequently, the optimal time T_o required to change the current speed to the target speed (the target is provided by the input from the user's controller) is calculated via the bisection method. Then, the parameters in Equation 5.13 are obtained to compute the theoretical speed and acceleration at the current frame, based on the last frame. Finally, the system compares the calculated theoretical speed with the target speed in order to avoid a sharp increase or decrease between two frames. As presented in *line 15 to line 18* of Algorithm 2, the system firstly checks if the user increases or decreases speed by comparing the input speed $\mathcal{I}$ and the last frame speed $\mathcal{V}_{-1}$: if increasing, the real speed is the smaller one between the optimized one $\mathcal{V}_o$ and the input speed $\mathcal{I}$; otherwise if decreasing, the real speed is the larger one between the optimized one $\mathcal{V}_o$ and the input speed $\mathcal{I}$. Therefore, when the speed protector is applied, the real navigation speed is not always the same as the optimized profile from the protector.

Algorithm 3 along with the supplementary Algorithm 4 and Algorithm 5 describes the pseudo-code of the bisection method used to compute the motion profile with minimum jerk and constraints. The motion profiles can be easily solved with Equation 5.13, Equation 5.14a and Equation 5.16 if the

constraints in subsubsection 5.2.2.4 are excluded. However, these constraints should be considered to improve user comfort during navigation. When the total time T is set to a small value, the peak value of speed, acceleration and jerk will exceed the constraints and miss comfort conditions; when T increases monotonously to a relatively large value, the peak values will become smaller correspondingly so that all the conditions will be fulfilled. In return, too much time will be taken to reach the desired states. A compromise must be found between the value of the total time and the required constraints, which is the reason why the bisection method is used here. As the peak value changes monotonously according to the total time T, we can set a large initial search interval (e.g., $[0.1, 60]$) to ensure the optimal time can be found with the bisection method.

Algorithm 4 can get the evolution of different motion states within a given terminal time T so that the algorithm is used in each iteration. In order to have a solution fulfilling the boundary conditions, the algorithm firstly tries to compute the polynomials parameterized with ξ_0, ξ_1, ξ_2 and ξ_3, in Equation 5.14a and Equation 5.16. Then, an equally spaced time vector t is generated in $[0, T]$; v, a and j are calculated for each element in vector t (time step). In such element-wise calculation, the results are also in vector form which represents the corresponding motion states at each time step.

Algorithm 5 is a module to check whether the constraint conditions satisfy the given range. It returns a boolean value, either **true** meaning that the solution meets all the requirements. On the contrary, if one of the motion states (e.g., speed, acceleration and jerk) cannot be met, the module returns **false** implying that the current motion profiles are not acceptable.

The implementation of these algorithms was done in Eigen (Guennebaud, Jacob, *et al.* 2010) which is a C++ template library for linear algebra, and the code was wrapped to be used in Unity3D.

The implementation of the linear version is much simpler as no optimization is required. *Line 22 to line 29* in Algorithm 2 presents the running process of the linear speed protector. The system has just to know $a_{\max}$ and the speed is changed accordingly depending on the variation of acceleration.

5.2.3 User validation study

We designed an experiment to validate whether user experience including cybersickness and cognitive workload could be improved with the proposed speed protector. The hypotheses were

H1 When speed protectors (especially the nonlinear one) are activated, users are less prone to

Algorithm 3 Bisection method to find a minimum jerk profile

function findOptimalTime
  $[T_m, T_n] \in \mathbb{R}^2$ ▷ Initial search domain
  $\eta \leftarrow |T_m - T_n|$, $\eta \in \mathbb{R}$ ▷ Runtime error
  $\kappa \leftarrow 0.01$, $\kappa \in \mathbb{R}$ ▷ Predefined accuracy
  while $\eta > \kappa$ **do**
    $v_m, a_m, j_m \leftarrow$ getStates(T_m, 0, **true**, $\mathcal{V}_{-1}$, $\mathcal{A}_{-1}$, $\mathcal{I}$) ▷ Vector
    $r_m \leftarrow$ checkLimits(v_m, a_m, j_m) ▷ Boolean
    $v_n, a_n, j_n \leftarrow$ getStates(T_n, 0, **true**, $\mathcal{V}_{-1}$, $\mathcal{A}_{-1}$, $\mathcal{I}$) ▷ Vector
    $r_n \leftarrow$ checkLimits(v_n, a_n, j_n) ▷ Boolean
    if $r_m \neq r_n$ **then**
      $T_k \leftarrow \frac{1}{2}(T_m + T_n)$ ▷ Bisection point
      $v_k, a_k, j_k \leftarrow$ getStates(T_k, 0, **true**, $\mathcal{V}_{-1}$, $\mathcal{A}_{-1}$, $\mathcal{I}$) ▷ Vector
      $r_k \leftarrow$ checkLimits(v_k, a_k, j_k)
      if $r_k \neq r_n$ **then**
        $T_m \leftarrow T_k$
      else
        $T_n \leftarrow T_k$
      end if
    end if
    $\eta \leftarrow |T_m - T_n|$ ▷ Update error
  end while
  $T_o \leftarrow \frac{1}{2}(T_m + T_n)$ ▷ Compute the final optimal time
  return T_o
end function

Algorithm 4 Get the evolution of the state within a total time T_g

function GETSTATES(T_g, Δ, vectorForm, $\mathcal{V}_{-1}$, $\mathcal{A}_{-1}$, I)
  Get the boundary condition required in Equation 5.5a and Equation 5.5b:
  $v(0) \leftarrow \mathcal{V}_{-1}$, $v(T_g) \leftarrow \mathcal{I}$
  $v'(0) \leftarrow \mathcal{A}_{-1}$, $v'(T_g) \leftarrow 0$
  Compute a_0 and a_1 as in Equation 5.14a
  Compute a_2 and a_3 with T as in Equation 5.16
  if vectorForm **then**
    Generate a linearly spaced vector t_v between and including 0 and T_g
  else
    $t_v = \Delta$ ▷ t is a scalar
  end if
  $v \leftarrow a_0 + a_1 t_v + a_2 t_v^2 + a_3 t_v^3$ ▷ Element-wise product
  $a \leftarrow a_1 + 2a_2 t_v + 3a_3 t_v^2$ ▷ Element-wise product
  $j \leftarrow 2a_2 + 6a_3 t_v$ ▷ Element-wise product
  return v, a, j ▷ Each is in vector form
end function

Algorithm 5 Check if the results meet the required limits

function CHECKLIMITS(v, a, j)
  $[v_{\min}, v_{\max}] \in \mathbb{R}^2$ ▷ Range of speed
  $[a_{\min}, a_{\max}] \in \mathbb{R}^2$ ▷ Range of acceleration
  $[j_{\min}, j_{\max}] \in \mathbb{R}^2$ ▷ Range of jerk
  $r \leftarrow$ **false** ▷ Default value
  if $\max(v) \leq v_{\max}$ **and** $\min(v) \geq v_{\min}$ **then**
    if $\max(a) \leq a_{\max}$ **and** $\min(a) \geq a_{\min}$ **then**
      if $\max(j) \leq j_{\max}$ **and** $\min(j) \geq j_{\min}$ **then**
        $r \leftarrow$ **true** ▷ Constraints satisfied
      end if
    end if
  end if
  return r ▷ Boolean value
end function

cybersickness and suffer from less cognitive workload.

H2 Acceleration and jerk in the nonlinear speed protector are the factors that are highly associated with cybersickness and cognitive workload.

Cybersickness was evaluated by the simulator sickness questionnaire (*SSQ*) (Kennedy, Lane, *et al.* 1993) and event-related skin conductance responses (ER-SCR), while cognitive workload was measured through the NASA-TLX (Hart 2006b). The *ER-SCR* during immersion is the physiological information

that contains the height of skin conductance signal peaks and the recovery time of an excitation; when VR users get frequent visual stimulation related to illusions of self-motion, the electrodermal activity (EDA) signal shows more peaks, that can be used to measure user experience (Tamura *et al.* 2018).

5.2.3.1 Platform design

In order to be comparable, user experiments were carried out in both a CAVE system designed by *Antycip Simulation*[3] and an HTC Vive head-mounted display (HMD). The CAVE, controlled by six PCs via MPI, is composed of five walls equipped with *Mirage 4k25* projectors for stereoscopic vision with a 4096×2160 pixel resolution at a maximal 120 Hz performance, one ART tracking system[4] to track users and interaction devices. An in-house software development interface called *iiVR* written in C++ was developed to connect the whole VR equipments such as the display system, navigation/interaction devices (e.g., a Flystick device) and infrared cameras. The HTC Vive has a refresh rate of 90 Hz and a display resolution of 2160×1200 pixels.

5.2.3.2 Participants

Fifteen subjects (11 males and 4 females: 24.52 ± 3.32 years, 67.11 ± 10.99 kg) from the university were invited to voluntarily participate to the experiment. There was a brief introduction to give supplementary information about the whole test procedure and probable effects prior to each experiment. Individual differences such as illness, gender and experience in videos games and VR application can affect the susceptibility to cybersickness (Davis *et al.* 2014). In order to measure their health conditions and have a better insight of their experience in the usage of computer applications, especially VR games, we designed a pre-exposure questionnaire for all participants to fill before the experiment. According to this questionnaire, no subject reported extreme disorders or unusual visual, hearing as well as balancing capabilities, indicating that they could perform the experiment. A consent form was also signed by participants.

5.2.3.3 Orthogonal experimental design

The orthogonal experimental design is an efficient and fast way to study phenomena that can be affected by many potential factors. Conventional methods normally study the effect of these factors

[3] www.antycipsimulation.com
[4] https://ar-tracking.com

separately by extracting one factor as the variable and fixing the remaining factors. Although such separation allows to check the significance of the factors, they converge only to a local significance which means that the significance might fail to reproduce when a combination of these factors are operated (Su 2013).

Considering many factors that would affect user experience, we investigated eight factors including the longitudinal speed modality, acceleration, jerk, the rotational speed modality, rotational acceleration, and rotational jerk. The speed modality referred to three different types: no speed protector (NP), nonlinear speed protector (non-LP), and linear speed protector (LP), through which we could verify the efficiency of the speed protector.

The VR platform and the scenario type were involved to reduce the effect of experiment repetition which can affect subjects' reporting (Clément *et al.* 2007). Two platforms and three scenarios were introduced to extend the generality of the speed protector and more importantly to reduce learning effects during the experiment. Again, it is important to keep in mind that the objective of the experiment is to validate the effect of the speed protector and its related parameters, not that of the platform and the scenario type.

The remaining parameters related to navigation dynamics were also examined to see the significance in terms of user satisfaction. With all these factors, we designed a $L_{18}(2^1 \times 3^7)$ table, as shown in Table 5.3: for example, in order to conduct the 3^{rd} experimental group, the user had to test with the HMD in a wide environment scenario, with both longitudinal and rotational speed protectors, a maximal acceleration of 2.4m/s^2, a maximal jerk of 3.0m/s^3, a maximal rotational acceleration of $45°/\text{s}^2$, and a maximal rotational jerk of $45°/\text{s}^3$. These parameters were determined through a trial and error procedure with magnitudes adapted from the literature (Kilinç and Baybura 2012; Förstberg 2000; Kemeny *et al.* 2017).

5.2.3.3.1 Protocol Three environments, consisting of a forest and a predefined route that users had to navigate through, were designed by controlling the density of trees and flowers in the forest from sparse to dense (low, medium, high), to reduce the accumulated familiarity of each environment. Two platforms (CAVE, HMD), three environments and other parameters were arranged in the orthogonal table as presented above. Participants had to pass a group of eighteen experiments in a random order and with one (minimum) to five (maximum) days between two sessions to avoid cumulative effects of

Table 5.3: Orthogonal experimental design with multi-factors and mixed levels (NP: no speed protector, LP: linear speed protector, non-LP: nonlinear speed protector)

Experiment Group	Platform	Scenario	Speed modality	Acceleration, m/s^2	Jerk, m/s^3	Rotational Speed modality	Rotational Acceleration, $°/s^2$	Rotational Jerk, $°/s^3$
1	HMD	Low	NP	-	-	NP	-	-
2	HMD	Low	non-LP	1.6	2.0	non-LP	30.0	30.0
3	HMD	Low	LP	2.4	-	LP	45.0	-
4	HMD	Medium	NP	-	-	non-LP	45.0	30.0
5	HMD	Medium	non-LP	1.6	1.0	LP	15.0	-
6	HMD	Medium	LP	2.4	-	NP	-	-
7	HMD	High	NP	-	-	LP	30.0	-
8	HMD	High	non-LP	2.4	1.0	NP	-	-
9	HMD	High	LP	0.8	-	non-LP	15.0	45.0
10	CAVE	Low	NP	-	-	non-LP	30.0	45.0
11	CAVE	Low	non-LP	0.8	2.0	LP	45.0	-
12	CAVE	Low	LP	1.6	-	NP	-	-
13	CAVE	Medium	NP	-	-	NP	-	-
14	CAVE	Medium	non-LP	2.4	3.0	non-LP	15.0	15.0
15	CAVE	Medium	LP	0.8	-	LP	30.0	-
16	CAVE	High	NP	-	-	LP	15.0	-
17	CAVE	High	non-LP	0.8	3.0	NP	-	-
18	CAVE	High	LP	1.6	-	non-LP	45.0	15.0

cybersickness after each immersion in the VE.

The experimental procedure was designed as follows:

1. A pre-exposure questionnaire was filled by each participant to check for any health issues. Since participants needed to know how to navigate using the Flystick or the HTC Vive, each of them was given a training period for about 2 minutes before being immersed in the VEs.

2. Before being introduced in the CAVE/HMD and exposed to visual stimuli, each participant was requested to fill a pre-exposure *SSQ* to detect any prior sickness symptoms. The E4 Empatica wristband[5] was used to get the EDA through two electrodes placed on the wrist at a 4 Hz sample rate with a unit of μS.

3. The participant started to navigate in the VE following a predefined checkpoint, during which he/she had to repeatedly accelerate, decelerate or make a turn in order to avoid obstacles on the path (note that frequent accelerations and decelerations aimed at provoking VR sickness more easily, and in this way, we were able to see the effects of the motion protector on user experience), as shown in Figure 5.8. The EDA was recorded for the whole navigation session in the VE.

4. When the participant reached the destination in the VE, he/she was removed from the CAVE/HMD system and was requested again to fill an *SSQ* and the NASA-TLX table according to the experience and impressions on the whole simulation without knowing the modality of the experiment. The final VR sickness score was evaluated by calculating the difference between the pre- and post-exposure scores in the VE and cognitive workload was analyzed through the NASA-TLX table.

5. Previous steps were repeated for each experiment and participant.

Each session lasted around 5.5 minutes on average, depending on the participants. If a participant got too sick during the experiment, he/she was asked to stop the experiment. Otherwise, he/she was asked to complete the remaining part of the path. Participants were free to stop the simulation at any time if they did not feel well. They were told by the experimenter to stop once the task was completed.

[5]https://www.empatica.com/research/e4/

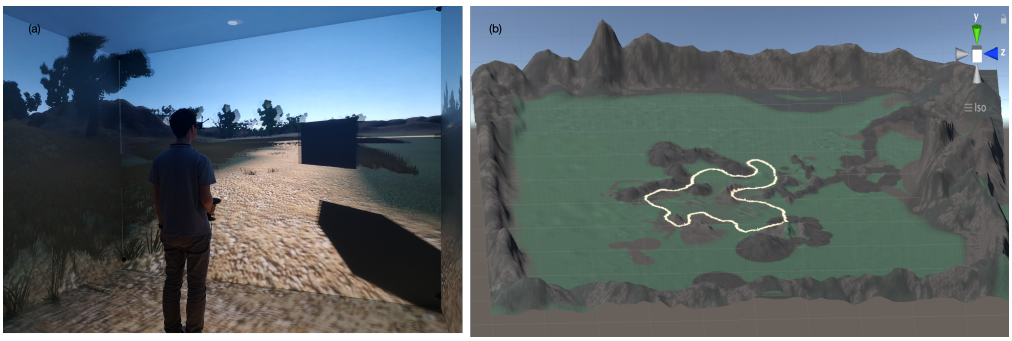

Figure 5.8: (a) Experiment inside a CAVE and (b) overview of the 3D virtual environment with the path to follow highlighted in yellow.

5.2.4 Results

Three participants did not finish all groups of the experiment due to their availability. Therefore, slightly different sample sizes were obtained for the different evaluation approaches, simulator sickness questionnaire (249), EDA signal (248), NASA-TLX (249). Under the same evaluation approach, the data sample size was not uniformly and evenly scattered over the different factor levels. As the sample size was no more balanced among the different settings, we decided to use a mixed-effects model. In order to avoid the effect of individual differences (recorded by the pre-exposure questionnaire) on the results as they could lead to potential variation, we set it as a random effect factor. The variables listed in Table 5.3 were set as fixed effect factors.

5.2.4.1 Significant factors

The significance level was set to .05. The number of *ER-SCR* of one EDA signal was computed via the *Neurokit2* (Makowski *et al.* 2020), and further statistical tests were performed in *R* (R Core Team 2020) and related packages including the *lme4*, *afex*, *lmerTest* and *effectsize*. Normality of distribution and equality of variance were verified for all data.

5.2.4.1.1 Optimal speed modality One mixed-effects model was conducted on the influence of five independent variables (platform, scenario, speed and rotational speed modality) on response variables including the total *SSQ* score, *Nausea*, *Oculomotor*, *Disorientation* (Table 5.4). Except the platform which contains only two levels (CAVE, HMD), all the other factors included three levels. The effect of the platform was found to be statistically significant concerning the total *SSQ* ($F_{1,235.84} = 25.60$,

$p < .01$, $\eta_p^2 = .10$), *Nausea* ($F_{1,236.24} = 16.05$, $p < .01$, $\eta_p^2 = .06$), *Oculomotor* ($F_{1,236.23} = 10.92$, $p < .01$, $\eta_p^2 = .04$) and *Disorientation* ($F_{1,235.74} = 20.70$, $p < .01$, $\eta_p^2 = .08$), while the effect of the speed modality was reported to be statistically significant regarding the total *SSQ* ($F_{2,235.41} = 4.36$, $p = .01$, $\eta_p^2 = .04$), *Nausea* ($F_{2,235.71} = 4.38$, $p = .01$, $\eta_p^2 = .04$) and *Oculomotor* ($F_{2,235.63} = 3.23$, $p = .04$, $\eta_p^2 = .03$). The interaction between the platform and the speed modality was also highly significant for *Disorientation* ($F_{2,235.23} = 4.71$, $p < .01$, $\eta_p^2 = .04$) and marginally significant for the total *SSQ* ($F_{2,235.40} = 2.88$, $p = .06$, $\eta_p^2 = .02$) and *Nausea* ($F_{2,236.68} = 2.57$, $p = .08$, $\eta_p^2 = .02$). As reported by the *Oculomotor* score, the effect of the rotational speed modality ($F_{2,235.57} = 3.45$, $p = .03$, $\eta_p^2 = .03$) was also statistically significant. No further significance ($p < .05$) was observed for the other main and interaction factors from the simulator sickness questionnaire.

Table 5.4: Effect of parameters on the simulator sickness questionnaire scores (**: $p < .01$, *:$p < .05$).

	Sum Sq	NumDF	DenDF	F	p-value	η_p^2	Sum Sq	NumDF	DenDF	F	p-value	η_p^2
	Total SSQ						Nausea					
Platform	2032.02	1	235.84	25.60	.00**	.10	1384.22	1	236.24	16.05	.00**	.06
Scenario	24.40	2	235.84	0.15	.86	<.01	96.50	2	236.23	0.56	.57	<.01
Speed Modality	692.55	2	235.41	4.36	.01*	.04	755.25	2	235.71	4.38	.01*	.04
Rotational Speed Modality	256.26	2	235.38	1.61	.20	.01	0.33	2	235.65	0.002	.99	<.01
Platform*Scenario	16.54	2	235.87	0.10	.90	<.01	8.42	2	236.28	0.05	.95	<.01
Platform*Speed Modality	458.54	2	235.40	2.88	.06	.02	444.41	2	236.68	2.57	.08	.02
Platform*Rot_Speed Modality	159.91	2	235.38	1.00	.37	<.01	284.31	2	236.66	1.65	.19	.01
	Oculomotor						Disorientation					
Platform	803.66	1	236.23	10.92	.00*	.04	3803.10	1	235.74	20.70	.00**	.08
Scenario	119.13	2	236.21	0.81	.45	<.01	477.20	2	235.74	1.30	.27	.01
Speed Modality	475.03	2	235.63	3.23	.04*	.03	589.00	2	235.24	1.60	.20	.01
Rotational Speed Modality	507.08	2	235.57	3.45	.03*	.03	389.50	2	235.20	1.06	.34	<.01
Platform*Scenario	104.56	2	236.27	0.71	.49	<.01	608.20	2	235.77	1.65	.19	.01
Platform*Speed Modality	33.45	2	235.60	0.23	.79	<.01	1730.90	2	235.23	4.71	.00**	.04
Platform*Rot_Speed Modality	16.54	2	235.58	0.11	.89	<.01	887.30	2	235.21	2.41	.09	.02

Another mixed-effects model was conducted on the influence of five independent variables (platform, scenario, speed modality and rotational speed modality) on the number of *ER-SCR* (Table 5.5). The platform ($F_{1,233.63} = 44.65$, $p < .01$, $\eta_p^2 = .16$) and the speed modality ($F_{2,234.42} = 3.27$, $p = .03$, $\eta_p^2 = .03$) showed significant differences, while the scenario ($F_{2,234.43} = 2.66$, $p = .07$, $\eta_p^2 = .02$) and the interaction between the platform and the rotational speed modality ($F_{2,233.21} = 2.76$, $p = .06$, $\eta_p^2 = .02$) were marginally significant. There was no significance for the rotational speed modality ($F_{2,233.24} = 0.54$, $p = .58$, $\eta_p^2 < .01$) and other interaction terms.

The effect of the platform, the scenario, the speed modality and the rotational speed modality on the NASA-TLX score is given in Table 5.6. For simplicity, we only presented the summarized p-values and effect size from the mixed-effects models. We can observe that none of the NASA-TLX sub-scales

Table 5.5: Effect of parameters on the number of *ER-SCR* (**: $p < .01$, *:$p < .05$).

	Sum Sq	NumDF	DenDF	F	p-value	η_p^2
Platform	185610	1	233.63	44.65	.00**	.16
Scenario	22136	2	234.43	2.66	.07	.02
Speed Modality	27254	2	233.42	3.27	.03*	.03
Rotational Speed Modality	4458	2	233.24	0.54	.58	<.01
Platform*Scenario	264	2	233.67	0.03	.96	<.01
Platform*Speed Modality	4008	2	233.04	0.48	.61	<.01
Platform*Rot_Speed Modality	22939	2	233.21	2.76	.06	.02

was significantly affected by the speed modality except the interaction between the platform and the speed modality ($p = .02$). *Performance* ($p < .05$, $\eta_p^2 = .03$) and *Effort* ($p = .04$, $\eta_p^2 = .02$) were however significantly influenced by the platform.

Table 5.6: Statistical summary of p-values and effect size for the NASA-TLX sub-scale scores (MD: Mental Demand, PD: Physical demand, TD: Temporal demand, Pe: Performance, Ef: Effort, Fr: Frustration, **: $p < .01$, *:$p < .05$).

	MD		PD		TD		Pe		Ef		Fr	
	p	η_p^2	p	η_p^2	p	η_p^2	p	η_p^2	p	η_p^2	p	η_p^2
Platform	.30	<.01	.49	<.01	.96	<.01	.00**	.03	.04*	.02	.87	<.01
Scenario	.00**	.07	.11	.02	.17	.02	.95	<.01	.00*	.04	.04	.03
Speed Modality	.31	<.01	.91	<.01	.21	.01	.31	<.01	.31	<.01	.17	.01
Rotational Speed Modality	.81	<.01	.56	<.01	.52	<.01	.99	<.01	.56	<.01	.73	<.01
Platform*Scenario	.79	<.01	.47	<.01	.00**	.04	.91	<.01	.66	<.01	.92	<.01
Platform*Speed Modality	.87	<.01	.02*	.03	.12	.02	.42	<.01	.27	.01	.44	<.01
Platform*Rot_Speed Modality	.93	<.01	.59	<.01	.34	<.01	.58	<.01	.85	<.01	.93	<.01

Tukey HSD tests were further performed to review the differences among the speed modalities, given in Table 5.7. The corresponding sample size, mean, standard deviation and median of each situation were reported in Table 5.8. According to the total *SSQ* score, a significant difference was found between NP ($mean = 15.49, SD = 15.87, median = 11.22$) and non-LP ($mean = 11.27, SD = 13.59, median = 7.48$), with $p < .01$ and $\eta_p^2 = .03$, and also between NP and LP ($mean = 12.94, SD = 14.37, median = 7.48$), with $p = .04$ and $\eta_p^2 = .02$. Both the *Nausea* and the *Oculomotor* scores reported significant differences between NP and non-LP, $p \leq .01$. The evaluation based on the number

Table 5.7: Post-hoc analysis for the speed modalities considering different measurements; Lower and Upper represent the boundaries of the 95% confidence interval (CI), (**: $p < 0.01$, *:$p < .05$).

	Speed Modality	Speed Modality	Lower	Upper	p-value	η_p^2
Total *SSQ*	NP	non-LP	1.26	6.81	.005**	.03
	NP.	LP	0.10	5.51	.04*	.02
	non-LP	LP	-4.00	1.54	.38	<.01
Nausea	NP	non-LP	1.39	7.18	.004**	.03
	NP	LP	-0.17	5.47	.07	.01
	non-LP	LP	-4.53	1.25	.26	<.01
Oculomotor	NP	non-LP	0.77	6.11	.01*	.03
	NP	LP	-1.05	4.16	.24	<.01
	non-LP	LP	-4.55	0.78	.16	<.01
Disorientation	NP	non-LP	-1.79	6.65	.25	<.01
	NP	LP	-0.43	7.81	.08	.01
	non-LP	LP	-2.95	5.47	.55	<.01
ER-SCR	NP	non-LP	-18.58	21.60	.88	<.01
	NP	LP	-41.39	-1.90	.03*	.02
	non-LP	LP	-43.32	-2.98	.02*	.02

Table 5.8: Descriptive statistics including the sample size (n), mean, standard deviation (SD) and median for the performance of each speed modality.

	NP				non-LP				LP			
	n	Mean	SD	Median	n	Mean	SD	Median	n	Mean	SD	Median
SSQ	85	15.49	15.87	11.22	87	11.27	13.59	7.48	77	12.94	14.37	7.48
Nausea	85	12.46	15.44	9.54	87	8.05	12.29	0	77	9.76	12.34	9.54
Oculomotor	85	11.33	12.69	7.58	87	7.88	10.32	7.58	77	10.11	11.99	7.58
Disorientation	85	18.67	21.54	13.92	87	15.73	21.35	13.92	77	15.36	19.8	13.92
ER-SCR	85	306.25	110.36	331	86	305.44	90.47	323	77	331.74	86.88	354

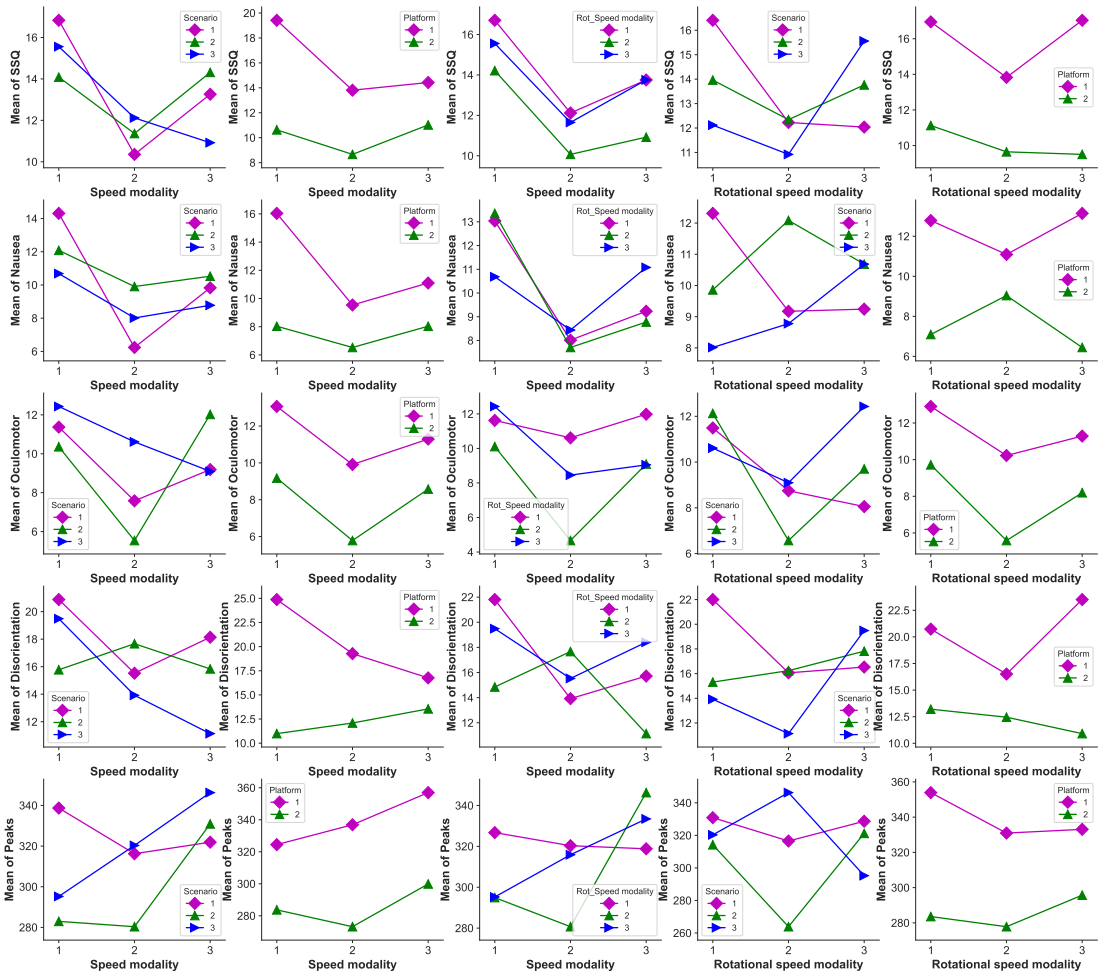

Figure 5.9: Interaction effects between factors; speed modality (1: NP, 2: non-LP, 3: LP), angular speed modality (1: NP, 2: non-LP, 3: LP), platform (1: HMD, 2: CAVE), scenario (1: low, 2: medium, 3: high).

of *ER-SCR* indicated supplementary differences which were not detected by the simulator sickness questionnaire: significant reduction from NP ($mean = 306.25, SD = 110.36, median = 331$) to LP ($mean = 331.74, SD = 86.88, median = 354$), with $p = .03$ and $\eta_p^2 = .02$, and from LP to non-LP ($mean = 305.44, SD = 90.47, median = 323$) were observed, with $p = .02$ and $\eta_p^2 = .02$. We did not perform post-hoc tests on the NASA-TLX criteria as no statistical differences were reported.

As the analysis of the interaction effects in the $L_{18}(2^1 \times 3^7)$ table between the two-three level factors was not allowed because of a rank deficiency (Frey 1998; Su 2013), we concentrated on the interaction between the platform and other related factors (Figure 5.9). To reduce the total *SSQ*, the *Nausea* and the *Oculomotor* scores and the number of *ER-SCR*, combining the CAVE and the non-LP speed modality as well as the non-LP and the rotational non-LP speed modalities present competitive advantages to alleviate side effects during virtual navigation.

Now, recalling hypothesis H1, we observed that the cognitive workload measured by the NASA-TLX table was not significantly affected by the speed protector (either non-LP or LP), which contrasts with our hypothesis. However, from NP to LP, and to non-LP, the total *SSQ* score, *Nausea*, *Oculomotor* and *Disorientation* showed obviously cybersickness levels reductions. Therefore, we can deduce that with a speed protector and especially the nonlinear one, users are less prone to cybersickness, validating part of H1.

5.2.4.1.2 Optimal acceleration and jerk As the rotational speed modality was not reported to affect much on user's experience except on the *Oculomotor* score, we focused on the analysis of the optimal acceleration and jerk along the longitudinal direction with the different speed modalities. We conducted again a mixed-effects model to determine the influence of different acceleration and jerk magnitudes in the nonlinear speed protector case. For the sake of simplification, we presented only the p-values and effect size in Table 5.9. The effect of acceleration and jerk was not significant in terms of the *SSQ* score, *Nausea*, *Oculomotor*, $p > .05$. However, *Disorientation*, the number of *ER-SCR*, *Mental Demand*, *Effort* and *Frustration* were significantly affected by the acceleration, $p < .05$, while only the number of *ER-SCR* and *Mental Demand* were influenced by the jerk, $p < .01$.

Tukey HSD post-hoc tests were performed to find the optimal magnitude of acceleration and jerk in the non-LP case (Table 5.9). No significant difference in the different accelerations and jerks were observed for the total *SSQ*, *Nausea*, *Oculomotor*, *Physical Demand*, *Temporal Demand* and

Table 5.9: Statistical summary for the effect of acceleration and jerk on the total *SSQ* score, *ER-SCR* and NASA-TLX criteria in the nonlinear speed protector case (N: Nausea, O: Oculomotor, D: Disorientation, **: $p < .01$, *:$p < .05$).

			SSQ		N		O		D		ER-SCR		MD		PD		TD		Pe		Ef		Fr	
			p	η_p^2	p	η_p^2	p	η_p^2	p	η_p^2	p	η_p^2	p	η_p^2	p	η_p^2	p	η_p^2	p	η_p^2	p	η_p^2	p	η_p^2
Mixed-effects	Acceleration		.14	.05	.18	.05	.39	.02	.06	.07	.00*	.15	.00**	.14	.51	.02	.97	<.01	.11	.06	.00**	.19	.01*	.12
	Jerk		.95	<.01	.89	<.01	.70	<.01	.38	.03	.00*	.16	.00**	.14	.25	.04	.44	.02	.43	.02	.14	.05	.08	.07
Post-hoc	Acceleration	0.8–1.6	.80	<.01	.44	<.01	.38	.01	.33	.01	.00*	.15	.00**	.12	.30	.02	.98	<.01	.04	<.06	.00**	.18	.04*	.06
		0.8–2.4	.11	.03	.27	.02	.63	<.01	.02*	.07	.06	.05	.01*	.09	.33	.01	.82	<.01	.16	<.03	.02*	.08	.00**	.11
		1.6–2.4	.07	.02	.06	.04	.18	.02	.18	.02	.10	.04	.55	<.01	.90	<.01	.85	<.01	.49	<.01	.11	.04	.46	<.01
Post-hoc	Jerk	1–2	.76	<.01	.91	<.01	.69	<.01	.21	.02	.00**	.13	.00*	.11	.15	.03	.24	.02	.25	.02	.05	.05	.08	.04
		1–3	.82	<.01	.72	<.01	.40	<.01	.26	.02	.93	<.01	.00*	.10	.93	<.01	.32	.01	.99	<.01	.22	.02	.66	<.01
		2–3	.93	<.01	.66	<.01	.72	<.01	.84	<.01	.00**	.12	.76	<.01	.13	.03	.79	<.01	.25	.02	.42	<.01	.03*	.06

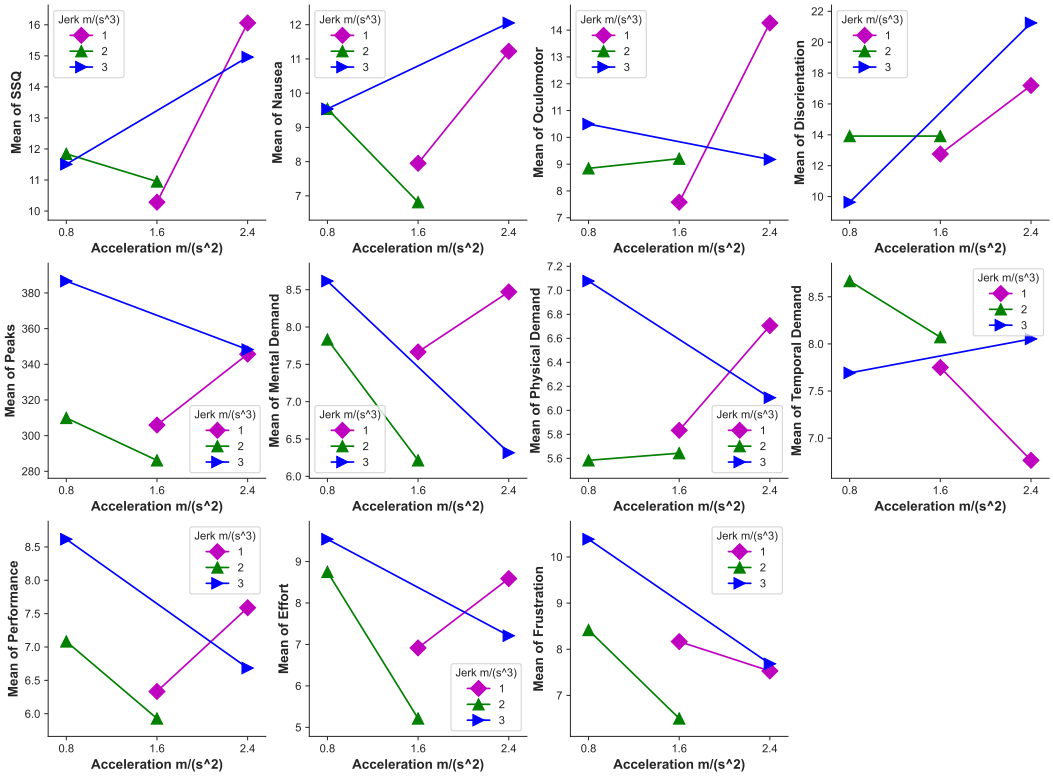

Figure 5.10: Interaction effects between acceleration and jerk in the non-LP case.

Table 5.10: Descriptive statistics including the sample size (n), mean, standard deviation (SD) and median for the performance of different acceleration and jerk magnitudes.

	n	Mean	SD	Median	n	Mean	SD	Median	n	Mean	SD	Median
						Acceleration						
		0.8				1.6				2.4		
Disorientation	25	11.69	17.37	13.92	26	13.38	21.01	0	36	19.33	20.32	13.92
ER-SCR	24	348.29	81.07	365.5	26	295.27	93.53	342	36	347.06	79.68	368
MD	25	8.24	4.01	8	26	6.88	4.48	5.5	36	7.33	3.32	7
Ef	25	9.16	4.53	10	26	6.00	3.39	5.5	36	7.86	3.97	8
Fr	25	9.44	4.73	7	26	7.27	3.13	7	36	7.61	3.03	7
						Jerk						
		1				2				3		
Disorientation	29	15.36	17.19	13.92	26	13.92	19.69	13.92	32	16.53	22.48	13.92
ER-SCR	29	329.24	84.93	349	26	297.12	91.72	333.5	31	363.13	75.27	376
MD	29	8.14	4.05	7	26	6.96	4.09	5	32	7.25	3.58	7
Ef	29	7.90	4.00	8	26	6.85	4.31	5.5	32	8.16	4.10	8
Fr	29	7.79	3.46	7	26	7.38	3.70	6.5	32	8.78	3.87	7.5

Performance, $p > .05$. The descriptive statistics for the remaining significant factors are shown in Table 5.10. An acceleration of 1.6m/s^2 led to a smaller number of *ER-SCR* ($mean = 295.27, SD = 93.53, median = 342$) than with an acceleration of 0.8m/s^2 ($mean = 348.29, SD = 81.07, median = 365.5$), $p < .01$, $\eta_p^2 = .15$. *Mental Demand*, *Effort* and *Frustration* showed larger values ($p < .05$) when the acceleration was 0.8m/s^2 compared to those with the other accelerations. These results validate hypothesis [H2] that acceleration affects user experience.

Likewise, the optimal jerk magnitude can be deduced. First, the simulator sickness questionnaire failed to distinguish between the three jerk magnitudes as no significant difference was observed among the jerk magnitudes as shown in Table 5.9, $p > .05$. However, we noticed that the number of *ER-SCR* was smaller ($p < .01$) when the jerk equaled 2m/s^3 ($mean = 297.12, SD = 91.72, median = 333.5$), than when it equaled 1m/s^3 ($mean = 329.24, SD = 84.93, median = 349$) with $\eta_p^2 = .13$ and 3m/s^3 ($mean = 363.13, SD = 75.27, median = 376$) with $\eta_p^2 = .12$. As jerk varied, *Mental Demand* dropped significantly ($p < .01$) from 1m/s^3 ($mean = 8.14, SD = 4.05, median = 7$) to 2m/s^3 ($mean = 6.96, SD = 4.09, median = 5$) with $\eta_p^2 = .11$, as well as from 1m/s^3 to 3m/s^3 ($mean = 7.25, SD = 3.58, median = 7$) with $\eta_p^2 = .10$. *Frustration* declined significantly ($p < .01$, $\eta_p^2 = .06$) from 3m/s^3 ($mean = 8.78, SD = 3.87, median = 7.5$) to 2m/s^3 ($mean = 7.78, SD = 3.70, median = 6.5$). These results complete the validation of hypothesis [H2] as jerk also affects user experience.

The interactions between acceleration and jerk are represented in Figure 5.10, which allows us to derive the best settings of acceleration and jerk. Based on the available combinations and among all

evaluations except *Disorientation* and *Temporal Demand*, an acceleration of 1.6m/s^2 and a jerk of 2m/s^3 represent the optimal settings to improve user experience.

Finally, we collected some general feedback from participants: they could tell intuitively the difference between the different speed modalities, in particular, they felt it was jerkier and less smooth without any speed protector while they felt better comfort with a speed protector. However when the speed protector was activated in the system, they reported that they could achieve a natural virtual navigation only under specific settings of acceleration and jerk.

5.2.4.2 Power spectral density (PSD) analysis

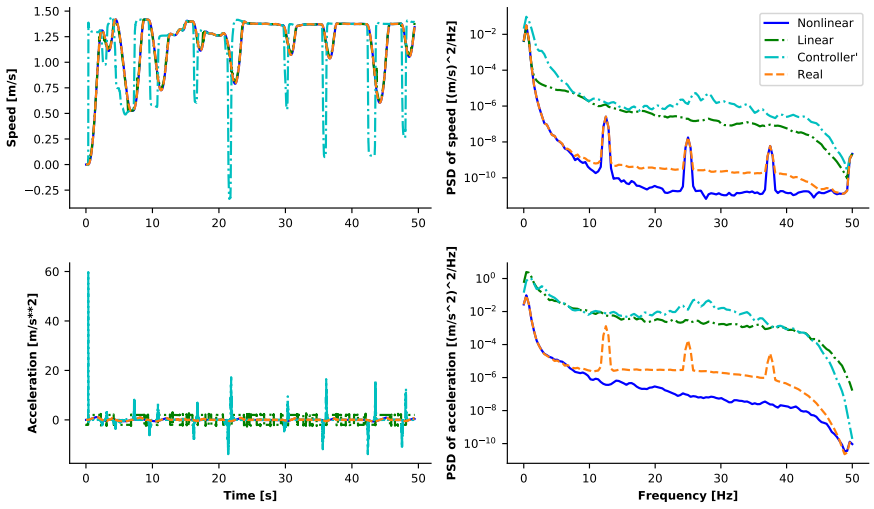

Figure 5.11: PSD of speed and acceleration from the nonlinear speed protector, the linear speed protector, the controller's input and the real navigation profile in the VE.

The frequency content of the speed and acceleration was calculated and inspected, through which the different speed modalities showed their difference, providing one reasonable explanation to previous results. Here we used the power spectral density (PSD) evaluated with the *Welch* method to find the spectrum of a piece of speed and acceleration profile during virtual navigation (Figure 5.11). As shown, the speed protectors can generate smoother speed by avoiding jumps or abrupt changes resulting from involuntary controller's inputs, which justifies the meaning of "speed protector". With a speed protector activated, speed still followed the controller's inputs but changed smoothly under the acceleration and jerk limits. For instance, without any speed protector, acceleration could reach 60.0m/s^2 in an abrupt change, which could induce discomfort, whereas with the speed protector it

stayed in a lower range thanks to navigation constraints.

The difference among different speed modalities shown in the frequency domain indicated that the PSD profiles (both speed and acceleration) from controller's input had high magnitude compared to those from the protector. The real speed and acceleration in the VE did not match exactly the ones computed from the speed protector; therefore, the PSD profile of the real speed and acceleration lay between the controller's input and the one optimized from the protector.

5.2.5 Discussion

Much research has been done over the last decades to better understand the rule of human walking and the profile of human-robot interaction in physical environments (Pham *et al.* 2007; Sidobre and Desormeaux 2019). Cirio *et al.* (2013) further analyzed the profile of a virtual walking in VEs. However, very little work has been done to apply these studies to virtual navigation design. Finding that a minimum-jerk trajectory has been used to simulate saccadic eye movements or goal-directed arm movements (C. M. Harris and Wolpert 1998), we applied the corresponding model to virtual navigation with the hypothesis that the minimum-jerk model could also alleviate side effects such as cybersickness and cognitive workload. We conducted a simulation to explain why the minimum-jerk model was more appropriate than the minimum-snap, minimum-crackle and minimum-pop models during navigation, and the results implied that only the minimum-jerk model best fitted for human controlled movements in which the ratio of peak speed to average was close to 1.75 (Flash and Hogan 1985).

To be sure that a speed protector could provide better user experience, we conducted a user test in a $L_{18}(2^1 \times 3^7)$ orthogonal table by arranging factors including the VR platform, the scenario density, acceleration, jerk, rotational acceleration and rotational jerk. The effect of the platform and the scenario density were analyzed through mixed-effects models: the score obtained from the simulator sickness questionnaire and *ER-SCR*, the *Performance* and the *Effort* scores from the NASA-TLX were strongly affected by the platform type, while *Mental Demand*, *Effort* and *Frustration* were influenced by the scenario density. When exposed to provocative vestibular stimulus repeatedly, users are less prone to sickness symptoms due to a learning effect (Clément *et al.* 2007). Therefore, the platform and the scenario density acted as artificial noise to reduce the accumulated familiarity of each experiment. Since many articles already discussed the effect of the VR platform and the scenario type (Riley and

Kaber 1999; Parsons *et al.* 2009; Cordeil *et al.* 2016) and that our aim was to investigate the effect of a speed protector on cybersickness and cognitive workload, we will not go further on how the platform type and the scenario density affected user experience.

From the three different measurements (*SSQ*, *ER-SCR* and NASA-TLX), results showed that the speed protector especially the nonlinear one could effectively improve user experience. The *SSQ* is a common method to measure simulator sickness in VR applications, and past work showed strong internal correlation among the scores of *SSQ*, *Nausea*, *Oculomotor* and *Disorientation* (Milleville-Pennel and Charron 2015; Y. Wang *et al.* 2019). We also found a consistent behavior of these scores to point out the merits of the minimum-jerk speed protector. We considered the EDA as an efficient approach to indicate the severity of VR sickness, together with the *SSQ*. Most work uses the absolute or relative variation of the EDA value (Plouzeau *et al.* 2018; Dennison *et al.* 2016), while we extracted other features like the skin conductance responses of the EDA signal through trough-to-peak analyses according to recent studies (Paschalidis *et al.* 2019; Magaki and Vallance 2019). Based on three different measurements, we found that the proposed speed protector could reduce cybersickness when the user navigated with such protector, but we did not find much significant effect of the rotational speed protector. Note that in our study we focused on both translational movements and rotational movements as the speed protector was embedded into the system to correct controller's inputs from the user. From past research (Nooij *et al.* 2017), it is known that rotational movements tend to cause also VR sickness, but we did not find much alleviation when the rotational speed protector was applied. Since the user had to navigate through a relatively long path in the 3D VE, such inconsistency with the literature could be due to the fact that here, the navigation relied mainly on translational movements, while rotational movements were less performed. In the future, we proposed to study the effect of a rotational speed protector by designing an appropriate experiment involving more rotational movements. Interestingly, we did not find any significant effect of the speed modality on the cognitive workload based on the NASA-TLX table, indicating that the different speed modalities had statistically equivalent workload in terms of cognition.

Knowing that the speed protector replaced irregular and jerky speed profiles with a minimum-jerk profile, we had to look for optimal settings of acceleration and jerk constraints to define the shape of the optimized profile. Indeed, even though a minimum-jerk profile was defined, inappropriate acceleration and jerk, e.g., very small limits, may lead to strong delays between the user's expectation

and the system response, resulting in unnatural perception of movement (Bos, Bles, *et al.* 2008). Therefore, a trade-off was found and the solution was to find the optimal acceleration and jerk settings. Although the different magnitudes of acceleration and jerk did not always show statistical differences, post-hoc analyses and interaction plots suggest that optimal acceleration and jerk should be 1.6m/s^2 and 2m/s^3 respectively. Note that the optimal acceleration (1.6m/s^2) is slightly larger than the one suggested in (*Mechanical Vibration and shock- Evaluation of human exposure to whole-body vibration- Part 1- General Requirements* 1997). This might be due to the inherent differences between the physical and the virtual environments and it may be therefore worth of further investigation with different magnitudes of acceleration. In the results, we found that only the *Mental Demand*, *Effort* and *Frustration* were significantly affected by the magnitudes of acceleration and jerk which was partly consistent with the work of Akyeampong *et al.* (2014), showing that the *Mental Demand* and *Frustration* are the top two important criteria; Milleville-Pennel and Charron (2015) also strengthened the importance of *Mental Demand* in simulators.

In addition to the comparison of speed modalities, we also performed a power spectral density (PSD) analysis on the acceleration and speed profiles obtained from the different speed modalities. Frequency analysis has been widely used in the automotive field to assess vehicle ride responses and human comfort, especially considering the amount of motion stimuli encountering for discomfort, e.g., Gao and K. Chen (2011) and Eriksson and Svensson (2015). By inspection of the PSD profile of speed, we saw that raw inputs from the controller contained more high magnitude components than for other control speeds, while regarding acceleration, the linear speed protector yielded more high magnitude components than with other speed modalities. When the nonlinear speed protector was used, the real speed followed the minimum-jerk speed profile which contained more low magnitude components. Findings through the PSD analysis suggested the following: when a user navigated without any speed protector, his/her inputs to the controller were directly transformed into the magnitude of speed used for navigation. However, this could lead to irregular speed profiles when the user frequently changed speed to be comfortable; consequently, speed and acceleration contained more high magnitude components. Conversely, when the minimum-jerk model was activated in the system, speed could be optimized so that speed and acceleration did not exceed comfort limits and changed smoothly.

The present work has however the following limitations. First, we tested three different values for

the acceleration and jerk whose magnitude were recommended from past literature and adapted here through a trial-and-error procedure, thus the efficiency of the speed protector was limited to these parameters. Second, we did not find any significant difference in cognitive workload when different magnitudes of the acceleration and jerk were applied, but the mental workload tended to decrease when the acceleration and jerk were set to 1.6m/s^2 and 2m/s^3 respectively. In fact, due to the inherent subjective property of the NASA-TLX evaluation, we failed to detect a significant difference[6]. Third, the data from the simulator sickness questionnaire were highly dispersed as the standard deviation was relatively large, posing a threat to the reliability of the work. Other measurement methods of cybersickness levels could be used to improve measurement reliability, such as postural sway (Chardonnet *et al.* 2017), especially since we based our speed protector on walking control. Fourth, instead of reporting full interaction effects in the mixed-effect model, we only considered the interaction between the VR platform and the other factors (i.e., scenario, speed modality and rotational speed modality). However, we presented other related interaction effects in subsubsection 5.2.4.1, in which the centrality regarding the mean still helped us compare users' feedback on different speed modalities and parameter settings. Put differently, the interaction plots emphasized the merits of the minimum-jerk model and helped determining the optimal magnitude of acceleration and jerk.

5.2.6 Conclusion

This work investigated the interest of a navigation protector based on the minimum-jerk model to optimize the user's inputs provided from a controller in a VR application. Despite the limitations described above, the current results indicated that the speed protector designed based on human motion and comfort conditions can significantly improve user experience by reducing VR sickness while keeping the same cognitive workload level. Significance could be assessed by the *SSQ*, *ER-SCR* and the NASA-TLX while speed profiles could be compared and analyzed through a PSD analysis.

We also found from some participants that, depending on the situation, they preferred to have different accelerations. Developing strategies to adapt the acceleration depending on individual factors might be a promising solution, in a similar way as presented in chapter 4: sickness symptoms could be predicted online during the navigation, and the magnitude of acceleration could be automatically adapted accordingly to provide better experience. Therefore, In the next section, we developed a

[6]Therefore, we proposed the TOPSIS method to improve the measuring quality of the NASA-TLX, presented in chapter 4

close-loop system that can adapt navigation based on physiological responses of the user.

5.3 Adaptive navigation with cybersickness susceptibility

5.3.1 Introduction

In chapter 4, we introduced two types of fuzzy logic, Mamdani-type fuzzy logic and adaptive neuro-fuzzy inference system (ANFIS). The former can be formulated based on expert knowledge or existing literature, while ANFIS is more like a nonlinear fitter. Both methods achieved equivalent performance in cybersickness detection. However, compared with ANFIS, Mamdani-type fuzzy logic can limit its output always between zero and one, which can be integrated into an adaptive system more easily and naturally. Therefore, ANFIS is not suitable in an adaptive model from a practical point as it can have a negative output. We designed an adaptive navigation method in which the navigation speed is computed from the individual proneness to cybersickness O_{fis} predicted from FIS, and we performed a user study to determine whether personalized navigation successfully mitigates cybersickness effects.

5.3.2 Adaptive speed model

Figure 5.12 represents the procedure to individualize navigation in virtual environments based on fuzzy logic. Depending on O_{fis} predicted from the user's characteristics, the navigation speed (So *et al.* 2001), acceleration (Plouzeau *et al.* 2018), and immersion time (Chardonnet *et al.* 2017) could be adapted accordingly. In this section, we chose the navigation speed as the adapted variable to control the occurrence of cybersickness.

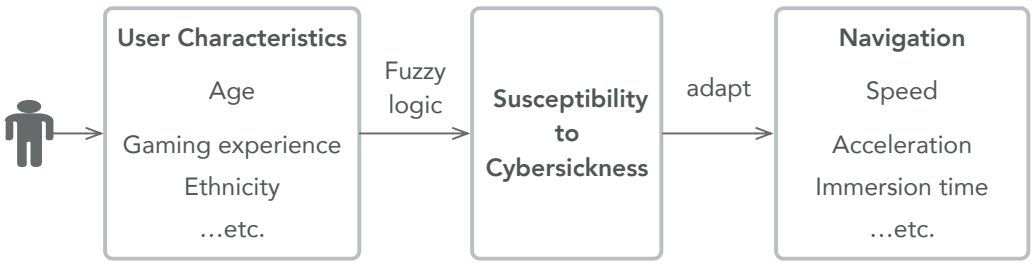

Figure 5.12: Process for using fuzzy logic methods to predict user's susceptibility to cybersickness and then adapt navigation parameters.

To clearly demonstrate the effect of adaptive navigation on the resulting cybersickness, we considered a baseline navigation speed higher than the normal walking speed – $3m/s$ –, so that cybersickness

could be easily induced. Then, we developed an adaptive speed model, where speed is computed from the output O_{fis} of the FIS taking as inputs the individual characteristics of the users. Recall that O_{fis} represents a cybersickness indicator and describes the proneness to cybersickness of the users taken individually. As O_{fis} ranges between zero and one, we introduced an amplification factor to ensure that the navigation speed was large enough to prompt cybersickness. The resulting adaptive speed model is described as follows:

$$Speed = O_{fis} * A_f \tag{5.23}$$

where A_f is the amplification factor and was arbitrarily set to 3, so that the maximum speed can be $3m/s$, the baseline navigation speed.

5.3.3 Experimental setup

A user test was performed to investigate the practical performance of our fuzzy system. We invited 48 subjects ($M_{age} = 26.42, SD_{age} = 3.50$) from the local city to participate in the experiment. Participants were rewarded with a gift. Upon arrival, they were requested to fill a pre-exposure questionnaire containing information about their age, gaming experience, and origins, that will be used as input parameters to the fuzzy inference system. The resulting O_{fis} for each subject is represented in Figure 5.13. Each participant followed a procedure similar to the one presented in Figure 4.13, this time using exclusively an HTC Vive head-mounted display:

1. A pre-exposure SSQ (SSQ_{pre}) was filled by the participants; SSQ_{pre} was used to get a pre-exposure cybersickness score. Since the participants needed to know how to use the controller for navigation, they were given a brief introduction about the tasks and devices at the beginning of the experiment.

2. Participants were immersed in the virtual environment and started to navigate through the scenario depicted in Figure 4.15 for four minutes.

3. When the time was up, they were removed from the HTC Vive and were asked to fill a post-exposure SSQ (SSQ_{post}). The final SSQ score was determined as the difference between SSQ_{post} and SSQ_{pre}.

4. The previous steps were repeated with three different speed settings in random order.

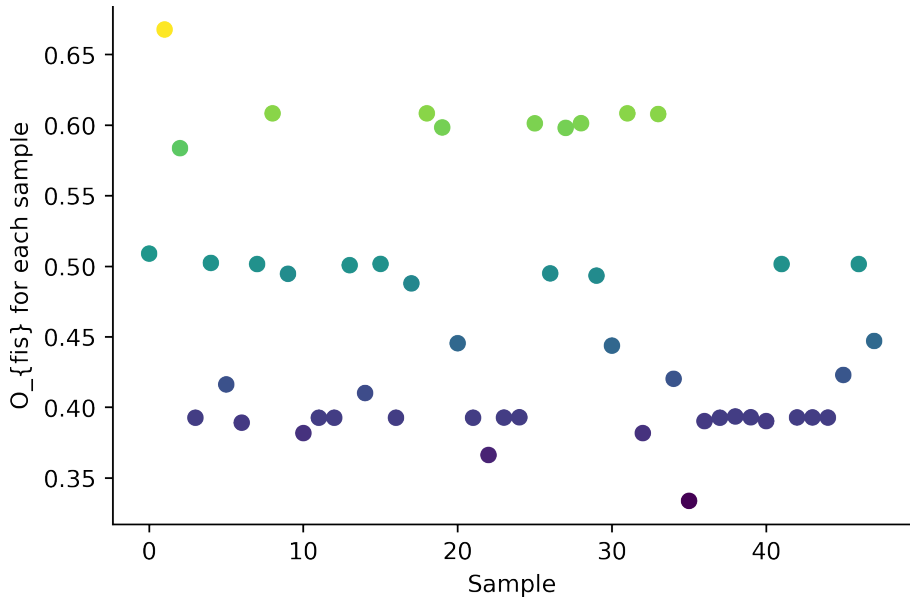

Figure 5.13: O_{fis} for each sample.

The three different navigation speed conditions were as follows:

A) 3m/s. As mentioned above, this speed represents a baseline condition.

B) Adapted speed with fuzzy logic, as represented in Equation 5.23.

C) 1.5m/s. We observed that the magnitude of O_{fis} was primarily scattered around 0.5 (Figure 5.13), therefore 1.5m/s $(0.5 * 3)$ was arranged as another baseline to be compared with.

In each condition, the indicated speed represented a maximum over which participants could not navigate. However, participants were allowed to control their navigation speed under these speeds with the controller.

We made the following hypothesis:

H1 The proportion of participants experiencing a reduction of cybersickness is higher with the adaptive navigation speed based on fuzzy logic.

Here, rather than considering how much the level of cybersickness could decrease thanks to our adaptation navigation, we were more interested in knowing to which extent personalization could increase the proportion of participants who felt a reduction of cybersickness severity, in other words,

whether a majority of participants could benefit from less cybersickness thanks to personalized navigation, compared to other navigation settings. Indeed, because of individual susceptibilities, measuring the amount of decrease of cybersickness levels may not be relevant here.

5.3.4 Results

Table 5.11 presents the pairwise comparisons between the different navigation speed conditions concerning the total *SSQ* score and its sub-scales (*Nausea*, *Oculomotor*, *Disorientation*). χ^2 tests were used to perform each comparison. Each result is accompanied by the corresponding p-value and the effect size ϕ. The significance level was set to .05.

With the adapted speed, significantly more participants reported smaller total SSQ scores compared to condition C ($\chi^2(1, N = 48) = 10.08, p < .01, \phi = .45$) and A ($\chi^2(1, N = 48) = 16.33, p < .01, \phi = .58$. Similar results were observed in the sub-scales of the SSQ. The fuzzy speed (condition B) allowed more participants to have less *Nausea* than in condition C ($\chi^2(1, N = 48) = 12.00, p < .01, \phi = .50$) and A ($\chi^2(1, N = 48) = 21.33, p < .01, \phi = .67$), less *Oculomotor* than in condition C ($\chi^2(1, N = 48) = 16.33, p < .01, \phi = .58$) and A ($\chi^2(1, N = 48) = 14.08, p < .01, \phi = .54$), and less *Disorientation* than in condition C ($\chi^2(1, N = 48) = 10.08, p < .01, \phi = .45$) and A ($\chi^2(1, N = 48) = 14.08, p < .01, \phi = .54$). In comparison to condition A, condition C resulted in less sick participants concerning the total SSQ score ($\chi^2(1, N = 48) = 8.33$, $p < .01$, $\phi = .42$), *Nausea* ($\chi^2(1, N = 48) = 21.33$, $p < .01$, $\phi = .67$), *Oculomotor* ($\chi^2(1, N = 48) = 4.08$, $p = .04$,$\phi = .29$) and *Disorientation* ($\chi^2(1, N = 48) = 16.33$, $p < .01$, $\phi = .58$), which validates the hypothesis.

Table 5.11: Comparisons between each speed condition of the number of participants who felt a decreased severity of cybersickness

				Total SSQ	Nausea	Oculomotor	Disorientation
Fuzzy speed	vs	Small speed	Decreased number	35	36	38	35
			χ^2 test	p<.01, χ^2=10.08	p<.01, χ^2=12.00	p<.01, χ^2=16.33	p<.01, χ^2=10.08
			ϕ	.45	.50	.58	.45
Fuzzy speed	vs	High speed	Decreased number	38	40	37	37
			χ^2 test	p<.01, χ^2=16.33	p<.01, χ^2=21.33	p<.01, χ^2=14.08	p<.01, χ^2=14.08
			ϕ	.58	.67	.54	.54
Small speed	vs	High speed	Decreased number	14	8	17	10
			χ^2 test	p<.01, χ^2=8.33	p<.01, χ^2=21.33	p=.04, χ^2=4.08	p<.01, χ^2=16.33
			ϕ	.42	.67	.29	.58

5.3.5 Discussion and conclusion

In this section, we designed an adaptive navigation speed model based on the output from Mamdani-type FIS, achieving a significantly larger proportion of users feeling less cybersickness. The results can also be regarded as a practical validation for the work in section 4.2.

We were aware that the the adaptive speed model may have two limitations. In the current context, fuzzy logic can predict the user's susceptibility to cybersickness, and based on it, we adapted the allowed maximal navigation speed. It implied that the speed is determined before the user is exposed to visual stimuli. However, in addition to the individual factors, the user's cybersickness states during the navigation are affected by many other factors such as the environmental conditions and task requirements (Bockelman and Lingum 2017). A speed adapted before the navigation may fail to involve these factors. Another limitation was associated with the limitation of the FIS method which had been reported in section 4.2: only three factors were considered to model the user characteristics, which may not be enough to cover all individual differences associated with cybersickness.

Aside to existing knowledge from the study of human characteristics, biofeedback-related knowledge may be interesting to consider, since past work has shown its feasibility to mitigate cybersickness effects (Plouzeau *et al.* 2018). In the next section, we will also investigate how information coming from physiological signals (e.g., galvanic skin response) could be utilized to increase the power of personalization of VR experience.

5.4 Adaptive navigation with physiological signals

5.4.1 Introduction

In this section, we proposed to use physiological signals, and particularly the electrodermal activity (EDA) that can be obtained from a wristband in real time (here an Empatica E4 wristband[7]), to adapt navigation in real time, and therefore mitigate cybersickness.

EDA signals can be decomposed into two components: skin conductance level (SCL) and skin conductance response (SCL) (Aqajari *et al.* 2020). SCL, also called the tonic level of the EDA signal, changes slowly with a time scale of tens of seconds to minutes. Because of the differences in hydration,

[7]https://www.empatica.com/research/e4/

skin dryness, or autonomic regulation of an individual respondent, the increase and decrease of SCL vary accordingly. SCL can be significantly different among respondents. On the other hand, SCR, also known as the phasic component of the EDA signal, rides on top of the tonic changes and demonstrates much faster variations. Alternations in SCR component of a EDA signal are observable as bursts or peaks in the signal. The phasic component is associated with specific emotionally arousing stimulus events (event-related SCRs, ER-SCRs). The rise of the phasic component can reach a peak within 1-5 seconds after the onset of stimuli.

By involving the EDA, we expected to further incorporate individual differences in the customized navigation experience. This method can be seen as an extension of (Plouzeau *et al.* 2018)'s work in which the navigation acceleration is adapted according to the variation of the EDA. Here, we proposed to use a PID controller associated with neural networks to further ensure the reliability of the adaptation.

5.4.2 PID controller

PID is the abbreviation of proportional-integral-derivative and is a control loop method with feedback that is widely used in industrial control systems and numerous applications needing constantly modulated control (L. Wang 2020). A PID controller continuously computes an error value *e(t)* representing the difference between the expected setpoint and the measured process value, and applies a correction determined by proportional, integral and derivative terms (denoted P, I, and D respectively). The overall control function is given as,

$$u(t) = K_P * e(t) + K_I * \int_0^T e(t) + K_D * \frac{de(t)}{dt} \tag{5.24}$$

where, $u(t)$ is the output of the PID controller, K_p, K_i and K_d are non-negative coefficients for the proportional, integral and derivative terms respectively. This controller contains three items with different control purpose:

- The proportional controller gives a feedback that is proportional to the error $e(t)$. If the error is large and positive, this term will also return a large and positive output, taking into account the coefficient K_p. However, it can not ensure that the system reaches the expected setpoint and maintains a steady-state error.

- The integral controller is involved to remedy the steady-state error. It integrates the historic cumulative value of the error until the error reduces to zero. However, the integral term decreases its output when a negative error appears, which will limit the speed of response and influence the stability of the system.

- The derivative controller enables the system to estimate the future trend of the error based on its rate of change along time. It improves the stability of the system by compensating for a phase lag resulting from the integral item.

5.4.3 1D convolutional neural network

We saw in section 4.1 that LSTM networks are efficient for processing sequential data. However, the LSTM model has to process each time step sequentially: each one needs the results from the previous one. Therefore, the LSTM hidden layers are particularly computationally expensive. Here, we will rather use a 1D convolutional neural network to process the sequential data.

1D CNNs can achieve competitive performance compared with LSTM on certain sequence-processing problems, usually at a significantly cheaper computational cost. Recently, 1D CNNs have been applied for audio generation and machine translation, obtaining great success (Kiranyaz *et al.* 2021).

5.4.4 Formulation of adaptive navigation

The SCR componment is associated with arousing stimulus events. When the user is exposed to visual stimuli in immersive virtual environments, an EDA burst or peak appears. The severer the visual stimuli, the more salient the burst or the higher the peak. In other words, in an ideal situation in which the user does not receive any visual stimuli, there should not be any observable bursts or peaks. Furthermore, it means that we should design a navigation technique in which the visual stimuli should not arouse excessive physiological responses. Our goal is to optimize navigation to stabilize the SCR componment of the EDA signal.

5.4.4.1 Formulation of adaptive navigation

The objective of this section is to deduce the mathematical formulations for the adaptive navigation technique based on the PID control system.

Firstly, we will give the mathematical formulations. $f(t)$ denotes the phasic component of the EDA signal at time t, and the objective is to stabilize the $f(t)$, given as,

$$E_f(t_i) = f(t_i) - f(t_{i-1}) \tag{5.25}$$

where $E_f(t_i)$ is the difference of the phasic component between time step t_i and previous time step t_{i-1}. In ideal state, $f(t_i)$ is expected to be 0 which means that there is no visual stimuli. Therefore, Equation 5.25 can be simplified as,

$$E_f(t_i) = -f(t_{i-1}) \tag{5.26}$$

As the EDA signal is decomposed into the phasic component and tonic component, it implies that the variation of the EDA signal is associated with the phasic component and tonic component. Knowing that the tonic component usually varies slowly and the phasic component varies rapidly overlying the tonic component (Benedek and Kaernbach 2010), in practice, we can use the phasic component to approximate the variation of the EDA signal. Mathematically, the variation of the EDA signal along time is noted as the temporal derivative of the EDA signal, i.e.,$f = \frac{dEDA}{dt}$. As depicted in Figure 5.14, the derivative of EDA and phasic component of EDA follow a similar variation trend.

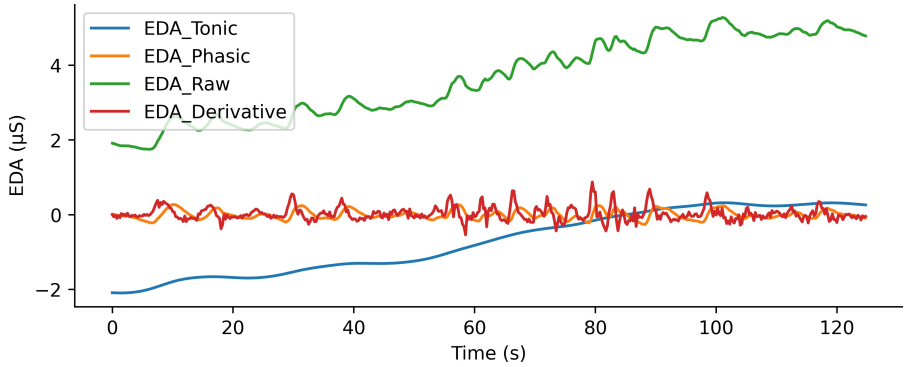

Figure 5.14: Demonstration of one EDA signal including the phasic component, tonic component, and temporal derivative.

The navigation acceleration $\mathbf{a}$ at time t_i can be parameterized in the following algebraic expression,

$$\mathbf{a}(t_i) = \mathbf{a}(t_{i-1}) + \underbrace{\psi_{\mathbf{a}}\mathbf{E}_{\mathbf{a}}(t_i)}_{\text{stabilize the acceleration}} + \underbrace{\text{diag}(\beta)\psi_f\mathbf{E}_{\mathbf{f}}(t_i)}_{\text{adaptation based on phasic EDA}} \tag{5.27}$$

where

$$\begin{aligned}\psi_{\mathbf{a}}(\cdot) &= \begin{bmatrix}\psi_{a_l}(\cdot) & 0\\ 0 & \psi_{a_r}(\cdot)\end{bmatrix}\\ &= \begin{bmatrix}K_{Pl}(\cdot) + K_{Il}\int_0^T(\cdot) + K_{Dl}\frac{d(\cdot)}{dt} & 0\\ 0 & K_{Pr}(\cdot) + K_{Ir}\int_0^T(\cdot) + K_{Dr}\frac{d(\cdot)}{dt}\end{bmatrix}\end{aligned} \tag{5.28}$$

$$\begin{aligned}\psi_{\mathbf{f}}(\cdot) &= \begin{bmatrix}\psi_f(\cdot) & 0\\ 0 & \psi_f(\cdot)\end{bmatrix}\\ &= \begin{bmatrix}K_{Pf}(\cdot) + K_{If}\int_0^T(\cdot) + K_{Df}\frac{d(\cdot)}{dt} & 0\\ 0 & K_{Pf}(\cdot) + K_{If}\int_0^T(\cdot) + K_{Df}\frac{d(\cdot)}{dt}\end{bmatrix}\end{aligned} \tag{5.29}$$

$$\mathbf{E}_{\mathbf{a}}(t_i) = \begin{bmatrix}E_{a_l}(t_i)\\ E_{a_r}(t_i)\end{bmatrix} = \begin{bmatrix}a_{le}(t_i) - a_l(t_i)\\ a_{re}(t_i) - a_r(t_i)\end{bmatrix} \tag{5.30}$$

$$\mathbf{E}_{\mathbf{f}}(t_i) = \begin{bmatrix}E_f(t_i)\\ E_f(t_i)\end{bmatrix} = \begin{bmatrix}-f(t_{i-1})\\ -f(t_{i-1})\end{bmatrix} \tag{5.31}$$

$$\mathrm{diag}(\beta) = \begin{bmatrix}\beta_l & 0\\ 0 & \beta_r\end{bmatrix} \tag{5.32}$$

In Equation 5.27, the second item $\psi_{\mathbf{a}}\mathbf{E}_{\mathbf{a}}(t_i)$ is to ensure that the acceleration can vary around an expected value, because if the third item keeps varying monotonously, the acceleration would also vary monotonously and reach an extremum. The third item $\psi_f\mathbf{E}_{\mathbf{f}}(t_i)$ represents the adaptive quantity due to the visual stimulus or physiological response. $\mathrm{diag}(\beta)$ is a diagonal coefficient matrix used to balance the importance between the longitudinal and rotational movements in Equation 5.27.

The navigation acceleration $\mathbf{a}$ includes both longitudinal and rotational parts. a_{le} is the expected longitudinal acceleration; a_{re} is expected rotational acceleration; a_l is the measured longitudinal acceleration; a_r is the measured rotational acceleration.

$\psi_{\mathbf{a}}(\cdot)$ and $\psi_{\mathbf{f}}(\cdot)$ are the PID operators. $\psi_{a_l}(\cdot)$ and $\psi_{a_r}(\cdot)$ are elements of $\psi_{\mathbf{a}}(\cdot)$ with the following coefficients: K_{Pl}, K_{Il}, K_{Dl}, and K_{Pr}, K_{Ir}, K_{Dr}, working on the longitudinal and rotational accelerations; they are used to ensure the accelerations to be around the expected values. $\psi_f(\cdot)$ is the element of $\psi_{\mathbf{f}}(\cdot)$ with the following coefficients: K_{Pf}, K_{If}, K_{Df}, working on the phasic component of the EDA signal. $\mathbf{E}_{\mathbf{a}}(t_i)$ and $\mathbf{E}_{\mathbf{f}}(t_i)$ are the errors between the expected steady states and measured states at time step t_i. The errors will be substituted to the PID operators to compute the corrections.

Overall, the adaptive navigation system can be described by Equation 5.27 and the supplementary equations: Equation 5.28, Equation 5.29, Equation 5.30, Equation 5.31, Equation 5.32. The inputs of the system at time step t_i are the measured longitudinal acceleration, rotational acceleration, and phasic component of EDA, and the outputs of the system are the corrected accelerations in both directions.

We had modeled the adaptive system in the parameterized form with the following eleven coefficients: K_{Pl}, K_{Il}, K_{Dl}, K_{Pr}, K_{Ir}, K_{Dr}, K_{Pf}, K_{If}, K_{Df}, β_l and β_r. As the objective of adaptation is to mitigate cybersickness, the nontrivial question becomes: can we find optimal parameters to adapt the acceleration so that cybersickness can be reduced?

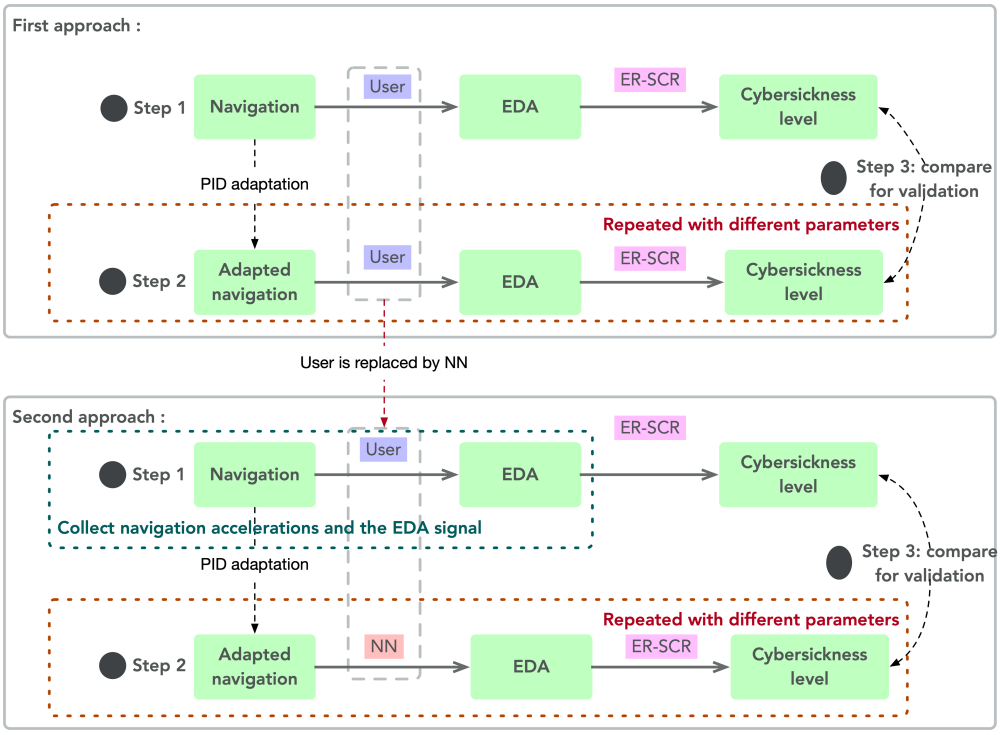

Figure 5.15: Strategies to find optimal parameters that can mitigate cybersickness in the adaptive model.

The answer is yes and there are two possibilities, given in Figure 5.15. The first approach is to assign different values to these coefficients and perform user studies to determine the best ones that can mitigate cybersickness. As there are eleven coefficients and each of them is independent to the other, the combination of optimal coefficients reaches at least hundreds or thousands of groups. To prove that a specific group of coefficients can reduce cybersickness with a statistical significance, we

will need around twenty users (to ensure a statistical significance) to evaluate the adaptation system. In general, there three steps for this approach:

- A group of users (around twenty users) navigate through a virtual environment without using adaptive navigation and evaluate the corresponding cybersickness level according to the EDA signal afterwards.
- The same group of users navigate through the same virtual environment with the PID adapted navigation. In this step, we have to manually adapt appropriate values for different parameters in this step.
- After they evaluate the cybersickness level, we can compare if the adapted navigation with current parameters can reduce cybersickness significantly.

Because of the global pandemic (Steed *et al.* 2020), in-person user studies have been much more difficult and expensive than ever before. However, in this approach, we have to ask a group of users to evaluate different settings of model parameters, which could be time consuming and challenging. The role of the users in this approach is to map the motion profiles during navigation to the corresponding EDA signal through which we can compute the cybersickness level. Fortunately, neural network (NN) models can work in this purpose as they are widely regarded as nonlinear fitters. Then, the question becomes: with an NN, how can we determine the performance of the adapted navigation with the minimum of user studies? This is where the second approach comes into play. It can bypass user studies, and instead use NN to evaluate the performance of different coefficients. The second approach includes three steps:

- The first step is similar to that of the first approach. While in this step we should collect longitudinal and rotational accelerations and the EDA signal during navigation in the immersive environments, the data will be used to train the NN model.
- The trained NN model can ingest the navigation accelerations and output the corresponding EDA signal. Therefore, in this step we can replace the user with the NN model, which shall avoid a vast number of user studies. The focus of the work becomes then to search for the appropriate parameters that can mitigate cybersickness, which is exactly a parameter optimization

problem. In mathematics, parametric optimization can be solved with different methods that have already been implemented in the open-source software *Optuna* (Akiba *et al.* 2019). Once the objective of the optimization is determined, *Optuna* can find the optimal parameters through Bayesian optimization, especially a sequential model-based optimization with Tree-Structured Parzen Estimator.

- Similar to that in the first approach, the third step compares if the adapted navigation can reduce cybersickness by comparing the ER-SCR feature of the EDA signal.

5.4.4.2 Experiment

Figure 5.16: Virtual scenario where the participants navigate along the highlighted path.

Compared to the first approach, the benefits of the second approach are: (1) replacing the user with an NN, which alleviates the challenge of recruiting experiments; (2) transposing the adaptation problem to an optimization problem that can solved with existing open-source software. In this case, the objective of the experiment is to collect enough data to train the NN model.

5.4.4.2.1 Data acquisition To avoid performing excessive user tests, we had to train an NN model that can map the navigation behavior (acceleration in this context) to the corresponding EDA signal. However, cutting down the number of user tests does not imply that we can get rid of them, we still

needed to collect enough data to train a high-quality NN model. Hence we carried out the following experiment to collect the required data:

1. We invited 53 participants from the local cities to participate in a navigation task in immersive environments. To obtain much more samples, all participants were asked to participate three times on three different days, hence we collected 159 samples. They were rewarded with different gifts afterwards. Upon arrival, they were asked to fill one questionnaire to investigate their health conditions and experience in playing games and using VR devices. From this questionnaire, no participants reported issues to perform the experiments.

2. Before the test, we gave the participant a brief introduction about the navigation tasks and how to control the VR devices. Due to the possible occurrence of cybersickness, they were informed that they could terminate the test whenever they felt sick or sever discomfort.

3. The experimenter put an HTC Vive Pro on the participant and the Empatica E4 wristband that can sample the EDA at a frequency of 4 Hz. The EDA signal during navigation is sent to the computer through Bluetooth.

4. The participant started to navigate in the virtual environment following a trajectory (brown color highlighted in Figure 5.16). Together with the EDA signal, the longitudinal and rotational accelerations were recorded synchronously. The navigation task lasted for four minutes.

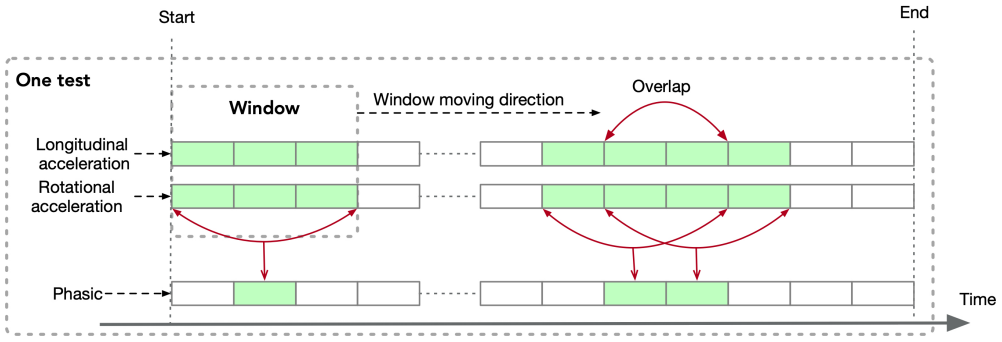

Figure 5.17: Schematic representation of the data collected from one user including the longitudinal and rotational accelerations, and the phasic component of EDA. Note that both accelerations were computed based on navigation speeds, and the phasic component of EDA was also preprocessed by the *Neurokit2* package.

5.4.4.2.2 Model architecture During the experiment, we had collected three signals with the same starting and ending time: longitudinal acceleration, rotational acceleration, and EDA signal. As the phasic component is associated with arousing stimulus events, the NN model should link the navigating accelerations to the phasic component of EDA. Therefore, we extracted the phasic component from the original EDA through *Neurokit2* (a Python toolbox for neurophysiological signal processing, Makowski *et al.* (2020)). Figure 5.17 represents a schematic representation of the data recorded from one user test. Individual differences (e.g., different magnitude) in the phasic response could make the model difficult to train, thus we normalized all the data to the range between zero and one.

To facilitate the model to learn the local relationship between the acceleration and phasic signal, we used a moving window on the signal and reformulated the data structure. The current time clip of the phasic signal was associated with the accelerations from the previous time clip and the next time clip. For example, with a clip length of 1 s, to predict the phasic signal between 1 s and 2 s, we used the acceleration data from 0 s to 3 s; to predict the phasic signal between 2 s and 3 s, we used the acceleration data from 1 s to 4 s. The duration of the window clip was considered as a hyper-parameter for the NN model. In total, we collected 159 pairs of data[8] among which we used 119 pairs to train the model, and the rest of them (40) to compare if the model could reduce the level of cybersickness. With 119 pairs of data, we obtained 90530 clips as the train set, and 22633 as the test set for the NN model.

The proposed model was implemented in the Tensorflow framework on an Nvidia GeForce RTX 2070 graphic card. Adam was chosen as the optimizer. Other hyper-parameters in the NN model (dropout rate, learning rate, the number of convolutional layer, the number of epoch, batch size) were optimally determined by *Optuna*. It took approximately three hours to train the model, and *Optuna* spent around ten days to find the optimal hyper-parameters inside the searching space. The hyper-parameters, with which we had achieved the best prediction accuracy, are given in Table 5.12. The model structure is given in Figure 5.18.

5.4.4.3 Computing the adaptive coefficients

We had obtained the best NN model that can map the acceleration to the phasic component of the EDA signal. At this stage, we can further find the optimal adaptive coefficients with the 40 pairs

[8] One pair of data includes longitudinal and rotational accelerations and one EDA signal from one user test.

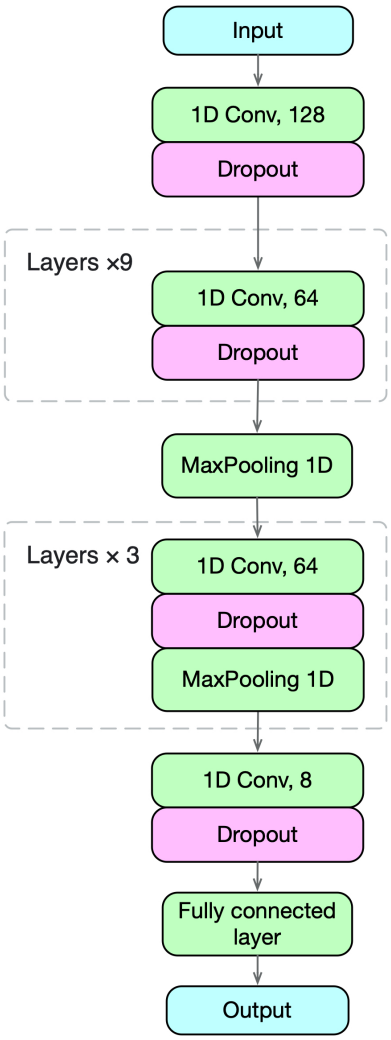

Figure 5.18: Architecture of the deep neural network. The network is composed of fourteen 1D convolutional layers and one fully connected layer; the kernel size for the convolutional is 3.

Table 5.12: Settings of the hyper-parameters obtained from *Optuna*.

Phasic signal length	2.25 s
Dropout rate	0.00099
Learning rate	0.000288
Convolutional layer	14
Epoch	1800
Batch size	256

of data mentioned above. The idea was to employ *Optuna* again to use the number of ER-SCR as the optimization objective, and search for the best adaptive coefficients that can reduce the number of ER-SCR. For the non-adapted navigation, the phasic component of EDA was obtained from the user study while for the adapted navigation with the coefficients in Table 5.13, the phasic component of EDA needed predicting from the pre-trained NN model. The detailed steps about the process are,

1. With the 40 pairs of data, we can compute the number of ER-SCR for the non-adapted navigation, denoted by N_{raw}, used as a baseline to be compared with the adapted one.

2. *Optuna* will randomly choose the values for eleven unknow coefficients. With the proposed model in Equation 5.27, we can compute the adapted acceleration based on the non-adapted one.

3. After obtaining the adapted accelerations, we can use the pre-trained NN model to compute the phasic component of EDA. As the pre-trained model only reads and returns the clipped data (shown in Figure 5.17), an additional step is required to reconstruct the phasic component from multiple clipped data to a single sequence. The number of ER-SCR obtained from the adapted model is denoted by $N_{adapted}$.

4. To record the reduction of the number of ER-SCR, *Optuna* will compute the difference ($N_{adapted} - N_{raw}$) . Further, it will randomly choose another group of coefficients and investigate if it can reduce the ER-SCR.

5. Above-mentioned step 2, 3 and 4 are repeated until ($N_{adapted} - N_{raw}$) converges to a stable value. Meanwhile, the corresponding coefficients are the optimal ones, given in Table 5.13.

Figure 5.19 demonstrates the difference between the non-adapted and adapted acceleration in longitudinal and rotational directions. The data came from one single test within 4 minutes. During the navigation, the acceleration might reach extremely large magnitudes because the user move in short time (as seen in section 5.2). The adaptive navigation can compensate the variation, and therefore, we observed the difference between the non-adapted and adapted acceleration profiles.

To validate if the adapted model with the coefficients presented in Table 5.13 can mitigate cybersickness, we had to compare the non-adapted navigation and the adapted one from a statistical viewpoint. As the data did not have equality of variance (*Levene's* test) nor have normality (*Shapiro–Wilk*

Table 5.13: Optimal coefficients of the adaptive model obtained from *Optuna*.

Coefficient	Value
K_{Pl}	0.0029
K_{Il}	0.0234
K_{Dl}	0.0173
K_{Pr}	0.0540
K_{Ir}	0.0078
K_{Dr}	0.1399
K_{Pf}	-0.3490
K_{If}	0.5845
K_{Df}	0.0560
β_l	0.0119
β_r	0.0226

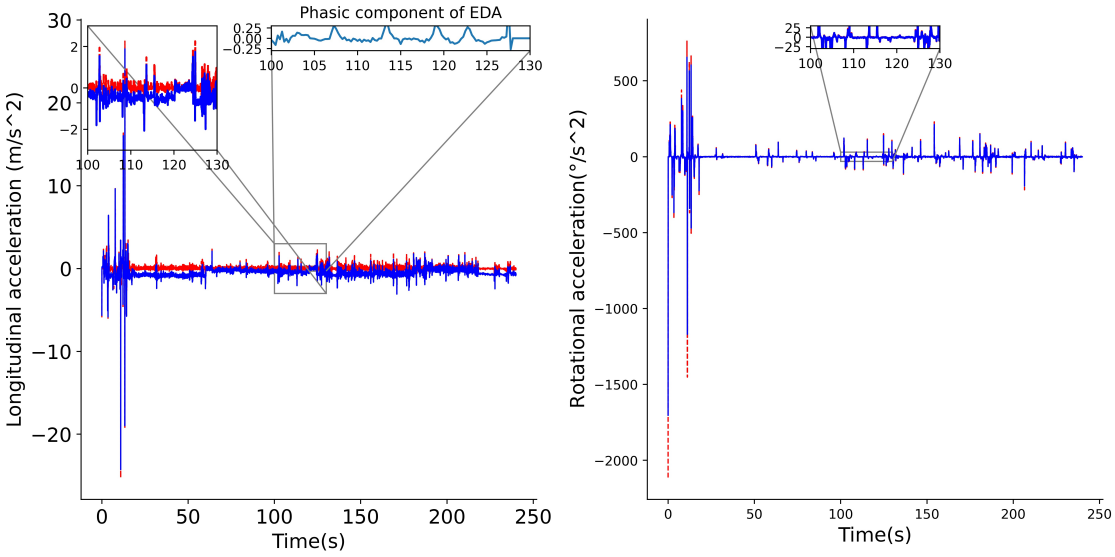

Figure 5.19: Comparison of non-adapted and adapted longitudinal and rotational acceleration.

test), we decided to employ the *Mann–Whitney* U test to compare the level of cybersickness between the navigation modes. The significance level was set to .05.

We used *Neurokit2* to compute the ER-SCR, and the result suggested that there was a significant reduction in cybersickness between the non-adapted navigation ($Median = 0.675$, normalized) and the adapted navigation ($Median = 0.451$, normalized) ($Mann–Whitney\ U = 1151.0, n_{adapted} = 40, n_{raw} = 40, p < 0.05$ one-tailed), which validated the performance of the adapted navigation.

5.4.5 Discussion

This work can be regarded as an extension of the previous work Plouzeau *et al.* (2018) in which the adaptive formulation is given as,

$$a(t_i) = a(t_{i-1}) - 0.5 * \frac{dEDA(t_i)}{dt} \tag{5.33}$$

where $a(t_i)$ and $a(t_{i-1})$ are the accelerations of two successive frames, longitudinal or rotational, $EDA(t_i)$ is the magnitude of EDA signal at time t_{i-1}. This formulation is designed for an acceleration-based control with which the joystick can control the longitudinal or rotational acceleration directly until reaching a speed limit. However, the user might fail to control the acceleration when $EDA(t_i)$ keeps increasing or decreasing, which was the reason that we added the second item in Equation 5.27 to stabilize the acceleration. Our model extended such equation into an algebraic form to incorporate all accelerations and coefficients thanks to the PID controller. In Equation 5.33 the factor 0.5 is derived empirically considering the physiological reaction time of the EDA, while in our model, all coefficients were optimized based on an existing dataset.

The adaptive navigation model was used to adapt the acceleration, while it is worth noting that it can adapt other navigation settings, e.g., the field of view (FOV) (Fernandes and Feiner 2016) or the geometry deformation (Lou and Chardonnet 2019). To adapt different navigation parameters, we can replace the acceleration in Equation 5.27 by these new parameters and then follow a similar procedure in this study to find the best parameters. The objective was not to compare the performance of different adaptive navigation settings for mitigating cybersickess, but to design a model of an adaptive strategy. For example, Islam *et al.* (2021) developed a closed-loop framework to detect cybersickness and adapt the FOV accordingly; this work has gained advantage by using a deep LSTM neural network to predict

the real-time cybersickness with physiological data including heart rate, heart rate variability, EDA and breathing rate, while our work only used the phasic component of EDA to detect cybersickness. Therefore, we can wonder whether involving other physiological signals can improve the accuracy of adaptation. Even so, the main difference here was that after getting a feedback signal (i.e., the level of cybersickness), our model can make use of the proportional, integral and derivative relation for adaptation, which can process the problem with high nonlinearity.

Generally, *Optuna* is an automatic hyperparameter optimization framework designed for optimizing an NN model. We used *Optuna* twice in this work with different intentions. First, to avoid performing massive user studies, we needed an NN model to map from navigation accelerations to the phasic component of EDA, and *Optuna* can help find the optimal settings. Second, after proposing the adaptive model, we had to determine the optimal parameters also with the objective of mitigating the cybersickness level significantly; therefore, we can use *Optuna* again for this parameter optimization problem.

However, more validation studies were required. The optimal parameters for adaptive navigation were found from a theoretical point, but we believed that a supplementary group of user studies to compare the non-adapted and adapted navigation can further confirm the effectiveness of the model parameters. Put differently, the lack of user studies might weaken the reliability of the parameters. A user study after the theoretical study not only can validate the performance of the adaptive parameter, but also can help define the search space in *Optuna* and discover more relationships between model parameters, bring benefits to the tuning process. Therefore, we will carry out such studies in future research, and at this stage we encouraged the potential readers to focus on the adaptive model apart from the optimal parameters. In addition, our model involved eleven parameters in order to adapt navigation, future research can investigate the relationship between these parameters and simplify the model with less parameters.

5.4.6 Conclusion

We proposed a pioneering mathematical model for adaptive navigation in virtual environments by integrating a PID controller. The premise to run this model successfully requires the system to detect cybersickness accurately; otherwise the adaptive power from the PID controller is weakened. Many adaptive VR systems have been focusing on the detection and evaluation of cybersickness in

immersive environments, while we paied more attention to how to utilize cybersickness to optimize the navigation settings backward. Although we had found the optimal adaptive coefficients thanks to simulation in *Optuna*, we were planning to run more user studies to further validate its performance.

5.5 Summary

This chapter presented four navigation techniques aiming at improving the navigation experience. First, semiautomatic navigation allows the user to navigate through a smooth trajectory with path planning algorithms. However, it still enables the user to adjust the path with the gaze-directed navigation technique manually. As the semiautomatic navigation only corrects the trajectory, we were further wondering whether the speed may also affect the navigation experience. Therefore, a speed protector was proposed to prevent the user from side effects arising from varying speeds. However, the speed protector only adapts the speed by avoiding a large magnitude of the acceleration and jerk, which does not involve the user factors. Therefore, we demonstrated how to use the cybersickness susceptibility obtained from the fuzzy logic to adapt the allowed maximal navigation speed; to make an online adaptive navigation, we proposed a PID-controlled system that can control the navigation acceleration based on the phasic component of the EDA signal. The closed-loop system models the navigation acceleration process with eleven parameters found through simulation. With the optimal parameters, the user shall experience less cybersickness. However, due to the limitation of the thesis schedule and the Covid-19 situation, we could not perform user studies to validate the model further.

Chapter 6

Conclusion and perspectives

Contents

6.1 General conclusion

Recalling the research questions, our objectives in this thesis were to improve navigation experience. In this frame, the questions dealt about the evaluation of user experience (cybersickness and cognitive workload) and the design of natural navigation techniques that can mitigate cybersickness and cognitive workload. For the former, we developed evaluation techniques based on the LSTM and the TOPSIS model, proving to be effective. For the latter, several techniques were proposed, including semiautomatic navigation, navigation with a speed protector, navigation with human factors, and adaptive navigation. Through experiments, their performance was validated.

The main contributions of this thesis can be summarized as follows:

1. We focused on evaluating user's experience when using VR applications, including cybersickness and cognitive workload. We summarized the explanation of cybersickness based on several theories. The subjective evaluation process can bias the results because of unperceived internal changes and unknown factors among users. It was necessary to have a method to handle and analyze this uncertainty, finding that the defects of the simulator sickness questionnnaire (SSQ) was of great significance in developing objective metrics for cybersickness. One of the well-known objective metrics is postural instability. So we trained an LSTM model for each participant using a normal-state postural signal captured before exposure. If the post-exposure postural sway signal were sufficiently different from the pre-exposure signal, the model would fail to reconstruct the input signal properly; the jump in the reconstruction error was called the loss error and indicated the level of cybersickness. In addition, regarding cognitive workload, we proposed to use the Technique for Order Performance by Similarity to Ideal Solution (TOPSIS) model to analyze the NASA-TLX table for measuring the overall cognitive workload instead of using the classical weighted sum method. To show the advantage of the TOPSIS approach, we performed one user experiment to validate the approach and its application to VR, considering factors including the VR platform and the scenario density.

2. We presented a semiautomatic navigation method based on path planning algorithms, aiming at reducing the generation of conflicting signals that may confuse the central nervous system (CNS). We carried out experiments where participants were asked to navigate through a VE equipped with an HTC Vive headset. Compared to joystick-based navigation, semiautomatic

navigation was more effective and accurate, enabling more concentration and immersion, achieving a significant reduction of visually-induced cybersickness.

3. We designed a speed protector that can be embedded into the navigation system to provide optimal speed profiles. With current technologies, the virtual navigation speed for most VR systems relies primarily on rate-control devices (e.g., joystick). The user has to manage manual adaptation of the speed based on the size of the VE and personal preferences. However, this method cannot provide optimal speeds for navigation as the user tends to change the speed involuntarily due to non-desired issues, including collisions or simulator sickness; in this case, the user may have to adjust the speed frequently and unsmoothly, worsening the situation. The speed protector can minimize the total jerk when the user navigates from an initial position to a target. In addition, we put constraints on speed, acceleration, and jerk so that they did not exceed specific thresholds. The speed protector was formulated mathematically and solved analytically to provide a smooth navigation experience with a minimum jerk of trajectory.

4. We proposed to understand the individual differences in the tolerance to cybersickness and the reason for its happening. Individual factors such as gender, age, postural stability, ethnic origin and genetic influences, gaming experience, personality, and visual acuity were analyzed. We argued that prior expert knowledge accumulated over decades of intense research should not be dismissed or ignored. However, the lack of strategy to integrate the influence of each factor on cybersickness made it challenging to utilize the results of existing research. We developed two approaches based on the fuzzy logic theory: the knowledge-based Mamdani-type fuzzy inference system and the data-driven Adaptive neuro-fuzzy inference system (ANFIS) to involve three individual differences (Age, Gaming experience, and Ethnicity). We correlated the corresponding outputs with the simulator sickness questionnaire (SSQ) scores in a simple navigation scenario. Such work provided insights to establish customized experiences for VR navigation by involving individual differences.

5. We presented an online strategy to adapt navigation acceleration based on physiological response. Currently, an approach to evaluate cybersickness is using subjective questionnaires (e.g., SSQ), but questionnaire-based evaluation will interrupt the experiment and introduce huge individual variances. During the navigation process, we can adapt the navigation speed based on these

signals. We used the PID control to adapt navigation and used neural networks to find an optimal PID setting. By doing this, we expected to mitigate cybersickness.

6.2 Limitations

The proposed methods have some limitations for the evaluation and the development of navigation techniques.

1. We had mentioned in chapter 3 that we expected to report cybersickness in real-time according to physiological signals such as EDA, Heart Rate, EEG, posture sway. While in our study, we only used EDA to measure the cybersickness of the proposed navigation techniques. EDA was chosen because collecting EDA signals with a wristwatch (Empatica E4[1]) was much convenient. Because the relationship between physiological signals and cybersickness is ambiguous and interpreting from one to another is an undergoing research topic, we did not involve EEG and heart rate to keep simplicity.

2. We developed adaptive navigation in chapter 5 based on the PID control. However, due to the Covid-19 pandemic, we only performed the validation from a theoretical point, which implies that the lack of user study might weaken the reliability of the proposed adaptive strategy.

6.3 Research perspectives

Based on our work in this thesis, we have some long-term perspectives for future developments.

1. **Measuring cybersickness with more physiological signals:** we proposed to measure cybersickness with the LSTM model by comparing the difference of posture sway signal between pre-exposure and post-exposure. However, measuring the posture sway signal when a user is immersed in VR application is infeasible, which means that we could not develop online adaptive navigation based on the posture sway signal. In the future, we plan to verify this method with other signals such as EEG, pupil dilation, and saccades in time series, which are supposed to be more convenient for real-time implementation and applications. In addition, it would be attractive to couple different physiological signals to improve prediction accuracy.

[1] https://www.empatica.com/research/e4/

2. **Developing standard dataset for user study:** artificial intelligence (AI) is gaining fast development thanks to easy access to public datasets. For instance, with datasets (KITTI, Cityscapes, ApolloScape, Waymo Open Dataset) for public transports, domain researchers can optimize the traffic flow and develop driverless vehicles. Considering that user experience in VR is generally individually different, we believe that a data-driven model can help solve the problem. However, when applying state-of-the-art algorithms to user interaction in immersive environments, limited datasets are available. Standard datasets are necessary to make use of the power of AI. These datasets should include the information from both virtual and physical environments: all visual information coming to the user and all corresponding physiological signals during the visual stimuli. We propose to develop a standardized process to create such datasets: (1) choosing the specific domain issue (e.g., cybersickness, cognitive workload) in VR, which helps determine the type of collected data; (2) choosing the widely accepted biosensors and questionnaires that are available to all researchers, and with this information, we can obtain different standard datasets that can be published for domain researchers. We believe that such datasets would enable researchers to compare their studies efficiently. And also, as the data collection process is standardized, different research teams also can contribute to the datasets.

3. **Using brain-computer interfaces (BCI) to improve immersive experience:** BCI can acquire brain signals and interpret them into executable actions performed by external devices. In VR, BCI can be used to analyze brain activities synchronously in real-time, through which we can evaluate user's responses in navigation tasks and adapt navigation settings accordingly. However, current BCI rely on many electrodes on the brain, posing a threat to natural interaction with virtual environments. Therefore, the development of non-invasive BCI with fewer electrodes and customized for VR devices is promising for future VR consumers. Moreover, BCI could be integrated into head-mounted devices during their design.

6.4 Scientific publications

All the research results were presented in the following scientific publications including journals and international conferences.

1. Journals

- Y. Wang, J.-R. Chardonnet, and F. Merienne, "Enhanced cognitive workload evaluation in 3D immersive environments with TOPSIS model," Int. J. Hum. Comput. Stud., vol. 147, p. 102572, Mar. 2021, doi: 10.1016/j.ijhcs.2020.102572.
- Y. Wang, J.-R. Chardonnet, and F. Merienne, "Development of a speed protector to optimize user experience in 3D virtual environments," Int. J. Hum. Comput. Stud., vol. 147, p. 102578, Dec. 2021, doi: 10.1016/j.ijhcs.2020.102578.

2. Conferences

- Y. Wang, J.-R. Chardonnet, F. Merienne, and J. Ovtcharova, "Using Fuzzy Logic to Involve Individual Differences for Predicting Cybersickness during VR Navigation," in 2021 IEEE Virtual Reality and 3D User Interfaces (VR), Mar. 2021, pp. 373–381, doi: 10.1109/VR50410.2021.00060.
- Y. Wang, J.-R. Chardonnet, and F. Merienne, "Design of a Semiautomatic Travel Technique in VR Environments," in 2019 IEEE Conference on Virtual Reality and 3D User Interfaces (VR), Mar. 2019, pp. 1223–1224, doi: 10.1109/VR.2019.8798004.
- Y. Wang, J.-R. Chardonnet, and F. Merienne, "VR Sickness Prediction for Navigation in Immersive Virtual Environments using a Deep Long Short Term Memory Model," in 2019 IEEE Conference on Virtual Reality and 3D User Interfaces (VR), Mar. 2019, pp. 1874–1881, doi: 10.1109/VR.2019.8798213.
- Y. Wang, J.-R. Chardonnet, and F. Merienne, "Speed Profile Optimization for Enhanced Passenger Comfort: An Optimal Control Approach," in 2018 21st International Conference on Intelligent Transportation Systems (ITSC), Nov. 2018, pp. 723–728, doi: 10.1109/ITSC.2018.8569420.
- Y. Wang, J.-R. Chardonnet, and F. Merienne, "A Semiautomatic Navigation Interface to Reduce Visually Induced Motion Sickness in Virtual Reality," in Journées de la Réalité Virtuelle, 2018, pp. 47–52.

Bibliography

[1] S. Chang and W. Chen, "Does visualize industries matter? a technology foresight of global virtual reality and augmented reality industry", in *2017 International Conference on Applied System Innovation (ICASI)*, May 2017, pp. 382–385. DOI: 10.1109/ICASI.2017.7988432.

[2] H. Bellini, W. Chen, M. Sugiyama, M. Shin, S. Alam, and D. Takayama, "Virtual and augmented reality: Understanding the race for the next computing platform, the goldman sachs group", *The Goldman Sachs Group,Inc*, 2016.

[3] M. Framingham, "Worldwide revenues for augmented and virtual reality forecast to reach $162 billion in 2020, according to idc", *IDC Report*, vol. 15, 2016.

[4] T. Merel, "After a mixed year, mobile ar to drive $108 billion vrar market by 2021", *Digi-Capital*, 2017.

[5] F. Merienne, "Virtual Reality: Principles and Applications", in *Encyclopedia of Computer Science and Technology, Second Edition*, vol. 2017, CRC Press, Dec. 2016, pp. 1–11, ISBN: 1482254948. DOI: 10.1081/E-ECST2-140000194.

[6] M. Javaid and A. Haleem, "Virtual reality applications toward medical field", *Clinical Epidemiology and Global Health*, 2019, ISSN: 2213-3984. DOI: 10.1016/j.cegh.2019.12.010.

[7] J. Radianti, T. A. Majchrzak, J. Fromm, and I. Wohlgenannt, "A systematic review of immersive virtual reality applications for higher education: Design elements, lessons learned, and research agenda", *Computers & Education*, vol. 147, p. 103 778, 2020, ISSN: 0360-1315. DOI: 10.1016/j.compedu.2019.103778.

[8] J. Negrillo-Cárdenas, J.-R. Jiménez-Pérez, and F. R. Feito, "The role of virtual and augmented reality in orthopedic trauma surgery: From diagnosis to rehabilitation", *Computer Methods and Programs in Biomedicine*, vol. 191, p. 105 407, 2020, ISSN: 0169-2607. DOI: 10.1016/j.cmpb.2020.105407.

[9] S. Gibbons, *How businesses are using vr to survive the covid-19 era*, Online, May 2020.

[10] G.-Z. Yang, B. J. Nelson, R. R. Murphy, H. Choset, H. Christensen, S. H. Collins, P. Dario, K. Goldberg, K. Ikuta, N. Jacobstein, D. Kragic, R. H. Taylor, and M. McNutt, "Combating covid-19—the role of robotics in managing public health and infectious diseases", *Science Robotics*, vol. 5, no. 40, 2020. DOI: 10.1126/scirobotics.abb5589.

[11] W. R. Sherman and A. B. Craig, *Understanding Virtual Reality: Interface, Application, and Design*. Morgan Kaufmann Publishers Inc., 2003, ISBN: 1-55860-353-0.

[12] S. M. Lavalle, A. Yershova, M. Katsev, and M. Antonov, "Head tracking for the oculus rift", in *In IEEE International Conference on Robotics and Automation (ICRA). IEEE*, 2014, pp. 187–194.

[13] J. Bolton, M. Lambert, D. Lirette, and B. Unsworth, "Paperdude: A virtual reality cycling exergame", in *CHI '14 Extended Abstracts on Human Factors in Computing Systems*, ser. CHI EA '14, Toronto, Ontario, Canada: ACM, 2014, pp. 475–478, ISBN: 978-1-4503-2474-8. DOI: 10.1145/2559206.2574827.

[14] T. Aslandere, D. Dreyer, and F. Pankratz, "Virtual hand-button interaction in a generic virtual reality flight simulator", in *2015 IEEE aerospace conference*, IEEE, 2015, pp. 1–8. DOI: 10.1109/AERO.2015.7118876.

[15] J. Jankowski and M. Hachet, "Advances in interaction with 3d environments", *Comput. Graph. Forum*, vol. 34, no. 1, pp. 152–190, Feb. 2015, ISSN: 0167-7055. DOI: 10.1111/cgf.12466.

[16] J. J. LaViola Jr, E. Kruijff, R. P. McMahan, D. Bowman, and I. P. Poupyrev, *3D user interfaces: theory and practice*. Redwood City, CA, USA: Addison-Wesley Professional, 2017, ISBN: 9780134034461.

[17] H. Hicheur, Q.-C. Pham, G. Arechavaleta, J.-P. Laumond, and A. Berthoz, "The formation of trajectories during goal-oriented locomotion in humans. I. A stereotyped behaviour", *European Journal of Neuroscience*, vol. 26, no. 8, pp. 2376–2390, Oct. 2007, ISSN: 0953816X. DOI: 10.1111/j.1460-9568.2007.05836.x.

[18] C. Papaxanthis, V. Dubost, and T. Pozzo, "Similar planning strategies for whole-body and arm movements performed in the sagittal plane", *Neuroscience*, vol. 117, no. 4, pp. 779–783, 2003, ISSN: 0306-4522. DOI: 10.1016/S0306-4522(02)00964-8.

[19] C. M. Harris and D. M. Wolpert, "Signal-dependent noise determines motor planning", *Nature*, vol. 394, no. 6695, pp. 780–784, Aug. 1998, ISSN: 0028-0836. DOI: 10.1038/29528.

[20] N. Hogan, "An organizing principle for a class of voluntary movements", *Journal of Neuroscience*, vol. 4, no. 11, pp. 2745–2754, 1984, ISSN: 0270-6474. DOI: 10.1523/JNEUROSCI.04-11-02745.1984.

[21] T. Flash and N. Hogan, "The coordination of arm movements: An experimentally confirmed mathematical model", *Journal of Neuroscience*, vol. 5, no. 7, pp. 1688–1703, 1985, ISSN: 0270-6474.

[22] Y. Uno, M. Kawato, and R. Suzuki, "Formation and control of optimal trajectory in human multijoint arm movement", *Biological Cybernetics*, vol. 61, no. 2, pp. 89–101, Jun. 1989, ISSN: 1432-0770. DOI: 10.1007/BF00204593.

[23] A. Kulik, "Building on realism and magic for designing 3d interaction techniques", *IEEE Computer Graphics and Applications*, vol. 29, no. 6, pp. 22–33, Nov. 2009, ISSN: 0272-1716. DOI: 10.1109/MCG.2009.115.

[24] J. L. Souman, P. R. Giordano, M. Schwaiger, I. Frissen, T. Thümmel, H. Ulbrich, A. D. Luca, H. H. Bülthoff, and M. O. Ernst, "Cyberwalk: Enabling unconstrained omnidirectional walking through virtual environments", *ACM Trans. Appl. Percept.*, vol. 8, no. 4, 25:1–25:22, Dec. 2008, ISSN: 1544-3558. DOI: 10.1145/2043603.2043607.

[25] S. Razzaque, "Redirected walking", Ph.D. dissertation, University of North Carolina at Chapel Hill, USA, 2005, ISBN: 0542340534.

[26] W. E. Marsh, M. Putnam, J. W. Kelly, V. J. Dark, and J. H. Oliver, "The cognitive implications of semi-natural virtual locomotion", in *2012 IEEE Virtual Reality Workshops (VRW)*, IEEE, 2012, pp. 47–50. DOI: 10.1109/VR.2012.6180878.

[27] *Ergonomics of human system interaction-part 210: Human-centred design for interactive systems*, Standard, International Organization for Standardization, Geneva, Switzerland, 2019.

[28] F. Rebelo, P. Noriega, E. Duarte, and M. Soares, "Using Virtual Reality to Assess User Experience", *Human Factors: The Journal of the Human Factors and Ergonomics Society*, vol. 54, no. 6, pp. 964–982, Dec. 2012, ISSN: 0018-7208. DOI: 10.1177/0018720812465006.

[29] K. M. Stanney, R. R. Mourant, and R. S. Kennedy, "Human factors issues in virtual environments: A review of the literature", *Presence*, vol. 7, no. 4, pp. 327–351, 1998. DOI: 10.1162/105474698565767.

[30] J. Takatalo, T. Kawai, J. Kaistinen, G. Nyman, and J. Häkkinen, "User experience in 3d stereoscopic games", *Media Psychology*, vol. 14, no. 4, pp. 387–414, 2011. DOI: 10.1080/15213269.2011.620538.

[31] M. Sheik-Nainar, D. Kaber, S. Hsiang, C. Pankok Jr, and M. Zahabi, "Influence of cognitive and perceptual processing on multitask performance with locomotion", *Theoretical Issues in Ergonomics Science*, vol. 16, no. 3, pp. 273–298, 2015. DOI: 10.1080/1463922X.2014.1001005.

[32] E. P. Shaw, J. C. Rietschel, B. D. Hendershot, A. L. Pruziner, M. W. Miller, B. D. Hatfield, and R. J. Gentili, "Measurement of attentional reserve and mental effort for cognitive workload assessment under various task demands during dual-task walking", *Biological psychology*, vol. 134, pp. 39–51, 2018. DOI: 10.1016/j.biopsycho.2018.01.009.

[33] T. Igarashi, R. Kadobayashi, K. Mase, and H. Tanaka, "Path drawing for 3d walkthrough", in *Proceedings of the 11th Annual ACM Symposium on User Interface Software and Technology*, ser. UIST '98, San Francisco, California, USA: ACM, 1998, pp. 173–174, ISBN: 1-58113-034-1. DOI: 10.1145/288392.288599.

[34] P. Renner, T. Dankert, D. Schneider, N. Mattar, and T. Pfeiffer, "Navigating and Selecting in the Virtual Supermarket: Review and Update of Classic Interaction Techniques", in *Virtuelle und Erweiterte Realität 7 Workshop der GIFachgruppe VRAR*, Stuttgart, 2010, pp. 71–82.

[35] N. Elmqvist and P. Tsigas, "A taxonomy of 3d occlusion management techniques", in *2007 IEEE Virtual Reality Conference*, IEEE, Mar. 2007, pp. 51–58. DOI: 10.1109/VR.2007.352463.

[36] M. Mohanan and A. Salgoankar, "A survey of robotic motion planning in dynamic environments", *Robotics and Autonomous Systems*, vol. 100, pp. 171–185, 2018, ISSN: 0921-8890. DOI: 10.1016/j.robot.2017.10.011.

[37] J. Yao, C. Lin, X. Xie, A. J. Wang, and C.-C. Hung, "Path planning for virtual human motion using improved a* star algorithm", in *Proceedings of the 2010 Seventh International Conference on Information Technology: New Generations*, ser. ITNG '10, Washington, DC, USA: IEEE Computer Society, 2010, pp. 1154–1158, ISBN: 978-0-7695-3984-3. DOI: 10.1109/ITNG.2010.53.

[38] A. Sud, E. Andersen, S. Curtis, M. Lin, and D. Manocha, "Real-time path planning for virtual agents in dynamic environments", in *ACM SIGGRAPH 2008 Classes*, ser. SIGGRAPH '08, Los Angeles, California: ACM, 2008, 55:1–55:9. DOI: 10.1145/1401132.1401206.

[39] Y. Liu, M.-k. Li, C.-l. Xie, M.-j. Peng, S.-y. Wang, N. Chao, and Z.-k. Liu, "Minimum dose method for walking-path planning of nuclear facilities", *Annals of Nuclear Energy*, vol. 83, pp. 161–171, 2015, ISSN: 0306-4549. DOI: 10.1016/j.anucene.2015.04.019.

[40] N. Chao, Y.-k. Liu, H. Xia, C.-l. Xie, A. Ayodeji, H. Yang, and L. Bai, "A sampling-based method with virtual reality technology to provide minimum dose path navigation for occupational workers in nuclear facilities", *Progress in Nuclear Energy*, vol. 100, pp. 22–32, 2017, ISSN: 0149-1970. DOI: 10.1016/j.pnucene.2017.05.024.

[41] F. Argelaguet and C. Andujar, "Automatic speed graph generation for predefined camera paths", in *Smart Graphics*, R. Taylor, P. Boulanger, A. Krüger, and P. Olivier, Eds., Berlin, Heidelberg: Springer Berlin Heidelberg, 2010, pp. 115–126. DOI: 10.1007/978-3-642-13544-6_11.

[42] F. Argelaguet, "Adaptive navigation for virtual environments", in *2014 IEEE Symposium on 3D User Interfaces (3DUI)*, IEEE, Mar. 2014, pp. 123–126, ISBN: 978-1-4799-3624-3. DOI: 10.1109/3DUI.2014.7027325.

[43] G. Cirio, M. Marchal, A.-H. Olivier, and J. Pettre, "Kinematic evaluation of virtual walking trajectories", *IEEE Transactions on Visualization and Computer Graphics*, vol. 19, no. 4, pp. 671–680, Apr. 2013, ISSN: 1077-2626. DOI: 10.1109/TVCG.2013.34.

[44] M. J. E. Richardson and T. Flash, "Comparing smooth arm movements with the two-thirds power law and the related segmented-control hypothesis", *Journal of Neuroscience*, vol. 22, no. 18, pp. 8201–8211, 2002, ISSN: 0270-6474.

[45] Q.-C. Pham, H. Hicheur, G. Arechavaleta, J.-P. Laumond, and A. Berthoz, "The formation of trajectories during goal-oriented locomotion in humans. II. A maximum smoothness model", *European Journal of Neuroscience*, vol. 26, no. 8, pp. 2391–2403, Oct. 2007, ISSN: 0953816X. DOI: 10.1111/j.1460-9568.2007.05835.x.

[46] K. Mombaur, J.-P. Laumond, and E. Yoshida, "An optimal control model unifying holonomic and nonholonomic walking", in *Humanoids 2008 - 8th IEEE-RAS International Conference on Humanoid Robots*, Daejeon, South Korea: IEEE, Dec. 2008, pp. 646–653, ISBN: 978-1-4244-2821-2. DOI: 10.1109/ICHR.2008.4756020.

[47] A. Somrak, I. Humar, M. S. Hossain, M. F. Alhamid, M. A. Hossain, and J. Guna, "Estimating VR Sickness and user experience using different HMD technologies: An evaluation study", *Future Generation Computer Systems*, vol. 94, pp. 302–316, May 2019, ISSN: 0167739X. DOI: 10.1016/j.future.2018.11.041.

[48] L. L. Arns and M. M. Cerney, "The relationship between age and incidence of cybersickness among immersive environment users", *Proceedings - IEEE Virtual Reality*, vol. 2005, pp. 267–268, 2005. DOI: 10.1109/vr.2005.80.

[49] B. D. Lawson, D. A. Graeber, A. M. Mead, and E. R. Muth, "Signs and symptoms of human syndromes associated with synthetic experiences.", in *Handbook of virtual environments: Design, implementation, and applications.* Ser. Human factors and ergonomics. Lawrence Erlbaum Associates Publishers, 2002, pp. 589–618, ISBN: 0-8058-3270-X (Hardcover).

[50] D. L. Harm, "Physiology of motion sickness", in *Motion and Space Sickness*, G. H. Crampton, Ed., Florida: CRC Press, 1990, pp. 153–178.

[51] E. M. Kolasinski, "Simulator sickness in virtual environments.", Army Research Inst for the Behavioral and Social Sciences Alexandria Va, Tech. Rep., 1995.

[52] S. Davis, K. Nesbitt, and E. Nalivaiko, "A Systematic Review of Cybersickness", in *Proceedings of the 2014 Conference on Interactive Entertainment - IE2014*, New York, New York, USA: ACM Press, 2014, pp. 1–9, ISBN: 9781450327909. DOI: 10.1145/2677758.2677780.

[53] F. Biocca, "Will simulation sickness slow down the diffusion of virtual environment technology?", *Presence: Teleoper. Virtual Environ.*, vol. 1, no. 3, pp. 334–343, Jan. 1992, ISSN: 1054-7460. DOI: 10.1162/pres.1992.1.3.334.

[54] L. Liu, M. Miyazaki, and B. Watson, "Norms and validity of the drivr: A virtual reality driving assessment for persons with head injuries", *Cyberpsychology & Behavior*, vol. 2, no. 1, pp. 53–67, 1999. DOI: 10.1089/cpb.1999.2.53.

[55] S.-N. Yang, T. Schlieski, B. Selmins, S. C. Cooper, R. A. Doherty, P. J. Corriveau, and J. E. Sheedy, "Stereoscopic viewing and reported perceived immersion and symptoms", *Optometry and vision science*, vol. 89, no. 7, pp. 1068–1080, 2012, PMID: 22733100. DOI: 10.1097/OPX.0b013e31825da430.

[56] J. T. Reason and J. J. Brand, *Motion sickness*. Academic press, 1975.

[57] A. C. Paillard, G. Quarck, F. Paolino, P. Denise, M. Paolino, J. F. Golding, and V. Ghulyan-Bedikian, "Motion sickness susceptibility in healthy subjects and vestibular patients: Effects of gender, age and trait-anxiety", *Journal of Vestibular Research: Equilibrium and Orientation*, vol. 23, no. 4-5, pp. 203–210, 2013, ISSN: 09574271. DOI: 10.3233/VES-130501.

[58] B. Bergström, "Morphology of the vestibular nerve: Ii. the number of myelinated vestibular nerve fibers in man at various ages", *Acta oto-laryngologica*, vol. 76, no. 1-6, pp. 173–179, 1973. DOI: 10.3109/00016487309121496.

[59] E. Richter, "Quantitative study of human scarpa's ganglion and vestibular sensory epithelia", *Acta oto-laryngologica*, vol. 90, no. 1-6, pp. 199–208, 1980. DOI: 10.3109/00016488009131716.

[60] M. Treisman, "Motion sickness: An evolutionary hypothesis", *Science*, vol. 197, no. 4302, pp. 493–495, 1977. DOI: 10.1126/science.301659.

[61] B. Bowins, "Motion sickness: A negative reinforcement model", *Brain Research Bulletin*, vol. 81, no. 1, pp. 7–11, 2010, ISSN: 0361-9230. DOI: 10.1016/j.brainresbull.2009.09.017.

[62] S. P. Smith and S. Du'Mont, "Measuring the effect of gaming experience on virtual environment navigation tasks", in *2009 IEEE Symposium on 3D User Interfaces*, IEEE, 2009, pp. 3–10, ISBN: 978-1-4244-3965-2. DOI: 10.1109/3DUI.2009.4811198.

[63] J. Häkkinen, M. Liinasuo, J. Takatalo, and G. Nyman, "Visual comfort with mobile stereoscopic gaming", in *Stereoscopic Displays and Virtual Reality Systems XIII*, A. J. Woods, N. A. Dodgson, J. O. Merritt, M. T. Bolas, and I. E. McDowall, Eds., International Society for Optics and Photonics, vol. 6055, SPIE, 2006, pp. 85–93. DOI: 10.1117/12.641210.

[64] M. M. Knight and L. L. Arns, "The relationship among age and other factors on incidence of cybersickness in immersive environment users", in *ACM SIGGRAPH 2006 Research Posters*, ser. SIGGRAPH '06, Boston, Massachusetts: ACM, 2006, ISBN: 1-59593-364-6. DOI: 10.1145/1179622.1179846.

[65] A. Iskenderova, F. Weidner, and W. Broll, "Drunk Virtual Reality Gaming:Exploring the Influence of Alcohol on Cybersickness", in *Proceedings of the Annual Symposium on Computer-Human Interaction in Play - CHI PLAY '17*, New York, New York, USA: ACM Press, 2017, pp. 561–572, ISBN: 9781450348980. DOI: 10.1145/3116595.3116618.

[66] M. S. Dennison, A. Z. Wisti, and M. D'Zmura, "Use of physiological signals to predict cybersickness", *Displays*, vol. 44, pp. 42–52, Sep. 2016. DOI: 10.1016/j.displa.2016.07.002.

[67] P. Gamito, J. Oliveira, D. Morais, A. Baptista, N. Santos, F. Soares, T. Saraiva, and P. Rosa, "Training presence: The importance of virtual reality experience on the "sense of being there"", *Annual Review of Cybertherapy and Telemedicine 2010*, pp. 128–133, 2010.

[68] P. Gamito, J. Oliveira, P. Santos, D. Morais, T. Saraiva, M. Pombal, and B. Mota, "Presence, immersion and cybersickness assessment through a test anxiety virtual environment", *Annual Review of CyberTherapy and Telemedicine*, vol. 6, pp. 83–90, 2008.

[69] S. Klosterhalfen, S. Kellermann, F. Pan, U. Stockhorst, G. Hall, and P. Enck, "Effects of ethnicity and gender on motion sickness susceptibility", *Aviation Space and Environmental Medicine*, vol. 76, no. 11, pp. 1051–1057, 2005, ISSN: 00956562.

[70] R. Stern, S. Hu, R. LeBlanc, and K. Koch, "Chinese hyper-susceptibility to vection-induced motion sickness", *Aviation, space, and environmental medicine*, vol. 64, no. 9 Pt 1, pp. 827–830, Sep. 1993, ISSN: 0095-6562.

[71] R. M. Stern, S. Hu, S. H. Uijtdehaage, E. R. Muth, L. H. Xu, and K. L. Koch, "Asian hypersusceptibility to motion sickness", *Human heredity*, vol. 46, no. 1, pp. 7–14, 1996. DOI: 10.1159/000154318.

[72] T. M. Yanus and F. V. Malmstrom, "Is motion sickness hereditary?", *Proceedings of the Human Factors and Ergonomics Society Annual Meeting*, vol. 38, no. 13, pp. 796–800, 1994. DOI: 10.1177/154193129403801304.

[73] G. W. Knox, "Motion Sickness: An Evolutionary and Genetic Basis for the Negative Reinforcement Model", *Aviation, Space, and Environmental Medicine*, vol. 85, no. 1, pp. 46–49, Jan. 2014, ISSN: 00956562. DOI: 10.3357/ASEM.3519.2014.

[74] K. Abe, N. Oda, and H. Hatta, "Behavioural genetics of early childhood: Fears, restlessness, motion sickness and enuresis", *Acta geneticae medicae et gemellologiae: twin research*, vol. 33, no. 2, pp. 303–306, 1984. DOI: 10.1017/S0001566000007340.

[75] C. M. Reavley, J. F. Golding, L. F. Cherkas, T. D. Spector, and A. J. MacGregor, "Genetic influences on motion sickness susceptibility in adult women: A classical twin study", *Aviation, space, and environmental medicine*, vol. 77, no. 11, pp. 1148–1152, 2006.

[76] K. Sharma, P. Sharma, A. Sharma, and G. Singh, "Phenylthiocarbamide taste perception and susceptibility to motion sickness: Linking higher susceptibility with higher phenylthiocarbamide taste acuity", *The Journal of Laryngology & Otology*, vol. 122, no. 10, pp. 1064–1073, 2008. DOI: 10.1017/S0022215107001442.

[77] H. Bakwin, "Car-sickness in twins", *Developmental Medicine & Child Neurology*, vol. 13, no. 3, pp. 310–312, 1971. DOI: 10.1111/j.1469-8749.1971.tb03267.x.

[78] J. C. Finley Jr, M. O'Leary, D. Wester, S. MacKenzie, N. Shepard, S. Farrow, and W. Lockette, "A genetic polymorphism of the α2-adrenergic receptor increases autonomic responses to stress", *Journal of applied physiology*, vol. 96, no. 6, pp. 2231–2239, 2004. DOI: japplphysiol.00527.2003.

[79] L. Liu, L. Yuan, H.-B. Wang, L.-S. Yu, J. Zheng, C.-Q. Luo, and Y. Wang, "The human alpha (2a)-ar gene and the genotype of site-1296 and the susceptibility to motion sickness", *Sheng wu hua xue yu sheng wu wu li xue bao Acta biochimica et biophysica Sinica*, vol. 34, no. 3, pp. 291–297, 2002.

[80] B. K. Jaeger and R. R. Mourant, "Comparison of simulator sickness using static and dynamic walking simulators", *Proceedings of the Human Factors and Ergonomics Society Annual Meeting*, vol. 45, no. 27, pp. 1896–1900, 2001. DOI: 10.1177/154193120104502709.

[81] S. R. Holmes and M. J. Griffin, "Correlation between heart rate and the severity of motion sickness caused by optokinetic stimulation.", *Journal of Psychophysiology*, vol. 15, no. 1, p. 35, 2001. DOI: 10.1027//0269-8803.15.1.35.

[82] J. Hakkinen, T. Vuori, and M. Paakka, "Postural stability and sickness symptoms after hmd use", in *IEEE International Conference on Systems, Man and Cybernetics*, IEEE, vol. 1, 2002, pp. 147–152. DOI: 10.1109/ICSMC.2002.1167964.

[83] M. B. Flanagan, J. G. May, and T. G. Dobie, "Sex differences in tolerance to visually-induced motion sickness", *Aviation, space, and environmental medicine*, vol. 76, no. 7, pp. 642–646, 2005.

[84] G. D. Park, R. W. Allen, D. Fiorentino, T. J. Rosenthal, and M. L. Cook, "Simulator sickness scores according to symptom susceptibility, age, and gender for an older driver assessment study", *Proceedings of the Human Factors and Ergonomics Society Annual Meeting*, vol. 50, no. 26, pp. 2702–2706, 2006. DOI: 10.1177/154193120605002607.

[85] T. Dobie, D. McBride, J. T. Dobie, and J. May, "The effects of age and sex on susceptibility to motion sickness.", *Aviation, Space, and Environmental Medicine*, vol. 72, no. 1, pp. 13–20, 2001.

[86] K.-H. Ladwig, B. Marten-Mittag, B. Formanek, and G. Dammann, "Gender differences of symptom reporting and medical health care utilization in the german population", *European Journal of Epidemiology*, vol. 16, no. 6, pp. 511–518, Jun. 2000, ISSN: 1573-7284. DOI: 10.1023/A:1007629920752.

[87] W. E. Collins and J. M. Lentz, "Some psychological correlates of motion sickness susceptibility", *Aviation, space, and environmental medicine*, vol. 48, no. 7, pp. 587–594, Jul. 1977, ISSN: 0095-6562.

[88] O. Robin, H. Vinard, E. Vernet-Maury, and J. Saumet, "Influence of sex and anxiety on pain threshold and tolerance", *Functional neurology*, vol. 2, no. 2, pp. 173–179, 1987, ISSN: 0393-5264.

[89] S. Weech, S. Kenny, and M. Barnett-Cowan, "Presence and Cybersickness in Virtual Reality Are Negatively Related: A Review", *Frontiers in Psychology*, vol. 10, pp. 1–19, Feb. 2019, ISSN: 1664-1078. DOI: 10.3389/fpsyg.2019.00158.

[90] L. Rebenitsch and C. Owen, "Review on cybersickness in applications and visual displays", *Virtual Reality*, vol. 20, no. 2, pp. 101–125, 2016. DOI: 10.1007/s10055-016-0285-9.

[91] M. Melo, J. Vasconcelos-Raposo, and M. Bessa, "Presence and cybersickness in immersive content: Effects of content type, exposure time and gender", *Computers & Graphics*, vol. 71, pp. 159–165, Apr. 2018, ISSN: 00978493. DOI: 10.1016/j.cag.2017.11.007.

[92] B. G. Witmer and M. J. Singer, "Measuring Presence in Virtual Environments: A Presence Questionnaire", *Presence: Teleoperators and Virtual Environments*, vol. 7, no. 3, pp. 225–240, Jun. 1998, ISSN: 1054-7460. DOI: 10.1162/105474698565686.

[93] I. Viaud-Delmon, Y. P. Ivanenko, A. Berthoz, and R. Jouvent, "Sex, lies and virtual reality", *Nature Neuroscience*, vol. 1, no. 1, p. 15, 1998. DOI: 10.1038/215.

[94] R. Schwab, "The nonlabyrinthine causes of motion sickness.", *International record of medicine and general practice clinics*, vol. 167, no. 12, pp. 631–637, 1954.

[95] J. F. Golding, P. Kadzere, and M. A. Gresty, "Motion sickness susceptibility fluctuates through the menstrual cycle", *Aviation, space, and Environmental medicine*, vol. 76, no. 10, pp. 970–973, 2005.

[96] R. L. Matchock, M. E. Levine, P. J. Gianaros, and R. M. Stern, "Susceptibility to Nausea and Motion Sickness as a Function of the Menstrual Cycle", *Women's Health Issues*, vol. 18, no. 4, pp. 328–335, Jul. 2008, ISSN: 10493867. DOI: 10.1016/j.whi.2008.01.006.

[97] R. S. Kennedy and L. H. Frank, "A review of motion sickness with special reference to simulator sickness", CANYON RESEARCH GROUP INC WESTLAKE VILLAGE CA, Tech. Rep., 1985.

[98] J. J. LaViola Jr, "A discussion of cybersickness in virtual environments", *ACM Sigchi Bulletin*, vol. 32, no. 1, pp. 47–56, 2000.

[99] N. A. Dodgson, "Variation and extrema of human interpupillary distance", in *Stereoscopic Displays and Virtual Reality Systems XI*, International Society for Optics and Photonics, vol. 5291, 2004, pp. 36–46. DOI: 10.1117/12.529999.

[100] J. C. Read and I. Bohr, "User experience while viewing stereoscopic 3D television", *Ergonomics*, vol. 57, no. 8, pp. 1140–1153, Aug. 2014, ISSN: 0014-0139. DOI: 10.1080/00140139.2014.914581.

[101] R. S. Kennedy, N. E. Lane, K. S. Berbaum, and M. G. Lilienthal, "Simulator Sickness Questionnaire: An Enhanced Method for Quantifying Simulator Sickness", *The International Journal of Aviation Psychology*, vol. 3, no. 3, pp. 203–220, Jul. 1993, ISSN: 1050-8414. DOI: 10.1207/s15327108ijap0303{_}3.

[102] Y. Ling, H. T. Nefs, W.-P. Brinkman, C. Qu, and I. Heynderickx, "The relationship between individual characteristics and experienced presence", *Computers in Human Behavior*, vol. 29, no. 4, pp. 1519–1530, 2013. DOI: 10.1016/j.chb.2012.12.010.

[103] G. E. Riccio and T. A. Stoffregen, "An ecological Theory of Motion Sickness and Postural Instability", *Ecological Psychology*, vol. 3, no. 3, pp. 195–240, Sep. 1991, ISSN: 1040-7413. DOI: 10.1207/s15326969eco0303{_}2.

[104] N. Owen, A. G. Leadbetter, and L. Yardley, "Relationship between postural control and motion sickness in healthy subjects", *Brain Research Bulletin*, vol. 47, no. 5, pp. 471–474, Nov. 1998, ISSN: 03619230. DOI: 10.1016/S0361-9230(98)00101-4.

[105] T. A. Stoffregen and L. Smart, "Postural instability precedes motion sickness", *Brain Research Bulletin*, vol. 47, no. 5, pp. 437–448, 1998, ISSN: 0361-9230. DOI: 10.1016/S0361-9230(98)00102-6.

[106] B. E. Maki, P. J. Holliday, and A. K. Topper, "Fear of falling and postural performance in the elderly", *Journal of gerontology*, vol. 46, no. 4, pp. M123–M131, 1991. DOI: 10.1093/geronj/46.4.M123.

[107] B. Maki and W. Mcllroy, "Influence of arousal and attention on the control of postural sway", *Journal of Vestibular Research*, vol. 6, no. 1, pp. 53–59, 1996. DOI: 10.3233/VES-1996-6107.

[108] K. S. Hale and K. M. Stanney, "Effects of low stereo acuity on performance, presence and sickness within a virtual environment", *Applied Ergonomics*, vol. 37, no. 3, pp. 329–339, May 2006, ISSN: 00036870. DOI: 10.1016/j.apergo.2005.06.009.

[109] E. J. Rinalducci, "Characteristics of visual fidelity in the virtual environment", *Presence: Teleoperators & Virtual Environments*, vol. 5, no. 3, pp. 330–345, 1996. DOI: 10.1162/pres.1996.5.3.330.

[110] N. A. Webb and M. J. Griffin, "Optokinetic stimuli: Motion sickness, visual acuity, and eye movements", *Aviation, space, and Environmental Medicine*, vol. 73, no. 4, pp. 351–358, 2002, PMID: 11952055.

[111] B. Allen, T. Hanley, B. Rokers, and C. S. Green, "Visual 3D motion acuity predicts discomfort in 3D stereoscopic environments", *Entertainment Computing*, vol. 13, pp. 1–9, Mar. 2016, ISSN: 18759521. DOI: 10.1016/j.entcom.2016.01.001.

[112] A. Graybiel, "Susceptibility to acute motion sickness in blind persons.", *Aerospace medicine*, vol. 41, no. 6, pp. 650–653, 1970, PMID: 5446920.

[113] J. O. Brooks, R. R. Goodenough, M. C. Crisler, N. D. Klein, R. L. Alley, B. L. Koon, W. C. Logan, J. H. Ogle, R. A. Tyrrell, and R. F. Wills, "Simulator sickness during driving simulation studies", *Accident Analysis and Prevention*, vol. 42, no. 3, pp. 788–796, 2010, ISSN: 00014575. DOI: 10.1016/j.aap.2009.04.013.

[114] J. T. Reason, "Motion sickness adaptation: A neural mismatch model", *Journal of the Royal Society of Medicine*, vol. 71, no. 11, pp. 819–829, 1978.

[115] C. M. Oman, "A heuristic mathematical model for the dynamics of sensory conflict and motion sickness hearing in classical musicians", *Acta Oto-Laryngologica*, vol. 94, no. sup392, pp. 4–44, 1982. DOI: 10.3109/00016488209108197.

[116] T. A. Stoffregen and G. E. Riccio, "An Ecological Critique of the Sensory Conflict Theory of Motion Sickness", *Ecological Psychology*, vol. 3, no. 3, pp. 159–194, Sep. 1991, ISSN: 1040-7413. DOI: 10.1207/s15326969eco0303_1.

[117] D. M. Hoffman, A. R. Girshick, K. Akeley, and M. S. Banks, "Vergence–accommodation conflicts hinder visual performance and cause visual fatigue", *Journal of vision*, vol. 8, no. 3, pp. 33–33, 2008. DOI: 10.1167/8.3.33.

[118] M. Lambooij, M. Fortuin, I. Heynderickx, and W. IJsselsteijn, "Visual discomfort and visual fatigue of stereoscopic displays: A review", *Journal of Imaging Science and Technology*, vol. 53, no. 3, pp. 30 201–1, 2009. DOI: 10.2352/J.ImagingSci.Technol.2009.53.3.030201.

[119] T. Shibata, J. Kim, D. M. Hoffman, and M. S. Banks, "The zone of comfort: Predicting visual discomfort with stereo displays", *Journal of vision*, vol. 11, no. 8, pp. 11–11, 2011. DOI: 10.1167/11.8.11.

[120] L. Warwick-Evans, N. Symons, T. Fitch, and L. Burrows, "Evaluating sensory conflict and postural instability. theories of motion sickness", *Brain Research Bulletin*, vol. 47, no. 5, pp. 465–469, Nov. 1998, ISSN: 03619230. DOI: 10.1016/S0361-9230(98)00090-2.

[121] L. Warwick-Evans and S. Beaumont, "An experimental evaluation of sensory conflict versus postural control theories of motion sickness", *Ecological Psychology*, vol. 7, no. 3, pp. 163–179, 1995. DOI: 10.1207/s15326969eco0703-1.

[122] J. N. Templeman, P. S. Denbrook, and L. E. Sibert, "Virtual Locomotion: Walking in Place through Virtual Environments", *Presence: Teleoperators and Virtual Environments*, vol. 8, no. 6, pp. 598–617, Dec. 1999, ISSN: 1054-7460. DOI: 10.1162/105474699566512.

[123] R. P. Darken, W. R. Cockayne, and D. Carmein, "The omni-directional treadmill:a locomotion device for virtual worlds", in *Proceedings of the 10th annual ACM symposium on User interface software and technology - UIST '97*, New York, New York, USA: ACM Press, 1997, pp. 213–221, ISBN: 0897918819. DOI: 10.1145/263407.263550.

[124] Z. Cao, J. Jerald, and R. Kopper, "Visually-Induced Motion Sickness Reduction via Static and Dynamic Rest Frames", in *2018 IEEE Conference on Virtual Reality and 3D User Interfaces (VR)*, IEEE, Mar. 2018, pp. 105–112, ISBN: 978-1-5386-3365-6. DOI: 10.1109/VR.2018.8446210.

[125] A. K. Ng, L. K. Chan, and H. Y. Lau, "A study of cybersickness and sensory conflict theory using a motion-coupled virtual reality system", *Displays*, p. 101 922, 2019. DOI: 10.1016/j.displa.2019.08.004.

[126] W. Bles, J. E. Bos, B. de Graaf, E. Groen, and A. H. Wertheim, "Motion sickness: only one provocative conflict?", *Brain Research Bulletin*, vol. 47, no. 5, pp. 481–487, Nov. 1998, ISSN: 03619230. DOI: 10.1016/S0361-9230(98)00115-4.

[127] J. E. Bos, W. Bles, and E. L. Groen, "A theory on visually induced motion sickness", *Displays*, vol. 29, no. 2, pp. 47–57, Mar. 2008. DOI: 10.1016/j.displa.2007.09.002.

[128] H. Khalid, O. Turan, and J. E. Bos, "Theory of a subjective vertical-horizontal conflict physiological motion sickness model for contemporary ships", *Journal of Marine Science and Technology*, vol. 16, no. 2, pp. 214–225, 2011, ISSN: 09484280. DOI: 10.1007/s00773-010-0113-y.

[129] L. J. Smart Jr, T. A. Stoffregen, and B. G. Bardy, "Visually induced motion sickness predicted by postural instability", *Human factors*, vol. 44, no. 3, pp. 451–465, 2002.

[130] J.-R. Chardonnet, M. A. Mirzaei, and F. Mérienne, "Features of the Postural Sway Signal as Indicators to Estimate and Predict Visually Induced Motion Sickness in Virtual Reality", *International Journal of Human–Computer Interaction*, vol. 33, no. 10, pp. 771–785, Oct. 2017, ISSN: 1044-7318. DOI: 10.1080/10447318.2017.1286767.

[131] O. Merhi, E. Faugloire, M. Flanagan, and T. A. Stoffregen, "Motion sickness, console video games, and head-mounted displays", *Human Factors*, vol. 49, no. 5, pp. 920–934, 2007, PMID: 17915607. DOI: 10.1518/001872007X230262.

[132] T. A. Stoffregen, E. Faugloire, K. Yoshida, M. B. Flanagan, and O. Merhi, "Motion sickness and postural sway in console video games", *Human Factors*, vol. 50, no. 2, pp. 322–331, 2008, PMID: 18516842. DOI: 10.1518/001872008X250755.

[133] B. Keshavarz, A. C. Novak, L. J. Hettinger, T. A. Stoffregen, and J. L. Campos, "Passive restraint reduces visually induced motion sickness in older adults.", *Journal of experimental psychology: applied*, vol. 23, no. 1, p. 85, 2017. DOI: 10.1037/xap0000107.

[134] F. Koslucher, E. Haaland, and T. A. Stoffregen, "Sex differences in visual performance and postural sway precede sex differences in visually induced motion sickness", *Experimental brain research*, vol. 234, no. 1, pp. 313–322, 2016. DOI: 10.1007/s00221-015-4462-y.

[135] J. Munafo, M. Diedrick, and T. A. Stoffregen, "The virtual reality head-mounted display Oculus Rift induces motion sickness and is sexist in its effects", *Experimental Brain Research*, vol. 235, no. 3, pp. 889–901, Mar. 2017, ISSN: 0014-4819. DOI: 10.1007/s00221-016-4846-7.

[136] J. D. Prothero, "The Role of Rest Frames in Vection, Presence and Motion Sickness", Ph.D. dissertation, University of Washington, 1998.

[137] J. D. Prothero and D. E. Parker, "A unified approach to presence and motion sickness", *Virtual and adaptive environments: Applications, implications, and human performance issues*, p. 47, 2003.

[138] J. D. Prothero, M. H. Draper, D. Parker, M. Wells, *et al.*, "The use of an independent visual background to reduce simulator side-effects.", *Aviation, space, and environmental medicine*, vol. 70, no. 3 Pt 1, pp. 277–283, 1999.

[139] D. Whitinghill, B. Ziegler, J. Moore, and T. Case, "Nasum virtualis: A simple technique for reducing simulator sickness in head mounted vr", in *Game Developers Conference. San Francisco*, 2015, p. 74.

[140] J. J. W. Lin, J. J. W. Lin, H. Abi-Rached, and M. Lahav, "Virtual guiding avatar: An effective procedure to reduce simulator sickness in virtual environments", in *Proceedings of the SIGCHI Conference on Human Factors in Computing Systems*, ser. CHI '04, Vienna, Austria: ACM Press, 2004, pp. 719–726, ISBN: 1-58113-702-8. DOI: 10.1145/985692.985783.

[141] S. M. Ebenholtz, "Motion sickness and oculomotor systems in virtual environments", *Presence: Teleoperators & Virtual Environments*, vol. 1, no. 3, pp. 302–305, 1992. DOI: 10.1162/pres.1992.1.3.302.

[142] S. M. Ebenholtz, M. M. Cohen, and B. J. Linder, "The possible role of nystagmus in motion sickness: A hypothesis.", *Aviation, space, and environmental medicine*, vol. 65, no. 11, pp. 1032–1035, 1994, PMID: 7840743.

[143] N. A. Webb and M. J. Griffin, "Eye movement, vection, and motion sickness with foveal and peripheral vision", *Aviation Space and Environmental Medicine*, vol. 74, no. 6, pp. 622–625, 2003, PMID: 12793532, ISSN: 00956562.

[144] S. M. Ebenholtz, *Oculomotor systems and perception*. Cambridge University Press, 2001.

[145] J. T. T. Ji, R. H. Y. So, and R. T. F. Cheung, "Isolating the effects of vection and optokinetic nystagmus on optokinetic rotation-induced motion sickness", *Human Factors*, vol. 51, no. 5, pp. 739–751, 2009, PMID: 20196298. DOI: 10.1177/0018720809349708.

[146] C. M. Oman, "Are evolutionary hypotheses for motion sickness "just-so" stories?", *Journal of Vestibular Research*, vol. 22, no. 2,3, pp. 117–127, 2012, ISSN: 09574271. DOI: 10.3233/VES-2011-0432.

[147] K. Money and B. Cheung, "Another function of the inner ear: Facilitation of the emetic response to poisons.", *Aviation, space, and environmental medicine*, vol. 54, no. 3, p. 208, 1983, PMID: 6847555.

[148] D. G. Watt, L. J. Bouyer, I. T. Nevo, A. V. Smith, and Y. Tiande, "What is motion sickness? a", *Annals of the New York Academy of Sciences*, vol. 656, no. 1, pp. 660–667, 1992, PMID: 1599171. DOI: 10.1111/j.1749-6632.1992.tb25243.x.

[149] D. L. Harm, "Physiology of motion sickness", in *Motion and Space Sickness*, G. H. Crampton, Ed., Florida: CRC Press, 1990, pp. 153–178.

[150] L. Frank, R. S. Kennedy, R. S. Kellogg, and M. E. McCauley, "Simulator sickness: A reaction to a transformed perceptual world. 1. scope of the problem", ESSEX CORP ORLANDO FL, Tech. Rep., 1983.

[151] Ł. Dziuda, M. P. Biernacki, P. M. Baran, and O. E. Truszczyński, "The effects of simulated fog and motion on simulator sickness in a driving simulator and the duration of after-effects", *Applied Ergonomics*, vol. 45, no. 3, pp. 406–412, 2014, ISSN: 0003-6870. DOI: 10.1016/j.apergo.2013.05.003.

[152] W. Chen, A. Plancoulaine, N. Férey, D. Touraine, J. Nelson, and P. Bourdot, "6dof navigation in virtual worlds: Comparison of joystick-based and head-controlled paradigms", in *Proceedings of the 19th ACM Symposium on Virtual Reality Software and Technology*, ser. VRST '13, Singapore: ACM, 2013, pp. 111–114, ISBN: 978-1-4503-2379-6. DOI: 10.1145/2503713.2503754.

[153] A. Alshaer, H. Regenbrecht, and D. O'Hare, "Immersion factors affecting perception and behaviour in a virtual reality power wheelchair simulator", *Applied Ergonomics*, vol. 58, pp. 1–12, 2017, ISSN: 0003-6870. DOI: 10.1016/j.apergo.2016.05.003.

[154] M. Meehan, S. Razzaque, M. C. Whitton, and F. P. Brooks Jr., "Effect of latency on presence in stressful virtual environments", in *Proceedings of the IEEE Virtual Reality 2003*, ser. VR '03, Washington, DC, USA: IEEE Computer Society, 2003, p. 141, ISBN: 0-7695-1882-6. [Online]. Available: http://dl.acm.org/citation.cfm?id=832289.835964.

[155] N. Padmanaban, T. Ruban, V. Sitzmann, A. M. Norcia, and G. Wetzstein, "Towards a Machine-Learning Approach for Sickness Prediction in 360° Stereoscopic Videos", *IEEE Transactions on Visualization and Computer Graphics*, vol. 24, no. 4, pp. 1594–1603, Apr. 2018, ISSN: 1077-2626. DOI: 10.1109/TVCG.2018.2793560.

[156] H. K. Kim, J. Park, Y. Choi, and M. Choe, "Virtual reality sickness questionnaire (VRSQ): Motion sickness measurement index in a virtual reality environment", *Applied Ergonomics*, vol. 69, no. March 2017, pp. 66–73, May 2018, ISSN: 00036870. DOI: 10.1016/j.apergo.2017.12.016.

[157] P. Bimberg, T. Weissker, and A. Kulik, "On the usage of the simulator sickness questionnaire for virtual reality research", in *2020 IEEE Conference on Virtual Reality and 3D User Interfaces Abstracts and Workshops (VRW)*, IEEE, 2020, pp. 464–467. DOI: 10.1109/VRW50115.2020.00098.

[158] J. E. Bos, S. N. MacKinnon, and A. Patterson, "Motion sickness symptoms in a ship motion simulator: Effects of inside, outside, and no view", *Aviation Space and Environmental Medicine*, vol. 76, no. 12, pp. 1111–1118, 2005, ISSN: 00956562.

[159] J. E. Bos, S. C. de Vries, M. L. van Emmerik, and E. L. Groen, "The effect of internal and external fields of view on visually induced motion sickness", *Applied Ergonomics*, vol. 41, no. 4, pp. 516–521, Jul. 2010, ISSN: 00036870. DOI: 10.1016/j.apergo.2009.11.007.

[160] B. Keshavarz and H. Hecht, "Validating an Efficient Method to Quantify Motion Sickness", *Human Factors: The Journal of the Human Factors and Ergonomics Society*, vol. 53, no. 4, pp. 415–426, Aug. 2011, ISSN: 0018-7208. DOI: 10.1177/0018720811403736.

[161] J. F. Golding, "Motion sickness susceptibility questionnaire revised and its relationship to other forms of sickness", *Brain research bulletin*, vol. 47, no. 5, pp. 507–516, 1998. DOI: 10.1016/S0361-9230(98)00091-4.

[162] J. F. Golding, "Predicting individual differences in motion sickness susceptibility by questionnaire", *Personality and Individual Differences*, vol. 41, no. 2, pp. 237–248, Jul. 2006, ISSN: 01918869. DOI: 10.1016/j.paid.2006.01.012.

[163] S. B. Brundage, J. M. Brinton, and A. B. Hancock, "Utility of virtual reality environments to examine physiological reactivity and subjective distress in adults who stutter", *Journal of Fluency Disorders*, vol. 50, pp. 85–95, 2016, ISSN: 0094-730X. DOI: 10.1016/j.jfludis.2016.10.001.

[164] J. L. Higuera-Trujillo, J. L.-T. Maldonado, and C. L. Millán, "Psychological and physiological human responses to simulated and real environments: A comparison between photographs, 360° panoramas, and virtual reality", *Applied Ergonomics*, vol. 65, pp. 398–409, 2017, ISSN: 0003-6870. DOI: 10.1016/j.apergo.2017.05.006.

[165] J. Plouzeau, J.-R. Chardonnet, and F. Merienne, "Using Cybersickness Indicators to Adapt Navigation in Virtual Reality: A Pre-Study", in *2018 IEEE Conference on Virtual Reality and 3D User Interfaces (VR)*, vol. 6, IEEE, Mar. 2018, pp. 661–662, ISBN: 978-1-5386-3365-6. DOI: 10.1109/VR.2018.8446192.

[166] Y. Matsuura and H. Takada, "Evaluation of motion sickness induced by 3d video clips", *Nippon Eiseigaku Zasshi (Japanese Journal of Hygiene)*, vol. 71, no. 1, pp. 2–11, 2016. DOI: 10.1265/jjh.71.2.

[167] S. Wibirama and K. Hamamoto, "Investigation of visually induced motion sickness in dynamic 3D contents based on subjective judgment, heart rate variability, and depth gaze behavior", in *2014 36th Annual International Conference of the IEEE Engineering in Medicine and Biology Society*, IEEE, Aug. 2014, pp. 4803–4806, ISBN: 978-1-4244-7929-0. DOI: 10.1109/EMBC.2014.6944698.

[168] L. Deng and D. Yu, "Deep learning: Methods and applications", *Foundations and trends in signal processing*, vol. 7, no. 3–4, pp. 197–387, 2014. DOI: 10.1561/2000000039.

[169] I. Goodfellow, Y. Bengio, A. Courville, and Y. Bengio, *Deep learning*, 2. MIT press Cambridge, 2016, vol. 1.

[170] S. Khan and T. Yairi, "A review on the application of deep learning in system health management", *Mechanical Systems and Signal Processing*, vol. 107, pp. 241–265, 2018, ISSN: 0888-3270. DOI: 10.1016/j.ymssp.2017.11.024.

[171] O. Faust, Y. Hagiwara, T. J. Hong, O. S. Lih, and U. R. Acharya, "Deep learning for healthcare applications based on physiological signals: A review", *Computer Methods and Programs in Biomedicine*, vol. 161, pp. 1–13, 2018, ISSN: 0169-2607. DOI: 10.1016/j.cmpb.2018.04.005.

[172] C.-T. Lin, S.-F. Tsai, and L.-W. Ko, "EEG-based learning system for online motion sickness level estimation in a dynamic vehicle environment.", *IEEE transactions on neural networks and learning systems*, vol. 24, no. 10, pp. 1689–700, Oct. 2013, ISSN: 2162-2388. DOI: 10.1109/TNNLS.2013.2275003.

[173] R. S. Kennedy, J. Drexler, and R. C. Kennedy, "Research in visually induced motion sickness", *Applied Ergonomics*, vol. 41, no. 4, pp. 494–503, 2010, Special Section - The First International Symposium on Visually Induced Motion Sickness, Fatigue, and Photosensitive Epileptic Seizures (VIMS2007), ISSN: 0003-6870. DOI: 10.1016/j.apergo.2009.11.006.

[174] A. Wertheim, J. Bos, and A. Krul, *Predicting motion induced vomiting from subjective misery (MISC) ratings obtained in 12 experimental studies*. TNO Human Factors, 2001.

[175] C. A. Zanbaka, B. C. Lok, S. V. Babu, A. C. Ulinski, and L. F. Hodges, "Comparison of path visualizations and cognitive measures relative to travel technique in a virtual environment", *IEEE Transactions on Visualization and Computer Graphics*, vol. 11, no. 6, pp. 694–705, 2005. DOI: 10.1109/TVCG.2005.92.

[176] B. Reimer and B. Mehler, "The impact of cognitive workload on physiological arousal in young adult drivers: A field study and simulation validation", *Ergonomics*, vol. 54, no. 10, pp. 932–942, 2011. DOI: 10.1080/00140139.2011.604431.

[177] L. Zhang, J. Wade, D. Bian, J. Fan, A. Swanson, A. Weitlauf, Z. Warren, and N. Sarkar, "Cognitive load measurement in a virtual reality-based driving system for autism intervention", *IEEE transactions on affective computing*, vol. 8, no. 2, pp. 176–189, 2017. DOI: 10.1109/TAFFC.2016.2582490.

[178] S. G. Hart, "Nasa-task load index (nasa-tlx); 20 years later", *Proceedings of the Human Factors and Ergonomics Society Annual Meeting*, vol. 50, no. 9, pp. 904–908, 2006. DOI: 10.1177/154193120605000909.

[179] C. D. Wickens, J. G. Hollands, S. Banbury, and R. Parasuraman, *Engineering psychology and human performance*. Psychology Press, 2015.

[180] W. O. Blackwood, *Human factors in the design of tactical display systems for the individual soldier*. National Academies Press, 1900. [Online]. Available: https://www.nap.edu/read/9107/chapter/9.

[181] F. Paas, J. E. Tuovinen, H. Tabbers, and P. W. Van Gerven, "Cognitive load measurement as a means to advance cognitive load theory", *Educational psychologist*, vol. 38, no. 1, pp. 63–71, 2003.

[182] G. B. Reid and T. E. Nygren, "The subjective workload assessment technique: A scaling procedure for measuring mental workload", in *Advances in psychology*, vol. 52, Elsevier, 1988, pp. 185–218.

[183] K. J. Kilmer, R. Bateman, and D. Malzahn, "Techniques of subjective assessment: A comparison of the swat and modified cooper-harper scales", *Proceedings of the Human Factors Society Annual Meeting*, vol. 32, no. 2, pp. 155–159, 1988.

[184] S. G. Hart and L. E. Staveland, "Development of nasa-tlx (task load index): Results of empirical and theoretical research", in *Human Mental Workload*, ser. Advances in Psychology, P. A. Hancock and N. Meshkati, Eds., vol. 52, North-Holland, 1988, pp. 139–183. DOI: 10.1016/S0166-4115(08)62386-9.

[185] J. Katicic, P. Häfner, and J. Ovtcharova, "Methodology for emotional assessment of product design by customers in virtual reality", *Presence: Teleoperators and Virtual Environments*, vol. 24, no. 1, pp. 62–73, 2015. DOI: 10.1162/PRES_a_00215.

[186] R. P. Harper and G. E. Cooper, "Handling qualities and pilot evaluation", *Journal of Guidance, Control, and Dynamics*, vol. 9, no. 5, pp. 515–529, 1986.

[187] R. Ma and D. B. Kaber, "Presence, workload and performance effects of synthetic environment design factors", *International Journal of Human-Computer Studies*, vol. 64, no. 6, pp. 541–552, 2006. DOI: 10.1016/j.ijhcs.2005.12.003.

[188] A. Cannavò, F. De Pace, F. Salaroglio, and F. Lamberti, "A visual editing tool supporting the production of 3d interactive graphics assets for public exhibitions", *International Journal of Human-Computer Studies*, p. 102 450, 2020. DOI: 10.1016/j.ijhcs.2020.102450.

[189] S. M. Casner and B. F. Gore, "Measuring and evaluating workload: A primer", *NASA Technical Memorandum*, vol. 216395, p. 2010, 2010.

[190] E. Eraslan, G. F. Can, and K. D. Atalay, "Mental workload assessment using a fuzzy multi-criteria method", *Tehnicki vjesnik - Technical Gazette*, vol. 23, no. 3, pp. 667–674, Jun. 2016, ISSN: 13303651. DOI: 10.17559/TV-20140401112509.

[191] S. Miller, "Workload measures", *National Advanced Driving Simulator. Iowa City, United States*, 2001.

[192] L. Gerry, B. Ens, A. Drogemuller, B. Thomas, and M. Billinghurst, "Levity: A virtual reality system that responds to cognitive load", in *Extended Abstracts of the 2018 CHI Conference on Human Factors in Computing Systems*, 2018, pp. 1–6. DOI: 10.1145/3170427.3188479.

[193] A. Hoover, A. Singh, S. Fishel-Brown, and E. Muth, "Real-time detection of workload changes using heart rate variability", *Biomedical Signal Processing and Control*, vol. 7, no. 4, pp. 333–341, 2012, ISSN: 1746-8094. DOI: 10.1016/j.bspc.2011.07.004.

[194] G. Mulder, "The concept and measurement of mental effort", in *Energetics and human information processing*, Springer, 1986, pp. 175–198.

[195] S. Metalis, "Heart period as a useful index of pilot workload in commercial transport aircraft", *The International Journal of Aviation Psychology*, vol. 1, no. 2, pp. 107–116, 1991. DOI: 10.1207/s15327108ijap0102_2.

[196] T. Kosch, M. Hassib, D. Buschek, and A. Schmidt, "Look into my eyes: Using pupil dilation to estimate mental workload for task complexity adaptation", in *Extended Abstracts of the 2018 CHI Conference on Human Factors in Computing Systems*, ser. CHI EA '18, Montreal QC, Canada: ACM, 2018, LBW617:1–LBW617:6, ISBN: 978-1-4503-5621-3. DOI: 10.1145/3170427.3188643.

[197] A. Gevins, M. E. Smith, H. Leong, L. McEvoy, S. Whitfield, R. Du, and G. Rush, "Monitoring working memory load during computer-based tasks with eeg pattern recognition methods", *Human factors*, vol. 40, no. 1, pp. 79–91, 1998.

[198] J. Son and S. Park, "Cognitive workload estimation through lateral driving performance", SAE Technical Paper, Tech. Rep., 2011.

[199] M. Shakouri, L. H. Ikuma, F. Aghazadeh, and I. Nahmens, "Analysis of the sensitivity of heart rate variability and subjective workload measures in a driving simulator: The case of highway work zones", *International Journal of Industrial Ergonomics*, vol. 66, pp. 136–145, Jul. 2018, ISSN: 01698141. DOI: 10.1016/j.ergon.2018.02.015.

[200] O. Janeh, E. Langbehn, F. Steinicke, G. Bruder, A. Gulberti, and M. Poetter-Nerger, "Walking in Virtual Reality: Effects of Manipulated Visual Self-Motion on Walking Biomechanics", *ACM Transactions on Applied Perception*, vol. 14, no. 2, pp. 1–15, Feb. 2017, ISSN: 1544-3558. DOI: 10.1145/3022731.

[201] F. Zhang, S. Chu, R. Pan, N. Ji, and L. Xi, "Double hand-gesture interaction for walk-through in vr environment", in *2017 IEEE/ACIS 16th International Conference on Computer and Information Science (ICIS)*, IEEE, May 2017, pp. 539–544. DOI: 10.1109/ICIS.2017.7960051.

[202] N. G. Vinson, J.-F. Lapointe, A. Parush, and S. Roberts, "Cybersickness induced by desktop virtual reality", in *Proceedings of Graphics Interface 2012*, ser. GI '12, Toronto, Ontario, Canada: Canadian Information Processing Society, 2012, pp. 69–75, ISBN: 978-1-4503-1420-6. [Online]. Available: http://dl.acm.org/citation.cfm?id=2305276.2305288.

[203] I. Milleville-Pennel and C. Charron, "Do mental workload and presence experienced when driving a real car predispose drivers to simulator sickness? An exploratory study", *Accident Analysis and Prevention*, vol. 74, pp. 192–202, 2015, ISSN: 00014575. DOI: 10.1016/j.aap.2014.10.021.

[204] R. Zhou and A. H. Chan, "Using a fuzzy comprehensive evaluation method to determine product usability: A proposed theoretical framework", *Work*, vol. 56, no. 1, pp. 9–19, 2017.

[205] K. P. Yoon and C.-L. Hwang, *Multiple attribute decision making: an introduction*. Sage publications, 1995, vol. 104.

[206] M. Behzadian, S. [Otaghsara], M. Yazdani, and J. Ignatius, "A state-of the-art survey of topsis applications", *Expert Systems with Applications*, vol. 39, no. 17, pp. 13 051–13 069, 2012, ISSN: 0957-4174. DOI: 10.1016/j.eswa.2012.05.056.

[207] Y. Bengio, P. Simard, and P. Frasconi, "Learning long-term dependencies with gradient descent is difficult", *IEEE transactions on neural networks*, vol. 5, no. 2, pp. 157–166, 1994, ISSN: 1045-9227. DOI: 10.1109/72.279181.

[208] N. Srivastava, G. Hinton, A. Krizhevsky, I. Sutskever, and R. Salakhutdinov, "Dropout: A simple way to prevent neural networks from overfitting", *Journal of Machine Learning Research*, vol. 15, no. 56, pp. 1929–1958, 2014. [Online]. Available: http://jmlr.org/papers/v15/srivastava14a.html.

[209] M. Hasan, J. Choi, J. Neumann, A. K. Roy-Chowdhury, and L. S. Davis, "Learning temporal regularity in video sequences", in *2016 IEEE Conference on Computer Vision and Pattern Recognition (CVPR)*, Jun. 2016, pp. 733–742. DOI: 10.1109/CVPR.2016.86.

[210] S. D. Young, B. D. Adelstein, and S. R. Ellis, "Demand characteristics in assessing motion sickness in a virtual environment: Or does taking a motion sickness questionnaire make you sick?", *IEEE Transactions on Visualization and Computer Graphics*, vol. 13, no. 3, pp. 422–428, May 2007, ISSN: 1077-2626. DOI: 10.1109/TVCG.2007.1041.

[211] Z. Yang, Y. Liu, and C. Li, "Interpolation of missing wind data based on anfis", *Renewable Energy*, vol. 36, no. 3, pp. 993–998, 2011. DOI: 10.1016/j.renene.2010.08.033.

[212] Y.-S. Chen, C.-H. Cheng, C.-L. Chiu, and S.-T. Huang, "A study of anfis-based multi-factor time series models for forecasting stock index", *Applied Intelligence*, vol. 45, no. 2, pp. 277–292, 2016. DOI: 10.1007/s10489-016-0760-8.

[213] K. Benmouiza and A. Cheknane, "Clustered ANFIS network using fuzzy c-means, subtractive clustering, and grid partitioning for hourly solar radiation forecasting", *Theoretical and Applied Climatology*, vol. 137, no. 1-2, pp. 31–43, 2019, ISSN: 14344483. DOI: 10.1007/s00704-018-2576-4.

[214] J.-S. R. Jang and C.-T. Sun, *Neuro-Fuzzy and Soft Computing: A Computational Approach to Learning and Machine Intelligence*. USA: Prentice-Hall, Inc., 1996, ISBN: 0132610663.

[215] J.-S. Jang, "Anfis: Adaptive-network-based fuzzy inference system", *IEEE transactions on systems, man, and cybernetics*, vol. 23, no. 3, pp. 665–685, 1993. DOI: 10.1109/21.256541.

[216] M. K. Goyal, B. Bharti, J. Quilty, J. Adamowski, and A. Pandey, "Modeling of daily pan evaporation in sub tropical climates using ann, ls-svr, fuzzy logic, and anfis", *Expert systems with applications*, vol. 41, no. 11, pp. 5267–5276, 2014. DOI: 10.1016/j.eswa.2014.02.047.

[217] P. Srisaeng, G. S. Baxter, and G. Wild, "An adaptive neuro-fuzzy inference system for forecasting australia's domestic low cost carrier passenger demand", *Aviation*, vol. 19, no. 3, pp. 150–163, 2015. DOI: 10.3846/16487788.2015.1104806.

[218] D. Wu, C. G. Courtney, B. J. Lance, S. S. Narayanan, M. E. Dawson, K. S. Oie, and T. D. Parsons, "Optimal arousal identification and classification for affective computing using physiological signals: Virtual reality stroop task", *IEEE Transactions on Affective Computing*, vol. 1, no. 2, pp. 109–118, Jul. 2010, ISSN: 1949-3045. DOI: 10.1109/T-AFFC.2010.12.

[219] D. Ota, B. Loftin, T. Saito, R. Lea, and J. Keller, "Virtual reality in surgical education", *Computers in Biology and Medicine*, vol. 25, no. 2, pp. 127–137, 1995, Virtual Reality for Medicine, ISSN: 0010-4825. DOI: 10.1016/0010-4825(94)00009-F.

[220] G. Cueva-Fernandez, J. P. Espada, V. García-Díaz, R. G. Crespo, and N. Garcia-Fernandez, "Fuzzy system to adapt web voice interfaces dynamically in a vehicle sensor tracking application definition", *Soft Computing*, vol. 20, no. 8, pp. 3321–3334, 2016. DOI: 10.1007/s00500-015-1709-2.

[221] H. O. Nyongesa, T. Shicheng, S. Maleki-Dizaji, S.-T. Huang, and J. Siddiqi, "Adaptive web interface design using fuzzy logic", in *Proceedings IEEE/WIC International Conference on Web Intelligence (WI 2003)*, IEEE, 2003, pp. 671–674. DOI: 10.1109/WI.2003.1241293.

[222] A. Hamam, M. Eid, A. El Saddik, and N. D. Georganas, "A fuzzy logic system for evaluating quality of experience of haptic-based applications", in *International Conference on Human Haptic Sensing and Touch Enabled Computer Applications*, Springer, 2008, pp. 129–138. DOI: 10.1007/978-3-540-69057-3_14.

[223] *Fuzzy logic toolbox: User's guide (r2020a)*, The MathWorks, Inc., Natick, Massachusetts, United State, 2020. [Online]. Available: https://www.mathworks.com/help/fuzzy/.

[224] T. Takagi and M. Sugeno, "Derivation of fuzzy control rules from human operator's control actions", *IFAC Proceedings Volumes*, vol. 16, no. 13, pp. 55–60, 1983. DOI: 10.1016/S1474-6670(17)62005-6.

[225] M. Şahin and R. Erol, "A Comparative Study of Neural Networks and ANFIS for Forecasting Attendance Rate of Soccer Games", *Mathematical and Computational Applications*, vol. 22, no. 4, p. 43, 2017. DOI: 10.3390/mca22040043.

[226] R. Taylor, "Interpretation of the Correlation Coefficient: A Basic Review", *Journal of Diagnostic Medical Sonography*, vol. 6, no. 1, pp. 35–39, Jan. 1990, ISSN: 8756-4793. DOI: 10.1177/875647939000600106.

[227] R. R. Picard and R. D. Cook, "Cross-validation of regression models", *Journal of the American Statistical Association*, vol. 79, no. 387, pp. 575–583, 1984. DOI: 10.1080/01621459.1984.10478083.

[228] Y. Bengio and Y. Grandvalet, "No unbiased estimator of the variance of k-fold cross-validation", *Journal of machine learning research*, vol. 5, no. Sep, pp. 1089–1105, 2004.

[229] J. Katicic, P. Häfner, and J. Ovtcharova, "Methodology for Emotional Assessment of Product Design by Customers in Virtual Reality", *Presence: Teleoperators and Virtual Environments*, vol. 24, no. 1, pp. 62–73, Feb. 2015, ISSN: 1054-7460. DOI: 10.1162/PRES_a_00215.

[230] B. Khoshnevisan, S. Rafiee, M. Omid, and H. Mousazadeh, "Development of an intelligent system based on ANFIS for predicting wheat grain yield on the basis of energy inputs", *Information Processing in Agriculture*, vol. 1, no. 1, pp. 14–22, 2014, ISSN: 22143173. DOI: 10.1016/j.inpa.2014.04.001.

[231] H. L. Tubbs-Cooley, C. A. Mara, A. C. Carle, and A. P. Gurses, "The nasa task load index as a measure of overall workload among neonatal, paediatric and adult intensive care nurses", *Intensive and Critical Care Nursing*, vol. 46, pp. 64–69, 2018, ISSN: 0964-3397. DOI: 10.1016/j.iccn.2018.01.004.

[232] D. C. Kamaraj, B. E. Dicianno, H. P. Mahajan, A. M. Buhari, and R. A. Cooper, "Stability and workload of the virtual reality–based simulator-2", *Archives of physical medicine and rehabilitation*, vol. 97, no. 7, pp. 1085–1092, 2016.

[233] C.-S. Yu, "A gp-ahp method for solving group decision-making fuzzy ahp problems", *Computers & Operations Research*, vol. 29, no. 14, pp. 1969–2001, 2002. DOI: 10.1016/S0305-0548(01)00068-5.

[234] H. Singh, M. M. Gupta, T. Meitzler, Z.-G. Hou, K. K. Garg, A. M. Solo, and L. A. Zadeh, "Real-life applications of fuzzy logic", 2013. DOI: 10.1155/2013/581879.

[235] A. T. Gumus, "Evaluation of hazardous waste transportation firms by using a two step fuzzy-AHP and TOPSIS methodology", *Expert Systems with Applications*, vol. 36, no. 2, pp. 4067–4074, Mar. 2009, ISSN: 09574174. DOI: 10.1016/j.eswa.2008.03.013.

[236] M. Mouzé-Amady, E. Raufaste, H. Prade, and J.-P. Meyer, "Fuzzy-tlx: Using fuzzy integrals for evaluating human mental workload with nasa-task load index in laboratory and field studies", *Ergonomics*, vol. 56, no. 5, pp. 752–763, 2013. DOI: 10.1080/00140139.2013.776702.

[237] D.-Y. Chang, "Applications of the extent analysis method on fuzzy AHP", *European Journal of Operational Research*, vol. 95, no. 3, pp. 649–655, Dec. 1996, ISSN: 03772217. DOI: 10.1016/0377-2217(95)00300-2.

[238] D. Harris, M. Wilson, and S. Vine, "Development and validation of a simulation workload measure: the simulation task load index (SIM-TLX)", *Virtual Reality*, pp. 1–10, Dec. 2019, ISSN: 1359-4338. DOI: 10.1007/s10055-019-00422-9.

[239] M. R. Wilson, J. M. Poolton, N. Malhotra, K. Ngo, E. Bright, and R. S. Masters, "Development and validation of a surgical workload measure: The surgery task load index (surg-tlx)", *World journal of surgery*, vol. 35, no. 9, p. 1961, 2011. DOI: 10.1007/s00268-011-1141-4.

[240] V. Novák and I. Perfilieva, "Evaluating linguistic expressions and functional fuzzy theories in fuzzy logic", in *Computing with Words in Information/Intelligent Systems 1*, Springer, 1999, pp. 383–406. DOI: 10.1007/978-3-7908-1873-4_17.

[241] Y. Hong, X. Zeng, P. Bruniaux, Y. Chen, and X. Zhang, "Development of a new knowledge-based fabric recommendation system by integrating the collaborative design process and multi-criteria decision support", *Textile Research Journal*, vol. 88, no. 23, pp. 2682–2698, Dec. 2018, ISSN: 0040-5175. DOI: 10.1177/0040517517729383.

[242] R. Saaty, "The analytic hierarchy process—what it is and how it is used", *Mathematical Modelling*, vol. 9, no. 3, pp. 161–176, 1987, ISSN: 0270-0255. DOI: 10.1016/0270-0255(87)90473-8.

[243] C.-L. Hwang and K. Yoon, "Methods for multiple attribute decision making", in *Multiple attribute decision making: methods and applications a state-of-the-art survey*, Springer, 1981, pp. 58–191. DOI: 10.1007/978-3-642-48318-9_3.

[244] V. Sevinc and M. I. Berkman, "Psychometric evaluation of Simulator Sickness Questionnaire and its variants as a measure of cybersickness in consumer virtual environments", *Applied Ergonomics*, vol. 82, p. 102 958, Jan. 2020, ISSN: 00036870. DOI: 10.1016/j.apergo.2019.102958.

[245] T. D. Parsons, L. Cosand, C. Courtney, A. Iyer, and A. A. Rizzo, "Neurocognitive workload assessment using the virtual reality cognitive performance assessment test", in *Engineering Psychology and Cognitive Ergonomics*, D. Harris, Ed., Berlin, Heidelberg: Springer Berlin Heidelberg, 2009, pp. 243–252, ISBN: 978-3-642-02728-4.

[246] A. Galecki and T. Burzykowski, *Linear Mixed Effects Models Using R. : A Step-by-Step Approach*. Mar. 2013. DOI: 10.1007/978-1-4614-3900-4.

[247] R Core Team, *R: A language and environment for statistical computing*, R Foundation for Statistical Computing, Vienna, Austria, 2020. [Online]. Available: https://www.R-project.org/.

[248] D. K. Lee, "Alternatives to p value: Confidence interval and effect size", *Korean journal of anesthesiology*, vol. 69, no. 6, p. 555, 2016. DOI: 10.4097/kjae.2016.69.6.555.

[249] G. Kesteven, "The coefficient of variation", *Nature*, vol. 158, no. 4015, pp. 520–521, 1946. DOI: 10.1038/158520c0.

[250] P. Lovie, "Coefficient of variation", *Encyclopedia of statistics in behavioral science*, 2005. DOI: 10.1002/0470013192.bsa107.

[251] J. M. Riley and D. B. Kaber, "The effects of visual display type and navigational aid on performance, presence, and workload in virtual reality training of telerover navigation", *Proceedings of the Human Factors and Ergonomics Society Annual Meeting*, vol. 43, no. 22, pp. 1251–1255, 1999. DOI: 10.1177/154193129904302218.

[252] T. Porssut and J.-R. Chardonnet, "Asymetric telecollaboration in virtual reality", in *2017 IEEE Virtual Reality (VR)*, IEEE, 2017, pp. 289–290, ISBN: 978-1-5090-6647-6. DOI: 10.1109/VR.2017.7892290.

[253] J. D. C. Freitas, "KAVE - Kinect Cave Design, tools and comparative analysis with other VR technologies", Ph.D. dissertation, Universidade da Madeira, 2018.

[254] J. Harrison, K. Izzetoglu, H. Ayaz, B. Willems, S. Hah, U. Ahlstrom, H. Woo, P. A. Shewokis, S. C. Bunce, and B. Onaral, "Cognitive workload and learning assessment during the implementation of a next-generation air traffic control technology using functional near-infrared spectroscopy", *IEEE Transactions on Human-Machine Systems*, vol. 44, no. 4, pp. 429–440, Aug. 2014. DOI: 10.1109/THMS.2014.2319822.

[255] R. McKendrick, B. Feest, A. Harwood, and B. Falcone, "Theories and methods for labeling cognitive workload: Classification and transfer learning", *Frontiers in Human Neuroscience*, vol. 13, p. 295, 2019, ISSN: 1662-5161. DOI: 10.3389/fnhum.2019.00295.

[256] A. Gevins and M. E. Smith, "Neurophysiological measures of cognitive workload during human-computer interaction", *Theoretical Issues in Ergonomics Science*, vol. 4, no. 1-2, pp. 113–131, 2003.

[257] C. J. Patten, A. Kircher, J. Östlund, L. Nilsson, and O. Svenson, "Driver experience and cognitive workload in different traffic environments", *Accident Analysis & Prevention*, vol. 38, no. 5, pp. 887–894, 2006, ISSN: 0001-4575. DOI: 10.1016/j.aap.2006.02.014.

[258] M. Sterman and C. Mann, "Concepts and applications of eeg analysis in aviation performance evaluation", *Biological psychology*, vol. 40, no. 1-2, pp. 115–130, 1995.

[259] B. H. Kantowitz and P. A. Casper, "Human workload in aviation", in *Human Error in Aviation*, Routledge, 2017, pp. 123–153.

[260] T. A. Galyean, "Guided navigation of virtual environments", in *Proceedings of the 1995 symposium on Interactive 3D graphics - SI3D '95*, New York, New York, USA: ACM Press, 1995, 103–ff. ISBN: 0897917367. DOI: 10.1145/199404.199421.

[261] R. Tiwari, R. Tiwari, A. Shukla, and R. Kala, *Intelligent Planning for Mobile Robotics: Algorithmic Approaches*, 1st. Hershey, PA, USA: IGI Global, 2012.

[262] D. Gonzalez Bautista, "Functional architecture for automated vehicles trajectory planning in complex environments", Theses, PSL Research University, Apr. 2017. [Online]. Available: https://pastel.archives-ouvertes.fr/tel-01568505.

[263] L. Rebenitsch and C. Owen, "Review on cybersickness in applications and visual displays", *Virtual Reality*, vol. 20, no. 2, pp. 101–125, 2016. DOI: 10.1007/s10055-016-0285-9.

[264] D. Bowman, D. Koller, and L. Hodges, "Travel in immersive virtual environments: an evaluation of viewpoint motion control techniques", in *Proceedings of IEEE 1997 Annual International Symposium on Virtual Reality*, IEEE Comput. Soc. Press, 1997, pp. 45–52, ISBN: 0-8186-7843-7. DOI: 10.1109/VRAIS.1997.583043.

[265] S. Tregillus, M. Al Zayer, and E. Folmer, "Handsfree omnidirectional vr navigation using head tilt", in *Proceedings of the 2017 CHI Conference on Human Factors in Computing Systems*, ser. CHI '17, Denver, Colorado, USA: ACM, 2017, pp. 4063–4068, ISBN: 978-1-4503-4655-9. DOI: 10.1145/3025453.3025521.

[266] G. Llorach, A. Evans, and J. Blat, "Simulator sickness and presence using hmds: Comparing use of a game controller and a position estimation system", in *Proceedings of the 20th ACM Symposium on Virtual Reality Software and Technology*, ser. VRST '14, Edinburgh, Scotland: ACM, 2014, pp. 137–140, ISBN: 978-1-4503-3253-8. DOI: 10.1145/2671015.2671120.

[267] J. Eriksson and L. Svensson, "Tuning for Ride Quality in Autonomous Vehicle Application to Linear Quadratic Path Planning Algorithm", Ph.D. dissertation, Uppsala University, 2015. [Online]. Available: http://www.teknat.uu.se/student.

[268] R. H. Y. So, "The search for a cybersickness dose value", in *Proceedings of HCI International (the 8th International Conference on Human-Computer Interaction) on Human-Computer Interaction: Ergonomics and User Interfaces-Volume I - Volume I*, Hillsdale, NJ,USA: L. Erlbaum Associates Inc., 1999, pp. 152–156, ISBN: 0-8058-3391-9.

[269] P. Crossland and K. Rich, "Validating a model of the effects of ship motion on postural stability", in *International Conference of Environmental Ergonomics*, vol. 77, Oct. 1998, pp. 385–388.

[270] A. S. Kilinç and T. Baybura, "Determination of minimum horizontal curve radius used in the design of transportation structures, depending on the limit value of comfort criterion lateral jerk", *TS06G-Engineering Surveying, Machine Control and Guidance*, May 2012.

[271] J. Förstberg, "Ride Comfort and Motion Sickness in Tilting Trains", Ph.D. dissertation, KTH Royal Institute of Technology, 2000.

[272] "Mechanical vibration and shock- evaluation of human exposure to whole-body vibration- part 1- general requirements", International Organization for Standardization, Geneva, CH, Standard, 1997.

[273] G. Guennebaud, B. Jacob, *et al.*, *Eigen v3*, 2010. [Online]. Available: http://eigen.tuxfamily.org.

[274] S. G. Hart, "Nasa-task load index (nasa-tlx); 20 years later", *Proceedings of the Human Factors and Ergonomics Society Annual Meeting*, vol. 50, no. 9, pp. 904–908, 2006. DOI: 10.1177/154193120605000909.

[275] A. Tamura, T. Iwamoto, H. Ozaki, M. Kimura, Y. Tsujimoto, and Y. Wada, "Wrist-Worn Electrodermal Activity as a Novel Neurophysiological Biomarker of Autonomic Symptoms in Spatial Disorientation", *Frontiers in Neurology*, vol. 9, no. December, pp. 1–11, Dec. 2018, ISSN: 1664-2295. DOI: 10.3389/fneur.2018.01056.

[276] C. Su, "Chapter 4: Utilization of orthogonal arrays", in *Quality Engineering: Off-Line Methods and Applications*, Florida: CRC Press, USA, 2013, pp. 57–77. DOI: 10.1201/b13909.

[277] G. Clément, O. Deguine, M. Bourg, and A. P.-L. Traon, "Effects of vestibular training on motion sickness, nystagmus, and subjective vertical", *Journal of Vestibular Research*, vol. 17, no. 5, 6, pp. 227–237, 2007.

[278] A. Kemeny, P. George, F. Mérienne, and F. Colombet, "New vr navigation techniques to reduce cybersickness", *Electronic Imaging*, vol. 2017, no. 3, pp. 48–53, 2017, ISSN: 2470-1173. DOI: 10.2352/ISSN.2470-1173.2017.3.ERVR-097.

[279] D. Makowski, T. Pham, Z. J. Lau, J. C. Brammer, F. Lespinasse, H. Pham, C. Schölzel, and A. S H Chen, *Neurokit2: A python toolbox for neurophysiological signal processing*, 2020. DOI: 10.5281/ZENODO.3597887. [Online]. Available: https://github.com/neuropsychology/NeuroKit.

[280] D. Frey, *16.881 robust system design*, License: Creative Commons BY-NC-SA., Massachusetts Institute of Technology: MIT OpenCourseWare, 1998. [Online]. Available: https://ocw.mit.edu.

[281] D. Sidobre and K. Desormeaux, "Smooth cubic polynomial trajectories for human-robot interactions", *Journal of Intelligent & Robotic Systems*, vol. 95, no. 3, pp. 851–869, 2019. DOI: 10.1007/s10846-018-0936-z.

[282] M. Cordeil, T. Dwyer, K. Klein, B. Laha, K. Marriott, and B. H. Thomas, "Immersive collaborative analysis of network connectivity: Cave-style or head-mounted display?", *IEEE transactions on visualization and computer graphics*, vol. 23, no. 1, pp. 441–450, 2016. DOI: 10.1109/TVCG.2016.2599107.

[283] Y. Wang, J.-R. Chardonnet, and F. Merienne, "VR Sickness Prediction for Navigation in Immersive Virtual Environments using a Deep Long Short Term Memory Model", in *2019 IEEE Conference on Virtual Reality and 3D User Interfaces (VR)*, Osaka, Japan: IEEE, Mar. 2019, pp. 1874–1881, ISBN: 978-1-7281-1377-7. DOI: 10.1109/VR.2019.8798213.

[284] E. Paschalidis, C. F. Choudhury, and S. Hess, "Combining driving simulator and physiological sensor data in a latent variable model to incorporate the effect of stress in car-following behaviour", *Analytic Methods in Accident Research*, vol. 22, p. 100 089, 2019, ISSN: 2213-6657. DOI: 10.1016/j.amar.2019.02.001.

[285] T. Magaki and M. Vallance, "Developing an accessible evaluation method of vr cybersickness", in *2019 IEEE Conference on Virtual Reality and 3D User Interfaces (VR)*, Mar. 2019, pp. 1072–1073. DOI: 10.1109/VR.2019.8797748.

[286] S. A. E. Nooij, P. Pretto, D. Oberfeld, H. Hecht, and H. H. Bülthoff, "Vection is the main contributor to motion sickness induced by visual yaw rotation: Implications for conflict and eye movement theories", *PLOS ONE*, vol. 12, no. 4, pp. 1–19, Apr. 2017. DOI: 10.1371/journal.pone.0175305.

[287] J. Akyeampong, S. Udoka, G. Caruso, and M. Bordegoni, "Evaluation of hydraulic excavator human–machine interface concepts using nasa tlx", *International Journal of Industrial Ergonomics*, vol. 44, no. 3, pp. 374–382, 2014, ISSN: 0169-8141. DOI: 10.1016/j.ergon.2013.12.002.

[288] J. Gao and K. Chen, "Frequency-Domain Simulation and Analysis of Vehicle Ride Comfort based on Virtual Proving Ground", *International Journal of Intelligent Engineering and Systems*, vol. 4, no. 3, pp. 1–8, Sep. 2011, ISSN: 21853118. DOI: 10.22266/ijies2011.0930.01.

[289] R. H. Y. So, W. T. Lo, and A. T. K. Ho, "Effects of navigation speed on motion sickness caused by an immersive virtual environment", *Human Factors*, vol. 43, no. 3, pp. 452–461, 2001, PMID: 11866200. DOI: 10.1518/001872001775898223.

[290] P. Bockelman and D. Lingum, "Factors of cybersickness", in *International Conference on Human-Computer Interaction*, Springer, 2017, pp. 3–8.

[291] S. A. H. Aqajari, E. K. Naeini, M. A. Mehrabadi, S. Labbaf, A. M. Rahmani, and N. Dutt, "GSR Analysis for Stress: Development and Validation of an Open Source Tool for Noisy Naturalistic GSR Data", no. 1, May 2020. arXiv: 2005.01834. [Online]. Available: http://arxiv.org/abs/2005.01834.

[292] L. Wang, *PID control system design and automatic tuning using MATLAB/Simulink*. John Wiley & Sons, 2020.

[293] S. Kiranyaz, O. Avci, O. Abdeljaber, T. Ince, M. Gabbouj, and D. J. Inman, "1D convolutional neural networks and applications: A survey", *Mechanical Systems and Signal Processing*, vol. 151, p. 107 398, Apr. 2021, ISSN: 08883270. DOI: 10.1016/j.ymssp.2020.107398. arXiv: 1905.03554.

[294] M. Benedek and C. Kaernbach, "A continuous measure of phasic electrodermal activity", *Journal of neuroscience methods*, vol. 190, no. 1, pp. 80–91, 2010. DOI: 10.1016/j.jneumeth.2010.04.028.

[295] A. Steed, F. R. Ortega, A. S. Williams, E. Kruijff, W. Stuerzlinger, A. U. Batmaz, A. S. Won, E. S. Rosenberg, A. L. Simeone, and A. Hayes, "Evaluating immersive experiences during covid-19 and beyond", *Interactions*, vol. 27, no. 4, pp. 62–67, 2020. DOI: 10.1145/3406098.

[296] T. Akiba, S. Sano, T. Yanase, T. Ohta, and M. Koyama, "Optuna: A next-generation hyperparameter optimization framework", in *Proceedings of the 25th ACM SIGKDD international conference on knowledge discovery & data mining*, Jul. 2019, pp. 2623–2631. DOI: 10.1145/3292500.3330701.

[297] A. S. Fernandes and S. K. Feiner, "Combating vr sickness through subtle dynamic field-of-view modification", in *2016 IEEE symposium on 3D user interfaces (3DUI)*, IEEE, 2016, pp. 201–210. DOI: 10.1109/3DUI.2016.7460053.

[298] R. Lou and J.-R. Chardonnet, "Reducing cybersickness by geometry deformation", in *2019 IEEE Conference on Virtual Reality and 3D User Interfaces (VR)*, IEEE, 2019, pp. 1058–1059. DOI: 10.1109/VR.2019.8798164.

[299] R. Islam, S. Ang, and J. Quarles, "Cybersense: A closed-loop framework to detect cybersickness severity and adaptively apply reduction techniques", in *2021 IEEE Conference on Virtual Reality and 3D User Interfaces Abstracts and Workshops (VRW)*, IEEE, 2021, pp. 148–155. DOI: 10.1109/VRW52623.2021.00035.

Appendix A

Questionnaires

A.1 Fuzzy comparison questionnaire

A.1.1 Questionnaire design

- Name:
- The Nasa Task Load Index (NASA-TLX) is a widely used, subjective, multidimensional assessment tool that rates perceived workload in order to assess a task, system, or team's effectiveness or other aspects of performance; more precisely: mental demand, physical demand, temporal demand, performance, effort, frustration.
- In order to create individual weighting of these sub-scales, please fill the following table (see Table A.1) using the pre-defined language expressions considering: which one do you think is more important during the task you have just performed?
- Language expressions: equally important (EI), weakly more important (WI), strongly more important (SI), very strongly more important (VI), absolutely important (AI).

A.1.2 Example of a filled questionnaire

See Table A.2.

Table A.1: Fuzzy comparison table to be filled with the linguistic expressions (MD: mental demand; PD: physical demand; TD: temporal demand; P: performance; F: frustration)

	MD	PD	TD	P	E	F
MD	EI					
PD		EI				
TD			EI			
P				EI		
E					EI	
F						EI

Table A.2: One filled questionnaire from the experiment (MD: mental demand; PD: physical demand; TD: temporal demand; P: performance; F: frustration); the cells with "-" are automatically filled during the data analysis as it has a reciprocal relationship with the item from the other side of the diagonal

	MD	PD	TD	P	E	F
MD	EI	-	WI	WI	WI	EI
PD	WI	EI	WI	-	-	SI
TD	-	-	EI	-	-	WI
P	-	SI	SI	EI	EI	-
E	-	WI	SI	-	EI	SI
F	-	-	-	WI	-	EI

Appendix B

Résumé substantiel en langue française

B.1 Introduction

La réalité virtuelle (RV) nécessite qu'un utilisateur soit immergé dans un environnement synthétisé par ordinateur pour effectuer des tâches (Merienne 2016). Par conséquent, la RV est centrée sur l'utilisateur, et toutes les applications créées doivent pleinement intégrer l'utilisateur pour améliorer l'acceptation de la RV. Selon un ensemble minimal d'évaluations, la capacité de prédire la susceptibilité humaine au cybermalaise est un travail prometteur pour développer des paramètres personnalisés pour les utilisateurs de réalité virtuelle, réduisant ou évitant ainsi les effets secondaires pendant et après l'expérience d'immersion. Depuis longtemps, la communauté scientifique recherche des solutions pour réduire le cybermalaise et offrir aux utilisateurs de réalité virtuelle une meilleure expérience. Les utilisateurs souffrent de cybermalaise lorsqu'ils sont exposés à des tâches de navigation dominées par la locomotion. Bien que de nombreuses techniques aient été proposées pour atténuer le cybermalaise dans de telles applications de navigation, peu de travaux ont impliqué des facteurs individuels et une boucle de rétroaction physiologique. De nombreux articles proposent de nouvelles techniques pour réduire le cybermalaise mais manquent d'explications substantielles quant à leur efficacité. L'insuffisance de support théorique est un problème. Nous pensons que toute approche pour traiter les effets secondaires de la réalité virtuelle doit commencer par la raison de leur apparition. De plus, la gravité et la susceptibilité au cybermalaise varient généralement selon les utilisateurs, ce qui entraîne des difficultés dans leurs mesures.

B.1.1 Objectifs

Notre premier objectif était d'évaluer les états de l'utilisateur, y compris le niveau de mal-être et la charge de travail cognitive, lors de la navigation dans des environnements de RV. Par conséquent, nous devions d'abord synthétiser le mécanisme du cybermalaise sur la base des études existantes et rapporter leurs relations. Sur la base de ces théories, nous pourrions concevoir de nouvelles stratégies de navigation et comparer leurs performances. Grâce à l'analyse de la littérature, notre attente était d'améliorer les méthodes d'évaluation actuelles concernant la précision de la mesure et l'implication des facteurs humains.

Le deuxième objectif portait sur la proposition de techniques adaptatives de navigation virtuelle en menant plusieurs études expérimentales. Sur la base d'une étude exhaustive sur l'effet des facteurs humains, nous avons proposé un "protecteur" de vitesse pour limiter le profil de mouvement. De plus, nous avons étudié la possibilité d'impliquer les différences individuelles pour adapter la navigation. Les résultats de l'évaluation ont démontré que les techniques adaptatives pouvaient réduire le cybermalaise des utilisateurs dans les environnements virtuels où la navigation est prépondérante.

B.1.2 Contenu de la thèse

La Figure B.1 décrit la structure de la thèse et la relation entre chaque chapitre. Le contenu de la recherche s'en tient à la navigation en réalité virtuelle en améliorant l'expérience de navigation. Nous avons conçu différentes techniques de navigation en nous concentrant principalement sur le cybermalaise ainsi que sur la cognition. Ci-dessous, nous résumons le contenu des autres chapitres (à l'exclusion du chapitre en cours) :

Dans le chapitre 2, nous effectuons une revue de littérature sur la navigation et l'expérience utilisateur. Nous étudions les différences individuelles dans la tolérance au cybermalaise et la raison de son apparition. Les effets de facteurs individuels tels que le sexe, l'âge, la stabilité posturale, l'origine ethnique et les influences génétiques, l'expérience de jeu, la personnalité, l'acuité visuelle sont analysés. Ce chapitre résume également les explications du cybermalaise basées sur plusieurs théories et met en évidence les corrélations et les différences de notre point de vue. Sur la base de ces théories, nous avons proposé des recommandations pour des travaux futurs sur les interfaces d'interaction 3D, la réduction ou l'évitement du cybermalaise et d'autres problèmes liés à l'expérience utilisateur. De plus,

nous étudions dans ce chapitre des approches pour mesurer la charge de travail cognitive.

Dans le chapitre 3, nous définissons plus en détail les objectifs de la thèse. En outre, nous exposons les questions de recherche associées.

Dans le chapitre 4, nous proposons nos solutions pour mesurer le cybermalaise et la charge de travail cognitive. Pour mesurer le cybermalaise, nous entraînons un modèle LSTM pour chaque participant en utilisant un signal postural à l'état normal capturé avant immersion. Si le signal de balancement postural après immersion est suffisamment différent du signal avant immersion, cela suggère qu'il existe un niveau de cybermalaise élevé. Pour prédire la susceptibilité au cybermalaise en fonction de la différence individuelle, nous introduisons en outre un modèle de logique floue qui peut analyser les caractéristiques humaines liées au cybermalaise. Enfin, pour améliorer la qualité de mesure de la charge cognitive, nous proposons une nouvelle méthode d'analyse du NASA-TLX basée sur TOPSIS.

Dans le chapitre 5, nous présentons quatre techniques de navigation différentes pour améliorer l'expérience de navigation. L'idée est d'adapter les paramètres de navigation tels que les facteurs humains, la dynamique du mouvement (trajectoire, vitesse ou accélération). Dans un premier temps, nous proposons une navigation semi-automatique pour lisser la trajectoire de navigation lors de la navigation. Deuxièmement, connaissant l'importance du profil de vitesse de navigation, nous concevons un protecteur de vitesse pour minimiser les à-coups lorsque l'utilisateur navigue dans des environnements virtuels tout en garantissant une faible charge de travail cognitive. De plus, nous développons une navigation adaptative basée sur la susceptibilité des utilisateurs au cybermalaise calculée à partir du modèle de logique floue présenté dans chapter 4, et nous concevons également une stratégie en ligne adaptative pour adapter la vitesse de navigation basée sur la théorie du contrôle PID.

Dans le chapitre 6, nous résumons brièvement la thèse et proposons plusieurs perspectives liées à notre travail pour des recherches ultérieures.

B.2 État de l'art

La particularité de la RV est de permettre à un utilisateur d'être immergé dans un environnement virtuel (EV) et d'interagir avec lui (Sherman and Craig 2003), ce qui signifie des allers-retours entre l'utilisateur et l'EV. Actuellement, la recherche en réalité virtuelle se concentre sur de nombreux sous-domaines liés à l'interaction homme-machine (IHM), par exemple, des dispositifs d'affichage plus

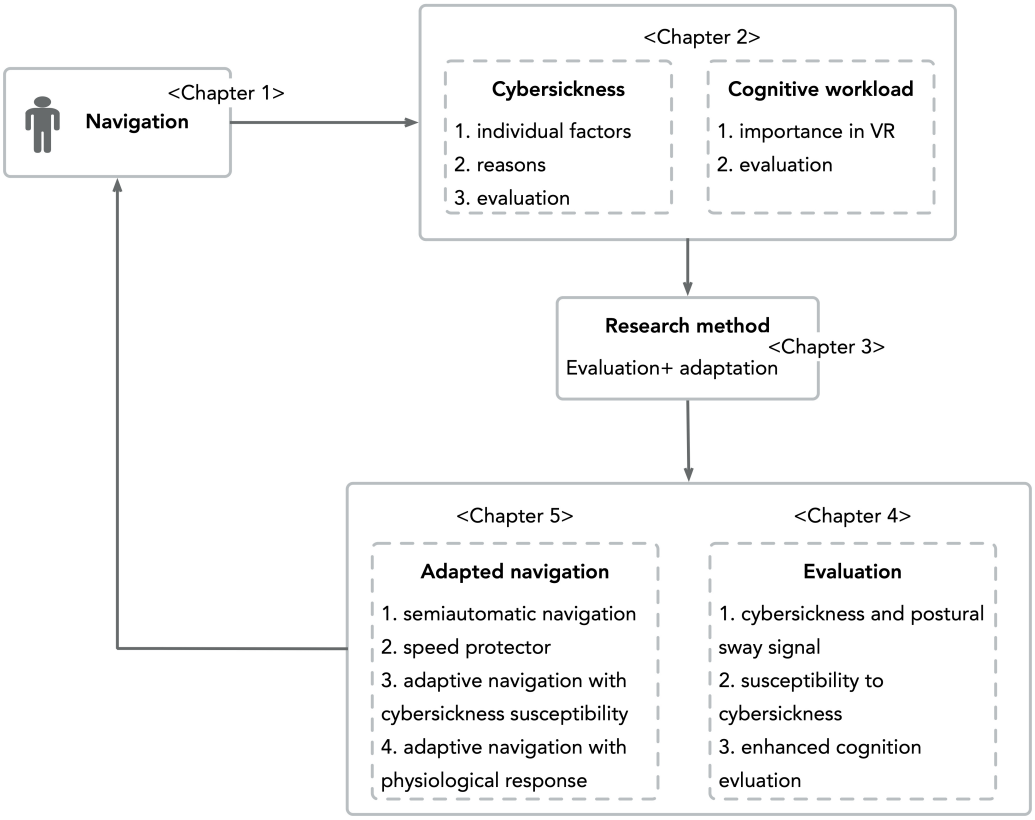

Figure B.1: Aperçu de la structure de la thèse.

immersifs, l'interaction avec un retour multisensoriel, les facteurs humains. Merienne (2016) a affirmé que le sujet est au centre d'une application de RV, et que la connaissance des technologies et des facteurs humains est essentielle pour promouvoir l'efficacité de l'application. Les ingénieurs essaient de produire des environnements aussi immersifs que possible basés sur les nouvelles technologies (Lavalle *et al.* 2014; Bolton *et al.* 2014), tandis que les chercheurs académiques ont tendance à concevoir et vérifier de nouveaux types d'interfaces utilisateur et de techniques d'interaction dans un environnement virtuel immersif (Aslandere *et al.* 2015; Jankowski and Hachet 2015). Avec le développement rapide des technologies issues des jeux vidéo, de nouveaux dispositifs sont fréquemment mis sur le marché, améliorant continuellement les interfaces utilisateur et les techniques d'interaction. Nous pensons que la réalité virtuelle devrait offrir une expérience plus orientée sur l'utilisateur et personnalisée en impliquant des facteurs humains plutôt que des aspects technologiques.

Dans cette thèse, nous nous concentrons sur la navigation, en tant que tâche clé dans les environnements virtuels.

B.2.1 Navigation

La navigation est une tâche fondamentale pour un grand nombre de domaines utilisant des applications de réalité virtuelle. Avant d'effectuer cette tâche principale, les utilisateurs doivent adapter leur point de vue afin d'explorer des environnements virtuels inconnus (Kulik 2009). Les humains peuvent effectuer une navigation dans des environnements physiques grâce à des retours multisensoriels provenant de systèmes visuels, proprioceptifs et vestibulaires, tandis qu'en réalité virtuelle, le seul moyen de conserver des retours sensoriels identiques et cohérents pendant la marche virtuelle est de permettre aux utilisateurs de marcher réellement et de transposer ces mouvements en environnements virtuels. Cependant, en raison des limites des dispositifs de RV, des écrans de RV et du faible espace de travail disponible avec les écrans immersifs de grande taille, les utilisateurs doivent être contraints dans un espace physique limité, ce qui signifie qu'il est impossible de faire correspondre directement la marche réelle à la marche virtuelle, ce qui conduit à un retour sensoriel non naturel. Ce problème a attiré beaucoup d'attention avec le développement de nombreux dispositifs et métaphores de navigation, par exemple, le système de tapis roulant omnidirectionnel CyberWalk qui permet aux utilisateurs de marcher sans fin dans n'importe quelle direction sans quitter les limites de l'espace physique (Souman *et al.* 2008), ou des techniques de marche redirigée permettant une véritable marche dans des espaces physiques contraints en manipulant subtilement le point de vue des utilisateurs (Razzaque 2005).

Les interfaces de navigation naturelle sont privilégiées car elles visent à minimiser l'inadéquation entre les informations proprioceptives liées aux actions et les retours sensoriels issus du système de RV (Marsh *et al.* 2012). Une technique de navigation naturelle devrait envisager de fournir la meilleure expérience aux utilisateurs. Dans la conception de produits, l'expérience utilisateur est définie comme "les perceptions et les réponses d'une personne résultant de l'utilisation prévue d'un produit, d'un système ou d'un service" (*Ergonomics of human system interaction-Part 210: Human-centred design for interactive systems* 2019). Elle ne se concentre pas uniquement sur le retour de l'utilisateur lors de l'interaction avec un produit (par exemple, les mesures subjectives et les préférences d'action), mais plutôt sur les réactions (par exemple, physiologiques) qui apparaissent lors de l'interaction. Étant donné que ces réponses et réactions sont influencées par divers facteurs tels que les attentes, les croyances, les préférences, les perceptions, les sentiments et les émotions, et les réalisations de l'utilisateur, les concepteurs sont invités à déterminer l'importance des facteurs différenciants en fonction du type de produit et de l'application prévue (Rebelo *et al.* 2012). En ce qui concerne la réalité virtuelle, de nom-

breux travaux antérieurs (Stanney *et al.* 1998; Takatalo *et al.* 2011; Sheik-Nainar *et al.* 2015; Shaw *et al.* 2018) ont étudié le cybermalaise et la charge de travail cognitive lors de tâches multiples impliquant la navigation dans des environnements virtuels 3D. Par conséquent, malgré les différentes explications de l'expérience utilisateur fournies dans différents domaines (Rebelo *et al.* 2012; *Ergonomics of human system interaction-Part 210: Human-centred design for interactive systems* 2019), tout au long de la thèse, nous définissons l'expérience utilisateur comme étant le niveau effectif de cybermalaise et de charge de travail cognitive car ces deux éléments sont explicitement associées à la navigation.

B.2.2 Cybermalaise

La navigation dans des environnements virtuels conduit généralement à un cybermalaise qui nuit à la convivialité des applications de réalité virtuelle. Il existe une corrélation significative entre les niveaux d'inconfort liés au mal de la réalité virtuelle et le confort de l'utilisateur (Somrak *et al.* 2019). Actuellement, de nombreuses interfaces de navigation ont été développées dans le but d'améliorer le confort de l'utilisateur, mais le cybermalaise reste un problème inhérent à surmonter. Dans cette partie, nous résumons les différences individuelles pouvant affecter la susceptibilité au cybermalaise et différentes hypothèses pour expliquer le cybermalaise, à partir desquelles nous pouvons proposer nos solutions pour l'atténuer.

B.2.2.1 Facteurs individuels

Environ 80 % à 95 % des utilisateurs de RV ressentent des symptômes de mal-être lorsqu'ils sont exposés à des environnements virtuels (EV), parmi lesquels 5 percent à 30 % doivent quitter l'immersion (Arns and Cerney 2005). Pour les utilisateurs novices de la technologie de RV, environ 60 % souffrent de ces symptômes indésirables et la gravité des symptômes varie généralement d'un individu à l'autre (Lawson *et al.* 2002). Par conséquent, nous avons cherché à examiner les caractéristiques individuelles qui pourraient affecter le cybermalaise lors de la navigation dans des environnements 3D immersifs. Bien que de nombreux travaux aient été réalisés pour réduire le cybermalaise en fonction de facteurs liés à la technologie (par exemple, le champ de vision, le type de dispositif, la résolution, la fréquence d'images, le contenu de la scène et la latence), très peu d'attention est accordée aux facteurs humains de manière systématique. Ces caractéristiques humaines doivent être clairement étudiées pour déterminer et expliquer la raison principale du cybermalaise chez les individus. Par

conséquent, Table B.1 résume l'effet des différences individuelles (par exemple, le sexe, l'âge, la posture, l'expérience de jeu, l'influence ethnique, etc.) sur l'occurrence et la gravité du cybermalaise. Ces facteurs sont étudiés car ils sont liés à l'homme et individuellement indépendants, expliquant pourquoi certains participants souffrent plus que d'autres.

Table B.1: Résumé de l'influence des facteurs individuels sur le cybermalaise

Facteurs individuels	**Relation avec le cybermalaise**	**Références**
Âge	1. La sévérité du cybermalaise augmente jusqu'à 12 ans, et diminue ensuite Constat opposé : 2. Les personnes âgées sont plus sujettes au cybermalaise que les jeunes	L. Harm (1990a), Kolasinski (1995), Davis *et al.* (2014), Constat opposé : Arns and Cerney (2005)
Expérience de jeu	Plus l'expérience de jeu est forte, moins le cybermalaise est présent	S. P. Smith and Du'Mont (2009), Häkkinen *et al.* (2006), Knight and Arns (2006), Iskenderova *et al.* (2017), Gamito, Oliveira, Morais, *et al.* (2010)
Origine ethnique et influences génétiques	1. Les caucasiens ont une tolérance plus longue lors de rotations que les sujets asiatiques 2. Le cybermalaise présente des caractéristiques héréditaires , selon si les parents sont sensibles au cybermalaise 3. Le cybermalaise est associé à la fréquence de l'alpha-2 phénotype du récepteur adrénergique "gg".	Klosterhalfen *et al.* (2005), R. Stern *et al.* (1993), Yanus and Malmstrom (1994), Knox (2014), Abe *et al.* (1984), Reavley *et al.* (2006), Sharma *et al.* (2008), Bakwin (1971), L. Liu, Yuan, *et al.* (2002)
Genre	Les femmes sont plus sensibles que les hommes quel que soit le type de malaise	Reason and Brand (1975), Jaeger and Mourant (2001), Holmes and Griffin (2001), Hakkinen *et al.* (2002), S.-N. Yang *et al.* (2012), Flanagan *et al.* (2005), Häkkinen *et al.* (2006), G. D. Park *et al.* (2006)
Stabilité posturale	1. La stabilité posturale avant immersion est fortement associée à des nausées et une désorientation. 2. Un mauvais contrôle postural est lié au cybermalaise	Kolasinski (1995), Riccio and Stoffregen (1991), N. Owen *et al.* (1998), Stoffregen and Smart (1998), N. Owen *et al.* (1998)
Acuité visuelle	1. Les sujets ayant une mauvaise acuité visuelle subissent généralement un cybermalaise Constats opposés : 2. Aucune relation significative entre l'acuité visuelle et le cybermalaise	Rinalducci (1996), Hale and Stanney (2006) Opposite findings: Hale and Stanney (2006), Read and Bohr (2014), Allen *et al.* (2016)
Maladies	La maladie peut augmenter le risque de cybermalaise élevé	LaViola Jr (2000)

B.2.2.2 Théories du cybermalaise

La communauté cherche depuis longtemps des théories pour expliquer "pourquoi" et "comment" le cybermalaise peut survenir. Cependant, aucune théorie unifiée ne peut tout expliquer, de sorte que ces théories sont développées par affinement des unes des autres pour une application dans différentes situations. Par exemple, les théories du conflit sensoriel, de l'instabilité posturale et des mouvements oculaires sont considérées comme des théories du "comment", tandis que la théorie de l'évolution est considérée comme la théorie du "pourquoi" (Brooks *et al.* 2010). Table B.2 résume et compare sept théories différentes pour expliquer le cybermalaise.

Table B.2: Résumé des théories pour expliquer le cybermalaise

Théorie	**Explications**	**Références**
Théorie du conflit sensoriel	L'information de conflit provenant de différents organes entraîne un cybermalaise	Reason and Brand (1975), Oman (1982), Brooks *et al.* (2010)
Théorie de la verticale subjective	Le cybermalaise apparaît lorsque la verticale ressentie entre en conflit avec la verticale subjective	Bles *et al.* (1998)
Théorie de l'instabilité posturale	Le cybermalaise résulte d'instabilités prolongées, et précède les symptômes decybermalaise	Stoffregen and Riccio (1991), Riccio and Stoffregen (1991), Smart Jr *et al.* (2002), Chardonnet *et al.* (2017)
Théorie du cadre fixe	Les cadres fixes sont essentiels pour la perception spatiale, et l'incapacité de choisir un cadre fixe approprié génère du cybermaladie	Prothero (1998), Prothero, Draper, *et al.* (1999), Prothero and D. E. Parker (2003)
Théorie du mouvement des yeux	Toute condition produisant une erreur dans le contrôle des mouvements oculaires, précédant avec un signal de retour et de correction d'erreur, est une raison potentielle du cybermalaise	Riccio and Stoffregen (1991), Ebenholtz (1992), Ebenholtz *et al.* (1994), Ebenholtz (2001)
Théorie du poison	1. Le corps réagit aux conflits sensoriels comme s'il avait ingéré des toxines 2. Les nausées et vomissements dans la réponse aux stimuli visuels pourraient être une réponse accidentelle de ce système de protection	Treisman (1977)
Modèle de renforcement négatif	Avec les symptômes du cybermalaise, les utilisateurs réduiraient naturellement ou cesseraient les activités correspondantes pour échapper à une expérience désagréable.	Bowins (2010)

B.2.3 Charge de travail cognitive

Concernant le développement d'interfaces de navigation dans une application de réalité virtuelle, la charge de travail cognitive est un autre facteur important à considérer car le choix de la technique de navigation peut influencer la cognition dans un environnement virtuel (Zanbaka *et al.* 2005). Reimer and Mehler (2011) a montré une tendance positive entre une vitesse croissante et une charge de travail cognitive croissante. Les stratégies de contrôle de la vitesse adoptées pendant la navigation virtuelle jouent un rôle important vis-à-vis de la charge de travail cognitive. Marsh *et al.* (2012) a montré qu'une navigation non naturelle est susceptible d'aggraver les performances de l'utilisateur et d'entraîner une charge de travail cognitive élevée car elle nécessite une mémoire de travail supplémentaire pour établir et prendre en charge un modèle mental ; les auteurs ont en outre proposé de développer une technique de navigation basée sur le corps qui nécessite moins de ressources cognitives, car une telle navigation est basée sur des compétences naturelles déjà existantes, par exemple une vraie marche dans l'environnement physique.

Malgré la croissance du marché de la RV et les capacités des derniers dispositifs, si une tâche en réalité virtuelle n'est pas conçue avec un niveau de charge de travail cognitive approprié pour correspondre à l'expertise d'un utilisateur, les performances de réalisation de la tâche peuvent être limitées (L. Zhang *et al.* 2017). La charge de travail cognitive dans ce cas est un terme qui fait référence au coût de réalisation d'une tâche (Hart 2006a). Il peut être défini comme la quantité de ressources cognitives utilisées par unité de temps pour atteindre la performance requise par la tâche (Wickens *et al.* 2015). De manière pragmatique, Blackwood (1900) a proposé une définition simple selon laquelle la charge de travail est le rapport entre le temps requis et le temps disponible (temps requis/temps disponible). Lorsque le temps nécessaire pour accomplir une tâche est plus long que le temps disponible, il s'agit d'une surcharge cognitive, et vice versa. Par exemple, lorsqu'un utilisateur navigue dans un environnement virtuel en tant que tâche principale, il peut avoir à interagir avec des objets de cet environnement en tant que tâche secondaire, et de ce fait, un utilisateur non qualifié pourrait voir sa charge cognitive devenir importante plus longtemps. Une introduction détaillée à la charge de travail cognitive peut être consultée dans (Paas *et al.* 2003).

Bien que la charge de travail soit définie selon un niveau qualitatif, les chercheurs tentent toujours de trouver des critères mesurables sur une base multidimensionnelle pour quantifier ce phénomène.

Les approches utilisées dans la littérature pour mesurer la charge de travail cognitive comprennent des mesures subjectives telles que des questionnaires, des mesures physiologiques à travers des capteurs, et des mesures de performance (Paas *et al.* 2003; L. Zhang *et al.* 2017). Les méthodes d'évaluation subjective et physiologique sont similaires à celles utilisées pour mesurer le cybermalaise et, par conséquent, elles partagent le même défaut d'être potentiellement sources d'erreur. Les mesures de performance doivent rapporter la charge de travail cognitive en fonction de certaines variables de performance liées à la réalisation des tâches telles que le temps de réaction, la précision et le taux d'erreur.

Les moyens physiologiques de mesure de la charge de travail cognitive ont progressé grâce au développement de nouveaux types de capteurs, tandis que les méthodes de mesure subjectives sont principalement basées sur des questionnaires existants depuis longtemps tels que la Subjective Workload Assessment Technique (SWAT) (Reid and Nygren 1988), l'échelle modifiée de Cooper Harper (MCH) (Kilmer *et al.* 1988), ou le NASA-TLX (Hart and Staveland 1988; Hart 2006a). Les questions prédéfinies permettent aux expérimentateurs de réaliser des expériences et d'analyser les données plus facilement qu'avec du retour physiologique. Cependant, le processus d'évaluation subjective peut biaiser les résultats en raison de changements internes non perçus et de facteurs inconnus parmi les utilisateurs. De plus, cette méthode d'évaluation ne parvient généralement pas à réduire les effets de dispersion, le bruit et l'incertitude lors d'une enquête subjective (Katicic *et al.* 2015a), ce qui constitue une problématique pour ce que nous appelons la précision de la mesure.

B.3 Questions de recherche

Les fabricants de casques de RV essaient de proposer une immersion plus élevée avec leurs produits. La contrepartie est que les utilisateurs ont tendance à souffrir davantage du cybermalaise, qui s'aggrave à mesure que le temps d'immersion augmente (Padmanaban *et al.* 2018). La susceptibilité au cybermalaise varie selon les utilisateurs de réalité virtuelle. Jusqu'à présent, le manque de méthodes efficaces pour évaluer et atténuer ce mal-être dans les environnements virtuels attire beaucoup l'attention des communautés académiques et industrielles. Ainsi, les problématiques de recherche liées au cybermalaise sont:

Q1 Comment évaluer le cybermalaise en tenant compte des caractéristiques individuelles, ainsi qu'en fonction de signaux physiologiques tels que l'activité électro-dermale ou la balance posturale ?

Q2 Comment concevoir des techniques de navigation adaptées à l'utilisateur afin d'atténuer le mal de la réalité virtuelle ?

Parce que la complexité d'une tâche dans un environnement virtuel peut affecter le traitement de l'information, les performances et l'attention de l'utilisateur (Ma and Kaber 2006), un environnement virtuel peut agir sur l'utilisateur à la fois au niveau cognitif et perceptif (Milleville-Pennel and Charron 2015). Bien qu'il existe plusieurs méthodes subjectives pour évaluer la charge de travail cognitive, le manque de précision entraîne des difficultés à comparer différents niveaux de charge de travail. Ainsi, la problématique de recherche pour la charge de travail cognitive est :

Q3 Comment améliorer l'évaluation de la charge cognitive ?

B.3.1 Approche proposée

B.3.1.1 Modèle LSTM de mesure du cybermalaise (Q1)

La susceptibilité au cybermalaise est affectée par de nombreux facteurs, notamment les caractéristiques individuelles et les dispositifs d'affichage. Il est important d'étudier comment mesurer et quantifier la quantité de cybermalaise après qu'un utilisateur s'est servi de systèmes de RV. Le modèle LSTM est l'un des algorithmes de la famille de l'apprentissage profond, et il présente un avantage particulier pour l'analyse de données séquentielles. Cette thèse propose d'aborder cette question en introduisant le modèle LSTM pour évaluer le cybermalaise à partir de signaux physiologiques.

B.3.1.2 Navigation adaptative en VR (Q2)

Nous souhaitons concevoir un système d'évaluation en ligne de l'expérience utilisateur pour optimiser les interfaces de navigation en RV en fonction du niveau de cybermalaise de l'utilisateur. Un système de navigation adaptative en temps réel a été développé suivant l'évaluation du cybermalaise. Quatre techniques ont été développées, telles qu'un protecteur de vitesse qui peut optimiser la vitesse de navigation, et un modèle adaptatif qui peut ajuster l'accélération de la navigation en fonction d'un contrôleur PID et des signaux physiologiques de l'utilisateur (par exemple, activité électro-dermale).

B.3.1.3 TOPSIS pour mesurer la charge de travail cognitive (Q3)

Considérant que la plupart des méthodes actuelles ne prennent pas souvent en compte les incertitudes inhérentes au processus de jugement subjectif et de comparaison (Zhou and Chan 2017), nous proposons d'utiliser la *Technique for Order of Preference by Similarity to Ideal Solution* (TOPSIS) (K. P. Yoon and Hwang 1995) pour améliorer la précision de l'évaluation subjective de la charge de travail. TOPSIS a été développé pour que les décideurs mesurent et comparent les performances relatives entre différentes alternatives ; il a été largement utilisé dans de nombreux processus d'évaluation tels que la gestion d'une chaîne d'approvisionnement, la conception de systèmes de fabrication, la gestion commerciale et marketing, et dans le domaine de la santé (Behzadian *et al.* 2012). Dans cette thèse, la méthode TOPSIS est utilisée pour analyser le NASA-TLX et mesurer la charge de travail cognitive globale, à la place de la méthode classique de la somme pondérée.

B.4 Mesure de l'expérience utilisateur

Grâce à l'étude de la littérature dans la section B.2, nous avons constaté qu'il existe de nombreuses méthodes d'évaluation du cybermalaise et de la charge de travail cognitive. Cependant, ces méthodes sont pointées du doigt pour être sources de multiples erreurs, détériorant la fiabilité des résultats évalués. Constatant l'importance d'évaluer l'expérience utilisateur dans une tâche de navigation, nous avons proposé différentes méthodes d'évaluation de l'expérience utilisateur, c'est-à-dire le cybermalaise et la charge de travail cognitive dans ce contexte. La mesure du cybermalaise comprend deux aspects. L'un consiste à mesurer le cybermalaise après la navigation de l'utilisateur dans un environnement virtuel. Par exemple, en comparant le signal de balance postural avant immersion et après immersion aux stimuli visuels, nous pouvons calculer le niveau de mal-être de l'utilisateur. Cependant, il s'agit d'une mesure a posteriori, insuffisante pour prédire la susceptibilité des utilisateurs au cybermalaise. Par conséquent, nous avons utilisé la logique floue pour impliquer les différences individuelles afin de prédire la susceptibilité au cybermalaise, avant que l'utilisateur ne soit exposé à des stimuli visuels. De plus, il est essentiel de mesurer la charge de travail cognitive : lorsqu'il navigue dans un environnement virtuel, l'utilisateur utilise également la cognition pour traiter l'information, interagir avec des objets virtuels et effectuer des tâches. Cependant, les méthodes d'évaluation subjective actuelles ne parviennent généralement pas à contrôler les effets de dispersion, le bruit et l'incertitude. Par conséquent,

nous avons proposé le modèle TOPSIS pour améliorer la précision de l'évaluation subjective de la charge de travail cognitive.

B.4.1 Évaluation du cybermalaise par la balance posturale[1]

B.4.1.1 Introduction

Un ensemble de symptômes peuvent apparaître selon la susceptibilité des utilisateurs au cybermalaise pendant ou après avoir été exposés à un dispositif d'affichage visuel dynamique pendant une longue durée. L'instabilité posturale est un des phénomènes comportementaux ayant montré son efficacité pour mesurer le cybermalaise (Chardonnet *et al.* 2017). Pour mesurer le niveau de cybermalaise, nous avons proposé une nouvelle méthode basée sur les réseaux profonds *long short term memory* (LSTM) et construit un réseau pour caractériser le niveau individuel de cybermalaise. Comparé à d'autres réseaux de neurones tels que les perceptrons multi-couches (MLP) et les réseaux de neurones convolutifs (CNN) qui ne possèdent pas de mémoire interne et ne traitent que chaque donnée de manière indépendante, le modèle LSTM peut avoir de meilleures performances dans le traitement de dépendances sur le long terme parmi des données séquentielles grâce à des portes incluant une porte d'oubli, une porte d'entrée et une porte de sortie, et surmonter les problèmes d'explosion et de disparition des gradients en même temps (Bengio, Simard, *et al.* 1994). Cela a motivé notre choix pour le modèle LSTM pour détecter le cybermalaise. Ici le modèle LSTM sera utilisé pour analyser les signaux de balance posturale.

B.4.1.2 Méthodologie

La Figure B.2 présente une vue d'ensemble de la méthode proposée pour mesurer objectivement le niveau de cybermalaise basé sur le modèle LSTM. Cette figure montre que le modèle consiste en un encodeur qui tente de représenter le signal brut de balance posturale dans un espace latent, suivi d'un décodeur qui tente de reconstruire le signal original à partir des caractéristiques encodées. Deux étapes composent la méthode : une étape d'entraînement et une étape d'évaluation. Comme le réseau profond est entraîné avec le signal de balance posturale obtenu avant que l'utilisateur ne soit immergé dans l'environnement virtuel, le modèle entraîné est censé capturer les caractéristiques d'une personne non malade. Par conséquent, il peut reconstruire le signal de balance original. Cependant, lorsqu'un

[1]Nous renvoyons à la section 4.1 pour une description détaillée.

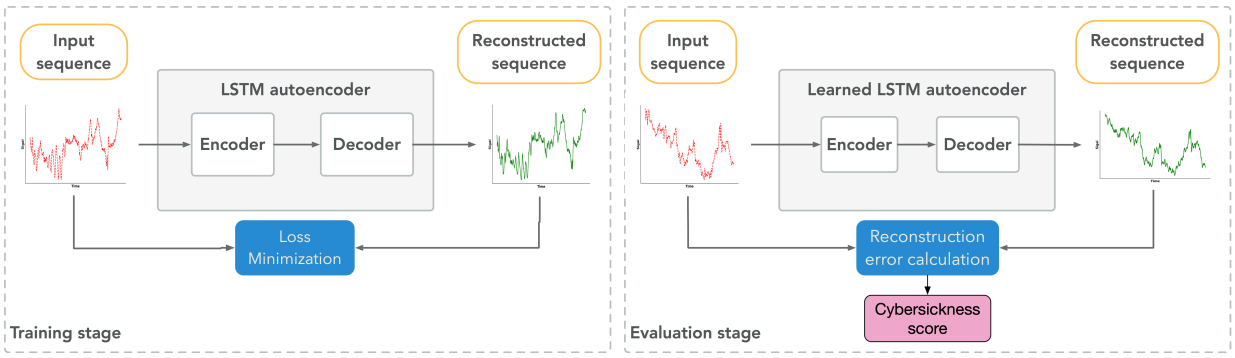

Figure B.2: Présentation de la méthode proposée pour estimer le niveau de cybermalaise à l'aide d'un modèle LSTM.

tel modèle entraîné est utilisé dans l'étape d'évaluation où le signal de balance posturale est obtenu après que l'utilisateur a été exposé à un environnement virtuel, l'erreur de reconstruction sera plus importante. Par conséquent, en évaluant le score de cybermalaise avec un modèle entraîné sur la base de la perte de reconstruction, le niveau de cybermalaise devrait être estimé et prédit en temps réel sans fournir d'informations supplémentaires.

Une erreur de reconstruction plus faible signifie que notre modèle peut récupérer le signal avec plus de précision. En d'autres termes, lorsque nous entraînons le modèle avec un signal de balance posturale obtenu à partir d'un état normal de la personne (sans aucune sensation de cybermalaise), l'encodeur extrait les caractéristiques de cet état et le décodeur reconstruit le signal en conséquence avec une grande précision. Cependant, lors de la phase d'évaluation, lorsque nous alimentons le réseau avec un signal de balance posturale obtenu à partir d'un état corporel différent, le décodeur ne sera pas en mesure de reconstituer le signal d'entrée avec précision car le réseau ne reconnaît pas les caractéristiques apprises : l'erreur de reconstruction est donc supposée grande, indiquant la présence d'un cybermalaise.

B.4.1.3 Résultats

Pour évaluer les performances du LSTM, nous avons demandé à 11 participants de naviguer dans un environnement virtuel et de récupérer 30 pièces de monnaies virtuelles le plus rapidement possible. Les signaux de balance posturale avant et après immersion ont été acquis grâce à une plateforme de mesure de balance posturale. Un questionnaire sur le mal simulateur (SSQ) a également été administré avant et

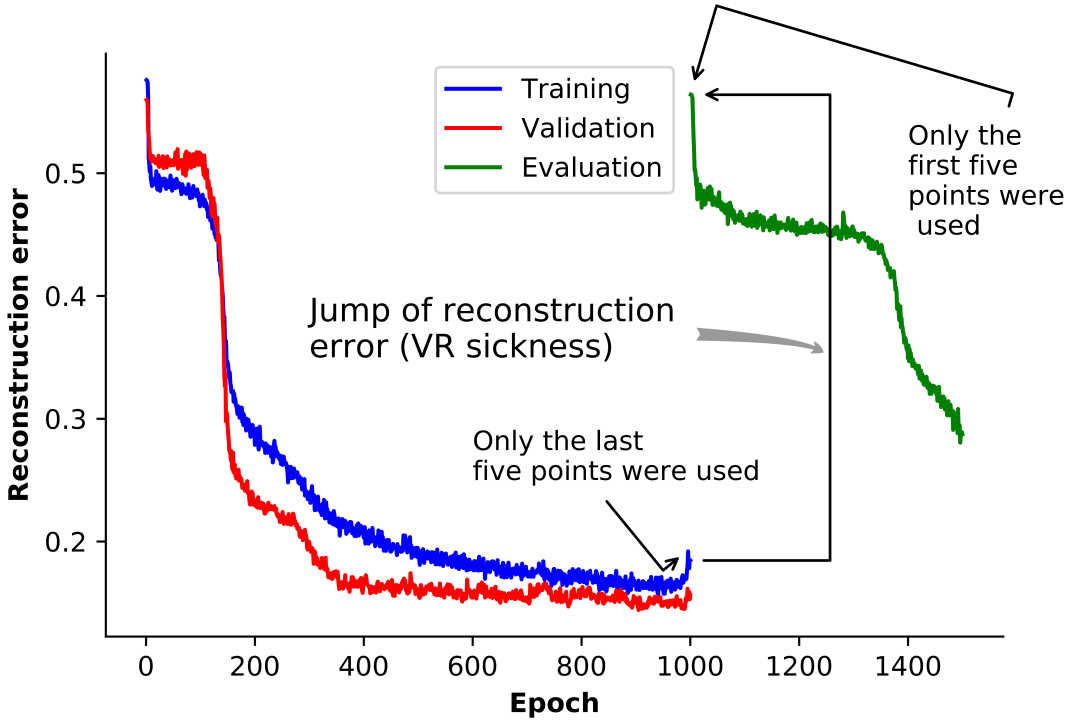

Figure B.3: Démonstration de la méthode proposée pour détecter le cybermalaise à partir des signaux d'un participant.

après immersion. Les données avant immersion ont été transmises au réseau LSTM, conduisant à une valeur d'erreur de reconstruction de référence. La différence d'erreur de reconstruction après immersion a ensuite été calculée. La moyenne des cinq dernières valeurs minimisées d'erreur de reconstruction avant immersion et la moyenne des cinq premières valeurs d'erreur de reconstruction après immersion ont été utilisées pour le calcul. Un exemple d'évolution de l'erreur de reconstruction pour un participant déterminée à partir des signaux de balance posturale à l'état normal (avant immersion, courbe bleue) et après immersion (courbe verte) est montré dans la Figure B.3. Un score de SSQ a également été calculé pour chaque participant à partir de la différence entre les scores de SSQ après et avant immersion. Des coefficients de corrélation de Pearson ont ensuite été calculés entre les erreurs de reconstruction et les scores de SSQ, ainsi que ceux des sous-échelles du SSQ. Les résultats montrent que la fiabilité de prédiction est validée car les coefficients de corrélation de Pearson sont suffisamment élevés.

Étant donné que le modèle est conçu pour apprendre les caractéristiques lorsque l'utilisateur ne

ressent aucun cybermalaise, il peut détecter et alerter sur la présence de signaux anormaux lorsque l'utilisateur se trouve dans un autre état physiologique et ressent un cybermalaise. Comme nous avons formé le modèle pour chaque utilisateur indépendamment, le modèle est personnalisé, ce qui signifie que la méthode proposée peut être utilisée de manière personnalisée dans une navigation en RV pour détecter le cybermalaise avec des performances en temps réel.

B.4.2 Prédiction du cybermalaise par les facteurs humains[2]

B.4.2.1 Introduction

Nous avons proposé de développer des modèles flous intégrant le système d'inférence floue (FIS) et le système d'inférence neuro-flou adaptative (ANFIS) pour prédire la susceptibilité au cybermalaise résultant de la navigation virtuelle immersive, en se basant sur les différences individuelles (par exemple, l'âge, l'expérience de jeu et ethnicité), ce qui permet aux concepteurs d'applications de réalité virtuelle de définir des paramètres de navigation pouvant offrir une expérience personnalisée à l'utilisateur. Notre choix pour la logique floue était dû au fait que les innombrables techniques de régression sont des modèles basés sur des données qui peuvent prédire la susceptibilité individuelle au cybermalaise. Cependant, ils ne sont pas adaptés à la situation actuelle. Les modèles de logique floue sont formulés à partir de règles existantes ou appris à partir de données pour formuler les règles, permettant aux chercheurs d'appliquer des connaissances spécialisées à une application. Par ailleurs, les techniques de régression ne sont qu'un ajustement non linéaire de la corrélation des données. De plus, les techniques de régression reposent fortement sur la qualité de l'ensemble des données, ce qui est problématique et ne permet donc pas de tirer parti de manière optimale d'informations antérieures basées sur des connaissances d'experts. Nous soutenons le fait que les connaissances d'experts antérieures, accumulées au cours de décennies de recherches intenses, ne doivent pas être rejetées et ignorées.

B.4.2.2 Méthodologie

Un système d'inférence floue (FIS) est une application non linéaire qui déduit des sorties selon un raisonnement flou et une classe de règles floues si-alors. Le FIS est particulièrement approprié pour des situations où soit l'expression des problèmes étudiés est vague et incertaine, soit les systèmes sont difficiles à modéliser de manière exacte (Z. Yang *et al.* 2011). Le FIS s'appuie fortement sur

[2]Nous renvoyons à la section 4.2 pour une description détaillée.

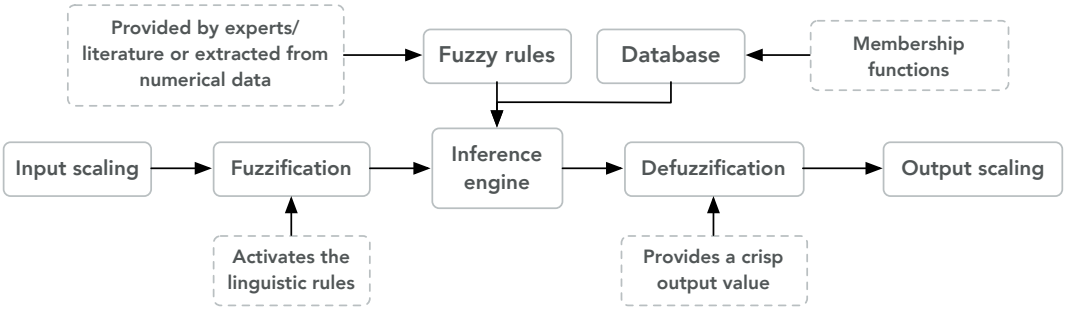

Figure B.4: Schéma fonctionnel d'un système d'inférence floue.

les connaissances et l'expérience des professionnels et des experts du domaine, et il est donc difficile d'obtenir des résultats satisfaisants si trop d'informations préalables font défaut (Y.-S. Chen *et al.* 2016; Benmouiza and Cheknane 2019). La structure d'un FIS est représentée dans la Figure B.4. La base de données définit des fonctions d'appartenance (MF) utilisées pour partitionner les variables linguistiques (petites, moyennes, grandes, etc.), puis le moteur d'inférence effectue une procédure de raisonnement basée sur les règles floues et les entrées fournies pour déterminer une sortie ou conséquence. Dans ce travail, comme la corrélation entre les facteurs d'influence et le cybermalaise peut être connue des experts du domaine ou de la littérature antérieure, le FIS peut naturellement inclure ces connaissances et prédire facilement l'occurrence du cybermalaise.

De nombreux facteurs individuels peuvent affecter la susceptibilité au cybermalaise comme nous l'avons vu dans la Table B.1, cependant, en tant qu'étude exploratoire, nous avons choisi de ne considérer que l'*Age*, l'*Expérience de jeu* et l'*Ethnicité*, car nous pouvons obtenir ces informations facilement grâce à des questionnaires et les rendre floues directement grâce aux MF.

L'architecture d'ANFIS utilisée dans cette étude est illustrée dans la Figure B.5. Le système démarre avec trois entrées, x, y et z, représentant respectivement l'*Age*, l'*Expérience de jeu* et l'*Ethnicité*. La MF $O_{1,i}$ implique le degré auquel le t donné appartient à un quantificateur, par exemple, petit, moyen et haut. Les MF sont au minimum égal à 0 et au maximum égal à 1. Certaines MF, telles que la triangulaire, trapézoïdale et gaussienne, sont celles généralement utilisées, mais la plus courante est la fonction gaussienne en cloche, donnée par :

$$MF(t) = \frac{1}{1 + (\frac{t-c_i}{a_i})^{2b_i}} \tag{B.1}$$

où a_i, b_i et c_i sont les paramètres à optimiser par l'algorithme d'apprentissage. Lors de la modifica-

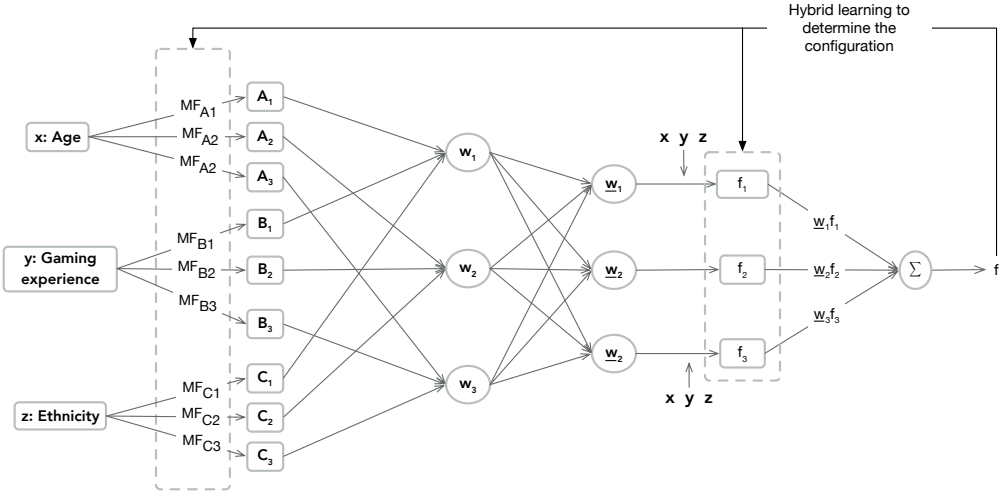

Figure B.5: Architecture du système d'inférence neuro-floue adaptative ; à noter que les MF et les fonctions qui en découlent sont déterminées par des connaissances expertes dans le FIS, ce qui constitue la principale différence entre l'ANFIS et le FIS.

tion de leurs valeurs, les fonctions en cloche varient en conséquence, affichant différentes configurations de MF.

A partir des caractéristiques individuelles de chaque utilisateur, des règles sont construites, et le FIS et l'ANFIS fournissent par conséquent un score individuel de susceptibilité au cybermalaise.

B.4.2.3 Résultats

Pour valider l'utilisation de la logique floue pour prédire individuellement le cybermalaise, nous avons collecté des données d'expériences passées impliquant la navigation dans des environnements virtuels. Pour chacun d'eux, des questionnaires démographiques ont fourni des informations sur chaque participant en termes d'âge, d'origine ethnique et d'expérience de jeu. Pour chaque donnée, le score de susceptibilité au cybermalaise a été calculé et corrélé avec les scores de SSQ rapportés par chaque participant après immersion. Les résultats indiquent des corrélations significatives, peu importe avec le FIS ou l'ANFIS, entre les scores de susceptibilité respectifs et les scores de SSQ. D'autres corrélations ont été déterminées avec l'ethnicité ainsi qu'avec l'expérience de jeu, tandis que l'âge n'a pas montré une forte corrélation.

Nous n'avons impliqué que trois facteurs individuels (âge, origine ethnique et expérience de jeu) dans cette étude, ce qui a réduit l'ampleur des corrélations observées, mais la significativité de ces

valeurs a permis de montrer la fiabilité du score de susceptibilité au cybermalaise prédit par la logique floue. D'autres caractéristiques individuelles, telles que la maladie, la contrôlabilité de la stabilité posturale, l'acuité visuelle, les traits de personnalité et les états émotionnels, peuvent être facilement intégrées dans le FIS grâce à son architecture évolutive, ce qui peut renforcer encore la fiabilité du modèle proposé.

B.4.3 Amélioration de l'évaluation de la charge de travail cognitive[3]

Nous avons proposé des méthodes d'évaluation du cybermalaise, soit par les signaux de balance posturale, soit par les facteurs individuels. Comme nous l'avons analysé dans la section B.2, la charge de travail cognitive est un autre élément important de l'expérience lors de l'exécution de tâches dans des environnements virtuels, mais les évaluations actuelles de la cognition par des méthodes subjectives sont critiquées pour leur faible précision en raison de diverses erreurs. Nous présentons une méthode d'amélioration de l'évaluation de la charge de travail cognitive.

B.4.3.1 Introduction

Cette partie ne vise pas à développer une nouvelle approche pour déduire des opérations et des équations mathématiques pour mesurer la charge de travail cognitive, mais plutôt à améliorer la précision et la qualité des approches d'évaluation avec les modèles existants. L'amélioration de la précision peut permettre aux concepteurs et aux expérimentateurs de RV de mieux discriminer les différences entre les paramètres et d'optimiser facilement leurs applications. Le domaine de la RV nécessite de nombreuses méthodes d'évaluation pour mesurer le retour d'expérience des utilisateurs sur le design d'interaction, cependant l'application de méthodes appropriées assurant une qualité du retour d'information dans ce domaine est plutôt rare, ce qui nous a motivé à utilisr TOPSIS et la méthode de procédure hiérarchique floue d'analyse (*fuzzy AHP*) pour améliorer la qualité de mesure de charge de travail cognitive en RV. Il convient de noter que la méthode proposée peut être appliquée non seulement à la RV, mais également à toute application d'interaction homme-machine pour laquelle la charge cognitive est importante à prendre en compte.

[3]Nous nous référons à la section 4.3 pour une description détaillée.

B.4.3.2 Méthodologie

La Figure B.6 présente le schéma complet de la méthode proposée pour évaluer la charge de travail cognitive à l'aide de TOPSIS à partir des approches de pondération de *Hart* et fuzzy AHP. La méthode nécessite deux étapes. La première étape consiste à calculer les coefficients de pondération à partir de l'approche fuzzy AHP, de comparaisons par paires suggérées par Hart and Staveland (1988) et Hart (2006a), ou l'approche de pondération uniforme. La deuxième étape consiste à utiliser TOPSIS pour calculer le coefficient de proximité relative (RCC) en utilisant les informations de pondération obtenues à partir de la première étape.

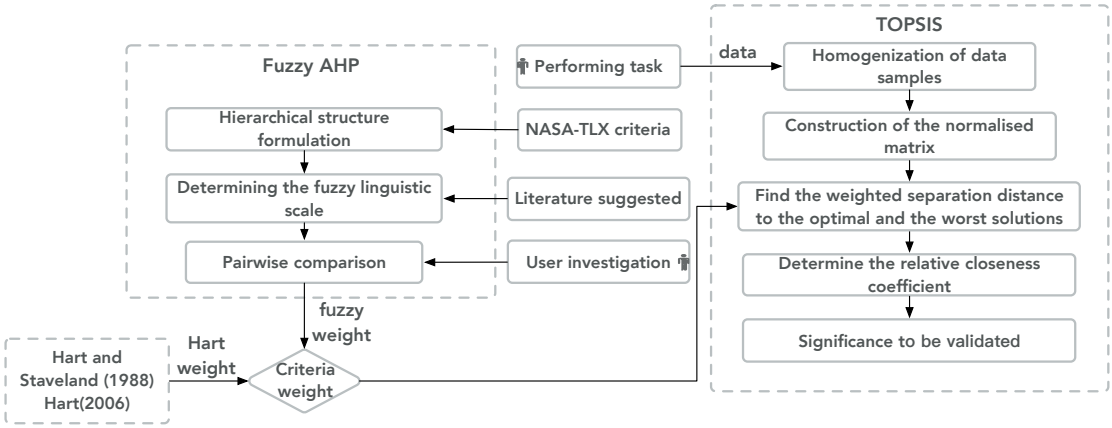

Figure B.6: Processus schématique de la procédure d'évaluation TOPSIS proposée ; la méthode TOPSIS peut utiliser différentes approches de pondération.

B.4.3.3 Résultats

Nous avons validé notre méthode en menant une expérience à la fois dans un système CAVE et un visiocasque HTC Vive. Puisque l'objectif était d'évaluer notre méthode pour améliorer la précision de la quantification de la charge de travail cognitive, nous avons conçu un environnement virtuel dans lequel 15 participants devaient naviguer en considérant plusieurs niveaux de densité d'objets environnants et d'obstacles sur le chemin de navigation à suivre. Une table NASA-TLX a été remplie par chaque participant à la fin de l'expérience. Les participants ont également été invités à remplir une matrice de comparaison individuelle par paires en utilisant des expressions linguistiques relatives à l'importance de chaque critère du NASA-TLX. La charge de travail cognitive a ensuite été calculée avec notre méthode et comparée à une méthode classique de somme pondérée. La plateforme de réalité

virtuelle et la densité de scénarios ont été les deux facteurs étudiés pour comparer les performances de chaque méthode d'évaluation. Les résultats montrent une dispersion des données significativement plus faible avec TOPSIS qu'avec la méthode classique.

Le *RCC* calculé à partir de TOPSIS s'est avéré être une mesure complète pour quantifier et comparer le niveau de charge de travail entre diverses applications de RV, avec un CV réduit sur l'évaluation subjective par rapport à la méthode classique de la somme pondérée. Les résultats sont cohérents avec la littérature correspondante, ce qui suggère que notre nouvelle méthode peut être utile pour évaluer la charge de travail tout en réduisant l'incertitude subjective et améliorer la qualité de la mesure.

En raison de la popularité croissante de la RV, il est important de considérer la charge de travail cognitive dans ce domaine. Par conséquent, la méthode TOPSIS de mesure de la charge de travail cognitive a été conçue et validée dans le domaine de la RV, alors qu'elle peut également bénéficier à d'autres domaines en suivant nos étapes expérimentales. Néanmoins, une limitation importante est que seuls deux facteurs ont été pris en compte pour déterminer l'efficacité de notre approche ; les travaux futurs prendront en compte plus de facteurs ainsi que plus de cas d'utilisation pour tester entièrement la généricité de cette approche.

B.4.4 Déploiement des outils d'évaluation

Les parties précédentes ont présenté et validé différentes méthodes de mesure du cybermalaise et de la charge de travail cognitive. Cette partie résume les méthodes d'évaluation proposées et, en outre, transforme explicitement les méthodes en outils de mesure efficaces pour le cybermalaise et la charge de travail cognitive. L'objectif n'est pas de proposer un nouveau résultat de recherche, mais de donner une procédure simple concernant la façon d'utiliser nos méthodes d'évaluation comme outils standard.

B.4.4.1 Procédure de mesure du cybermalaise

B.4.4.1.1 Utilisation du signal postural La procédure de mesure du cybermalaise en fonction du signal postural est la suivante :

1. Un utilisateur se tient debout sur une plateforme d'équilibre tout en regardant un point fixe devant soi, à travers lequel l'expérimentateur peut collecter le signal de balance posturale lorsque

l'utilisateur est dans un état normal.

2. L'expérimentateur crée un modèle d'auto-encodeur avec lequel la caractéristique de l'état normal peut être extraite et enregistrée dans le modèle.

3. L'utilisateur commence à naviguer dans l'environnement virtuel.

4. L'utilisateur se place à nouveau sur la plateforme de mesure tout en regardant un point fixe devant soi, à travers lequel l'expérimentateur recueillera le signal de balance posturale après immersion. Il est à noter que la fréquence et la durée du deuxième signal collecté doivent être les mêmes que pour le précédent.

5. L'expérimentateur substitue le deuxième signal dans l'auto-encodeur mentionné ci-dessus, et le modèle calcule l'erreur de reconstruction, qui indique le niveau de cybermalaise.

B.4.4.1.2 Utilisation de facteurs individuels En utilisant les facteurs individuels, nous pouvons obtenir la susceptibilité de l'utilisateur au cybermalaise avant qu'il ne soit exposé à des stimuli visuels, conférant un pouvoir de prédiction. La procédure pour prédire la susceptibilité au cybermalaise grâce au facteurs humains est la suivante :

1. L'expérimentateur prépare un questionnaire pour collecter des informations personnelles telles que l'âge, l'expérience de jeu et l'origine ethnique.

2. Sur la base des relations entre les facteurs individuels et le cybermalaise (comme présenté dans la Table B.1), l'expérimentateur peut formuler les règles à insérer dans le système d'inférence floue.

3. Avec le système d'inférence floue, l'expérimentateur peut calculer la susceptibilité de l'utilisateur au cybermalaise. Cette susceptibilité indique la probabilité individuelle d'avoir des symptômes de cybermalaise pendant la navigation.

Comme l'étude se base sur des facteurs liés à l'utilisateur, l'expérimentateur doit respecter les règles liées à la protection de la vie privée.

B.4.4.2 Procédure de mesure de la charge cognitive

La mesure de la charge de travail cognitive est développée à partir du questionnaire NASA-TLX. Par conséquent, le processus d'expérimentation est le même que dans les travaux antérieurs utilisant le NASA-TLX, mais la différence se situe au niveau du traitement des données du NASA-TLX, pour lequel la méthode TOPSIS sera utilisée.

La procédure de mesure de la charge de travail cognitive avec la méthode TOPSIS est la suivante :

1. L'utilisateur effectue la tâche de navigation dans un environnement virtuel, après quoi il doit remplir le NASA-TLX.

2. L'utilisateur doit également effectuer les comparaisons par paires entre les différents éléments du NASA-TLX. Les comparaisons peuvent refléter l'importance de chaque élément du NASA-TLX concernant la tâche en cours. Concernant les comparaisons par paires, nous avons mentionné trois méthodes différentes dans la section 4.3.

3. Une fois que l'expérimentateur a terminé toutes les études utilisateurs, TOPSIS calculera une charge de travail cognitive globale pour chaque utilisateur.

B.5 Amélioration de l'expérience de navigation

Cette partie présente quatre techniques de navigation visant à améliorer l'expérience de navigation. Premièrement, la navigation semi-automatique permet à l'utilisateur de naviguer selon une trajectoire fluide grâce à des algorithmes de planification de trajectoires. Cependant, elle permet toujours à l'utilisateur d'ajuster manuellement sa trajectoire grâce à la technique de navigation dirigée par le regard. Comme la navigation semi-automatique ne corrige que la trajectoire, nous nous sommes demandés en outre si la vitesse pouvait également affecter l'expérience de navigation. Par conséquent, un "protecteur" de vitesse a été proposé pour éviter à l'utilisateur de subir les effets secondaires résultant de vitesses variables. Cependant, le limiteur de vitesse n'adapte la vitesse qu'en évitant une grande amplitude de l'accélération et d'à-coup, indépendamment des caractéristiques individuelles. Par ailleurs, nous avons démontré comment utiliser la susceptibilité au cybermalaise obtenue à partir de la logique floue pour adapter la vitesse de navigation maximale autorisée. Enfin, pour permettre une navigation adaptative en ligne, nous avons proposé un système contrôlé par un PID qui peut

contrôler l'accélération de la navigation en fonction de la composante phasique du signal d'EDA. Le système en boucle fermée modélise le processus d'accélération de la navigation avec onze paramètres déterminés par simulation. Avec les paramètres optimaux, l'utilisateur éprouvera moins de cybermalaise. Cependant, en raison des contraintes du calendrier de thèse et de la situation de Covid-19, nous n'avons pas pu effectuer d'études utilisateurs pour valider ce modèle.

B.5.1 Navigation semi-automatique[4]

B.5.1.1 Introduction

Une technique de tracé de chemin a été conçue par Igarashi *et al.* (1998) pour naviguer dans des espaces virtuels en 3D. Cette méthode permet aux utilisateurs de suivre la trajectoire souhaitée en traçant un trait dans l'environnement virtuel qui sera ensuite projeté automatiquement sur la surface de navigation pour générer la trajectoire finale. Pour développer une interface de navigation permettant d'offrir une meilleure expérience utilisateur et réduire le cybermalaise, dans cette partie, nous proposons une nouvelle technique semi-automatique pour naviguer dans des environnements virtuels immersifs. L'algorithme de planification de trajectoire est similaire à celui utilisé en robotique humanoïde, à savoir A* (Tiwari *et al.* 2012).

Actuellement, de nombreuses interfaces de navigation ont été développées dans le but d'améliorer le confort de l'utilisateur mais le cybermalaise est toujours un problème inhérent à surmonter en réalité virtuelle (Davis *et al.* 2014). Considérant la théorie des conflits sensoriels, le problème devient : pouvons-nous concevoir une interface de navigation qui réduise autant que possible ce conflit ? Afin de répondre à cette question, nous avons conçu la navigation semi-automatique et nous avons émis l'hypothèse que l'utilisateur devrait souffrir de moins de cybermalaise.

B.5.1.2 Méthodologie

La Figure B.7 présente quatre exemples différents pour l'application de la technique de navigation semi-automatique. L'utilisateur doit naviguer vers la position C à partir de la position A, et dans le cas le plus simple, s'il n'y a pas de raison particulière le motivant à passer par la position D, le chemin proposé par le planificateur de trajectoire serait le meilleur choix. Cependant, un utilisateur peut ne pas vouloir suivre la trajectoire calculée par le planificateur mais naviguer avec un chemin personnalisé

[4]Nous renvoyons à la section 5.1 pour une description détaillée.

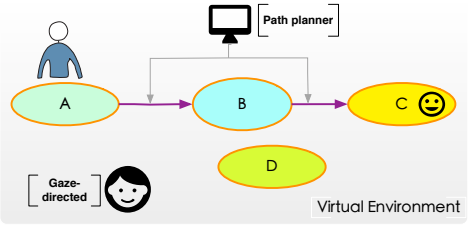

(a) L'utilisateur navigue simplement de A à C en suivant le chemin généré par le planificateur de trajectoire pendant tout le processus, en passant par la position B. Cela peut arriver lorsque l'utilisateur n'a pas à effectuer d'activités en position D.

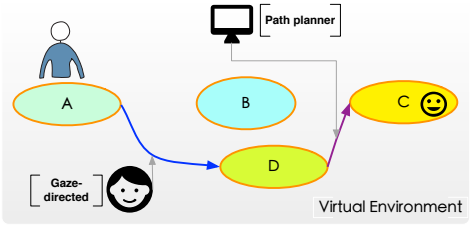

(b) L'utilisateur navigue d'abord vers la position D avec la technique du regard pour effectuer une tâche si B n'est pas la position souhaitée, puis il peut activer à nouveau le planificateur de trajectoire dans une étape ultérieure pour aller à la position C.

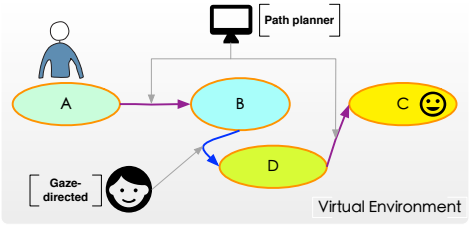

(c) L'utilisateur arrive d'abord à la position B avec le planificateur de trajectoire mais ensuite il/elle peut aller à la position D avec la méthode du regard pour effectuer une tâche ; enfin il utilise le planificateur de trajectoire pour se rendre à la position C.

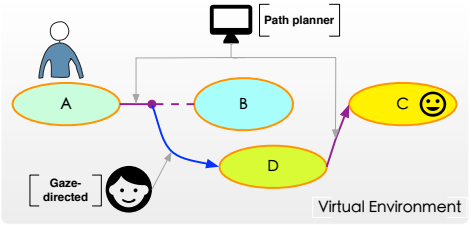

(d) L'utilisateur décide d'abord de naviguer avec le planificateur de trajectoire par défaut mais il/elle change d'avis avant d'arriver à la position B, donc la technique du regard lui permet de passer à la position D. Après avoir terminé la tâche en D, il/elle passe à C avec le planificateur de trajectoire.

Figure B.7: Technique de navigation semi-automatique pour naviguer de la position A à la position C dans un EV : la ligne violette est la trajectoire générée à partir du planificateur de trajectoire tandis que la ligne bleue est la trajectoire générée à partir de la technique du regard. A, B, C et D sont des positions arbitraires de la surface de navigation dans l'EV.

auquel cas la technique du regard dirigé fournit une interaction naturelle entre l'EV et l'utilisateur. Par exemple dans un jeu, les utilisateurs souhaitent ramasser des trésors en cours de route "$A \rightarrow D \rightarrow C$" au lieu de "$A \rightarrow B \rightarrow C$" dans l'EV, alors la technique de regard dirigé leur permet de modifier la trajectoire du mouvement vers une autre position D, qui fonctionne en complément du planificateur de mouvement automatique. Enfin, l'utilisateur sera déplacé avec succès vers la destination finale avec la trajectoire calculée par le planificateur ou par la méthode du regard dirigé, les deux fournissant des trajectoires fluides.

En général, la navigation semi-automatique suit le principe : les utilisateurs peuvent accepter le chemin par défaut et optimisé (le plus court) pour effectuer la tâche assignée, mais ils peuvent affiner

ou modifier le chemin avec la technique du regard si le plus court n'est pas préféré ou pour un tâche précise. Cependant, si les utilisateurs se perdent dans l'EV pendant la navigation, à n'importe quel moment et lieu, ils peuvent réactiver le planificateur de trajectoire.

B.5.1.3 Résultats

Pour montrer l'efficacité de la navigation semi-automatique, nous avons mis en place une expérience dans laquelle 13 participants ont été invités à naviguer dans un environnement virtuel et à ramasser des pièces de monnaie virtuelles le plus rapidement possible. Deux modalités de navigation ont été proposées aux participants et comparées : une navigation par joystick et notre navigation semi-automatique. Le temps de réalisation, la variation de la balance posturale, le score du SSQ et la qualité de la navigation ont été mesurés pour chaque modalité.

Les analyses statistiques ont montré une amélioration significative de la réduction du cybermalaise, en particulier des symptômes de nausée et oculomoteurs. Cela valide nos hypothèses selon lesquelles lors de la navigation à l'aide d'un joystick, les utilisateurs doivent fréquemment changer la vitesse et la direction du mouvement et toujours chercher la cible à atteindre, ce qui entraîne davantage de conflits sensoriels. A l'inverse, le planificateur de mouvement dans la navigation semi-automatique peut aider les utilisateurs à naviguer dans un EV avec moins de stimuli visuels inutiles et saccadés, réduisant ainsi le cybermalaise. De plus, la navigation semi-automatique permet d'obtenir de meilleures performances selon plusieurs facteurs qualitatifs tels que l'efficacité, la précision, l'immersion, la cohérence et la demande en concentration. Les travaux futurs se concentreront davantage sur l'intention de l'utilisateur ainsi que sur l'optimisation de la vitesse de navigation.

B.5.2 Navigation avec protecteur de vitesse[5]

B.5.2.1 Introduction

L'objectif principal est d'étudier si un profil de vitesse optimisé de la navigation avec une accélération et un à-coup appropriés peut améliorer l'expérience utilisateur. L'idée est de concevoir ce que nous appelons un *protecteur de vitesse* qui empêche les utilisateurs d'avoir une expérience négative due à des vitesses irrégulières. L'objectif à long terme est d'étendre davantage ce protecteur dans une interface de navigation en boucle fermée qui peut ajuster les conditions de mouvement en fonction de

[5]Nous renvoyons à la section 5.2 pour une description détaillée.

la réponse physiologique de l'utilisateur. Par exemple, si le système de navigation détecte qu'un utilisateur tombe malade ou subit une charge de travail cognitive élevée, il peut restreindre la navigation irrégulière et optimiser la vitesse en conséquence, et pas simplement s'arrêter brusquement, ce qui est susceptible d'induire un déséquilibre de sa posture dû à l'inertie (Merienne 2016). Notre objectif est donc plus vaste que de simplement optimiser la navigation. Cependant, cette partie se concentre sur la conception du limiteur de vitesse et la validation de ses performances avec une étude utilisateur.

Nous pensons que le contrôle de la marche physique sera bénéfique pour la navigation virtuelle notamment en améliorant le confort lors d'une expérience de RV. En outre, cela nous permet de répondre à certaines questions complexes, telles que comment réduire efficacement le cybermalaise et la charge de travail cognitive et obtenir une expérience plus confortable, d'étudier les comportements des utilisateurs lors d'une navigation complexe dans des environnements immersifs, et en outre de contribuer à l'utilisation de la réalité virtuelle dans divers domaines.

B.5.2.2 Méthodologie

Des études antérieures ont développé des techniques de navigation en utilisant des trajectoires pré-définies (Igarashi *et al.* 1998) à suivre ou en adaptant la vitesse (Argelaguet 2014) pour garder une navigation fluide. Nous proposons ici une nouvelle méthode d'adaptation de la vitesse en considérant que le principe de la marche humaine et du mouvement de la main est généralement un problème de minimisation. Il s'agit d'une nouvelle idée de traiter la navigation dans les EV 3D avec un principe similaire à celui des mouvements humains dans des environnements physiques. Nous avons développé deux types de protecteurs : un non linéaire et un linéaire. Le protecteur de vitesse non linéaire suggère que la vitesse est une fonction non linéaire tandis que le protecteur de vitesse linéaire implique que la vitesse est une fonction linéaire. Le protecteur de vitesse vise à minimiser les à-coups lorsque l'utilisateur navigue d'une position initiale à une cible, ce qui est une règle courante dans la réalité. En plus de la minimisation, nous imposons des contraintes sur la vitesse, l'accélération et les à-coups afin qu'ils ne dépassent pas des seuils spécifiques. Le protecteur de vitesse est formulé mathématiquement et résolu analytiquement afin de fournir une expérience de navigation fluide avec un minimum d'à-coups de trajectoire.

B.5.2.3 Résultats

Une expérimentation a été mise en place avec 15 participants amenés à naviguer dans un environnement virtuel pour évaluer les performances de notre protecteur de vitesse. Un système CAVE et un visiocasque HTC Vive ont été utilisés et le scénario a impliqué trois niveaux de densité d'environnements. Trois niveaux d'accélération et d'à-coups en translation et rotation ont été étudiés. Les scores de SSQ et les réponses de la conductance cutanée (ER-SCR) ont été mesurés pour le niveau de cybermalaise et le NASA-TLX a été utilisé pour mesurer la charge de travail cognitive.

Les résultats actuels indiquent que le protecteur de vitesse, conçu en fonction du mouvement humain et des conditions de confort, peut améliorer considérablement l'expérience de l'utilisateur en réduisant le mal de la réalité virtuelle tout en conservant le même niveau de charge de travail cognitive. La significativité de cette amélioration a pu être évaluée par le *SSQ*, l'*ER-SCR* et le NASA-TLX tandis que les profils de vitesse ont pu être comparés et analysés grâce à une analyse de densité spectrale de puissance.

Nous avons également constaté chez certains participants que, selon la situation, ils préféraient avoir des accélérations différentes. Développer des stratégies pour adapter l'accélération en fonction de facteurs individuels pourrait être une solution prometteuse : les symptômes du cybermalaise pourraient être prédits en ligne pendant la navigation, et l'amplitude de l'accélération pourrait être automatiquement adaptée en conséquence pour offrir une meilleure expérience. Par conséquent, dans les parties suivantes, nous avons développé un système en boucle fermée qui peut adapter la navigation en fonction des réponses physiologiques de l'utilisateur.

B.5.3 Navigation adaptative par les facteurs humains[6]

B.5.3.1 Introduction

Nous avons introduit deux modèles de logique floue dans les parties précédentes, la logique floue de type Mamdani et le système d'inférence neuro-floue adaptatif (ANFIS). Le premier peut être formulé sur la base des connaissances d'experts ou de la littérature existante, tandis que l'ANFIS ressemble davantage à un modèle d'ajustement non linéaire. Les deux méthodes ont atteint des performances équivalentes dans la détection du cybermalaise. Cependant, par rapport à l'ANFIS, la logique floue de

[6]Nous renvoyons à la section 5.3 pour une description détaillée.

type Mamdani peut limiter sa sortie toujours entre zéro et un, ce qui peut être intégré plus facilement et naturellement dans un système adaptatif. Par conséquent, l'ANFIS ne convient pas dans un modèle adaptatif d'un point de vue pratique car il peut fournir une sortie négative. Nous avons conçu une méthode de navigation adaptative dans laquelle la vitesse de navigation est calculée à partir du score de propension individuelle au cybermalaise O_{fis} prédite par le FIS, et nous avons réalisé une étude utilisateur pour déterminer si la navigation personnalisée atténue avec succès les effets du cybermalaise.

B.5.3.2 Méthodologie

La Figure B.8 représente la procédure pour individualiser la navigation dans les environnements virtuels sur la base de la logique floue. En fonction du score de propension O_{fis} prédit à partir des caractéristiques de l'utilisateur, la vitesse de navigation (So *et al.* 2001), l'accélération (Plouzeau *et al.* 2018), et le temps d'immersion (Chardonnet *et al.* 2017) pourraient être adaptés en conséquence. Ici, nous avons choisi la vitesse de navigation comme variable d'adaptation pour contrôler l'apparition d'un cybermalaise.

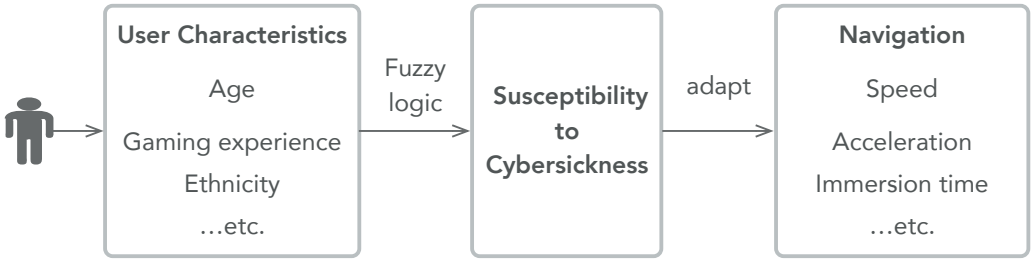

Figure B.8: Procédé d'utilisation des méthodes de logique floue pour prédire la susceptibilité de l'utilisateur au cybermalaise puis adapter les paramètres de navigation.

Pour démontrer clairement l'effet de la navigation adaptative sur le cybermalaise, nous avons considéré une vitesse de navigation de base supérieure à la vitesse de marche normale –$3m/s$–, afin que le cybermalaise puisse être facilement induit. Ensuite, nous avons développé un modèle de vitesse adaptatif, où la vitesse est calculée à partir de la sortie O_{fis} du FIS en prenant en entrée les caractéristiques individuelles des utilisateurs. Rappelons que O_{fis} représente un indicateur de cybermalaise et décrit la propension au cybermalaise des utilisateurs pris individuellement. Comme O_{fis} est compris entre zéro et un, nous avons introduit un facteur d'amplification pour garantir que la vitesse de navigation est suffisamment élevée pour provoquer un cybermalaise. Le modèle de vitesse adaptatif résultant est

décrit comme suit :

$$Vitesse = O_{fis} * A_f \tag{B.2}$$

où A_f est le facteur d'amplification et a été arbitrairement fixé à 3, de sorte que la vitesse maximale peut être de $3m/s$, la vitesse de navigation de base.

B.5.3.3 Résultats

Pour valider cette méthode, 48 participants ont été invités à participer à une expérimentation nécessitant de naviguer dans un environnement virtuel à l'aide d'un visiocasque et avec trois vitesses de navigation : une vitesse de base de $3m/s$, une vitesse adaptée telle que décrite dans l'Equation B.2, et une autre vitesse de base de $1,5m/s$ correspondant à la vitesse moyenne calculée par l'Equation B.2 avec les scores de propension déterminés. Ici, seuls les scores de SSQ ont été mesurés pour le niveau de cybermalaise.

Les résultats montrent que notre modèle de vitesse de navigation adaptative basé sur la sortie du FIS de type Mamdani a permis à une proportion significativement plus grande d'utilisateurs de ressentir moins de cybermalaise. Dans le contexte actuel, la logique floue permet de prédire la susceptibilité de l'utilisateur au cybermalaise, et sur cette base, nous avons adapté la vitesse de navigation maximale autorisée. Cela impliquait que la vitesse soit déterminée avant que l'utilisateur ne soit exposé à des stimuli visuels. Cependant, en plus des facteurs individuels, les états de cybermalaise de l'utilisateur pendant la navigation sont affectés par de nombreux autres facteurs tels que les conditions environnementales et les exigences de la tâche (Bockelman and Lingum 2017). Une vitesse adaptée avant la navigation peut échouer à impliquer ces facteurs.

B.5.4 Navigation adaptative par les signaux physiologiques[7]

B.5.4.1 Introduction

Nous proposons ici d'utiliser les signaux physiologiques, et notamment l'activité électrodermique (EDA) qui peut être obtenue à partir d'un bracelet en temps réel (ici un bracelet Empatica E4[8]), pour adapter la navigation en temps réel, et donc atténuer le cybermalaise. Les signaux d'EDA peuvent être décomposés en deux composantes : le niveau de conductance cutanée (SCL) et la réponse de

[7] Nous renvoyons à la section 5.4 pour une description détaillée.
[8] https://www.empatica.com/research/e4/

la conductance cutanée (SCR) (Aqajari *et al.* 2020). Le SCL, également appelé niveau tonique du signal d'EDA, varie lentement avec une échelle de temps de quelques dizaines de secondes à quelques minutes. En raison des différences d'hydratation, de sécheresse cutanée ou de régulation autonome d'un individu, l'augmentation et la diminution du SCL varient en conséquence. Le SCL peut être très différent selon les individus. D'autre part, la SCR, également connu sous le nom de composante phasique du signal d'EDA, surpasse les changements toniques et présente des variations beaucoup plus rapides. Les alternances dans la composante SCR d'un signal d'EDA sont observables sous forme de salves ou de pics dans le signal. La composante phasique est associée à des événements spécifiques de stimulation émotionnelle (SCR liée à des événements, appelée ER-SCR). L'augmentation de la composante phasique peut atteindre un pic en 1 à 5 secondes après le début des stimuli.

En impliquant l'EDA, nous proposons d'intégrer davantage les différences individuelles dans l'expérience de navigation. Cette méthode peut être vue comme une extension des travaux de (Plouzeau *et al.* 2018) dans lesquels l'accélération de la navigation est adaptée en fonction de la variation de l'EDA. Ici, nous proposons d'utiliser un contrôleur PID associé à des réseaux de neurones pour améliorer la fiabilité de l'adaptation.

B.5.4.2 Méthodologie

L'objectif est de déduire la formulation mathématique de la technique de navigation adaptative à partir d'un système de contrôle PID.

Si $f(t)$ désigne la composante phasique du signal d'EDA au temps t, l'objectif est de stabiliser $f(t)$ tel que,

$$E_f(t_i) = f(t_i) - f(t_{i-1}) \tag{B.3}$$

où $E_f(t_i)$ est la différence de la composante phasique entre le pas de temps t_i et le pas de temps précédent t_{i-1}. Idéalement, $f(t_i)$ devrait être nul, ce qui signifie qu'il n'y a pas de stimuli visuels. Par conséquent, l'Equation B.3 peut être simplifié de la manière suivante :

$$E_f(t_i) = -f(t_{i-1}) \tag{B.4}$$

L'accélération de navigation **a** à l'instant t_i peut être paramétrée de la manière suivante :

$$\mathbf{a}(t_i) = \mathbf{a}(t_{i-1}) + \psi_{\mathbf{a}}\mathbf{E}_{\mathbf{a}}(t_i) + \text{diag}(\beta)\psi_f\mathbf{E}_{\mathbf{f}}(t_i) \tag{B.5}$$

où

$$\begin{aligned}\psi_{\mathbf{a}}(\cdot) &= \begin{bmatrix}\psi_{a_l}(\cdot) & 0\\ 0 & \psi_{a_r}(\cdot)\end{bmatrix}\\ &= \begin{bmatrix}K_{Pl}(\cdot) + K_{Il}\int_0^T(\cdot) + K_{Dl}\frac{d(\cdot)}{dt} & 0\\ 0 & K_{Pr}(\cdot) + K_{Ir}\int_0^T(\cdot) + K_{Dr}\frac{d(\cdot)}{dt}\end{bmatrix}\end{aligned} \tag{B.6}$$

$$\begin{aligned}\psi_{\mathbf{f}}(\cdot) &= \begin{bmatrix}\psi_f(\cdot) & 0\\ 0 & \psi_f(\cdot)\end{bmatrix}\\ &= \begin{bmatrix}K_{Pf}(\cdot) + K_{If}\int_0^T(\cdot) + K_{Df}\frac{d(\cdot)}{dt} & 0\\ 0 & K_{Pf}(\cdot) + K_{If}\int_0^T(\cdot) + K_{Df}\frac{d(\cdot)}{dt}\end{bmatrix}\end{aligned} \tag{B.7}$$

$$\mathbf{E}_{\mathbf{a}}(t_i) = \begin{bmatrix}E_{a_l}(t_i)\\ E_{a_r}(t_i)\end{bmatrix} = \begin{bmatrix}a_{le}(t_i) - a_l(t_i)\\ a_{re}(t_i) - a_r(t_i)\end{bmatrix} \tag{B.8}$$

$$\mathbf{E}_{\mathbf{f}}(t_i) = \begin{bmatrix}E_f(t_i)\\ E_f(t_i)\end{bmatrix} = \begin{bmatrix}-f(t_{i-1})\\ -f(t_{i-1})\end{bmatrix} \tag{B.9}$$

$$\text{diag}(\beta) = \begin{bmatrix}\beta_l & 0\\ 0 & \beta_r\end{bmatrix} \tag{B.10}$$

Dans l'Equation B.5, le deuxième terme $\psi_{\mathbf{a}}\mathbf{E}_{\mathbf{a}}(t_i)$ a pour rôle de s'assurer que l'accélération peut varier autour d'une valeur attendue, car si le troisième terme continue de varier de façon monotone, l'accélération varierait aussi de façon monotone et atteindrait un extremum. Le troisième terme $\psi_f\mathbf{E}_{\mathbf{f}}(t_i)$ représente la quantité adaptative due au stimulus visuel ou à la réponse physiologique. diag(β) est une matrice diagonale utilisée pour équilibrer l'importance entre les mouvements de translation et de rotation dans l'Equation B.5.

L'accélération de navigation **a** comprend à la fois celles en translation et en rotation. a_{le} est l'accélération longitudinale attendue ; a_{re} est l'accélération de rotation attendue ; a_l est l'accélération longitudinale mesurée ; a_r est l'accélération de rotation mesurée.

$\psi_{\mathbf{a}}(\cdot)$ et $\psi_{\mathbf{f}}(\cdot)$ sont les opérateurs du PID. $\psi_{a_l}(\cdot)$ et $\psi_{a_r}(\cdot)$ sont des éléments de $\psi_{\mathbf{a}}(\cdot)$ avec les coefficients suivants : K_{Pl}, K_{Il}, K_{Dl}, et K_{Pr}, K_{Ir}, K_{Dr}, agissant sur les accélérations longitudinale

et de rotation ; ils sont utilisés pour assurer que les accélérations soient stables autour des valeurs attendues. $\psi_f(\cdot)$ est l'élément de $\psi_{\mathbf{f}}(\cdot)$ avec les coefficients suivants : K_{Pf}, K_{If}, K_{Df}, agissant sur la composante phasique du signal d'EDA. $\mathbf{E_a}(t_i)$ et $\mathbf{E_f}(t_i)$ sont les erreurs entre les états stationnaires attendus et les états mesurés au pas de temps t_i. Les erreurs seront substituées aux opérateurs du PID pour calculer les corrections.

Ce travail peut être considéré comme une extension du travail précédent Plouzeau *et al.* (2018) dans lequel la formulation adaptative est donnée comme,

$$a(t_i) = a(t_{i-1}) - 0,5 * \frac{dEDA(t_i)}{dt} \tag{B.11}$$

où $a(t_i)$ et $a(t_{i-1})$ sont les accélérations à deux pas de temps successifs, longitudinales ou de rotation, $EDA(t_i)$ est l'amplitude du signal d'EDA au temps t_{i-1}. Cette formulation est conçue pour un contrôle basé sur l'accélération avec lequel le joystick peut contrôler directement l'accélération longitudinale ou de rotation jusqu'à atteindre une limite de vitesse. Cependant, l'utilisateur peut ne pas contrôler l'accélération lorsque $EDA(t_i)$ continue d'augmenter ou de diminuer, c'est la raison pour laquelle nous avons ajouté le deuxième terme dans l'Equation B.5 pour stabiliser l'accélération. Notre modèle étend cette équation sous une forme algébrique pour incorporer toutes les accélérations et coefficients grâce au contrôleur PID. Dans l'Equation B.11, le facteur $0,5$ est déterminé de manière empirique en tenant compte du temps de réaction physiologique de l'EDA, tandis que dans notre modèle, tous les coefficients sont optimisés sur la base d'un ensemble de données existant.

Pour calculer tous les coefficients dans le contrôleur PID, un réseau de neurones a été créé grâce un ensemble de données constitué des données de 53 participants d'une expérience impliquant la navigation dans un environnement virtuel. Les données contiennent les comportements de navigation, à savoir les accélérations et les valeurs d'activité électrodermale (EDA). Une optimisation mathématique a été menée pour trouver les meilleurs coefficients faisant correspondre les comportements de navigation aux valeurs d'EDA.

B.5.4.3 Résultats

En raison de la pandémie de Covid-19, aucune étude utilisateur n'a pu être réalisée. Cependant, une simulation de navigation adaptative dans un environnement virtuel a été réalisée. Avec les coeffi-

cients calculés, des accélérations adaptées ont été simulées, générant des activités d'EDA simulées. Le scénario considéré ici était le même que celui pour constituer le jeu de données d'apprentissage. Une comparaison a ensuite été faite entre les modalités navigation non adaptée et adaptée en termes de niveaux de cybermalaise. Les résultats de simulation montrent une réduction significative du niveau de cybermalaise lorsque la navigation a été adaptée.

Nous avons proposé un modèle mathématique innovant pour la navigation adaptative dans les environnements virtuels en intégrant un contrôleur PID. Le pré-requis pour exécuter ce modèle avec succès est que le système détecte avec précision le cybermalaise ; autrement, la puissance adaptative du contrôleur PID est moindre. De nombreux systèmes de réalité virtuelle adaptatifs se sont concentrés sur la détection et l'évaluation du cybermalaise dans les environnements immersifs, tandis que nous avons accordé un plus grand intérêt à la façon d'utiliser le cybermalaise pour optimiser les paramètres de navigation. Bien que nous ayons trouvé les coefficients adaptatifs optimaux par la simulation, nous prévoyons de mener davantage d'études utilisateurs pour valider la performance de notre méthode.

B.6 Conclusion et perspectives

Si nous rappelons les questions de recherche, nos objectifs de cette thèse étaient d'améliorer l'expérience de navigation. Dans ce cadre, les questions portaient sur l'évaluation de l'expérience utilisateur (cybermalaise et charge de travail cognitive) et la conception de techniques de navigation naturelle pouvant atténuer le cybermalaise et la charge de travail cognitive. Pour les premières questions, nous avons développé des techniques d'évaluation basées sur le LSTM et le modèle TOPSIS, qui se sont avérées efficaces. Pour les autres questions, plusieurs techniques ont été proposées, dont la navigation semi-automatique, la navigation avec limiteur de vitesse, la navigation utilisant les facteurs humains et la navigation adaptative. Grâce à des expérimentations, leurs performances ont été validées.

Les principaux apports de cette thèse peuvent être résumés comme suit :

1. Nous nous sommes concentrés sur l'évaluation de l'expérience utilisateur lors de l'utilisation d'applications de réalité virtuelle, en particulier le cybermalaise et la charge de travail cognitive. Nous avons expliqué l'origine du cybermalaise sur la base de plusieurs théories. Le processus d'évaluation subjective peut biaiser les résultats en raison de changements internes non perçus

et de facteurs inconnus parmi les utilisateurs. Il était nécessaire de disposer d'une méthode pour gérer et analyser cette incertitude, constatant que les défauts du questionnaire sur le mal de simulateur (SSQ) étaient suffisamment importants pour le développement de métriques objectives pour la mesure du cybermalaise. L'instabilité posturale est l'une des métriques objectives bien connues. Nous avons donc formé un modèle LSTM pour chaque participant en utilisant un signal postural à l'état normal capturé avant immersion. Si le signal de balance posturale après immersion est suffisamment différent du signal avant immersion, le modèle ne parvient pas à reconstruire correctement le signal d'entrée ; la différence d'erreur de reconstruction est appelé erreur de perte et indique le niveau de cybermalaise. Par ailleurs, concernant la charge de travail cognitive, nous avons proposé d'utiliser le modèle *Technique for Order Performance by Similarity to Ideal Solution* (TOPSIS) pour analyser le NASA-TLX et mesurer la charge de travail cognitive globale, à la place de la méthode classique de la somme pondérée. Pour montrer l'avantage de l'approche TOPSIS, nous avons effectué une étude utilisateur pour valider l'approche et son application à la réalité virtuelle, en tenant compte de facteurs tels que la plate-forme de réalité virtuelle et la densité des environnements virtuels.

2. Nous avons présenté une méthode de navigation semi-automatique basée sur des algorithmes de planification de trajectoire, visant à réduire la génération de signaux conflictuels pouvant perturber le système nerveux central (CNS). Nous avons réalisé des expériences où les participants devaient naviguer dans un EV équipé d'un casque HTC Vive. Par rapport à la navigation basée sur un joystick, la navigation semi-automatique est plus efficace et précise, permettant plus de concentration et d'immersion, et donc une réduction significative du cybermalaise induit visuellement.

3. Nous avons conçu un limiteur de vitesse qui peut être intégré au système de navigation pour fournir des profils de vitesse optimaux. Avec les technologies actuelles, la vitesse de navigation virtuelle pour la plupart des systèmes de réalité virtuelle repose principalement sur des dispositifs de contrôle de type joystick. L'utilisateur doit gérer l'adaptation manuelle de la vitesse en fonction de la taille de l'EV et de ses préférences personnelles. Cependant, cette méthode ne peut pas fournir de vitesses optimales pour la navigation, car l'utilisateur a tendance à modifier la vitesse involontairement en raison de problèmes involontaires, notamment des collisions ou un mal de simulateur ; dans ce cas, l'utilisateur peut être amené à ajuster la vitesse fréquemment et

de manière irrégulière, ce qui aggrave la situation. Le protecteur de vitesse peut minimiser les à-coups lorsque l'utilisateur navigue d'une position initiale à une cible. De plus, nous avons imposé des contraintes sur la vitesse, l'accélération et les à-coups afin qu'ils ne dépassent pas des seuils spécifiques. Le protecteur de vitesse a été formulé mathématiquement et résolu analytiquement pour offrir une expérience de navigation fluide avec un minimum d'à-coups de trajectoire.

4. Nous avons proposé de comprendre les différences individuelles dans la tolérance au cybermalaise et les raisons de son apparition. Des facteurs individuels tels que le sexe, l'âge, la stabilité posturale, l'origine ethnique et les influences génétiques, l'expérience de jeu, la personnalité et l'acuité visuelle ont été analysés. Nous avons appuyé sur le fait que les connaissances d'experts antérieures accumulées au cours de décennies de recherche ne devaient pas être rejetées ou ignorées. Cependant, le manque de stratégie pour intégrer l'influence de chaque facteur sur le cybermalaise a rendu difficile l'utilisation des résultats des travaux existants. Nous avons développé deux approches basées sur la théorie de la logique floue : le système d'inférence floue de type Mamdani basé sur la connaissance, et le système d'inférence neuro-floue adaptative basé sur les données (ANFIS), pour impliquer trois différences individuelles (âge, expérience de jeu et origine ethnique). Nous avons corrélé les résultats correspondants avec les scores du questionnaire sur le mal de simulateur (SSQ) dans un scénario de navigation simple. Un tel travail a fourni des informations permettant de proposer des expériences personnalisées de navigation en réalité virtuelle impliquant les différences individuelles.

5. Nous avons présenté une stratégie pour adapter en ligne l'accélération de la navigation en fonction de la réponse physiologique. Actuellement, l'évaluation du cybermalaise s'effectue sur la base de questionnaires subjectifs (par exemple, SSQ), mais l'évaluation par questionnaire interrompt l'expérience et introduit de grands écarts individuels. Pendant le processus de navigation, nous pouvons adapter la vitesse de navigation en fonction de signaux physiologiques. Nous avons utilisé le contrôle PID pour adapter la navigation et utilisé des réseaux de neurones pour trouver un réglage du PID optimal.

B.7 Limites

Les méthodes proposées présentent certaines limites pour l'évaluation et le développement des techniques de navigation.

1. Nous avions mentionné dans la section B.3 que nous souhaitions évaluer le cybermalaise en temps réel à partir de signaux physiologiques tels que l'EDA, la fréquence cardiaque, l'EEG, la balance posturale. Cependant, dans notre étude, nous n'avons utilisé que l'EDA pour mesurer le cybermalaise induit par les techniques de navigation proposées. L'EDA a été choisie car la collecte des signaux d'EDA a pu se faire par un bracelet (Empatica E4[9]), ce qui était très pratique. Etant donné que la relation entre les signaux physiologiques et le cybermalaise est ambiguë et que l'interprétation de l'un à l'autre est un sujet de recherche en cours, nous n'avons pas impliqué l'EEG et la fréquence cardiaque pour rester simple.

2. Nous avons développé une navigation adaptative dans la subsection B.5.4 basée sur le contrôle PID. Cependant, en raison de la pandémie de Covid-19, nous n'avons effectué la validation que d'un point de vue théorique, ce qui signifie que le manque d'étude utilisateurs pourrait détériorer la fiabilité de la stratégie adaptative proposée.

B.8 Perspectives de recherche

Sur la base de nos travaux dans cette thèse, nous proposons des perspectives à long terme pour des développements futurs.

1. **Mesurer le cybermalaise avec davantage de signaux physiologiques :** nous avons proposé de mesurer le cybermalaise avec le modèle LSTM en comparant la différence de signal de la balance posturale avant et après immersion. Cependant, mesurer le signal de balance posturale lorsqu'un utilisateur est immergé dans une application de RV est impossible, ce qui signifie que nous n'avons pas pu développer une navigation adaptative en ligne basée sur le signal de balance posturale. À l'avenir, nous prévoyons de vérifier cette méthode avec d'autres signaux tels que l'EEG, la dilatation pupillaire et les saccades, qui sont censés être plus pratiques dans une

[9]https://www.empatica.com/research/e4/

implémentation et des applications temps réel. De plus, il serait intéressant de coupler différents signaux physiologiques pour améliorer la précision des prédictions.

2. **Développement d'un ensemble de données standard pour les études utilisateurs :** l'intelligence artificielle (IA) se développe rapidement grâce à un accès facilité à des ensembles de données publics. Par exemple, avec des jeux de données (KITTI, Cityscapes, ApolloScape, Waymo Open Dataset) pour les transports publics, les chercheurs du domaine peuvent optimiser le flux de trafic et contribuer au développement des véhicules sans conducteur. Considérant que l'expérience utilisateur en RV est généralement différente individuellement, nous pensons qu'un modèle basé sur les données peut aider à résoudre le problème. Cependant, lorsqu'il s'agit de considérer des algorithmes d'interaction dans des environnements immersifs, la disponibilité d'ensemble de données est très faible. Des ensembles de données standard sont nécessaires pour utiliser la puissance de l'IA. Ces ensembles de données doivent inclure des informations provenant à la fois des environnements virtuels et physiques : toutes les informations visuelles transmises à l'utilisateur et tous les signaux physiologiques correspondants pendant les stimuli visuels. Nous proposons de développer un processus standardisé pour créer de tels ensembles de données : (1) choisir une problématique à traiter (par exemple, le cybermalaise, la charge de travail cognitive) en RV, ce qui permet de déterminer le type de données collectées ; (2) choisir des capteurs physiologiques et des questionnaires largement acceptés et disponibles pour tous les chercheurs, et avec ces informations, nous pouvons créer différents ensembles de données standard qui peuvent être publiés pour les chercheurs du domaine. Nous pensons que de tels ensembles de données permettront aux chercheurs de comparer efficacement leurs études. Et aussi, comme le processus de collecte de données est standardisé, différentes équipes de recherche peuvent également contribuer à enrichir ces ensembles de données.

3. **Utilisation des interfaces cerveau-ordinateur (BCI) pour améliorer l'expérience immersive :** une BCI peut acquérir des signaux cérébraux et les interpréter en actions exécutables effectuées par des appareils externes. En RV, une BCI peut être utilisé pour analyser les activités cérébrales de manière synchrone en temps réel, à partir desquelles nous pouvons évaluer les réponses de l'utilisateur dans des tâches de navigation et adapter les paramètres de navigation en conséquence. Cependant, les BCI actuelles reposent sur la pose de nombreuses électrodes sur le cerveau, ce qui constitue une menace pour l'interaction naturelle avec les environnements

virtuels. Par conséquent, le développement de BCI non invasives avec moins d'électrodes et adaptées aux dispositifs de réalité virtuelle est prometteur pour les futurs consommateurs de réalité virtuelle. Ainsi, les BCI pourraient être intégrées dans les visio-casques lors de leur conception.

Arts Sciences et Technologies et Métiers

Yuyang WANG
Intelligent navigation in virtual reality

HESAM UNIVERSITÉ

Résumé: La réalité virtuelle connaît un développement rapide grâce aux technologies de jeux vidéo 3D et de casques immersifs abordables, facilitant l'interaction avec les environnements virtuels. Cette thèse s'est intéressée à comprendre les facteurs humains affectant l'expérience utilisateur. Ces facteurs sont cruciaux pour concevoir une navigation naturelle. Les techniques de navigation virtuelle peuvent être exigeantes sur le plan cognitif et provoquer un cybermalaise. Divers facteurs humains peuvent influencer l'expérience utilisateur. L'évaluation correcte de l'expérience utilisateur est un préalable pour concevoir des techniques de navigation appropriées. Nous avons introduit un modèle de logique floue capable d'analyser les caractéristiques individuelles liées au cybermalaise. En plus des approches d'évaluation actuelles, nous avons proposé de nouveaux moyens de mesurer le cybermalaise et la charge cognitive sur la base du modèle LSTM et TOPSIS. Les résultats suggèrent que le *deep learning* peut évaluer efficacement le niveau de cybermalaise à partir de mesures comportementales, et que TOPSIS peut améliorer la précision de mesure de la charge cognitive. Les progrès réalisés pour accroître le potentiel de la réalité virtuelle reposent également sur notre capacité à développer de nouvelles techniques de navigation. Nous avons introduit la navigation adaptative et conçu quatre techniques différentes et originales de navigation tenant compte de différents facteurs humains. Des expérimentations ont été menées pour valider leurs performances, et les résultats ont montré une réduction significative du niveau de cybermalaise.

Mots clés: Réalité virtuelle, navigation adaptative, cybermalaise, cognition

Abstract: Virtual reality is experiencing fast development thanks to technologies from 3D computer games and affordable head-mounted devices, making it convenient to interact with virtual environments. This thesis focused on understanding human-related factors affecting user experience. These factors are crucial for designing natural navigation. Virtual navigation techniques might be cognitively demanding and induce cybersickness. Various human-related factors can influence user experience. The evaluation of user experience is a premise for designing appropriate navigation techniques. We introduced a fuzzy logic model that can analyze individual characteristics related to cybersickness. On top of the current evaluation approaches, we proposed new means to measure cybersickness and cognitive workload based on the LSTM model and TOPSIS. The results suggest that deep learning can measure cybersickness through behavioral assets, and TOPSIS can improve the measuring accuracy for the cognitive workload. The progress in unlocking the potential of VR also relies on our ability to develop new navigation techniques. We introduced adaptive navigation and designed four different original navigation techniques considering different human-related factors. User experiments were performed to validate their performance, and the results showed a significant reduction in cybersickness severity.

Keywords: Virtual reality, adaptive navigation, cybersickness, cognition